FINAL REPORT

Development and Optimization of the Direct Carbon Fuel Cell

Professor Scott Donne
University of Newcastle
February 26, 2016
Final Report, 2016

Submitted to Coal Innovation NSW
Project Commence Date: April, 2011
Project Cessation Date: December 2015
Project Duration: 5 years
Funding Allocated: $564,748

Phone: (02) 4921 5477
Fax: (02) 4921 5472
Email: Scott.Donne@newcastle.edu.au
Address: Discipline of Chemistry, University Drive, Callaghan NSW 2308, Australia

Executive Summary

Professor Scott Donne and co-investigators at the University of Newcastle (UoN) are investigating the Direct Carbon Fuel Cell (DCFC), a technology that has the ability to efficiently utilize coal to produce electricity with minimal environmental greenhouse gas emissions.

The DCFC is not a new technology, having been first demonstrated by Grove in 1839, and then investigated further by Jacques in 1896 (US Patent 555,511) for the direct production of electricity. While this system demonstrated the concept, it was expensive at the time and encountered problems with system impurities. Since then a number of researchers have occasionally revisited the DCFC, gradually making fundamental and performance improvements, until the present time when the DCFC is now viewed as a viable alternative for coal-fired energy generation.

In fact, the basic chemical reaction used by a coal fired power station and a DCFC are the same. The only difference is that the DCFC directly converts solid carbon into electrical energy through an electrochemical process where oxygen is combined with the carbon, as shown in the following schematic.

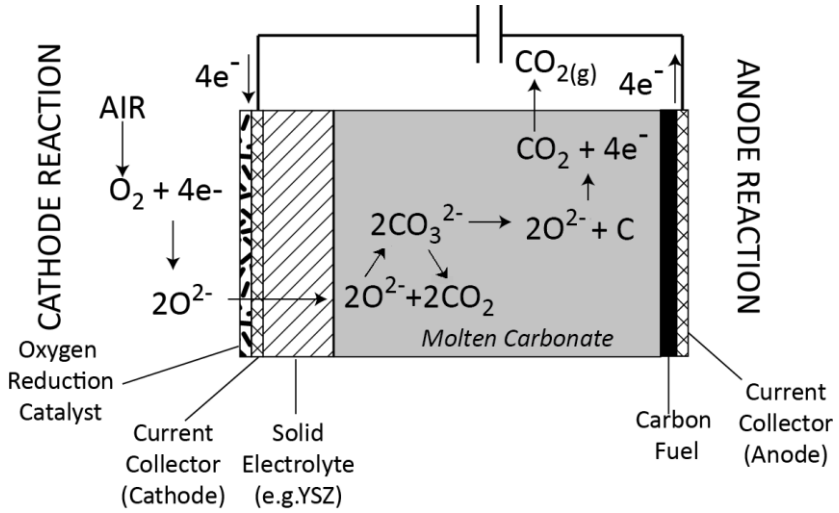

Here the cathodic process is the reduction of oxygen (O_2) in air with electrons (e^-) from the external circuit to form oxide anions (O^{2-}). These oxide anions then pass through a solid oxide ion conductor (electrolyte) to be combined with carbon dioxide (CO_2) to make carbonate ions (CO_3^{2-}). These carbonate ions act a carriers for the oxide anions to ultimately be combined with the carbon fuel via oxidation to make carbon dioxide and the electrons that pass through the external circuit. The potential difference between the anode and cathode in the DCFC produces a cell voltage, in a similar way that a battery works.

Current commercial systems operating in NSW generate electricity operate at most ~45% thermal efficiency and produce carbon dioxide (CO_2) that has to be subsequently captured and purified before storage (carbon sequestration). In contrast, the DCFC system is expected to operate at >80% thermal efficiency and produce pure CO_2. The CO_2 generated is approximately half the volume of that produced by current systems as well, which further diminishes greenhouse gas emissions.

This technology will enable rapidly declining coal reserves to be used in a highly efficient way. The DCFC will also minimize or remove associated by-process costs involved in capturing

the CO_2 (called post-combustion capture, PCC) and purifying the CO_2 prior to carbon sequestration.

This impact of this novel DCFC technology research has the potential to be world-changing and hold considerable significant commercialization advantages for the NSW Coal Industry. In summary, the DCFC offers the Australian and international coal industries:

(i) A way to extend their longevity (profitability and sustainability)
(ii) An effective tool to responsibly meet the ever increasing demands for electricity (social impact)
(iii) Reduce the carbon footprint imposed by the industry (environmental and social impact).

The overall objective of this project is to obtain proof of concept (POC) for the technology and progress towards commercialisation of the DCFC through further development and optimisation of bench-scale and then pilot-scale systems.

Coal Innovation NSW began funding Prof. Scott Donne at UoN in April 2011. This project revolves around the development and optimization of the Direct Carbon Fuel Cell (DCFC). The project objectives include:

(i) To understanding the mechanism through which coal is oxidized to form CO_2, and identifying and optimizing the important process variables for optimum performance, as defined by the kinetics of carbon oxidation to CO_2. The important process variables include the type and impurity level of the coal and whether coal washing is necessary, the nature and composition of the electrolyte (molten carbonate), the anodic catalyst, the operational temperature, and the gas-phase composition (CO_2/O_2 ratio).
(ii) Development of an operational (bench and pilot scale) DCFC, in particular, taking into account the mode of coal introduction to the catalyst surface.

The original concept of a fuel cell was first demonstrated by Grove in 1839. Although development of the DCFC has been underway since 1896, it is still in early developmental stages due to the substantial technical challenges that remain that require further research and development. This includes complex issues of materials degradation, reaction kinetics, stack fabrication, fuel delivery and system design.

The identified critical success factors for this project will be:

(i) Optimising performance of the coal oxidation process.
(ii) Overcoming limitations of the type of coal that can be used and preparation steps required.
(iii) Development of an operational bench and pilot scale DCFC (proof of concept).

A number of commercial partners have been approached during the course of this project, particularly in China where the market for small to medium size energy generation is quite large.

Fundamental investigations of the electrochemical oxidation if carbon carried out in this project have shown several avenues for improving performance of a pilot scale DCFC. These findings have allowed focus on optimisation work of the solid carbon anode to be planned including pre-treatment of the raw coal material using several different methods. Methods thought to increase electrochemical activity include pyrolysis and partial oxidation as well as the discovery of a high impact solid catalyst (kaolin) which enables dramatic enhancement of the oxidation kinetics. This catalyst is both cheap and abundant and easily incorporated into the solid

coal electrode through physical mixing.

Review of reported DCFC arrangements and performances has also allowed us to pin-point key areas which will allow a highly optimised and high performing pilot scale cell to be developed. In particular, it has been found that use of a solid anode in molten carbonate is the most advantageous arrangement and is expected to improve on reported performances. The final design of the pilot scale DCFC is thought to be superior to other designs as it is the only arrangement using a solid anode as well as the only arrangement to allow flexibility and optimisation in terms of the solid oxide electrolyte and cathode catalyst. The arrangement also allows off-gas sampling and analysis and careful control and monitoring of operational parameters such as temperature, pressure and purge gas composition.

Through application of findings from previously investigated milestones (including mechanistic investigations, catalyst development, coal type and pre-treatment effect, molten carbonate composition and contamination effects) and realisation of current cell design a highly optimised pilot-scale DCFC is expected to be realised on project completion.

Key scientific and technological outcomes from this project, compiled into their respective research areas, include:

(i) *Electrolyte Composition:* Common coal impurities were all found to affect the melt temperature of the electrolyte, either lowering or raising the melting point, indicating dissolution of the contaminant. Dissolution of these coal impurities had minimal impact on coal oxidation kinetics. This dissolution of impurities has also been discussed in terms of an opportunity to reclaim value added materials from the electrolyte component.

(ii) *Carbon Properties:* A range of different coal types (bother thermal and metallurgical) and their pre-pyrolysis has been investigated for their effect on coal oxidation kinetics. All coal samples behaved better than the baseline graphite because of their lower stability. It was found that thermal pre-treatment activated the coals via removing volatiles and functionality, and increased graphitisation. Lower pre-treatment temperatures removed volatiles but did not enhance coal conductivity to achieve good electrode performance. Higher pre-treatment temperatures led to significant loss of functionality, together with coal graphitisation. An optimum pre-treatment temperature was found depending on the coal type, established as a trade-off between functionalization and graphitization (conductivity).

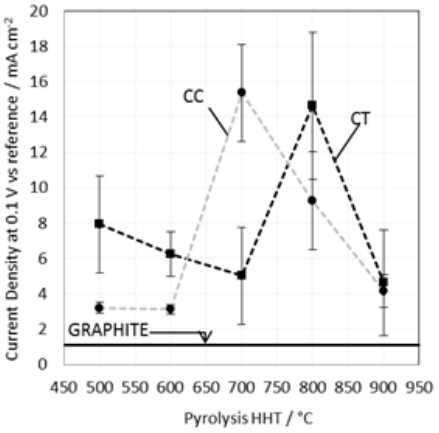

(iii) *Catalysis:* It was found that most common impurities in coal improve anode performance, and in the worst case, there was no effect on performance. A clay catalyst (kaolin) had a profound effect on performance; e.g., 5 wt% kaolin in coal doubled anodic current output. The distribution of kaolin in the anode was important, suggesting a surface mediated oxide ion transfer process. This is a new finding.

(iv) *Carbon Oxidation Mechanism:* A thorough electrochemical kinetic analysis of the carbon oxidation mechanism was carried out, assuming that each step in the mechanism was the rate determining step for electrochemical oxidation. Application of the predicted kinetic parameters to electrochemical data enabled identification of the rate determining step as a function of active material type and condition, as well as applied overpotential. In most

instances the first adsorption step and the first charge transfer step were identified as being rate determining. The addition of catalysts to the electrode enabled better adsorption, which is consistent with the previous hypothesis resulting from direct catalysis studies.

(v) *Electrolyte Design:* The baseline electrolyte used was the minimum melting temperature ternary molten alkali metal carbonate eutectic (Li_2CO_3:Na_2CO_3:K_2CO_3). The main conclusion is that binary carbonate combinations lead to better electrode performance, in particular those that contain a significant proportion of lithium carbonate, so much so that a binary sodium and potassium carbonate eutectic performed very poorly. The role of lithium has been hypothesized to involve lithium inclusion into the carbon structure, as in a Li-ion battery negative electrode, to facilitate superior anode performance.

(vi) *Bench- and Pilot-Scale DCFC Performance:* Another significant outcome of this project was the development and construction of two different size scale DCFC systems, both with the intent of implementing the fundamental project outcomes. While the bench-scale system successfully replicated the fundamental testing, the pilot-scale system enabled the introduction of advantageous fundamental findings on a larger scale. Specifically, the introduction of kaolin as a catalyst, the use of optimally pretreated coal, and the comparison between thermal and coking coals was evaluated. DCFC efficiency was evaluated here, with the efficiency ranging from 17% under high discharge loads, to 103% under low loads. This analysis identified the preferred material behaviours for high efficiency DCFC performance.

General Summary

Coal is a valuable resource for NSW, and indeed Australia. Its main use is in coal-fired power stations where it is used as the fuel for energy generation. This application, however, is limited in its scope for two main reasons:

(i) Coal combustion in power stations is responsible for significant emissions, including greenhouse gases (primarily CO_2), SO_x and NO_x gases, as well as particulates. None of these emissions is environmentally responsible.

(ii) Coal is a limited resource, and it is expected that our reserves of coal will be depleted in the near future.

These points are the main drivers for the development and implementation of more renewable and sustainable primary energy sources. While the transition from fossil-fuel based power to renewables is occurring, there is a need to implement strategies that enable the more efficient use of coal, all the while limiting the environmental emissions the arise conventionally from its use. One such technology is the Direct Carbon Fuel Cell (DCFC), which is the subject of this project.

Conventional use of coal in a coal-fired power station involves combustion, followed by a number of subsequent energy transformation steps to produce electrical energy. The overall efficiency of such a process is quite poor, typically around 35%. Alternately, the DCFC converts the chemical energy in coal directly to electrical energy with a theoretical efficiency of ~100%, and a practical efficiency of ~80%. This means that the DCFC operates at over twice the efficiency of a coal-fired power station. Additionally, the emissions coming from the DCFC are pure essentially CO_2 (no SO_x or NO_x gases or particulates) meaning that is can be captured and sequestered in a straightforward manner, unlike those from a coal-fired power station, for which post-combustion capture processes must be employed inducing a significant energy penalty.

This project has focused on the development of the DCFC. The project began with an extensive fundamental study into the factors that affect coal oxidation. This was then followed by the development of a functioning DCFC system into which the positive outcomes from the fundamental study were implemented.

Contents

Executive Summary 2
General Summary 6
Contents 7
1. INTRODUCTION 9
1.1. Project Description 9
1.1.1. Background and Project Aims 9
1.1.2. The University of Newcastle (Research Environment) Overview 9
1.1.3. Target Technology and Market 10
1.1.4. Potential Future Partnerships 11
1.1.5. Financial Projections 12
1.2. Project Objectives 12
1.3. Objectives and Relevance to Project 12
2. SUMMARY OF MILESTONES AND PROGRESS 17
2.1. Progress on Project Milestones 17
2.2. Overall Milestone Progress Summaries and Outcomes 17
3. TECHNICAL SUMMARY 29
3.1. Milestone 7: Molten Carbonate Impurity Effects on Performance 29
3.1.1. Milestone Background and Aims 29
3.1.2. Experimental Methods 29
3.1.3. Results 30
3.1.3. Conclusions 37
3.2. Milestone 8: Effect of Coal/Carbon Type on Performance 38
3.2.1. Milestone Background and Aims 38
3.2.2. Experimental Methods 38
3.2.3. Results 42
3.2.4. Conclusions 60
3.3. Milestone 11: Electrode Catalyst Effects on Oxidation 62
3.3.1. Milestone Background and Aims 62
3.3.2. Experimental Methods 62
3.3.3. Results 64
3.4. Milestone 12: Coal Oxidation Mechanism Characterisation 76
3.4.1. Milestone Background and Aims 76
3.4.2. Results 76
3.5. Milestone 13: Electrolyte Composition Design 83
3.5.1. Milestone Background and Aims 83
3.5.2. Experimental Methods 83
3.5.3. Results 84
3.5.4. Conclusions 90
Summary of Fundamental Outcomes 91
Applied Outcomes 93
3.6. Milestone 14 and Milestone 15: Construction and Performance Optimisation of a Bench-Scale DCFC 93
3.6.1. Milestone Background and Aims 93
3.6.2. Experimental Methods 93
3.6.3. Results 96
3.6.4. Summary and Conclusions From Bench-Scale DCFC Testing 96

3.7. Milestone 16: Construction of a Pilot Scale DCFC 98
3.7.1. Milestone Background and Aims 98
3.7.2. Pilot Cell Design 98
3.7.3. Commissioning 102
3.8. Milestone 18: Performance Optimisation of Pilot Scale DCFC 105
3.8.1. Milestone Background and Aims 105
3.8.2. Cell Component Fabrication 105
3.8.3. Anode Development 110
3.8.3.2. Performance Analysis – Literature Review 117
3.8.4. Coal Ash Distribution Investigation 120
3.8.5. Coal Pre-treatment Investigation 129
3.8.6. Materials Corrosion Investigation 137
3.8.7. Pilot Cell Commissioning and Initial Testing 141
3.8.8. First Pilot Cell Run 147
4. TECHNICAL OUTCOMES 161
4.1. Overall Outcomes and Learnings 161
4.2. Discussion of Project Challenges 161
4.3. Publications Arising from Project 161
5. CONCLUSIONS 163
5.1. Overall Progress in Meeting Project Objectives 163
5.1.1. Objective #1 163
5.1.2. Objective #2 163
6. References 164

1. INTRODUCTION

1.1. Project Description

1.1.1. Background and Project Aims

Currently NSW provides the eastern states of Australia with electricity produced primarily (90%) in coal-fired power stations. This is mainly because of an abundance of coal in the region. Fundamentally, electricity generated from coal (or fossil fuels in general) is very inefficient (limited by the Carnot efficiency), with even the best power stations, say for example using oxy-fuel technology, only operating at most 45% thermal efficiency. Furthermore, the combustion of coal in power stations is a major contributor to greenhouse gas emissions. Post-combustion capture (PCC) of CO_2 is also problematic, requiring a large footprint and energy consuming strippers to extract the CO_2 from the flue gas. Clearly a technology is required that capitalizes on the vast reserves of coal available in NSW, is efficient, and produces a flue gas that requires little if any processing before sequestration (pure CO_2).

The DCFC consists of a cathode and anode separated by an ionically conducting electrolyte. The electrolyte is also electronically insulating. A solid fuel (in this research, coal) is supplied to the fuel chamber and reacts directly at the electrode. From this reaction a gaseous exhaust product results. For the cell to operate at maximum efficiency, the overall chemical reaction is $C + O_2 = CO_2$.

The DCFC is a technology that transforms the oxidation of coal directly into electricity, thus avoiding the inefficiencies associated with a heat engine (i.e., using heat to produce steam which then turns a turbine). This direct generation of electricity also operates at close to 100% thermal efficiency, with all of the coal used as fuel converted into electricity. Furthermore, the flue gas coming from the DCFC is almost pure CO_2, immediately ready for sequestration.
Considering the impact of greenhouse gas emission, "in absolute terms, total CO_2 emissions from the production and use of energy in Australia were 95 per cent higher in 2000-01 than in 1973". As the DCFC produces approximately half the CO_2 as compared to the current systems and requires less energy impacts, it has the potential to directly contribute to a reduction in total CO_2 emissions.

Currently under development worldwide there are three basic families of DCFC. These are distinguished by the electrolyte type used in the reaction (aqueous and molten hydroxide, molten carbonate and solid oxygen ion conducting ceramic).

In this research project, the DCFC family being investigated is the molten carbonate which is the most commercially mature types of systems being investigated. The advantages of molten carbonate systems include long term CO_2 stability, high ionic conductivity and the ability to catalyse carbon oxidation. The operating temperature required though is between 600^{o}C and 850^{o}C .

Professor Scott Donne will attempt to develop and optimise a bench-scale and then pilot-scale DCFC, achieve proof of concept in preparation for future commercialisation.

1.1.2. The University of Newcastle (Research Environment) Overview

The research is to be conducted at the University of Newcastle (UoN), in the Faculty of Science and IT (FSCIT), in the Discipline of Chemistry. In 2015 in an independent Australian Government assessment (Excellence in Research for Australia, ERA), the UoN was ranked 8th in Australia for research that is well above world standard. 90% of UoN research was rated at world standard or above. Of particular relevance here was the ranking of Macromolecular and Materials Chemistry and Physical Chemistry as "Well Above World Standard", categories that

feed directly into this project.

Professor (Prof.) Scott Donne has worked at the UoN since 2001 in the Discipline of Chemistry. His research collaborations and Centres that he works within include the Newcastle Institute for Energy and Resources (NIER), the Priority Research Centre for Energy (PRCfE) and the Priority Research Centre for Organic Electronics (PRCOE). Prof. Donne's main research interests and significant experience lie in the general area of electrochemistry and materials science, applied to many varied areas including electrodeposition, the application of electroanalytical methods, energy storage systems, and corrosion.

Prof. Donne's research group (Applied Electrochemistry) is focused primarily on the development and fundamental understanding of various energy storage and conversion systems. He also has interests in materials science and corrosion. The Applied Electrochemistry group is based in the Newcastle Institute for Energy and Resources (NIER). The facilities available to this group are second to none across Australia and the world in terms of electrochemistry, while there are considerable centralized UoN facilities to support the materials science aspects of the group's research. The Applied Electrochemistry group also collaborates extensively with numerous academic and industrial partners from around Australia and across the world. Essentially these partners have recognized the capacity of this research group, seeking to capitalize on the skills and technologies available.

1.1.3. Target Technology and Market

Technology

The technology that is being investigated is the technique of obtaining thermal efficiency from coal required to produce electricity. This technology will be directly relevant to power stations. The benefits of the project will have implications to the economic and social aspects of all of the Australian community.

Electricity Market

Australia is the world's eighteenth largest energy consumer and ranks fourteenth on a per person basis. In 2009–10, Australia's primary energy production was 17,282 PJ. Net energy exports accounted for 68 per cent of domestic energy production in 2009–10, while domestic consumption accounted for the remaining 32 per cent. Australia is the world's ninth largest energy producer, accounting for around 2.5% of world energy production and 5% of world energy exports. In 2009–10, Australia's primary energy production was dominated by coal, which accounted for 61 per cent of total energy production in energy content terms.

Electricity Driver

Continuation of electricity is a primary concern for the Australian Government and the wider community. Coal is anticipated to continue to supply the majority of Australia's domestic needs despite the fact that natural gas and renewable energy sources are progressively increasing.

Electricity Demand Trends

Considering power consumption, during 2000-01, Australia used 93% more energy than it did 27 years earlier. Without reductions in energy intensity, it would have used 136% more. Energy consumption grew at an annual average rate of 2.5 per cent in Australia over the 27 years to 2000-01. Currently there are at least seven proposals for new coal power stations in Australia to meet projected future demand. Australia's energy mix is dominated by black and brown coal, accounting for around 37% of total primary energy supply in 2009–10.

New Legislative Requirements

From the 1st October 2011, all new power stations to be built have to meet new the NSW State Environmental Planning Policy and the Environmental Planning and Assessment Amendment (Part 3A Repeal) Act 2011. This act ensures that new stations are subjected to increased scrutiny in relation to environmental protection and the health and amenity of local communities. This involves a public and transparent assessment process. The DCFC will enable electricity providers to provide a 'cleaner' power station that has a reduced footprint and is twice as efficient as existing technology. The Australian Government released the Draft Energy White Paper, Strengthening the Foundations for Australia's Energy Future in December 2011. Four main policy priorities are identified: (1) enhancing energy policy through regular evaluations, (2) furthering competitiveness and efficiency in the energy market through reforms, (3) furthering the development of energy resources (with an emphasis on gas), and (4) promoting the transition towards clean energy technologies.

1.1.4. Potential Future Partnerships

This ultimate outcome of this project is to establish a sound pathway to commercialization through proof of concept and optimizations of the DCFC. It is imperative that potential relevant organizations be continually identified for possible future collaborations.

As described in the project agreement though, no collaborations will be undertaken without the prior consent of the project funders (Coal Innovation NSW and UoN).

Identified partners that may be approached for future development and commercialization discussions include:

Government/Regulatory Bodies

- Standing Council on Energy and Resources (formerly the Ministerial Council on Energy)
- Industry & Investment NSW – Minerals & Energy
- Environmental Protection Authority (EPA)
- Geoscience Australia

University Groups

- Tom Farrell Institute for the Environment (TFI) UoN
- NIER (Newcastle Institute for Energy and Resources)
- NSW Institute of Frontier Geoscience (NSW IFG)

Electricity Suppliers (full list see Annex 11.4)

- Ausgrid
- Endeavour Energy
- Essential Energy

Coal Mining Companies

- Peabody Pacific
- Rio Tinto Coal Australia Pty Ltd
- Vale

Industry Associations

- Australian Coal Association
- UNCOVER (Australian Academy of Science)
- Energy Supply Association of Australia

1.1.5. Financial Projections

The financial advantages of DCFC include:

(i) Wider range of applications to established markets
(ii) Avoidance of large infrastructure investments
(iii) High efficiency
(iv) Low CO_2 capture costs

At this stage financial projections have not been determined but it is expected that significant costs savings will be achieved through the increase in thermal efficiency, removal of the PCC process and purification of CO_2.

Eventual estimated costs are predicted to be US$1350 to $1600 per kW which is competitive with current coal fired power plants and the industry appears to be willing to accept a cost of up to $2000 per kW due to increased efficiency and lower associated running costs.

Anticipated process costs will include producing fuel cells (de-contamination) at approximately $2-3/MMBtu.

Currently DCFCs are expected to only have a lifetime of five years due to significant degradation and these needs to be investigated further to improve cell efficiency and value.

In the financial projections it is important to keep in mind that Australia's current commercial electricity infrastructure is aging which means that it may become increasingly unreliable in the coming decades.

Further details will be provided as the project proceeds through submission of quarterly and annual reports.

1.2. Project Objectives

Fundamentally, the DCFC has the potential to provide efficient and clean energy through the use of coal. However, there are a number of technological shortcomings of the DCFC that need to be addressed before its commercial implementation, and these are what we plan to address in this project. These include:

(i) Understanding the mechanism through which coal is oxidized to form CO_2, and identifying and optimizing the important process variables for optimum performance, as defined by the kinetics of carbon oxidation to CO_2. Following on from above, the important process variables include the type and impurity level of the coal and whether coal washing is necessary, the nature and composition of the electrolyte (molten carbonate), the anodic catalyst, the operational temperature, and the gas-phase composition (CO_2/O_2 ratio).
(ii) Development of an operational (bench and pilot scale) DCFC, in particular, taking into account the mode of coal introduction to the catalyst surface.

1.3. Objectives and Relevance to Project

This project on the development of the direct carbon fuel cell pre-dated the current project supported by Coal Innovation NSW. As such, some of the early milestones included into the

project outline for this project include details and activities of the prior project. A summary of all the project milestones and status is included in Table 1.

Table 1. Project Milestones and Relevance to Project.

Objectives	Status (%)	Relevance to Project and Comments
MILESTONE 1 Supervision and intellectual input of Professor Scott Donne	100%	Professor Donne conceived the project and contributed to its activities on an ongoing basis for the duration of the whole project.
MILESTONE 2 PhD student #1	100%	The first PhD student on this project (Dr. John Tulloch) completed his thesis and was awarded a PhD in 2012.
MILESTONE 3 Literature review of the DCFC	100%	Carried out on an ongoing basis by both PhD students as part of their theses.
MILESTONE 4 Prove-in of electrochemical test cell	100%	This milestone was completed as part of the activities of PhD student #1. This test cell played an integral part of the project as a whole, providing a vehicle through which many fundamental investigations were carried out.
MILESTONE 5 Postdoctoral research fellowship	100%	The appointment of a postdoctoral researcher was essential for the ongoing activities of the project, not only in terms of intellectual input but also day-to-day running of experiments and PhD student supervision.
MILESTONE 6 Undergraduate research scholarship	100%	During the initial stages of the project (2012) some delays were incurred and so it was necessary to appoint an undergraduate research student to make up for the lag. Not only did this enable the project to return to being on time, but also provided a valuable opportunity for the undergraduate student to gain experience in this research area.
MILESTONE 7 To investigate molten carbonate impurity effects on performance. (electrolyte properties). Includes examining the kinetic limitations/effects imposed on the molten carbonate electrolyte as a result of the presence of impurities and variation in composition.	100%	The medium in which carbon oxidation occurs greatly influences the oxidation interface including the shuttle mechanism for moving oxide anions from the cathode to the anode for reaction with carbon. Interactions which occur in the molten medium are of prime importance on both a fundamental and applied scale. Coal as a fuel contains many constituents other than pure carbon in the form of mineral ash. These 'impurities' are not expected to oxidise or react in the DCFC and are therefore able to accumulate in the molten carbonate medium. This is expected to affect both the thermal properties of the system (melting point, heat capacity) and electrochemical reactions (oxide

		anion diffusion, change in wettability at electrode surface, etc). This milestone has been completed within the bounds of this project. Nevertheless, there is still scope for further work in this aspect of the DCFC.
MILESTONE 8 Determine the effect of coal/carbon type on performance. Includes evaluation of various carbon types and pre-treatment conditions in both the half-cell and bench-top DCFC.	100%	In examining several types of carbon, more background information is required to optimize the DCFC. Coal sourced from various areas will have different ash composition and structure which may affect the activity of the carbon contained in the coal. Screening a variety of coals for activity gives a broad understanding of important variables in coal types to enable possible prediction of DCFC based on coal properties. Further, pre-treatment of coal prior to entry to the DCFC also changes the relative structure of the coal as well as altering the composition (for example, pyrolysis drives off volatiles and increases relative ash content depending on pyrolysis conditions). Pre-treatment methods and conditions may therefore change the reactivity of the coal in the DCFC and therefore the pre-treatment step is of great importance. This milestone has been completed for the limited number of carbon/coal samples examined in this project. Of course with the use of natural product such as coal, that is inherently variable, there still exists considerable scope for further research in this area.
MILESTONE 9 PhD student #2	90%	The second PhD student on this project (Mr. Michael Glenn) is nearing completion of his thesis. His work has been focused on the behavior of molten carbonate electrolytes and their impact on the performance of the DCFC, which is a fundamentally important aspect of system behavior.
MILESTONE 10 Completion of PhD student #1	100%	Thesis completed and degree awarded in 2012.
MILESTONE 11 Investigate electrode catalyst effects on oxidation.	100%	Catalysis in the carbon anodes can occur in two ways. The first involves the addition of foreign materials to the solid composite electrode. The second involves the addition of soluble species to the electrolyte. Both have the ability to catalyse or change the oxidation mechanism and identifying catalysts of this nature could

		significantly improve the performance of the DCFC. This milestone represents a significant outcome from this project. Within the scope of the current project this milestone has been completed, but there is much more research and benefits to DCFC performance that could result from further work in this area.
MILESTONE 12 Investigate carbon oxidation mechanism.	100%	Understanding the oxidation mechanism of the anodic reaction of the DCFC (carbon oxidation) is key fundamental knowledge and can be used to understand system effects and sensitivities. Understanding of the oxidation mechanism can also aid in catalyst development where identification of the rate determining step pinpoints where a catalyst may be applied and its nature. This milestone has been completed within the bounds of this project. As above for the previous milestone, further research is required here to better understand the effects of changing electrode parameters on anode performance.
MILESTONE 13 Optimise electrolyte composition design	100%	The composition of the molten carbonate has the ability to impact on the performance of the DCFC for reasons outlined in Milestone 7 (thermal and electrochemical). The eutectic composition (mixture of lowest melting temperature) has been chosen for investigations, however variation of the eutectic may result in more favourable outcomes electrochemically at the cost of thermal inputs (change in dissociation and dissolution of oxide anions, change in wetting characteristics of molten carbonate etc). It is therefore of interest to test both thermal and electrochemical properties of various eutectic mixtures in order to ensure the composition used on a larger scale is the most ideal both thermally and electrochemically. The electrolyte is a critical, but quite often overlooked, aspect of fuel cell performance. While preliminary research into molten carbonate electrolyte behavior has been carried out to satisfy this milestone, there is still much more that could be done to contribute to this milestone.
MILESTONE 14 Construction of Bench Scale	100%	Development of a workable bench-top DCFC allows several important parameters of the

DCFC		system to be tested and optimised prior to moving to a larger and less flexible set-up. Parameters identified to be of interest include those detailed in Milestones 7, 8, 11, 12 and 13. Further, in development of these milestones, practical cell set-up and assembly knowledge will be gained including materials handling and electrode construction issues. Workable reference and counter electrodes able to give reproducible results are key to the half-cell design while cathode design will impact heavily on the full bench scale operation. Throughout the course of this project an important aspect has been the transference of fundamental research findings into practical systems. The development of the bench-scale DCFC, and ultimately the pilot-scale DCFC, enable the transfer of fundamental information and findings into an operating full system. Within the bounds of this project, this milestone has been completed.
MILESTONE 15 Optimise performance of bench scale DCFC	100%	
MILESTONE 16 Construction of pilot-scale DCFC	100%	Scaling up the bench scale DCFC to a pilot scale is a key part of the DCFC commercialisation pathway and enables learning from the bench scale equipment to be applied on a larger scale. It is the intention of this project that the pilot scale rig is still flexible and able to be modified and optimised as new information comes to light. This milestone has been completed.
MILESTONE 17 Thesis completion of PhD student #2	90%	This milestone will be completed in June 2016.
MILESTONE 18 Performance Optimisation of Pilot Scale DCFC	100%	The practical and reliable operation of the pilot scale DCFC utilizing knowledge gained from previous milestones, including the bench scale arrangement, is the culmination of all work carried out to date. This milestone is essential for the commercial development of the DCFC. Throughout the course of this milestone the intent was to operate the pilot-scale DCFC in a way to demonstrate and implement the fundamental findings into a functioning larger scale full DCFC system. As such, this milestone has been completed.

2. SUMMARY OF MILESTONES AND PROGRESS

2.1. Progress on Project Milestones

A Gantt chart of the progress of project milestones is shown in Figure 1.

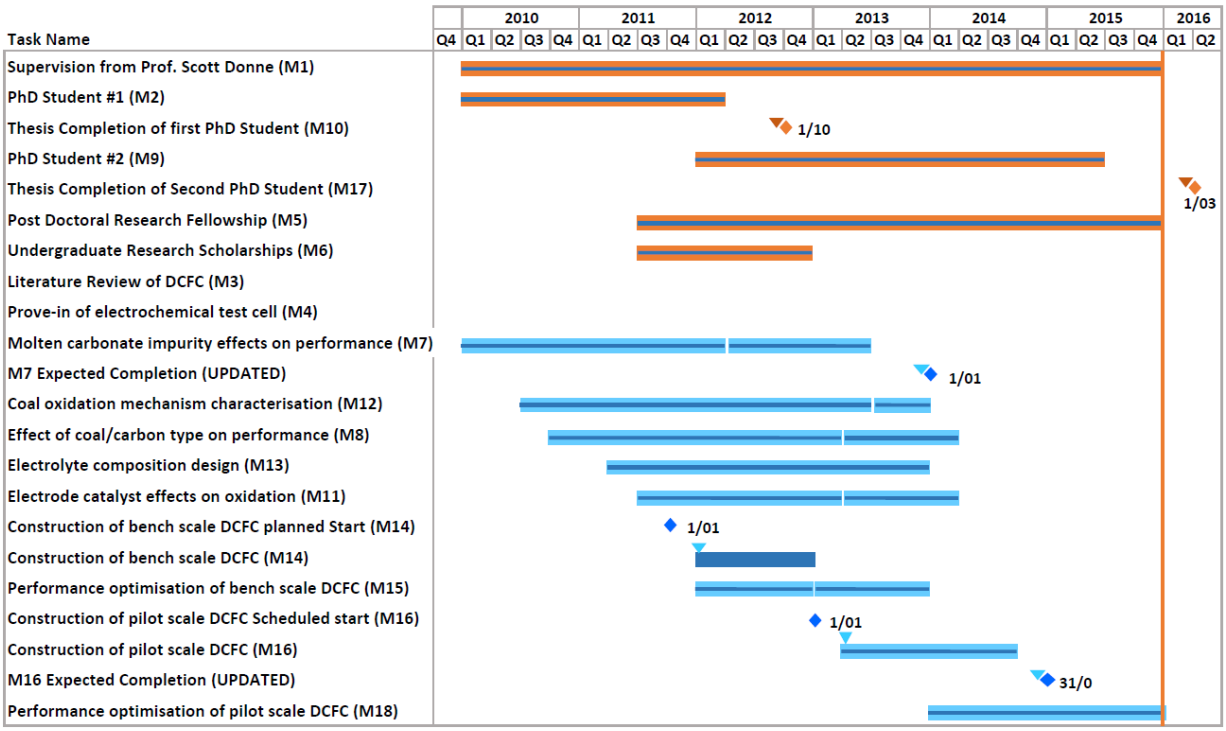

Figure 1 Gantt Chart of Project Progress

Staffing is shown in orange and grouped together at the top of . Research activities are shown in blue and grouped in order of ascending start date of milestone. In cases where the start or end-date of a milestone is different to original project projections, a marker has been used to indicate actual start and end dates. Milestones which are currently underway and are operating under extended time frames to initial projections are shown as a split in the indicator bar. The position of the split indicates where the milestone was initially planned for completion.

2.2. Overall Milestone Progress Summaries and Outcomes

MILESTONE 7: Molten Carbonate Impurity Effects on Performance

2013 Progress and Outcomes

(i) Tasks/Strategies:

Q1, 2013

⇒ A preliminary draft of the experimental outcomes was prepared.

⇒ The kinetic analysis model was been identified and applied to the experimental data. This dramatically improved the quality of the data analysis and understanding of the system under study.

Q2, 2013

⇒ Completed the kinetic modelling on the DTA data; and

⇒ Commenced writing a second article in relation to this work.

Q3, 2013

⇒ Development of an automated excel spreadsheet designed to enable fast analysis of DTA data and elucidation of melt phase activation energy

⇒ Analysis and collection of data for each impurity and at different concentrations to allow assessment of the effect of running the DCFC over time.

⇒ Ongoing documentation of analysis results and interpretation of data in a journal article format.

Q4, 2013

⇒ Finalization of analysis results and interpretation in journal article format.

⇒ Follow-up experimentation to confirm hypothesis for changes in melt behavior resulting from inclusion of particular contaminants

(ii) Performance Measures:

⇒ Development of technical information in the form of data analysis and review of relevant literature.

⇒ Organization of data into report and/or journal article format.

⇒ Application of knowledge to DCFC testing activities

(iii) Outcomes:

⇒ Analysis of all data to give activation energy as a function of conversion for each impurity at three concentrations

⇒ Development of a working hypothesis for differences observed in the DTA response of the ternary carbonate eutectic (use of various techniques on follow-up to confirm theory)

⇒ Reporting of data analysis outcomes in Q4 report, 2013 and here in Section 3.1. This report includes conclusions relevant to the application of knowledge to DCFC testing activities.

⇒ Finalization of a journal article to submission standard. Organization of data able to be formed into second journal article for consideration.

(iv) Comments:

⇒ This milestone has involved extensive data analysis and interpretation of results has not been trivial due to the variation in DTA response dependent on type and concentration of contaminant introduced. Initially, two journal articles were started; however due to a change in analysis method and follow-up experiments performed on initial results a single publication has been prepared at the completion of this Milestone (Glenn, M.J., J.A. Allen, and S.W. Donne, Energy and Fuels, 2015. 29(8): p. 5423-5433), with a number of others pending.

MILESTONE 8: **Effect of Coal/Carbon Type on Performance**

2013 Progress and Outcomes

(i) Tasks/Strategies:

Q1, 2013

⇒ Six additional carbon samples were analyzed electrochemically.

⇒ Physico-chemical analysis of these materials was also carried out.

Q2, 2013

⇒ Sourced four additional coal samples for analysis;

⇒ Conducted chemical and physical analysis on these materials; and

⇒ Evaluated their electrochemical performance in the DCFC.

Q3, 2013

⇒ Preparation, including milling and sieving, of four new coal materials sourced for electrochemical performance analysis.

Q4, 2013

⇒ Pyrolysis of coal samples under controlled and reproducible conditions

⇒ Characterization of pyrolysis behaviour of coals using TG/DTA

⇒ Development of electrochemical cup cell procedure for testing of coal materials

⇒ Fabrication of coal based electrodes for testing in DCFC bench scale cell

(ii) Performance Measures:

⇒ Development of technical information in the form of data analysis and review of relevant literature.

⇒ Organization of data into report and/or journal article format.

⇒ Application of knowledge to DCFC testing activities

(iii) Outcomes:

⇒ Testing of the majority of coal samples in the half-cell DCFC, prepared under identical pyrolysis conditions

⇒ Development of possible new methods for activity characterization of coals

2014 Progress and Outcomes

(i) Tasks/Strategies:

Q1, 2014

⇒ Testing of all 7 coal sources available in DCFC bench scale cell and assessment regarding activity

⇒ Collection of complimentary data for each coal type including TG/DTA, SEM, elemental analysis, ash analysis, pyrolysis behaviour and carbon dioxide adsorption affinity.

⇒ Analysis of the impact of thermal pre-treatment on electrochemical performance

⇒ Analysis of bubble formation at carbon electrode and effect of carbon type on bubble formation

(iv) Performance Measures:

⇒ Organization of data into journal article format.
⇒ Application of knowledge to DCFC testing activities

(v) Outcomes:
⇒ Highlight of pre-treatment effects and preliminary work on solid anode formula generation
⇒ Publication in high impact journal

(vi) Comments:
⇒ Understanding of impacts of coal type and pre-treatment, has led to an understanding of what an active, solid anode may consist of which may include coal of various rank and combination of pre-treatment options including coals which have been variously treated by ash removal, pyrolysis or partial oxidation. The results obtained for this milestone have been published (Allen, J.A., M. Glenn, and S.W. Donne, J. Power Sources, 2015. 279: p. 384-393).

MILESTONE 11: **Electrode Catalyst Effects on Oxidation**

2013 Progress and Outcomes
(i) Tasks/Strategies
Q1, 2013
⇒ Further kinetic analysis to characterize the behaviour of the beneficial catalysts on the oxidation of carbon in the DCFC.
⇒ Discussions were held with Mr. David Fleming from Newcastle Innovation to describe this invention and begin the patenting and commercialization process.
⇒ A preliminary literature survey was conducted to identify suitable soluble catalysts for use in the DCFC.

Q2, 2013
⇒ Examining the role that impurities/catalysts have on electrode performance at different temperatures; and
⇒ Modelling this data using previously developed electro-kinetic models.

Q3, 2013
⇒ Introduction of new additives to anode for electrochemical examination including transition metal oxides. Testing was performed over a range of temperatures. Review of electrode preparation procedure and test program for contaminants and temperatures of interest was also developed.
⇒ Preparation of a journal article (submission stage) based on previous work using common ash constituents as catalysts for the oxidation reaction. Involved an updated review of literature in the area which has expanded rapidly in the last 2-3 years.

Q4, 2013
⇒ Preparation of a library of stable, reproducible anodes incorporating different possible catalysts of interest

(ii) Performance Measures:

⇒ Development of technical information in the form of data analysis and review of relevant literature.

⇒ Organization of data into report and/or journal article format.

⇒ Application of knowledge to DCFC testing activities

(iii) Outcomes:

⇒ A summary of work carried out to date was prepared in the form of a journal article. The article was submitted, has been reviewed, approved and was published. Reference is as follows: J. Tulloch, J. A. Allen, L. Wibberley and S. W. Donne. "Influence of Selected Coal Contaminants on Graphitic Carbon Electro-Oxidation for Application to the Direct Carbon Fuel Cell." J. Power Sources, 2014. 260: p. 140-149.

⇒ Using the journal publication as a basis a patent on this work, specifically for the use of kaolin as a catalyst for graphite oxidation, has been prepared and submitted (S. W. Donne; "Coal Innovation", Australian Provisional Patent Application, IP Australia Reference SPBI-0000234234 (2014)).

⇒ Several active materials have been observed through interaction with the carbon at the electrode surface, the same results were not observed on addition of catalysts to the electrolyte.

2014 Progress and Outcomes

(i) Tasks/Strategies

Q1, 2014

⇒ Analysis of graphite electrodes with embedded impurities to determine activity using different catalytic materials to that tested previously

(ii) Performance Measures

⇒ Organization of data into journal article format.

⇒ Application of knowledge to DCFC testing activities

(iv) Outcomes:

⇒ Publication of results in high impact journal

⇒ Demonstration of catalyst effectiveness

(v) Comments

⇒ A solid catalyst was identified as giving the best promotional effects to the electrochemical oxidation of coal through simple mixing.

MILESTONE 12: **Coal Oxidation Mechanism Characterization**

2013 Progress and Outcomes

(i) Tasks/Strategies

Q1, 2013

⇒ The carbon oxidation model has been revised with a focus on surface oxidation processes.

Q2, 2013

⇒ Modelling the electrochemical response of electrodes discharged at elevated temperatures.

Q3, 2013

⇒ Assessment and testing of graphite electrodes at several temperatures to examine temperature effects on oxidation.

⇒ Review of kinetic method used to analyze mechanism and preparation of a journal article outlining this method and use of parameters for mechanistic interpretation of different carbon materials

Q4, 2013

⇒ Finalization and submission of journal article in this area

⇒ Development of a working hypothesis for oxidation mechanism and sensitivities

⇒ Development of repeatable electrochemical investigation model to gather further information and add to growing body of knowledge

(ii) Performance Measures

⇒ Development of technical information in the form of data analysis and review of relevant literature.

⇒ Organization of data into report and/or journal article format.

⇒ Application of knowledge to DCFC testing activities

(iii) Outcomes

⇒ A summary of work carried out to date was prepared in the form of a journal article. The article was submitted in December 2013 and is currently under review. Reference is: Allen, J.A., et al., Electrochim. Acta, 2014. 129: p. 389-395.

⇒ A working hypothesis for the activity of carbon in the DCFC has been established and is considered with respect to all results collected during this project. This hypothesis is presented here in Section 3.4**Error! Reference source not found.**.

(iv) Comments

⇒ Sound progress has been made on this milestone with the development of tools for assessment of experimental data in order to contrast and compared results and to add to understanding of the reaction mechanism. This knowledge will continue to be applied as testing on the pilot scale rig continues and new information about coal and carbon performance (Milestone 8) and the incorporation of different catalysts (Milestone 11) are collected. Due to the highly complicated nature of the oxidation mechanism, it is still not fully understood, however keys points as to how the mechanism proceeds and the rate of the reaction are hypothesized from current data.

MILESTONE 13: **Electrolyte Composition Design**

2013 Progress and Outcomes

(i) Tasks/Strategies:

Q1, 2013

⇒ Milestone was not furthered in this quarter due to a lack of equipment

Q2, 2013

⇒ Milestone activities were limited to testing of carbonate mixture containing contaminant species (Milestone 7)

Q3, 2013

⇒ Development of a research plan for a summer vacation student to analyze the effect of changing the eutectic composition on both thermal and electrochemical behavior of the DCFC.

⇒ Review of literature regarding wetting of carbon materials with carbonates and possible impact on oxidation reaction

Q4, 2013

⇒ Thermal analysis of six electrolyte compositions including melting temperature, activation energy and conversion behaviour

(ii) Performance Measures:

⇒ Development of technical information in the form of data analysis and review of relevant literature.

⇒ Organization of data into report and/or journal article format.

⇒ Application of knowledge to DCFC testing activities

(iii) Outcomes:

⇒ Data collected has been summarized in this report (Section 3.5) as well as in the Q4, 2013 report

⇒ Design of the electrolyte composition will require further refinement using the pilot scale arrangement, however key points of interest (including thermal behaviour) are now better understood and the eutectic composition currently remains the preferred composition.

(iv) Comments:

⇒ This milestone has been largely overshadowed by Milestone 7, however many of the techniques developed in Milestone 7 (including data analysis and interpretation) are applicable to this milestone and have been used for data analysis. Many of the learnings from Milestone 7 have also been applied to work in this milestone and a good understanding of the effect of varying the carbonate composition from the eutectic mixture on both thermal and electrochemical aspects of the system has been achieved.

MILESTONES 14 and 15: **Construction and Performance Optimisation of a Bench-Scale DCFC.**

2013 Progress and Outcomes

(i) Tasks/Strategies

Q1, 2013

- ⇒ A bench-scale DCFC system has been conceived, designed and constructed. It consists of a solid carbon anode, and air cathode, both of which are immersed in a molten carbonate electrolyte and separated by a solid yttria-stabilized zirconia membrane.
- ⇒ A range of different carbon materials have been evaluated in the bench-scale DCFC.

Q2, 2013

- ⇒ Continued implementation of our fundamental outcomes into the bench-scale DCFC. This includes features such as catalysts and electrolyte impurities.

Q3, 2013

- ⇒ Design and fabrication of cathode not prone to leakage of carbonate through alumina tube and use of new ceramic paste.
- ⇒ Design and commissioning of additional cell components required to allow extended testing of full cell as well as bench scale arrangement as anode AND cathode half-cell. This will allow quick determination of the limiting reaction and enable further optimization activities in this area.

Q4, 2013

- ⇒ A series of anodes were prepared using a more efficient and reproducible method for use in the bench scale DCFC

(ii) Performance Measures:

- ⇒ Ability to perform and complete other technical Milestones
- ⇒ Production of a workable, flexible and useful DCFC design for testing of various DCFC parameters
- ⇒ Design of a scaled up DCFC using learnings from bench scale cell.

(iii) Outcomes:

- ⇒ Completion of Milestones 7, 12 and 13.
- ⇒ Operation of DCFC as a full fuel cell (results presented in Section 3.6)
- ⇒ Design and start of procurement/construction of a pilot scale DCFC.

(iv) Comments:

- ⇒ Performance of the bench scale DCFC is essential to the completion of all technical milestones and refining electrode preparation and cell layout techniques have been integral to project work to date. Much progress has been made in this area through the extensive testing of the cell and techniques for producing stable (mechanical and electrochemically) anodes have been developed along with some cathode development. Some loss of knowledge occurred with research personnel turn-over and has led to some delay in testing of the full fuel-cell arrangement as well as some lost time in electrode fabrication techniques. Problems with laboratory and equipment availability also had an impact on this milestone.

MILESTONE 16: **Construction of a Pilot-Scale DCFC.**

2013 Progress and Outcomes

(i) Tasks/Strategies:

Q1, 2103

⇒ Initial system designs were considered.

Q2, 2103

⇒ Plans are continuing to be refined to construct a novel pilot-scale DCFC with either a solid or powdered anode construction.

Q3, 2013

⇒ Detailed design of a flexible pilot cell arrangement which will allow several fuel delivery configurations to be tested. Set-up will allow for both full and half-cell testing arrangements.

⇒ Patent review of commercial cell designs and new conceptual arrangement designed based on a slurry type commercial set-up.

Q4, 2013

⇒ Design finalization

⇒ Procurement of major unit required – vertical tube furnace

(ii) Performance Measures:

⇒ Construction of a working, pilot scale DCFC able to be run on coal fuels with air supplied at the cathode.

(iii) Outcomes:

⇒ Development of a design concept for a flexible pilot scale design able to test different fuel delivery methods on a larger scale than previous work.

⇒ Start of commissioning activities including ordering of key components (vertical tube furnace).

2014 Progress and Outcomes

(i) Tasks/Strategies:

Q1, 2014

⇒ Design modification according to supplier specifications

⇒ Practical build and component commissioning development for sourcing of parts and practical assembly/operation of pilot scale cell

⇒ Quotation of pilot cell components

Q2, 2014

⇒ Testing of cathode arrangement using both inner and outer pressure of carbonate to determine cathode attachment strength

⇒ Design of new test apparatus to enable more extensive cathode arrangement testing

⇒ Finalization of cell body design with manufacturer input and quotation on cell

⇒ Resbond sealing ability confirmation at 600°C

Q3, 2014

- ⇒ Use of test plate for molten carbonate leak testing on large commercial (>25 mm D) and small in-house (<20 mm D) cathode discs
- ⇒ Testing of silver contact adherence and function in a pseudo-DCFC arrangement (using test-plate)
- ⇒ Preparation of DCFC Pilot Cell lab space with connected services

Q4, 2014

- ⇒ Pilot cell components ordered including:
  - Cell body (Version 2 - Stainless Steel) – UoN Workshop
  - Thermocouple and reader (Dwyer)
  - Swagelok components including tubing, three-way valves, pressure sensor, gas connections, t-pieces
  - Gas flow meter (Dwyer)
  - High temperature gasket material (alumina felt)
- ⇒ Bulk fabrication of solid electrolyte membranes, required for assembly of pilot scale cell

(ii) Performance Measures:

- ⇒ Construction of a working, pilot scale DCFC able to be run on coal fuels with air supplied at the cathode.

(iii) Outcomes:

- ⇒ Design review and improvement
- ⇒ Commissioning of pilot cell body and components
- ⇒ Initial build of cell and preparation of facilities

2015 Progress and Outcomes

(i) Tasks/Strategies

Q1, 2015

- ⇒ Final assembly of full cell and components

(ii) Comments:

- ⇒ This milestone has experienced some delays, most significantly, the change in design required from an alumina cell to a stainless steel cell. Additionally, further delays were experienced when making changes to the cell design.

MILESTONE 18: **Performance Optimization of a Pilot-Scale DCFC**

2014 Progress and Outcomes

(i) Tasks/Strategies

Q1, 2014

- ⇒ Identification of key pilot design components and design of experiments to enable testing and confirmation of practicality

Q2, 2014

- ⇒ Literature review to determine most suitable membrane electrode assembly for cathode

and solid oxide membrane

⇒ Stability testing of YSZ in molten carbonate under mild treatment conditions

⇒ Development of design concept for anode including proposal for coal pyrolysed under different conditions for formation of a mechanically stable and electrochemically active solid anode

Q3, 2014

⇒ Spreadsheet prepared summarizing all DCFC arrangements trialled in the literature including membrane type and thickness, cathode type, anode type, arrangement, and best performance at various operating temperatures

⇒ Fabrication of YSZ solid electrolytes from YSZ powder including dry pressing and sintering

⇒ Preparation of LSM powder from pre-cursors

⇒ Preparation of LSM/YSZ mixture for cathode contact

⇒ Application and curing of cathode layers on YSZ discs including preparation of ink and spray coating followed by sintering. Testing of various spray coating formulas and adherence after sintering of different concepts (porous YSZ on YSZ, YSZ | LSM/YSZ | LSM, and YSZ | YSZ/LSM

⇒ Preparation and testing of two coal types with pyrolysis (under N_2) at various temperatures followed by electrochemical and physical characterization in order to develop the solid anode formula. Further samples have also been sent away for elemental analysis (CHNOS) to complement physical characterization

Q4, 2014

⇒ CGA/MLA analysis of coal chars to investigate electrochemical activation

⇒ Membrane and cathode fabrication and procedure optimization

⇒ Anode formulation and char acid washing investigation (de-ashing)

⇒ Review paper – DCFC optimization

(ii) Performance Measures

⇒ Successful operation of a functional and high performing DCFC

⇒ Publication of cell sensitivities and findings

(iii) Outcomes

⇒ In-house fabrication of major cell components (solid oxide membrane and cathode catalyst)

⇒ Testing aspects of pilot cell operability, i.e. sealing against carbonate leakage

⇒ Advanced characterisation of coal materials to enable optimised anode formulation

⇒ Submission of review paper regarding DCFC sensitivities and essential components

2015 Progress and Outcomes

(i) Tasks/Strategies

Q1, 2015

⇒ Corrosion investigation of different metals in molten carbonate environments including copper, stainless steel and titanium.

⇒ Ordering and preparation of further steel materials (four different alloys) for corrosion

testing and preparation of further pure metal electrodes for analysis including platinum, silver nickel and gold.

⇒ Preparation of coal for anode formulation testing including de-ashed coal, highly pyrolysed de-ashed coal (900°C) and partically oxidized coal (activated).

⇒ Continued preparation of solid oxide membranes and cathode components

⇒ Testing of thermal and coking coal at the Australian Synchrotron on the NEXAFS beamline

Q2, 2015

⇒ Coal ash distribution investigation using CGA and MLA data collected in late 2014

⇒ Investigation on performance of coal material undergoing various chemical and thermal treatments to optimize anode formation.

⇒ Corrosion investigation of stainless steel materials in molten carbonate

⇒ Pilot cell commissioning activities including preparation of YSZ/LSM membranes, leak testing of cell and gasket cutting and fitting, large area anode construction, corrosion protection of cell.

Q3, 2015

⇒ Construction of anode press and initial preparation of large scale anodes

⇒ Preparation of DCFC pilot in baseline performance arrangement – using graphite anode and YSZ/LSM cathode assembly

Q4, 2015

⇒ Testing of various anode compositions to implement fundamental understanding

⇒ Adjustment to pilot cell design and subsequent recommissioning

⇒ Leak testing

(ii) Performance Measures

⇒ Construction of a working, pilot scale DCFC able to be run on coal fuels with air supplied at the cathode.

(iii) Outcomes

⇒ Test run of pilot cell in baseline mode

⇒ Selected test runs with various anode compositions leading to design improvements in the cell

(iv) Comments

⇒ This milestone experienced some delays as a result of the delays experienced with Milestone 16. Useful results regarding the metal corrosion behaviour were obtained, which will help to improve the design of the cell. This is a challenging milestone but arguably the most important of work carried out as it combines findings from all previous work.

3. TECHNICAL SUMMARY

This section includes a technical description of the activities carried out over the course of this project in terms of milestones and broken up into fundamental and applied activities.

Fundamental Activities

3.1. Milestone 7: Molten Carbonate Impurity Effects on Performance

3.1.1. Milestone Background and Aims

The medium in which carbon oxidation occurs greatly influences the oxidation interface including the shuttle mechanism for moving oxide anions from the cathode to the anode for reaction with carbon. Interactions which occur in the molten medium are of prime importance on both a fundamental and applied scale. Coal as a fuel contains many constituents other than pure carbon in the form of mineral ash. These 'impurities' are not expected to oxidise or react in the DCFC and are therefore able to accumulate in the molten carbonate medium. This is expected to affect both the thermal properties of the system (melting point, heat capacity) and electrochemical reactions (oxide anion diffusion, change in wettability at electrode surface, etc). As such, the intent with this milestone was to investigate some of the effects that impurities in the molten carbonate electrolyte have on the electrochemical performance of the DCFC.

3.1.2. Experimental Methods

Carbonate Preparation

A ternary carbonate mixture, used as the electrolyte in the DCFC, was prepared from reagent grade purity chemicals (>99% purity). Lithium, sodium and potassium carbonates were sourced from Sigma Aldrich and used as received. Carbonates were mixed in the molar proportion of 43.5%, 31.5% and 25.0%, respectively manually using a mortar and pestle. The mixture was dried in a furnace at 110°C for 2 h in an alumina crucible immediately prior to DTA analysis. The final melting point of the eutectic composition we prepared was 397°C (measured from the DTA output), as expected from the literature [1].

Seven impurities common to coals sourced from Australian (NSW) mines (see Section 3.3) were added to the unmodified carbonate mixture at concentrations of 1, 2 and 5 wt% so that, in total, 21 samples were produced for analysis, in addition to the pure carbonate mixture. The impurities consisted of Fe_2O_3, FeS, TiO_2, $CaCO_3$, $CaSO_4$, the semi-metal oxide SiO_2, and the clay species kaolin. The impurities were ground to a fine consistency using a mortar and pestle before being added to the eutectic prior to DTA analysis.

Differential Thermo-gravimetric Analysis (DTA)

All thermal analysis experiments were carried out using a Perkin Elmer Diamond TGA/DTA instrument. The mass of the sample used for the TGA/DTA analysis was within the range 17-22 mg. In order to achieve acceptable thermal conductivity between the sample and the thermocouple aluminium crucibles were used. The TGA/DTA experiment consisted of heating and cooling cycles oscillating around the melting/freezing point of the electrolyte (397°C). In all experiments the thermal behaviour of the sample was monitored relative to a similar mass of α-Al_2O_3, which was used as the reference material.

Prior to each test the sample was placed in TGA/DTA instrument and held for 1 minute at 25°C with a nitrogen flow rate of 20.0 ml/min in order to equilibrate at the initial conditions. The sample was then heated at 15°C/min from 25°C to 150°C, where it was held for 1 min to ensure complete removal of water from the sample. After this equilibration period the sample was heated up to 600°C at 20°C/min, where it was again held for 1 min. The sample was then cooled at 20°C/min back down to 350°C, where it was again held for 1 min. This relatively fast rate melt/freeze cycling was intended to homogenize the sample. Multiple heating/cooling cycles of the sample were then carried out in the temperature range 350-500°C at 5°C/min. This cycling was conducted to further ensure homogenization, as well as ensure reproducibility of the results and steady state response of the carbonate mixture. The temperature program used is shown in Figure 2. DTA response results presented here have been taken from the third melt cycle.

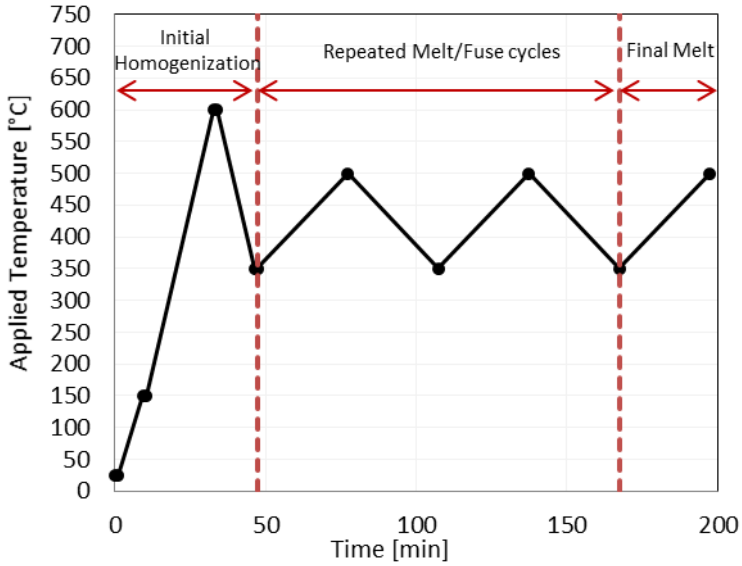

Figure 2: Heating profile used for collection of DTA data. Initial carbonate unfused to begin

3.1.3. Results

The inclusion of impurities into the eutectic is unavoidable in coal fuelled DCFC operation. Therefore, this milestone aims to explore the effects that these impurities exert on the physiochemical properties of the eutectic. It is predicted that the inclusion of impurities will likely alter the onset eutectic melting point; additionally thermal fusion may lead to formation of new crystal phases and chemical rearrangement of the material. This is important for DCFC operation as lower operating temperatures reduce energy expenditure and start-up costs.

This investigation aims to understand the influence of coal impurities on the thermal behaviour and properties of the electrolyte, specifically, the effect that mineral type and quantity have upon the onset temperature and activation energy of the eutectic (ternary composition of lowest melting point) melt/freeze cycle. This has implications for DCFC operation as well as the behaviour of coal fuels electrochemically.

The data obtained during this study has been used to further understand interactions taking place on the boundary between the electrolyte and impurity particles. It can also provide useful information for designing and improving operational conditions in order to maximize the power output and lifetime of molten carbonate fuel cells.

Differential Thermo-Gravimetric Analysis

In these DTA runs, the mass change associated with the melting and freezing cycles was negligible (as expected), and so our main focus is on the differential thermogravimetric analysis (DTA) response signal related to the heat transfer associated with the melting and freezing processes was the main feature of interest. An example of the DTA signal for a melt-freeze cycle is shown in Figure 3, in this case for the pure carbonate mixture.

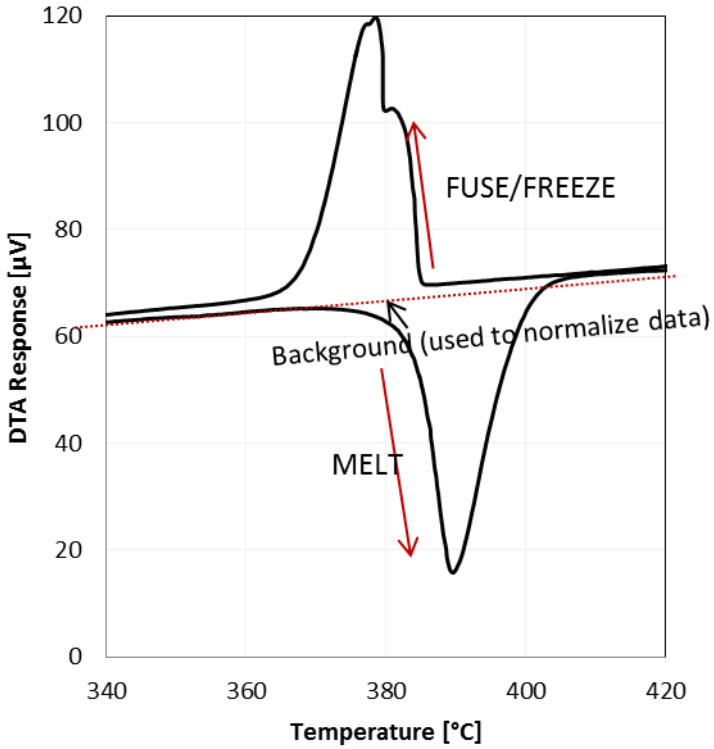

Figure 3: Eutectic carbonate final melt/freeze cycle unmodified DTA response

The data in this figure shows the expected negative (endothermic) peak for melting, and a positive (exothermic) peak for freezing. The peaks are offset by ~20°C, this is most likely due to a lag in nucleation during the freezing half cycle. Both peaks are also superimposed on a sloped linear background which represents changes in the heat capacity of the carbonate mixture and is offset from zero as a result of changes which occur in the initial fuse process.

For further analysis a linear background correction of the DTA data was used to focus specifically on the melting of the carbonate mixture. Additionally, the DTA data was normalized with respect to the initial sample mass (µV/mg) so that direct comparison between different samples and mixtures could be carried out. The background correction was aimed at isolating the single endothermic (melting) peak in the DTA response (seen in Figure 3), although in many experiments containing higher contaminant concentrations, such as kaolin, SiO_2 and TiO_2, a peak splitting phenomena was observed. In these cases the heating domain was limited to where the DTA response returned to baseline levels. Response curves for different contaminant concentrations are shown in Figure 4.

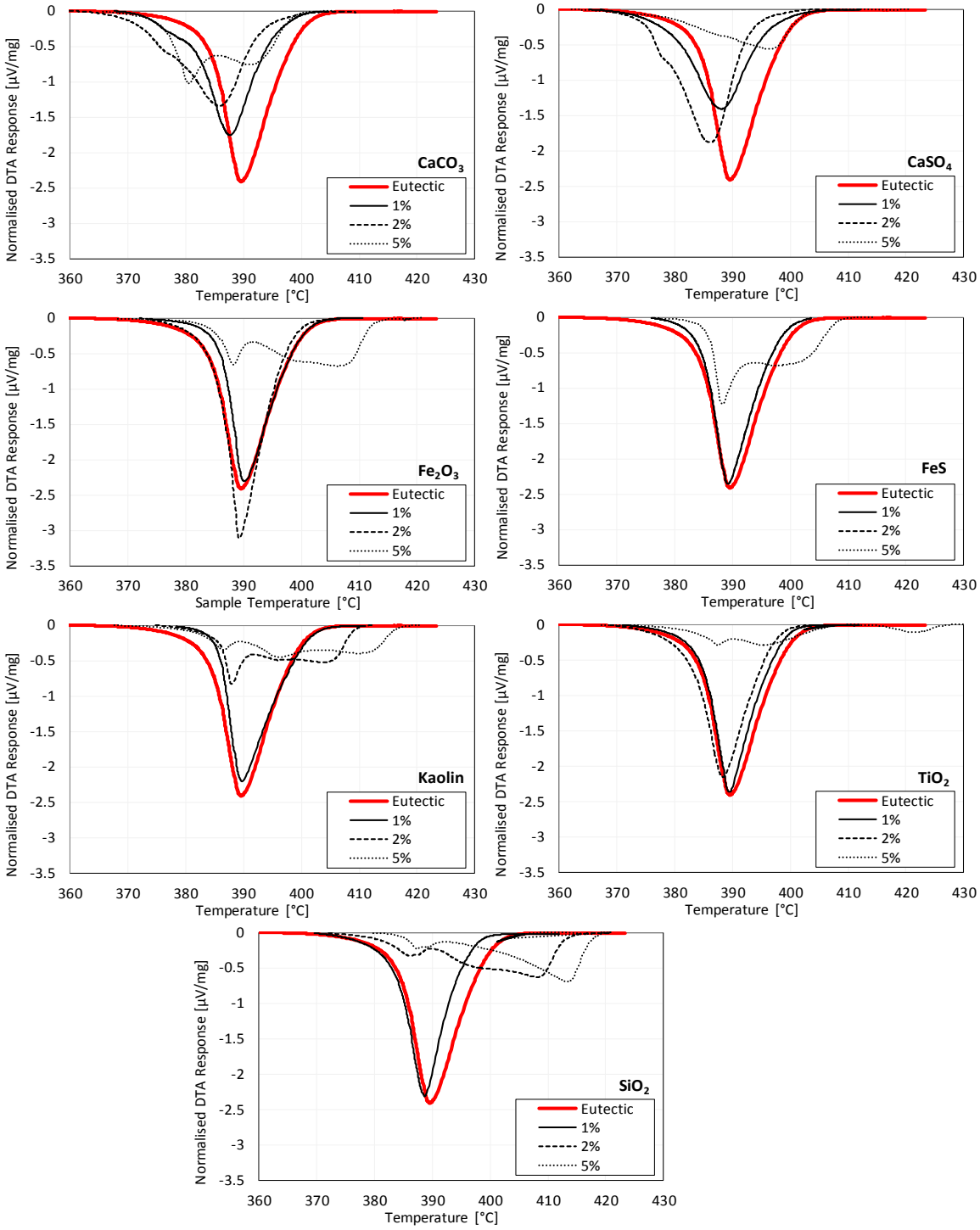

Figure 4: Background corrected and normalized DTA response (µV/mg) for the eutectic mixture of lithium, sodium and potassium carbonate deliberately contaminated with selected impurities at the 1, 2 and 5 wt% level.

The peaks observed in Figure 4 correspond to an endothermic process, predominately the melting of the carbonate eutectic. For the pure eutectic heating gave rise to a single peak, this was expected for a well homogenized system where a thorough mixing between the individual

carbonate salts; i.e. Li_2CO_3, Na_2CO_3 and K_2CO_3 had taken place. Upon the introduction of contaminants the system, behaviour varied considerably. Three distinct variations to the baseline reading were noted. These were (1) peak shifting to either lower or higher temperatures, (2) peak splitting, and (3) a change in area under the curve. The extent of these variations was enhanced by increasing the contaminant concentration and is more prevalent in some cases for specific contaminants.

Peak shifting towards lower temperatures was noted for all dopants, particularly those containing metal cations; i.e. Ca^{2+}, Fe^{2+} and Ti^{4+}. This peak shifting effect becomes more prominent with increasing contaminant concentrations. The shift is towards lower temperatures, meaning that less heat is required to bring about melting. This effect is analogous to freezing point depression, a colligative property of solutions brought about by increasing the solute concentration. In the case of freezing point depression the effect is attributed to an entropy increase in the system, and only takes place if the solvation of the introduced solute takes place. A similar affect being noted in the eutectic system implies a sound solvation of the metal ions in the carbonate melt. For DCFC applications this is favourable as the introduction of metal-oxide species into the melt may facilitate lower operating temperatures, meaning less energy expenditure to initialize the system.

There is also a peak spiting effect observed, which is also correlated with contaminant concentration. Where peak splitting occurs there is a sharp peak representing eutectic melting, but lower in intensity and also, shifted to lower temperatures by ~20°C compared to the control. There is also another broader peak at high temperatures observed, apparently due to the disruption of the crystal structure of the eutectic, resulting in the emergence of multiple crystal phases. This may be brought on by a phase shift in the dopant material, or even a chemical rearrangement borrowing from both the carbonate salts and the dopant. The reason for the emergence of the second peak would therefore vary according to the dopant, leading to the formation of unique phases depending upon the eutectic composition.

An exception to this trend was $CaSO_4$ at 5 wt% where there is only single broad peak shifted to high temperatures; indicating the formation of single phase, which includes the $CaSO_4$, and is different from the unmodified eutectic phase. Kaolin at 5 wt% presents three distinct peaks, this exception indicates the formation of an additional phase. This is not unexpected for kaolin as literature studies have cited kaolin to undergo phase transformations upon thermal treatment in air at atmospheric pressure [2]. Endothermic dehydration occurs between 550–600 °C, producing disordered metakaolin, i.e.

$$2\ Al_2Si_2O_5(OH)_4 \rightarrow 2\ Al_2Si_2O_7 + 2\ H_2O \quad (1)$$

This phase transition likely gives rise to one of the broader peaks noted in the DTA response.

Enthalpy on Melting

The area calculated under the curve [µV.°C/mg] is proportional to the enthalpy of the melting process, which is endothermic. A lower area implies that less heat is required to achieve a melt and is therefore beneficial from an operational point of view. In all cases the introduction of impurities into the melt causes a decrease in the area under the curve, which is reflective of a smaller DTA response, shown in Figure 5.

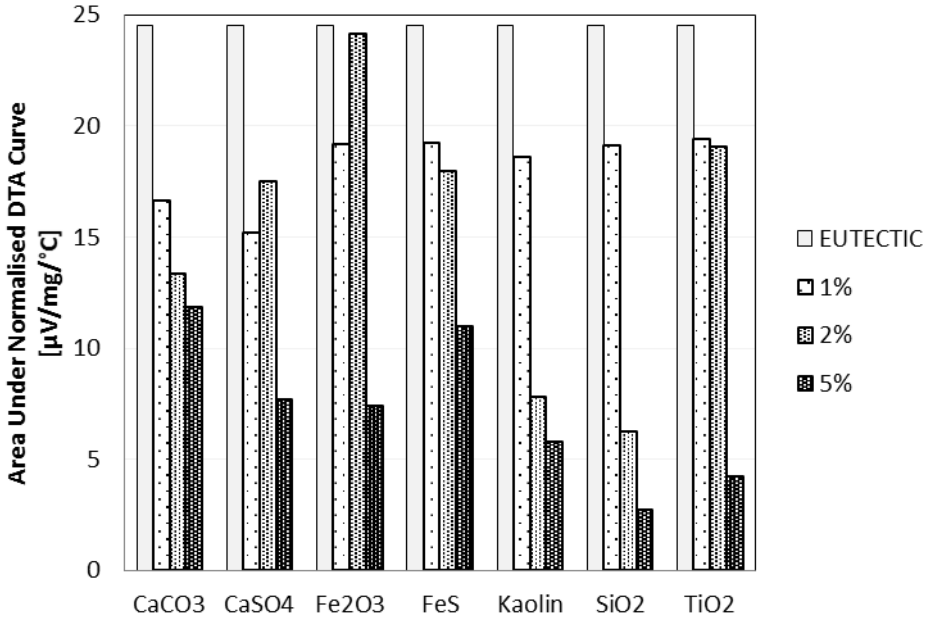

Figure 5: Area under the DTA response curve for contaminant concentrations at 1, 2 and 5%.

For the contaminants present in concentrations of 5 wt% there is a peak splitting effect which has been shown previously in 4. This is also true for many at the 2 wt% level barring those containing Fe and Ti cations. Multiple peaks imply the presence of separate materials with different thermal conductivities. This may be due to poor solvation of the impurities in the eutectic, such that when the eutectic melts the impurities remain solid, with minimal dissolution occurring.

If this were the case then the eutectic melting peak would be reduced in intensity by 5% compared to the control, and the melt temperature would not be shifted to lower values. This is not what is observed in Figure 4 and Figure 5, suggesting that there is disruption of the crystal structure by the dopants.

Greater reductions in the area under the curve have been noted for SiO_2 and Kaolin, a semimetal oxide and clay respectively. The addition of these dopants causes disruption of the alkali metal carbonate eutectic phase, due to the chemical dissimilarity between the materials. In these cases the area under the curve reduction is correlated smoothly with an increase in contaminant concentration.

Peak splitting, and therefore phase disruption is enhanced with increasing dopant concentration (5 wt%). Dopants containing heavy metal cations; i.e. FeS, Fe_2O_3 and TiO_2 included in low concentration impact the eutectic crystal structure minimally. When added in moderation, heavy metal cations blend coherently within the eutectic phase, which is comprised of alkali metal cations. Once the concentration rises to 5 wt%, the emergence of an additional crystal phase is evidenced by an increased intensity of the second peak relative to the eutectic melt peak, and also the reduced enthalpy upon melting, this is particularly so for TiO_2.

Single curve incremental isoconversional analysis

First order kinetic analysis has been applied to the DTA response to determine indicative activation energy for the melt process of the ternary carbonate in the presence of the

contaminants. This analysis was carried out using data from the final melt phase in the cycle using the rate equation:

$$\beta \frac{d\alpha}{dT} = Af(\alpha)exp\left(-\frac{E_A}{RT}\right) \quad \textbf{(2)}$$

Where A is the pre-exponential factor (min^{-1}), β is the heating rate ($°C.min^{-1}$), E_A is the activation energy, ($J\ mol^{-1}$), α is the extent of melting taking on a value from 0-1, and increasing as the experiment tends towards completion. f(α) denotes the model chosen to represent the mechanism of thermal decomposition. In this case we have used f(α) = 1-α for a system displaying first order kinetics.

An incremental integral approach was applied to the background-corrected DTA data. The extent of conversion for each melt was then determined by normalised numerical integration of the background-corrected data, with the normalisation taken for each point relative to the maximum area determined (point of 100% conversion).

To kinetically model this process, the above rate expression must be solved. This was performed using the Runge-Kutta method, an iterative technique for the approximation of ordinary differential equations. The initial condition was taken as:

$$\alpha(T_0) = \alpha_0 = 0 \quad \textbf{(3)}$$

This method begins with an estimated average of the slopes, arbitrary points are denoted (α_n, T_n), with the distances between points (h), the next consecutive point will be (α_{n+1}, T_{n+1}) and so on.

Applying the Runge-Kutta method gives (α_{n+1}, T_{n+1}); i.e.

$$\alpha_{n+1} = \alpha_n + \frac{1}{6}h(k_1 + 2k_2 + 2k_3 + k_4) \quad \textbf{(4)}$$

$$T_{n+1} = T_n + h \quad \textbf{(5)}$$

The interval size h, was arbitrarily set as 1 °C and k values are:

$$k_1 = f(T_n + \alpha_n) \quad \textbf{(6)}$$

$$k_2 = f(T_n + \frac{h}{2}, \alpha_n + \frac{hk_1}{2}) \quad \textbf{(7)}$$

$$k_3 = f(T_n + \frac{h}{2}, \alpha_n + \frac{hk_2}{2}) \quad \textbf{(8)}$$

$$k_4 = f(T_n + h, \alpha_n + hk_3) \quad \textbf{(9)}$$

This model gives rise to a theoretical curve for the extent of conversion against temperature, which was fitted to the experimental curve for a restricted temperature range using least squares regression (hence employing the incremental integral method) and assuming the conversion is initially zero. By varying the initial guess values for E_A and A the best achievable fit was achieved using this approach.

Figure 6 demonstrates that the model soundly fits the measured values of α over the range of temperatures fitted for the eutectic composition.

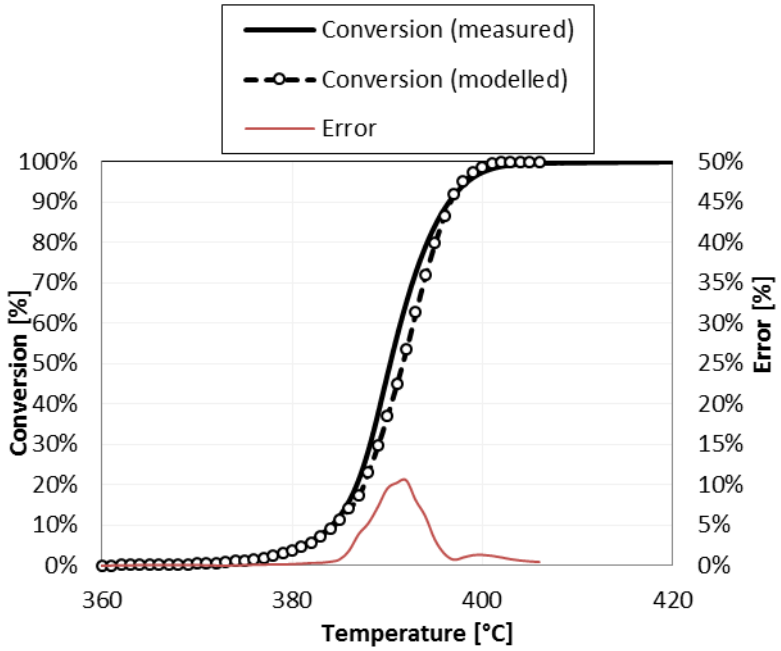

Figure 6: Conversion of carbonate from solid, fused material to liquid phase. Temperature increase 5°C/min

The quality of the fit is reflected by the magnitude of the error/residual; i.e. the difference between measured and modelled values at each data point. The error reaches a maximum value of only 10% in which is thought to be an acceptable margin.

Activation Energy vs. Conversion

The activation energy calculated using the isoconversional analysis outlined above for each contaminant concentration investigated is shown in Figure 7.

In the context of this study reaction rate is essentially the rate of conversion (α/sec) from a solid phase to a melt. An expedient conversion is desired because it allows the DCFC to become operational sooner thereby improving energy output (W.h). It is evident that the addition of certain impurities can considerably lower the E_A of the system which is reflective of the reaction rate.

It was discovered that with increasing contaminant concentration the variability in activation energy over the conversion extent increased. Furthermore the species SiO_2 and TiO_2 recorded considerably lower values at the 5% level.

Increasing contaminant concentration was shown to increase the variability in activation energy over the conversion. The activation energy varied only marginally within a range of ~50 kJ/mol for the 1wt% dopant concentrations. This variation is strongly correlated contaminant concentration as at the 2 wt% level the variation is ~150 kJ/mol, then ~250 kJ/mol at 5 wt%.

Consistently the presence of SiO_2 lowers the E_A value, a result reflected in earlier trends such as peak splitting and enthalpy reduction (4 and 5). Interestingly the presence of TiO_2 also causes a sharp decrease in E_A values, but only upon the addition a higher dopant concentration; i.e. 5 wt%. This was previously observed in the reduced area under the curve. This could in part be attributed to a phase transition from anatase to rutile under the imposed heating conditions. Alternatively, the formation of a titanate or generally a Ti containing anion (possibly $Ti(CO)_7]^{2-}$) species may be occurring; the occurrence of such species during heating could be confirmed

by elevated temp XRD or FTIR studies. Similarly, the transition to a Si containing anion from the dominant phase quartz may be the reason for considerable reduction in E_A, for the SiO_2 doped systems.

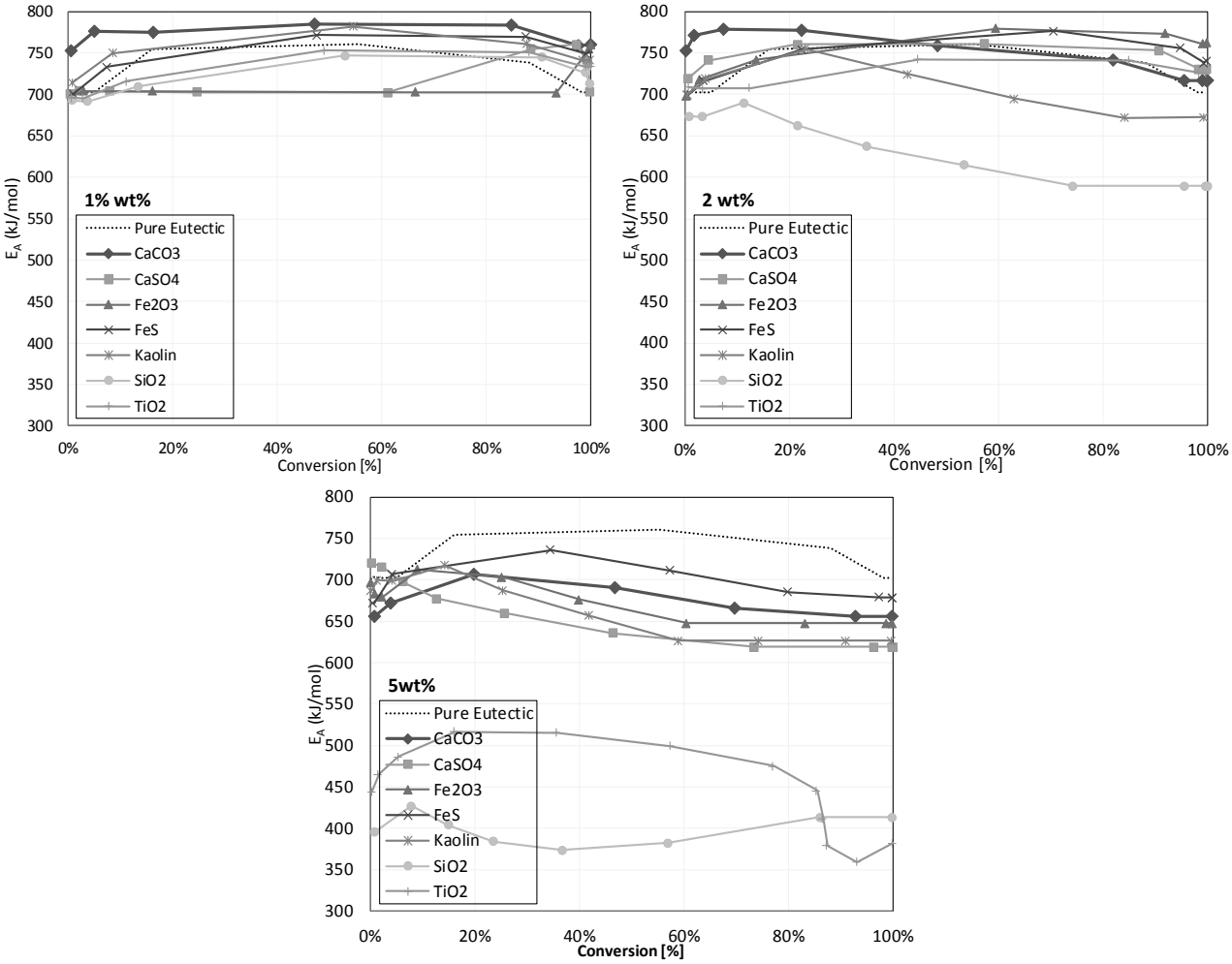

Figure 7: Calculated activation energy based on the isoconversional model for each contaminant and concentration

3.1.3. Conclusions

It is shown here that doping of the molten carbonate eutectic with various impurities often found in coals affects the activation energy and subsequently the kinetics of the melting process favourably for the DCFC. Clear evidence is shown for dissociation and interaction of ash constituents within the molten carbonate which vary with the dopant nature and often concentration. The activation energy of the doped electrolytes observed to decrease most notably with TiO_2 and SiO_2.

3.2. Milestone 8: Effect of Coal/Carbon Type on Performance

3.2.1. Milestone Background and Aims

Coal sourced from various areas will have different ash composition and structure which may affect the activity of the carbon contained in the coal. Screening a variety of coals for activity gives a broad understanding of important variables in coal types to enable possible prediction of DCFC based on coal properties. Further, pre-treatment of coal prior to entry to the DCFC also changes the relative structure of the coal as well as altering the composition (for example, pyrolysis drives off volatiles and increases relative ash content depending on pyrolysis conditions). Pre-treatment methods and conditions may therefore change the reactivity of the coal in the DCFC and therefore the pre-treatment step is of great importance. Therefore, the aim of this milestone was to examine the effect of pyrolysis temperature and coal type on the electrochemical activity of the fuel investigated.

3.2.2. Experimental Methods

Coal Preparation

Particle Size: Two parent coal samples were used, sourced from NSW Australia coal deposits, including a bituminous coal used for thermal applications (noted as CT) and a traditional coking coal (CC). The coal samples were firstly milled and sieved repeatedly to obtain a particle size of <45 μm. A stainless steel bowl and balls were used for milling in a Fritsch planetary monomill (Idar-Oberstein, Germany), while a shaker sieve platform was used for particle size separation. Larger fractions were milled until the required size was obtained for a full sample set. The temperature was kept below 100°C during milling to avoid thermal degradation during this procedure.

Pyrolytic Pre-Treatment of Coal: Samples of the milled coal were weighed into alumina crucibles and inserted into a tube furnace under constant nitrogen flow. The program used included heating initially to 110°C (to ensure sample is fully dried prior to pyrolysis) at a ramp rate of 10°C/min, followed by a wait of 1 h at this temperature. Following drying, the sample was heated to the highest heating temperature (HHT) of interest at a heating rate of 6°C/min, where it was held for 4 hours. The furnace was then turned off and allowed to cool to room temperature naturally under a nitrogen flow. Samples were not removed from the inert atmosphere until temperatures reached below 100°C. Once removed, samples were gently crushed to loosen prior to electrode preparation. Sample naming in this work consists of the parent coal identifier (CT or CC for thermal and coking coal, respectively) and the HHT of the char (500-900ºC).

Pyrolysis experiments involved the use of a specially designed, sealed reaction vessel where coal samples are placed under controllable nitrogen flow to prevent oxygen entering and partially oxidising coal during the pyrolysis process. The set-up for this process is shown in Figure 8 which also indicates safety measures used (propan-2-ol impinger bottles located in the laboratory fume hood) to ensure coal pyrolysis tars and combustible gases evolved during pyrolysis are not released to the laboratory atmosphere.

The coal processed is weighed both before and after pyrolysis to determine the final pyrolysis yield (on a dry basis). The heating rate and highest heating temperature (HHT) used during pyrolysis is kept consistent for each coal investigated with a heating rate of 5°C/min used and HHT of 700°C applied.

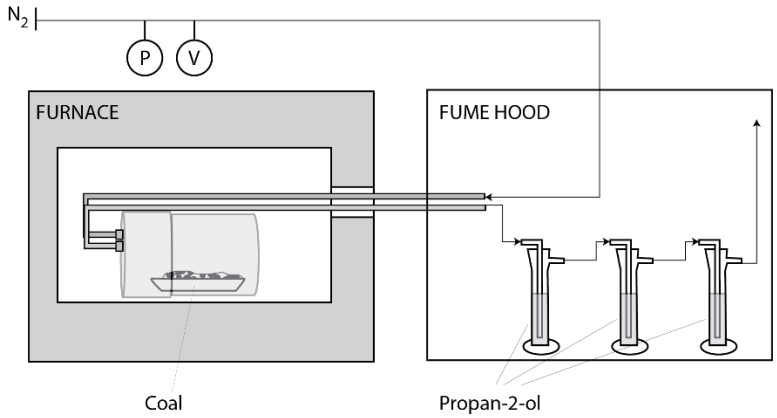

Figure 8: Coal Pyrolysis Arrangement. P and V indicate pressure and volumetric flow rate measurement points

Coal Characterisation

Thermogravimetric Analysis: A Perkin-Elmer (Massachusetts, USA) diamond TGA/DTA apparatus was used for sample analysis. In each case, a sample of ~ 20 mg was used, and samples were analysed in an alumina crucible set with α-Al_2O_3 used as a reference material. Samples were tested under both air flow (industrial grade, CoreGas) and under carbon dioxide flow (Food Grade, CoreGas) at 20 mL/min. In both cases, a heating rate of 15°C/min was used, and changes in mass measured as a function of temperature.

Elemental Analysis: Elemental analysis was carried out using an elemental analyzer (PerkinElmer PE2400 CHNS/O) using PE Datamanager 2400 and a PerkinElmer AD-6 ultra-micro balance. The instrument was run in CHNS and ash mode in duplicate with a sample size of 1-2 mg. Determination of the oxygen content was performed by difference in sample weight with other measured variables.

Resistivity Measurements: The resistivity of graphite and coal chars was measured using a purpose built cell with a Keithley Multimeter (sensitive to 0.0001 Ω). Pellets of pure coal char were made in-situ from ~1 g of material in the resistance measurement cell. The cell consisted of two conducting plates lined with an insulating ceramic material which could be held together at constant pressure. The cell was pressurized to 140 MPa initially, to ensure consistent contact with the coal char, before the cell was secured at this pressure and removed from press for a period of 10 minutes. Resistance was then measured in ohms. The compressed length was also recorded at this point using calipers in order to calculate the electronic resistivity according to:

$$R_{TOT} = R_0 + \rho \frac{l}{A} \quad \textbf{(10)}$$

where R_{TOT} is the total measured resistance (Ω), R_0 is the resistance measured with no coal char present (Ω), ρ is the electrical resisitivity (Ω.m), l is the pellet length (m), and A is the cross sectional area (m^2). R_0 was measured between each conductivity measurement to ensure there was no drift and was also measured after pressurizing the cell to 140 MPa.

Gas Adsorption: Approximately 0.2 g of each coal char was degassed under vacuum for a minimum of 8 hours at 300°C. The sample was then returned to room temperature and weighed in order to ensure adsorption measurements for the dry weight of the char added. The sample was then analysed using a Micrometrics ASAP 2020 Surface Area Analyser. Adsorption

isotherm data was collected using carbon dioxide as the adsorbate submersed in an ice-water bath (0°C).

Electrochemistry

Electrochemical Cup Cells: A cyclic voltammetry experiment is carried out on a small amount of the coal material, which is formed into a so called 'black-mix' prior to oxidation. The electrochemical apparatus and general set-up of the Electrochemical Cup Cell experiment is shown in Figure 9.

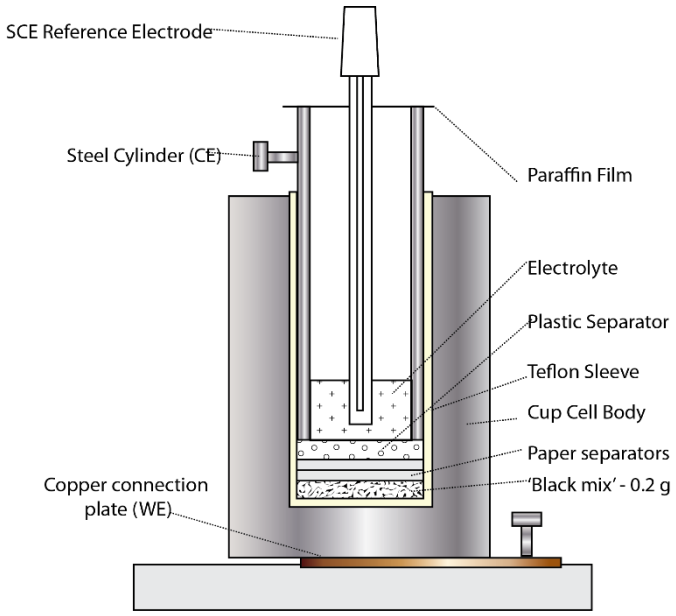

Figure 9: Electrochemical cup cell general arrangement

The electrochemical activity of the black mix is reflected in the experimental current response carried out on the cell which occurs over a period of several days (a very slow scan rate of 0.002 mV/s is used for this experimental set-up).

Electrode Preparation: Coal pellets for electrochemical assessment were formed using a mixture of graphite (SFG44 Timrex, Timcal Switzerland) and pyrolysed coal, using 25 wt% (dry basis) coal char for all pyrolysis temperature investigations. 0.8 g of the carbon mix in all cases was pressed into a pellet using an International Crystal Laboratories (Garfield, USA) 13 mm pellet die press under a pressure of 740 MPa. Once pressed, pellets were sintered at 500°C for 4 h under nitrogen flow. Pellets were then inserted into alumina electrode holders using the ceramic adhesive Resbond 989 (Ceramic Oxide Fabricators, VIC, Australia) and a paste of 1:1 Resbond 989 to graphite (weight percent) was compressed onto the back of the pellet over an electrical contact to ensure good connection.

The electrochemical cell used for these experiments is described in detail in Section 3.6. A general arrangement diagram of the anode is shown in Figure 10. The surface of the working electrode was polished flat on 1000 grit carbide abrasive paper and well rinsed with Milli-Q water to remove any surface contaminant. This procedure produced a working electrode with a cross sectional geometric area of 1.766 cm^2 (allowing for surface roughness), which has been used to normalise currents recorded in electrochemical testing (along with normalisation used for active carbon surface area as discussed in Section 3.1).

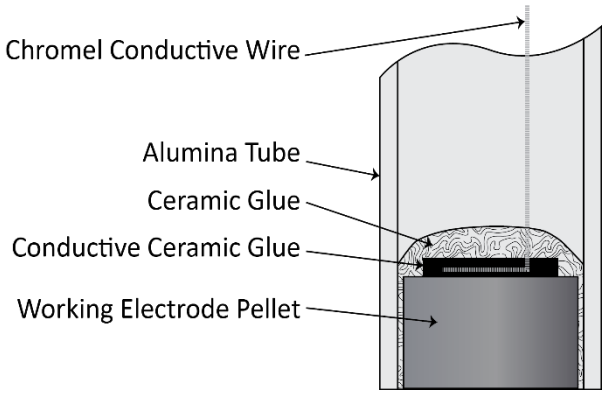

Figure 10: General arrangement of anode

Anodic Half-Cell Arrangement: The electrochemical half-cell used consisted of the working electrode as described above with counter and reference electrodes made from graphite rods. The rods were used several times and sanded back between experiments to refresh the surface, as well as renewing electrical connections which were inserted into a small hole drilled in the graphite rod. The electrodes were submersed in a pre-fused ternary carbonate eutectic once molten in an alumina bath with a weighted lid.

The eutectic was prepared from a mixture of lithium carbonate (Li_2CO_3, >99%), sodium carbonate (Na_2CO_3, >99%) and potassium carbonate (K_2CO_3, >99%, all Sigma-Aldrich) in the mole ratio 43.5:31.5:25 (eutectic composition [20]). The carbonates were firstly dried in air at 110°C for several days to remove moisture before being weighed separately and combined using a mortar and pestle. The eutectic was finally ball milled to ensure proper mixing (apparatus as described in Section 3.2.2). The eutectic was then fused at a temperature of 500°C in an alumina crucible before cooling.

Carbon dioxide (CO_2, Coregas, food-grade) was allowed to flow over the surface of the carbonate during electrochemical testing to maintain a carbon dioxide atmosphere (50 normal L/min flow rate, nitrogen basis) to ensure a stable reference electrode. Detailed cell and electrode drawings are provided in an earlier publication [19].

Electrochemical Test Procedure: In order to ensure consistent analysis, the same electrochemical method was used for assessment of all electrodes. Electrodes were at first partially inserted in the electrochemical half-cell to sit above the fused solid eutectic at room temperature. Carbon dioxide flow was started and the cell was heated at 6°C/min to the electrochemical assessment temperature of 600°C. The electrodes were immersed in the carbonate melt at 500°C prior to continuing to 600°C where the anode was held for 1 hour at open circuit potential (OCP) prior to testing to ensure good wetting of the carbon surface [21] and stable conditions within the cell (i.e., no temperature fluctuations from opening and closing the furnace door or movement of molten eutectic from insertion). Electrochemical testing was then carried out including sweeping of the electrode potential from the measured OCP to an overpotential of 0.5 V. Sweep rates of 1 and 5 mV/s were investigated.

For this work, the electrochemical apparatus used was a Pine Research Instrumentation (Durham, USA) WaveNow portable potentiostat, with AfterMath electrochemical software used for data collection. Current measured has been normalized for the geometric surface area of the pellet of 1.327 cm^2 (13 mm diameter) in all cases.

3.2.3. Results

Pyrolysis of Coals

Twelve (12) coal samples have been sourced for analysis over the course of this project; these are shown in Table 2.

Table 2: Coal Samples sourced for analysis in DCFC

Coal Name (Reference)	Coal Type	Date Sourced
Ashton (AS)	Bituminous	2010
Bulga (BG)	Bituminous	2010
HVO (HVO)	Bituminous	2010
Wombo (WB)	Bituminous	2010
Pittsburgh (PB)	Bituminous	2010
Airley Colliery (AR)	Bituminous	2012
Haystack Mountain (HS)	Bituminous	2012
Ivanhoe (IV)	Bituminous	2012
C083 (C83)	Coking Coal	2013
C084 (C84)	Coking Coal	2013
C085 (C85)	Coking Coal	2013
C086 (C86)	Coking Coal	2013

Materials designated with a 'C' are coking coals and are therefore expected to exhibit different behaviour to bituminous coals previously examined for the project. Procedures for milling and sieving the coal indeed were significantly slowed due to the more graphitic nature of the coal meaning milling did not result in loose particles following normal milling procedures but formed an agglomerated sample which required further treatment prior to size separation. It should also be noted that Coals 1-5 were used in early work on this project and procedures for preparation and use of coal (i.e. pyrolysis conditions etc) have been adjusted since this time. Samples of this coal are no longer available and therefore only coals 6-12 will be examined in more detail.

Pyrolysis of coal is a key preparation stage for the DCFC. Coal is composed of many different materials and can be classified in several ways. One of these is to separate the 'volatile', highly functionalised, component from the inorganic ash and the fixed carbon contained in the coal materials. Volatile, ash and fixed carbon components of coals 1-5 are shown in Figure 11.

Pyrolysis drives the majority of volatile species from the coal, along with some small amount of fixed carbon, leaving behind a residue consisting of mainly the fixed carbon and ash. The extent of pyrolysis, i.e. the HHT, can alter the extent to which volatiles are driven off (pyrolysis yield) as can the heating rate during pyrolysis. The pyrolysis yield can generally be related to coal properties with coals of higher volatile compositions giving a smaller solid yield following pyrolysis. In 2013, pyrolysis pre-treatment processes of the coal were examined and it was determined to be a possible variable in the behaviour of coal materials in the DCFC. Consistent preparation was therefore crucial. 700°C was chosen as the HHT to be applied in order to ensure the stability of the coal during oxidation in the DCFC. The effect of different HHT during pyrolysis on the coal is also of interest as, from an engineering and process point of view, a reduced HHT in the pyrolysis stage will mean a more efficient process depending on the nature of the volatile materials formed at that temperature (a process involving re-use of volatile,

combustible materials formed during pyrolysis to allow a self-sustaining pre-DCFC step is envisaged for the overall coal→electricity process). The overall process mass flow is shown generally in Figure 12 to demonstrate the flow of inputs and outputs in a DCFC plant (does not take into account molten carbonate cycling or use).

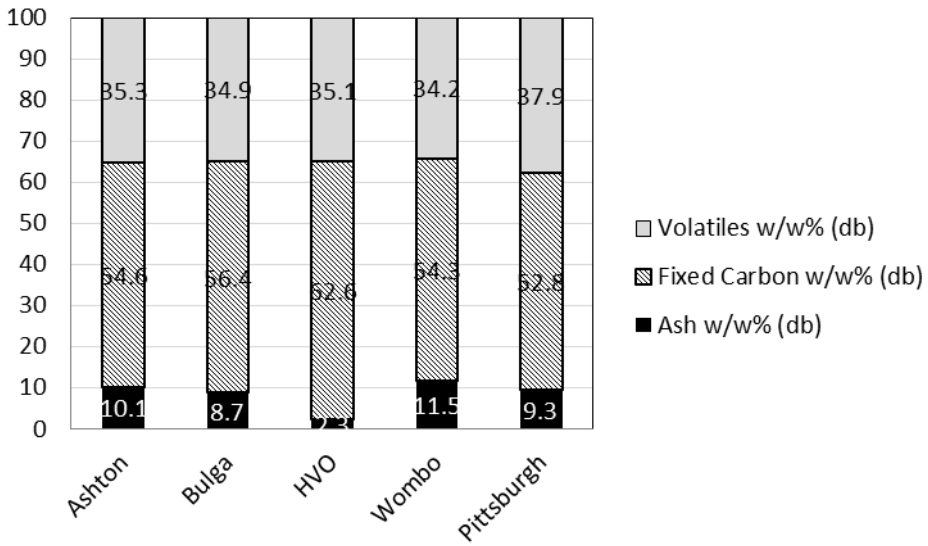

Figure 11: Proximate Analysis (Volatiles, Ash and Fixed Carbon) of initial coals sourced

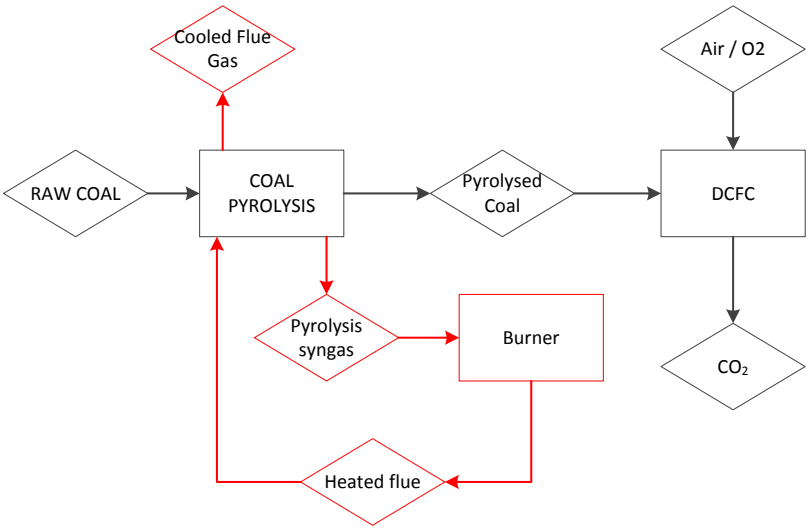

Figure 12: General Process Mass Flow Arrangement Envisaged

The extent of volatile evolution will determine whether the pyrolysis of coal will be a self-sustaining process or if supplementary heating is required in the pyrolysis step. The volatile composition therefore to a large extent control the final efficiency of the overall process since, although the DCFC can operate with extremely high efficiency, this applies only to material remaining after pyrolysis which is fed to the DCFC and some loss in the calorific value of the coal will occur during pyrolysis.

The pyrolysis conditions and subsequent yield are therefore highly relevant to the overall efficiency of the DCFC process. Further, the pyrolysis of the coal changes its structure in terms

of the carbon functionalization and surface properties. This may impact on the electrochemical performance of the DCFC. Optimisation of pyrolysis conditions as well as careful selection of starting materials is likely to be an important part of designing a high powered DCFC system. The measured pyrolysis yield of coals pyrolysed to date is shown in Figure 13.

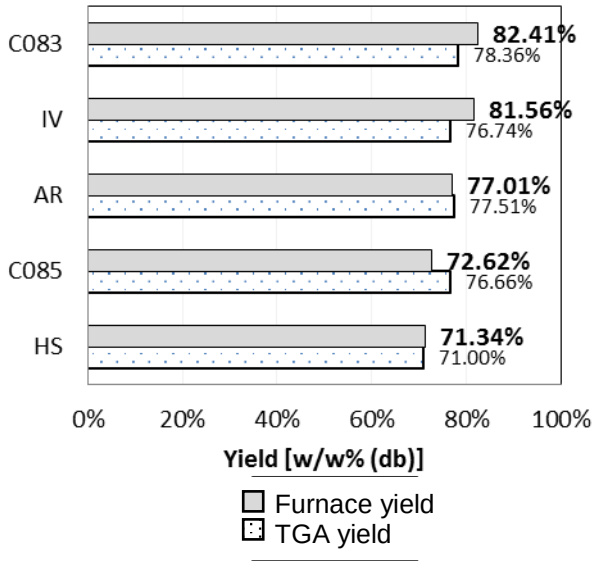

Figure 13: Pyrolysis yields of coal materials pyrolysed at 700°C using both TGA and muffle furnace methods

The pyrolysis program was run under nitrogen atmosphere at a heating rate of 6°C/min and held at 700°C for 4 hours. Results observed using bulk pyrolysis of coal using the arrangement in can then be compared to outcomes smaller coal samples run in the TGA. TGA is a useful method for characterizing and comparing thermal behaviour of different coal materials. It can be seen that the TGA analysis of coal samples prepared for use in the DCFC matches very closely with the measured pyrolysis yield. Typical pyrolysis behaviour of two example coals is shown in Figure 14. It can be seen that the majority of the mass change occurs during the heating ramp starting around 300°C where decomposition process begins and mass change levels out around 600°C. Only small mass loss occurs during the temperature hold period.

Coal Characterisation

Coal Char Composition: The coal samples used are NSW Australia bituminous thermal (CT) and coking (CC) coals. Elemental analysis is shown in along with the atomic H/C and O/C ratios measured from coal char samples.

Raw CT can be seen in Table 3 to have a substantial ash content (>20 wt% dry basis) while raw CC has a smaller ash content (<10 wt% dry basis). The ash is not removed from the solid product during pyrolysis and therefore the composition of ash will increase as the pyrolysis yield decreases. The carbon content of the char for both CC and CT chars is also seen to increase systematically with pyrolysis HHT.

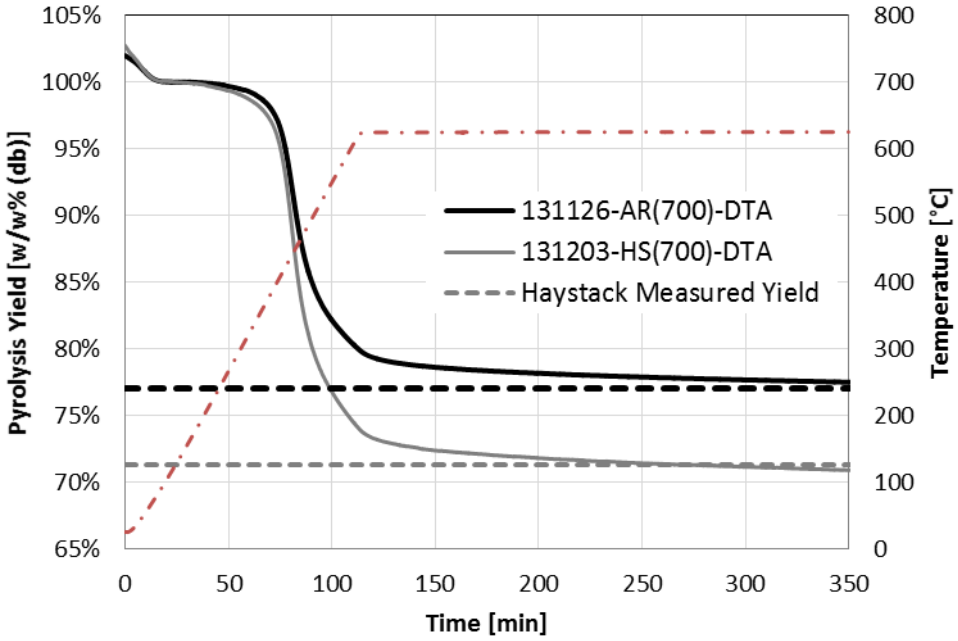

Figure 14: Pyrolysis mass change behaviour (LH axis) of HS and AR coal samples under applied temperature program (RH axis)

Table 3: Elemental analysis of coal and coal chars investigated (wt% dry basis)

	C	H	N	S	O	Ash	O/C	H/C
CT-RAW	62.58%	3.61%	1.53%	0.36%	9.51%	22.43%	0.152	0.686
CT-500	62.87%	2.30%	1.58%	0.29%	6.50%	26.47%	0.103	0.435
CT-600	64.22%	1.66%	1.55%	0.31%	4.33%	27.95%	0.067	0.307
CT-700	64.67%	1.03%	1.39%	0.21%	4.16%	28.55%	0.064	0.190
CT-800	65.50%	0.54%	1.29%	0.24%	3.41%	29.03%	0.052	0.098
CT-900	65.69%	1.18%	1.22%	0.09%	3.63%	28.20%	0.055	0.214
CC-RAW	78.73%	4.35%	1.60%	0.40%	5.48%	9.45%	0.070	0.658
CC-500	79.15%	3.16%	1.94%	0.29%	5.46%	10.01%	0.069	0.476
CC-600	79.45%	2.07%	1.77%	0.17%	5.54%	11.00%	0.070	0.310
CC-700	79.80%	2.40%	1.76%	0.22%	4.78%	11.05%	0.060	0.358
CC-800	82.25%	1.27%	1.74%	0.20%	3.13%	11.42%	0.038	0.183
CC-900	83.17%	1.43%	1.22%	0.09%	2.55%	11.56%	0.031	0.204

Increased pyrolysis temperature also results in a reduction in the oxygen and hydrogen containing groups present in the char. This is expected since more volatile material will be driven off with increasing temperatures during conversion to syngas and coal tars. These products contain large amounts of hydrogen and oxygen derived from the original parent coal [7] and their production will reduce the remaining functional groups. As functional groups are driven off, the coal char becomes more carbonized as indicated by comparison of H/C and O/C ratios for each char. Since aromaticity increases linearly as H/C ratio decreases [22], an increase in aromatic carbon groups and therefore partial graphitization of the carbon remaining is expected at higher pyrolysis temperatures [8].

Sulfur content is seen to change only slightly as the HHT increases for both parent coal types investigated and in both cases the sulfur content is almost identical. The sulfur is seen to

change dramatically above a temperature of 900°C where it is presumably evolved during pyrolysis.

The measured pyrolysis yields for the bulk samples produced for testing in the DCFC half-cell are compared in Figure 15.

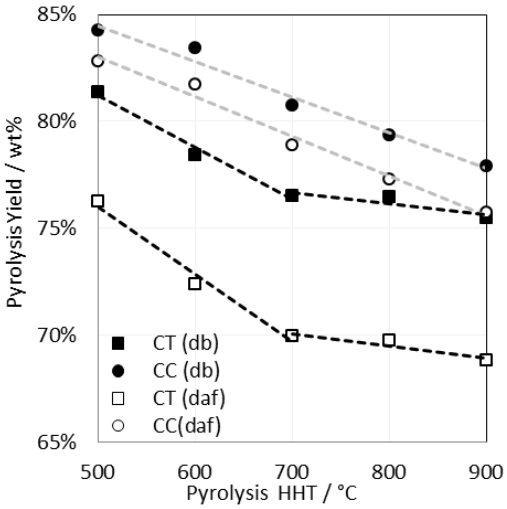

Figure 15: Pyrolysis yield as a function of HHT for CT and CC coal types on both dry basis (db) and dry ash free basis (daf)

Both the dry basis (db) and the dry ash free (daf) yields are shown in Figure 15 for each coal investigated. The pyrolysis char yield is seen in Figure 15to decrease as a function of HHT with an almost linear relationship observed for both coal types investigated. CT, however, demonstrates a plateau above 700°C while CC shows a consistent linear decrease with HHT, although the overall yield for each parent coal (db) is within 5wt% of each other. The yield of CT calculated on an ash free basis (daf) however is much lower than CC. In the case of CT-900 less than 70% of the organic matter present in the coal remains, while in CC almost 90% is retained. This difference is likely a result of the coking coal being of higher rank than the thermal coal, with high starting carbon content (see Table 3), this carbon content exacerbated as pyrolysis temperature increases.

Gasification Response: Each coal char generated has been investigated using thermogravimetric analysis in air and carbon dioxide to assess and compare activity towards chemical oxidation. Simplified reactions are shown in Eqs (11) and (12) respectively along with gasification agent:

$C_{(s)} + O_{2(g)} \rightarrow CO_{2(g)}$ AIR **(11)**

$C_{(s)} + CO_{2(g)} \rightarrow 2CO_{(g)}$ CARBON DIOXIDE **(12)**

The mass loss profiles of each char generated on an ash-free basis is shown as a function of temperature using both air and carbon dioxide in Figure 16 where a heating rate of 15°C/min was used.

Yield has been calculated in Figure 16 assuming 0% conversion at 110°C (i.e., starting point with dry coal). Clearly, oxidation in air results in a much larger loss of organic material compared to carbon dioxide. In the majority of chars examined, final yields in air of close to 0% organic matter at 900°C (i.e. only inorganic ash remains) while more than 80% of the starting material remains under CO_2 up to a higher temperature of 950°C. This result is not unexpected

as the relatively sluggish kinetics of coal gasification by CO_2 compared to combustion in air has been known for some time [23].

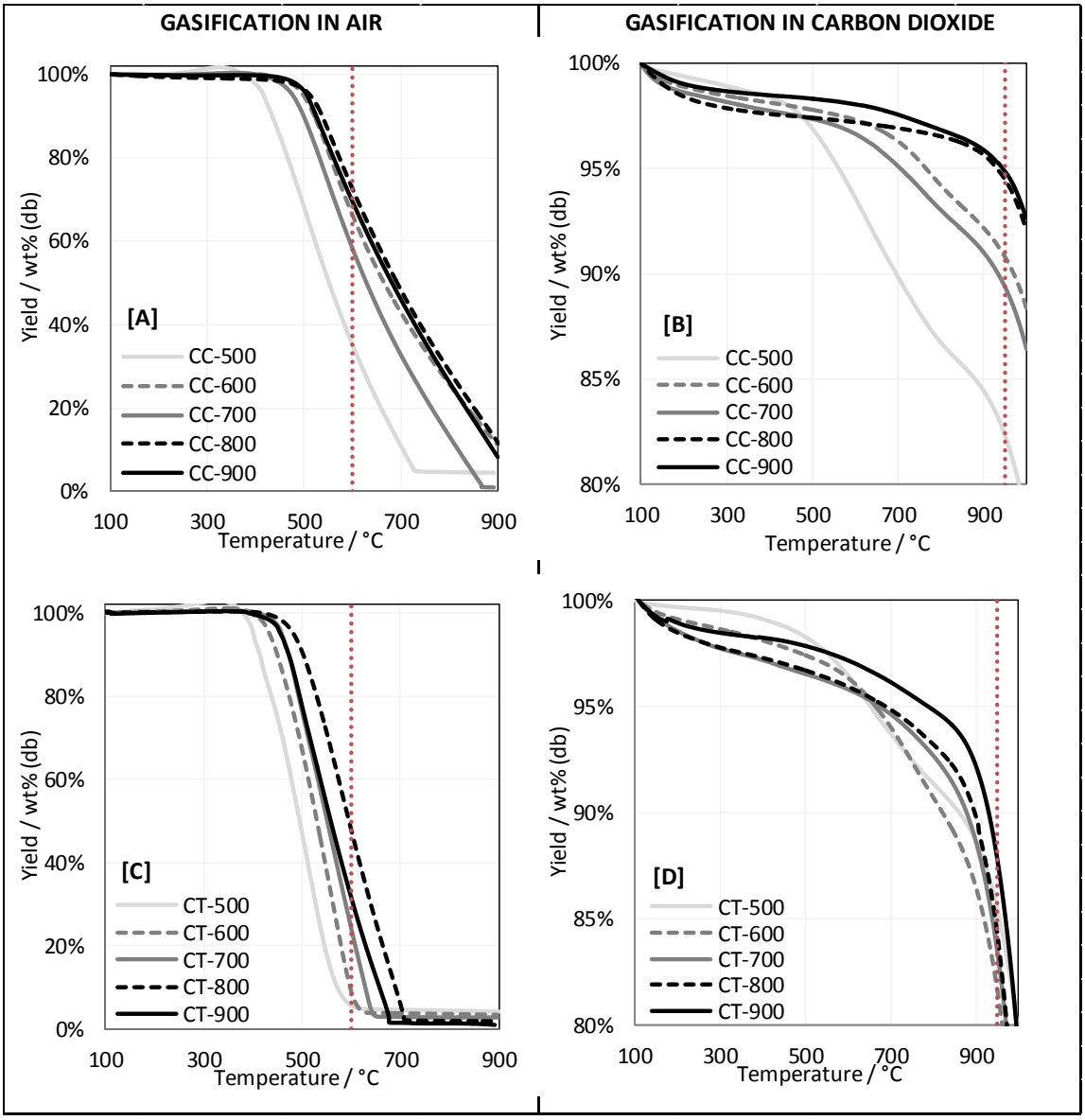

Figure 16: Dry ash free yield of coal chars (CC-[A] and [B], CT- [C] and [D]) during gasification by air ([A] and [C]) and carbon dioxide ([B] and [D]) at a heating rate of 15°C/min. Note y-axis limits are different for CO_2 and air experiments.

Difference between coal chars based on both parent coal and pyrolysis temperature can be observed in Figure 16 [A] and [C] under air. CT shows the majority of mass loss under air in the region 500-600°C with near complete conversion of organic material achieved by 700°C for all coal chars. CC however shows a slower oxidation process for all coal chars tested, excepting CC-500, with complete conversion not reached in the majority of cases in the temperature range shown. Differences in mass loss profiles are also observed between CC and CT examined under carbon dioxide. CC coal chars display two clear reaction regions starting at approximately 500°C and 700°C, the extent of conversion within each region varies with coal char HHT. CT chars

however generally show a single large mass loss beyond approximately 700°C which is not seen in the case of CC. The exception to these observations is the CT-500 which appears to be very similar in shape to CC-500. This material was the only coking coal char to approach similar mass loss to the thermal coals tested.

In order to assess performance quantitatively, the yield obtained in air and carbon dioxide has been assessed at 600°C and 950°C respectively (indicated in Figure 16) for comparison. At these temperatures, the coal chars are still undergoing gasification and have not stabilized. These values are plotted as a function of HHT of the original coal char in Figure 17.

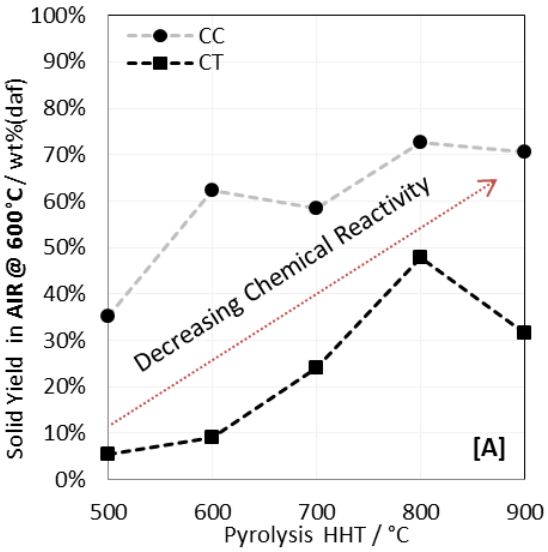

Figure 17: Solid yield of dry ash free coal char remaining for CC and CT in [A] air at 600°C and [B] carbon dioxide at 950°C. Note y-axis limits are different for CO_2 and air experiments

Both sets of coal chars investigated show a general trend of increasing yield with increase in pyrolysis temperature in both air and carbon dioxide. Activity towards chemical oxidation of coal and carbon materials in air is known to involve surface functional groups, with more highly functionalized materials showing comparatively faster kinetics [13, 24]. This does not however encompass all influences on chemical oxidation of carbon materials. As mentioned in Section 3.2.1, the increased ash material present in the thermal coal investigated might be expected to lead to a lower yield and better oxidation kinetics for thermal coal chars as observed due to the catalytic role of ash materials in chemical oxidation [25].

Coals chars reacted in carbon dioxide show large yields with relatively little variation, suggesting only small reactivity towards Bouduard gasification (chemical formation of carbon monoxide through reaction of carbon and carbon dioxide) which does not vary significantly with changes in pyrolysis temperature for the regime investigated here (<1000°C). CC chars investigated are seen to show a similar pattern towards activation under carbon dioxide as under air. CT chars tested however did not follow the same pattern, with a decrease in yield (increased activity) observed between 500-600°C and no observed increase in activity for CT-900.

Coal char gasification by carbon dioxide is not a new area of study [26], and it has been shown that coal type, based on rank generally (carbon content), has a significant effect on reaction kinetics with low rank coals performing better than high rank as a result of the presence of more oxygen-containing functional groups and inorganic ash components [26]. The inorganic

matter components contained in coal can act as catalysts for the gasification reaction [27], with the ash type and composition, as well as pyrolysis conditions all contributing to the final gasification behavior [26].

Overall, CT coal is seen to be more active towards chemical oxidation by both air and carbon dioxide for all pyrolysis conditions assessed here and both coals show a general trend of decreasing activity towards oxidation with increasing pyrolysis temperature.

BET Surface Area: The BET surface area of each char investigated was determined from a carbon dioxide adsorption isotherm. The measured BET surface area for each coal char produced is shown in Table 4 along with calculated total pore volume and average pore size (weighted based on volume adsorbed for specific pore size), calculated using the Frenkel-Halsey-Hill method.

Table 4: Surface area, pore volume and pore size

Pyrolysis HHT	BET SA / $m^2\ g^{-1}$		V_0 / $cm^3\ g^{-1}$		D_{AV} (Å)	
Parent Coal	*CC*	*CT*	*CC*	*CT*	*CC*	*CT*
500°C	57.8	59.2	229	143	1.809 ± 0.774	2.047 ± 0.861
600°C	98.9	89.3	308	188	2.832 ± 1.732	2.113 ± 0.931
700°C	69.7	96.1	273	188	2.139 ± 0.966	2.539 ± 1.035
800°C	66.3	98.1	181	182	1.380 ± 0.582	2.431 ± 1.118
900°C	36.7	74.2	70	140	2.358 ± 1.174	2.444 ± 1.260

CC – Coking Coal, CT – Thermal Coal

The BET surface area, micropore volume and average pore diameter measured for coal chars produced at low pyrolysis temperatures (< 700°C) exhibit little variation between each parent coal type. Increasing the pyrolysis temperature for both CT and CC chars from 500 to 600°C causes a distinct increase in BET surface area. CT chars are further shown to display an increase in BET surface area to a pyrolysis HHT of 800°C. Heat treatment of bituminous coal has previously been shown to increase BET surface area with pyrolysis HHT in the range investigated here [28]. Conversely, CC shows a sudden decrease in BET SA between 600 and 700°C which is not recovered at higher pyrolysis treatment temperatures. CC also shows a smaller micropore volume than CT beyond 600°C. It is likely that the coking nature of this coal contributes to this observation. Plasticization of the coking coal and subsequent formation of a molten component during pyrolysis is therefore assumed for CC to take place between 600 and 700°C under nitrogen based on the observed destruction of pores formed at lower temperatures. Surface area has been shown to influence the chemical oxidation activity of carbon materials [23] and indeed some correlation between the BET surface area and activity towards chemical oxidation activity can be observed, especially in the case of CT. Overall however the BET SA does not vary significantly with pyrolysis HHT or parent coal type (i.e. all chars have the same order of magnitude surface area).

Electrical Resistivity

The measured electrical resistivity of each coal char investigated is shown in Figure 18. An 8-order of magnitude variance in resistivity from coal char formed at 500°C to that at 900°C can be seen for both parent coals investigated. These results concur with a 5-order of magnitude drop in electrical resistance observed between 600 and 900°C HHT for biomass chars [29], where

a similar experimental set-up was used. A higher pressure was applied in the chars investigated here; however the results of Mochidzuki et al. suggest little variation to measured resistance using this method beyond a pressure of 7 MPa [29].

In general the resistivity of the coal char pyrolysed at temperatures higher than 700°C show much smaller variation than those pyrolysed at lower temperatures (Figure 18). This is especially true in the case of CC chars pyrolysed at HHT 800 and 900°C where the electrical resistance approaches that expected for pure graphite.

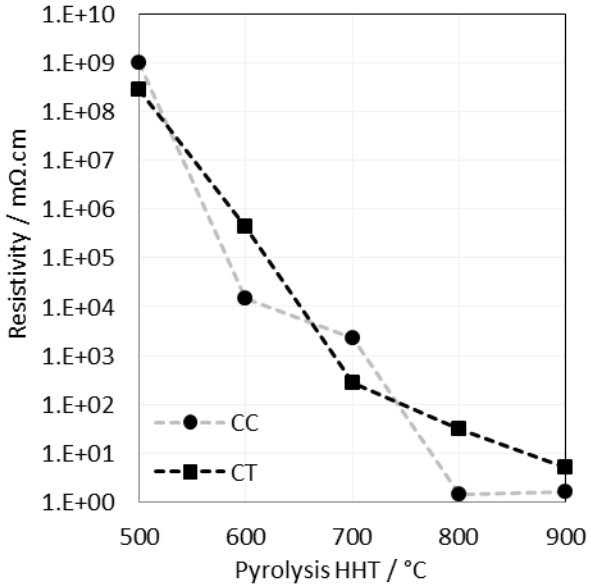

Figure 18: Electrical resistivity of coal chars under 140 MPa at room temperature.

Summary of Physical Properties

CT and CC coal chars studied here show similar general trends with increasing pyrolysis HHT including:

(i) Increasing solid yield under air and carbon dioxide (lower chemical reactivity)
(ii) Decreasing functionalization (including O/C and H/C ratios)
(iii) Decreasing electrical resistance, and,
(iv) Small changes in surface area and porosity

Comparison of the coking (CC) and thermal (CT) coal chars show that the thermal coal had higher ash content, as well as higher activity towards chemical oxidation in both air and carbon dioxide, especially for low pyrolysis HHT. The pyrolysis yield was also lower for CT chars suggesting a larger initial volatile composition for the parent thermal coal, which is also reflected in the lower carbon content of the thermal coal. Overall, the thermal coal also had higher surface area, micropore volume and average pore size than the coking coal, especially for char treated at pyrolysis temperatures above 600°C, although overall no large variation in pore size was observed. Degree of functionalization was similar between coal types pyrolysed at the same temperature with only small differences in H/C and O/C ratios observed between CC and CT. The exception is CC-700 which showed a larger H/C ratio than the equivalent CT, which may also account for non-linear behaviour observed for chemical activity, where CC-700 was seen to be more active than CC-600 under both air and carbon dioxide.

Electrochemical Analysis of Pyrolysed Coals

The pyrolysed material can then be formed into electrodes along with a graphite binder for analysis in the DCFC (see Section 3.6.2 for electrode preparation procedures). Electrodes of identical exposed surface area are therefore created. The surface of these electrodes has been examined under SEM prior to electrochemical oxidation as shown in Figure 19.

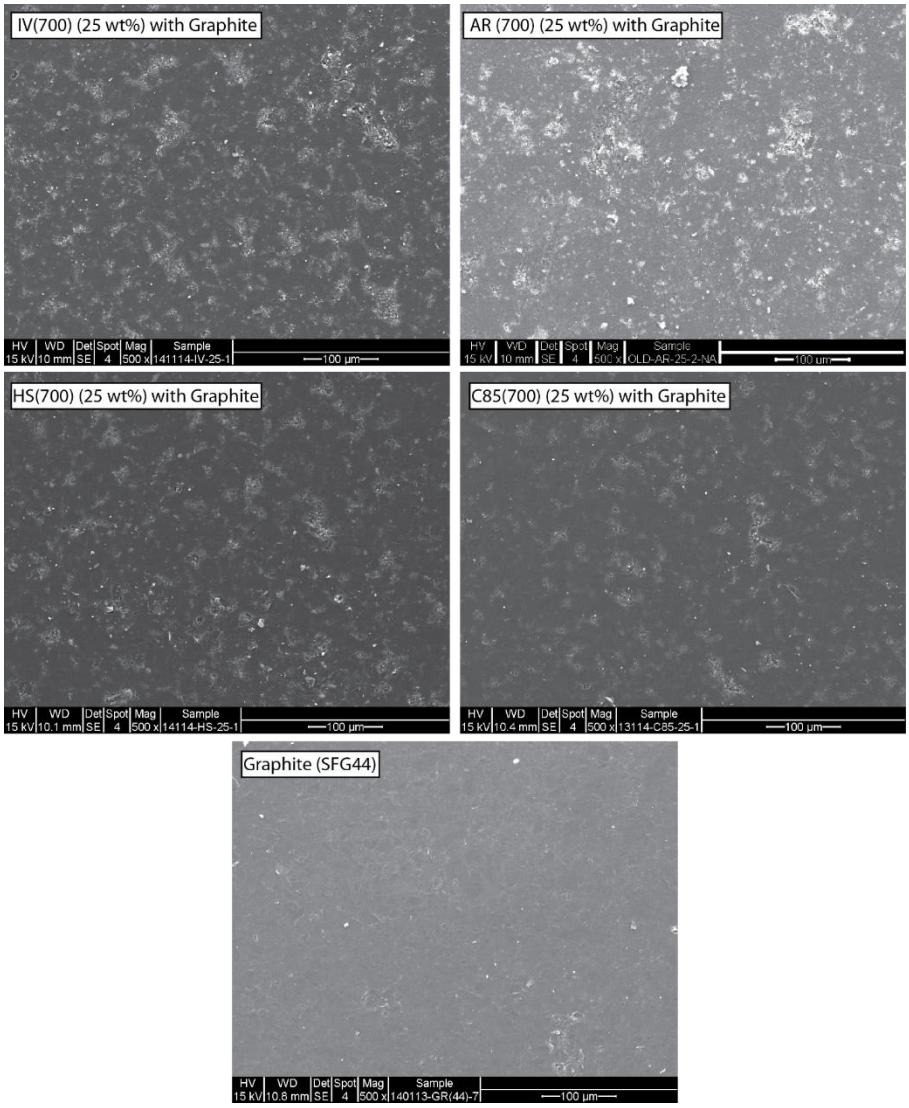

Figure 19: SEM Images of coal electrodes prepared in a 25wt% ratio with SFG44 graphite. 500 x magnification shown with coal identity shown in figure.

Although similar in the prevalence of coal, the roughness and apparent disorder of the electrodes appears different in the SEM with IV(700) and AR(700) showing more disorder than HS(700) and C85(700). This could be a result of different ash contents as well as the coal type and origin. Indeed IV(700) and AR(700) had higher pyrolysis yields than HS(700) and C85(700) suggesting lower and higher amounts of volatiles respectively – suggesting a loose relationship in the final structure of the electrode.

Electrodes examined under SEM were formed into electrodes and investigated for

electrochemical activity in the DCFC. Coal activity overshadows that of graphite and the behaviour of these coal based electrodes are therefore reflective of the coal rather than the graphite base. Results for AR(700), C85(700), IV(700) and HS(700) are shown compared with a graphite only electrode in Figure 20.

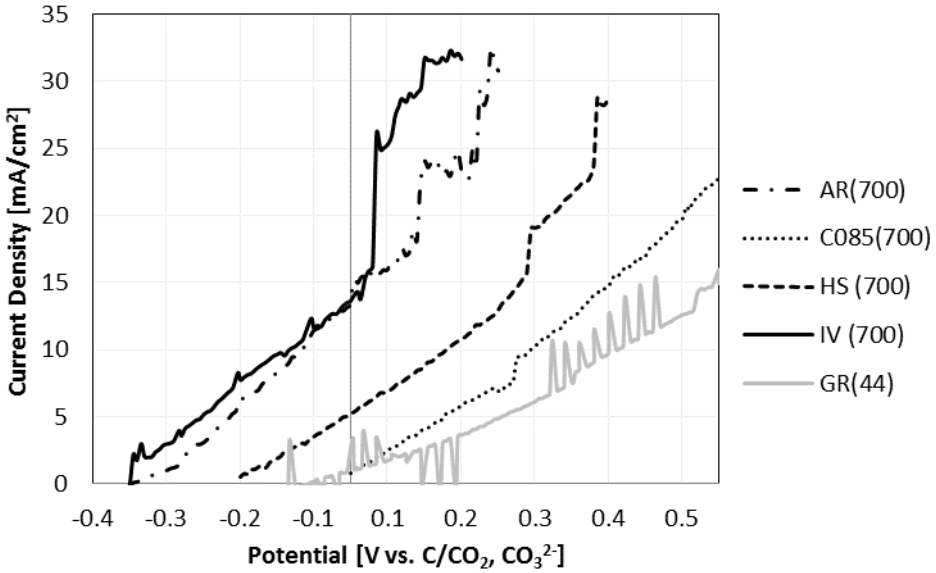

Figure 20: Electrochemical activity of coals investigated in half-cell arrangement, LSV at 5 mV/s after reading OCP

The electrochemical procedure used included firstly the measurement of the open circuit potential followed by a sweep from the measured open circuit potential to 0.5 V positive of this at a scan rate of 5 mV/s. Wide variation in electrochemical activity can be observed in Figure 20 where all coal materials gave a higher oxidation current at +0.5V OCP than graphite, although C85 coal can be seen to perform only marginally better than the graphite base. Highest performing coal materials are seen to be AR(700) and IV(700) which is reflected both in the current density achievable as well as the open circuit and onset potential. The OCP of each material investigated is shown in Figure 21.

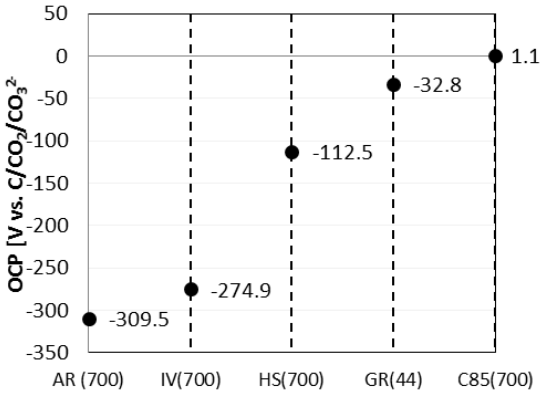

Figure 21: Averaged OCP taken over a period of 1 minute prior to linear sweep voltammetry on coal and graphite electrodes.

A more negative the OCP reflects a more active electrode towards carbon oxidation since a lower voltage is be required in a full DCFC arrangement versus the oxygen cathode for the same current density. It is therefore likely that the volatile composition and pyrolysis behaviour as well as physical structure of the electrode play key roles in activity of a particular coal material since AR and IV exhibit different physical structure (Figure 19) and pyrolysis yield (Figure 13) compared to HS and C85. More work is required in this area to confirm these observations.
Other methods used by the Applied Electrochemistry group at the University of Newcastle for electrochemical characterisation of carbonaceous materials in 2013 have also been applied to coals investigated for DCFC use. The most interesting method is that of the electrochemical cup cell (described in Section 3.2.2). It is believed that this method will allow the electrochemical assessment of coal materials for their activity in the DCFC without requiring DCFC anode construction and testing at highly elevated temperatures. Indeed this technique is carried out at room temperature and under pH neutral conditions.

Indicative results for coals samples which have been carried out at this stage are shown in Figure 22.

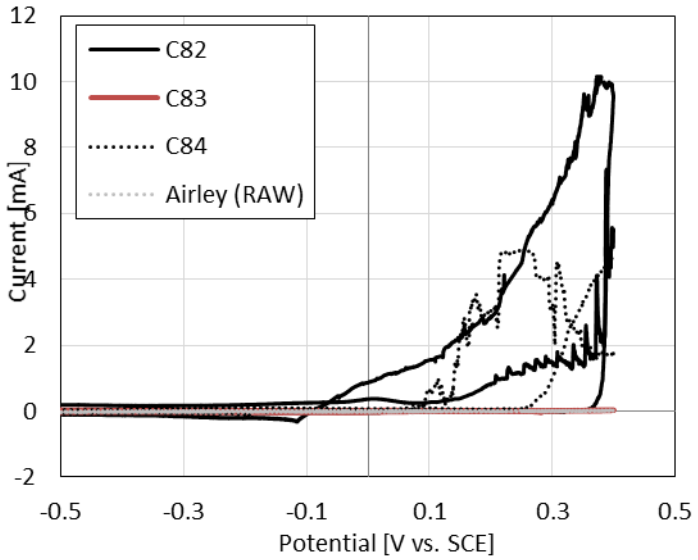

Figure 22: Cup cell electrochemical results for coals run to date

A higher response in terms of apparent oxidative activity of the black-mix investigated is observed for coal C82 and C84 compared to C83 and AR. Our hypothesis is that a correlation between these results and performance of each pyrolysed coal in the DCFC will be possible, although this will need to be confirmed with further work. It is expected that materials of higher volatile content will give better response in the cup cell. Since high volatile content and therefore low pyrolysis yield, has been indicated in this section to give lower electrochemical activity it may be a simple case of determining the volatile content of the coal to determine activity. In order to observe differences in behaviour in the electrochemical cup cell after pyrolysis, both raw and pyrolysed coals will also be run. An example of a raw and unpyrolysed coal run in the cell is shown in Figure 23.

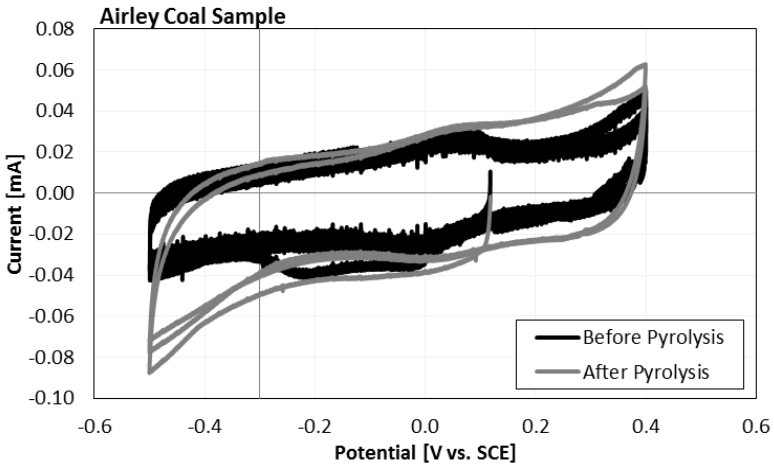

Figure 23: Comparative activity of both raw and un-pyrolysed AR Coal

AR shows limited activity in the electrochemical cup cell as shown in Figure 21. The pyrolysed version of this coal is no different and, although it appears as though a slight improvement in oxidative activity can be observed, the extent of oxidation is barely discernable for both raw and pyrolysed AR when compared to the apparently much higher activity of C82.

Comparative Performance versus Reference: The electrochemical activity of each coal char generated was assessed using a solid anode arrangement, as described in Section 3.6.2. The anode consisted of 25 wt% coal char with graphite as a binder. Since coal is expected to be more active than graphite [17, 30, 31], comparison of the 25 wt% loaded electrode will demonstrate key differences in electrochemical oxidative behavior for coal chars. Activity was assessed in a ternary carbonate eutectic (Li_2CO_3:Na_2CO_3:K_2CO_3) at 600°C in all cases for comparison. The same electrochemical procedure was used for consistency and included allowing the electrode to equilibrate at open circuit in the molten carbonate at temperature for 1 h. Three LSV sweeps were carried out consecutively (two at 5 mV/s followed by one at 1 mV/s) with a 2 minute wait at OCP between each. Results for CC-500 are shown in Figure 24.

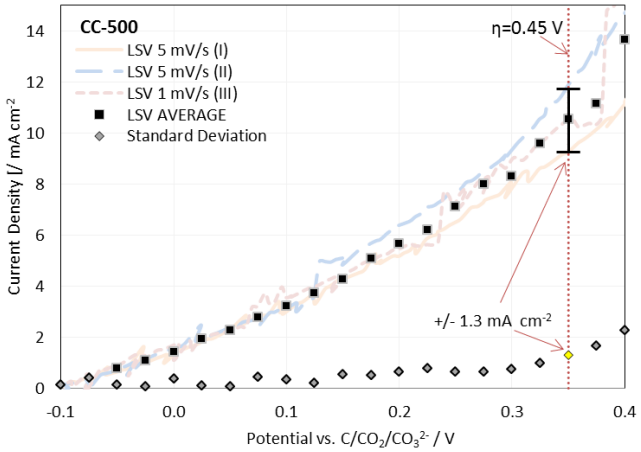

Figure 24: CC-500 electrochemical performance including LSV's at 1 and 5 mV/s, average current density at 0.025 V intervals and standard deviation at each potential.

Comparison of scan rates used shows no dependence on diffusion of reactants to the electrode, as expected in the carbonate/oxide rich electrolyte used here. In the potential region investigated the oxidation of carbon further occurs without reaching a diffusion plateau, commonly seen in slurry arrangements [32]. Standard deviation between the three LSVs measured in Figure 23 increases with polarization, reaching ~1.3 mA cm^{-2} at a polarisation of 0.45 V positive of the OCP (indicated in Figure 24). In order to encompass variations between LSV sweeps, it can be seen in Figure 24 that taking the average current density at 25 mV intervals, along with the standard deviation at a specific point, can be effectively used to encompass possible deviations in LSV curves observed with polarization. This has been done for each coal char produced as well as for pure graphite, shown in Figure 25.

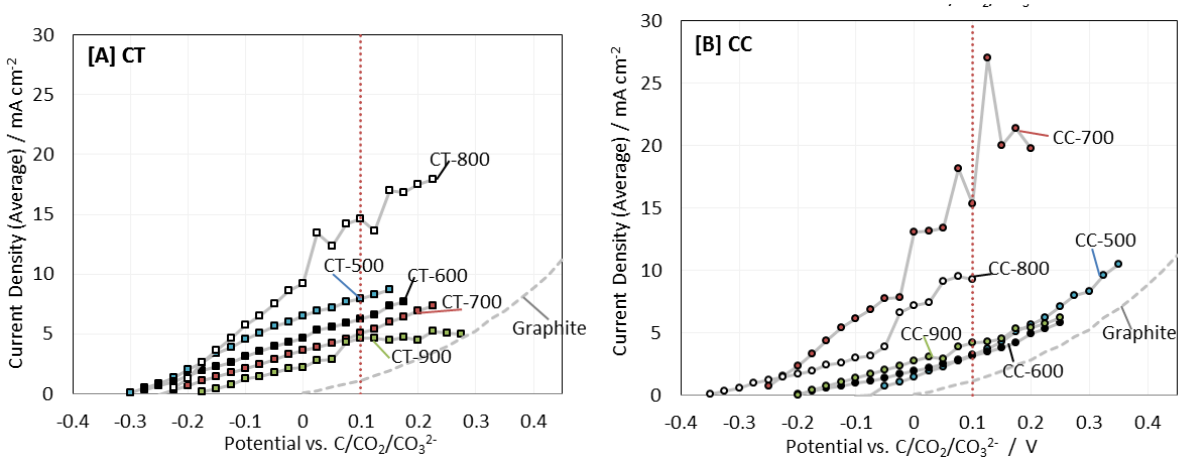

Figure 25: Comparative performance of each coal char investigated to an overpotential of 0.5 V

Each coal char investigated shows differences in OCP and in the maximum current density obtained. Variation in the stability (smoothness of curve) and general shape of the LSV can also be observed between chars. To compare overall performance, the current density at 0.1 V versus the reference (indicated by dashed line in Figure 25) has been plotted as a function of HHT. The standard deviation can also be included in this analysis, as outlined in , in order to show the reproducibility of the current density measured for each coal char at this polarization, results shown in Figure 26.

A clear activation can be observed for CC-700 and CT-800, also observed to a lesser extent for CT-500 and CC-800. A systematic decrease in activity can be seen for CT chars between 500 and 700°C HHT, while little to no difference is observed between CC chars below the activation HHT of 700°C. Both coal chars treated at 900°C HHT show limited activity. All coal chars investigated are shown in Figure 26 to perform better than graphite versus the reference system at the same polarization, this is in agreement with results found using slurry-type arrangements for the increased activity of coal materials compared to relatively inert graphite [3, 33].

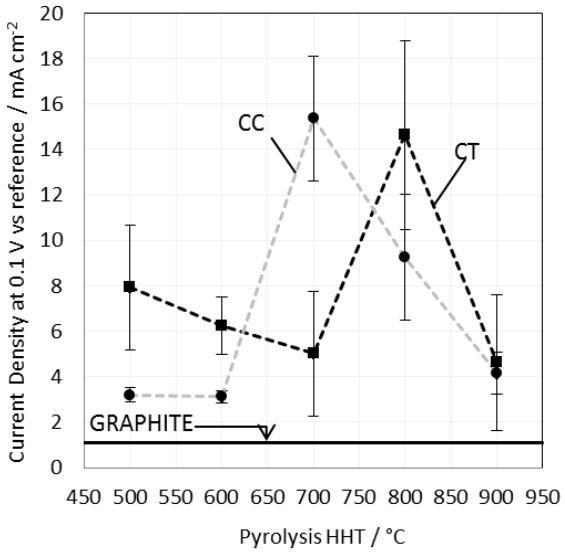

Figure 26: Average current density at 0.1 V vs reference from LSV results of 25 wt% coal chars at 600°C in ternary carbonate eutectic

OCP Assessment: Average OCP, measured between each LSV, as a function of pyrolysis HHT is shown for each parent coal type in Figure 27.

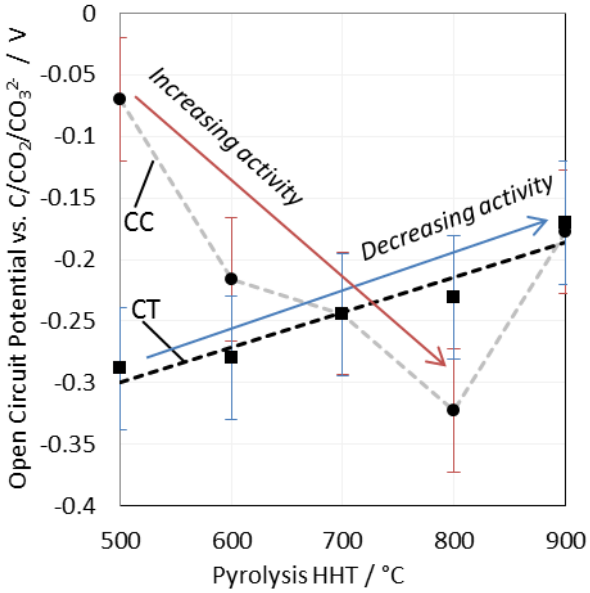

Figure 27: Average OCP measured versus reference for 25 wt% coal char working electrodes submersed in ternary carbonate eutectic at 600°C.

In the case of CT chars, the activation of the electrode apparently decreases with pyrolysis HHT while CC chars display an increase in relative activity, as marked in Figure 27. Change in the OCP could be due to (i) the presence of a mixed potential at the electrode surface, and/or (ii) change in the relative "activity" of solid carbon at the electrode surface.

Temperature, carbonate composition and carbon dioxide flow rate/partial pressure can affect the open circuit potential through the Nernst equation (Eq 13 and 14) for electrochemical

carbon oxidation in molten carbonate (Eq 2) [21]:

$$C + 2CO_3^{2-} \rightarrow 3CO_2 + 4e^- \quad \textbf{(13)}$$

$$E = E^0 - \frac{RT}{4F} ln\left(\frac{a_c {a_{CO_3^{2-}}}^2}{{p_{CO_2}}^3}\right) \quad \textbf{(14)}$$

where standard terms include E as the equilibrium potential and E_0 as the standard potential (V), R is the universal gas constant (J mol^{-1}K^{-1}), T is the temperature (K) and F is Faradays constant (C/mol). The activity of carbon and carbonate is described by a_C and $a_{CO_3^{2-}}$ respectively. Many investigations assume activity for both carbon and either carbonate or the oxide anion as unity, meaning the OCP is predicted to be affected only by the partial pressure of CO_2. Since, in our system, all variables are constant, the only variant is in fact the carbon source. Carbon activity was discussed by Li et al. [34] where changes in the OCP were modelled based on a calculated value for carbon activity. In this work, carbon activity was defined in limited terms by considering a model carbon (graphene) with the number of active carbon atoms defined as a function of several factors including the distance between two active carbon atoms, the diameter of the crystallites and carbon particle size. Although this idealized system is difficult to apply to results shown here, the systematic change in the OCP observed for CT chars as pyrolysis temperature increases suggests possible graphitization of the char and therefore a reduction in surface activity. In the case of the reference system used here, this causes the OCP to approach 0 V versus the reference since the reference electrode is also graphite.

Carbon activity with respect to relative graphitization however cannot be used to explain changes observed for the coking coal char investigated where increasing HHT appears to increase activity of the coal char, decreasing the OCP, until a HHT of 900°C where activity is lost. This is despite results suggesting that the carbon component of the coal char is also undergoing some degree of graphitization and presumably reduced carbon "activity" as defined by Li et al. [34]. Changes to the coking coal char OCP are also to a greater degree than that observed for the thermal coal investigated with variation of almost 0.3 V between most and least active OCP. It is therefore likely that a different effect on the OCP is observed in the case of CC compared to CT chars.

Chen et al. demonstrated that the open circuit potential is strongly affected by the extent of contact of the carbon sample tested (graphite) and the binary Li/K molten carbonate used by the authors, showing a sudden change in OCP of 0.3 V after flooding of a graphite sample at 650°C [21]. The authors discussed the OCP as representing a mixed/corrosion potential where the surface undergoes simultaneous reduction of carbon dioxide and oxidation of carbon, depending on whether the surface was wetted or not. They attributed large variation in OCP to progressive coverage of carbon by the molten carbonate and the subsequent generation of CO via the reverse Bouduard reaction, which can be electrochemically reduced to carbon. It is therefore likely that large variation in OCP observed for coking coal, in particular between 500 and 600°C HHT results from variation in the wetting of the coal char, possibly influenced by a change in properties of the ash component of the coking coal between these temperatures. It has previously been suggested that coal contaminants cause variation in the electrode polarity and therefore wettability with carbonate [19]. It is therefore suggested that pyrolysis of coal causes changes to the ash structure and distribution, effecting changes in the wetting behavior and therefore observed OCP of the electrode.

Comparative Performance versus Overpotential: It is useful to compare results independent of the OCP to assess the kinetic performance of the electrodes. Comparison of chars

produced versus their respective overpotential is therefore shown in Figure 28.

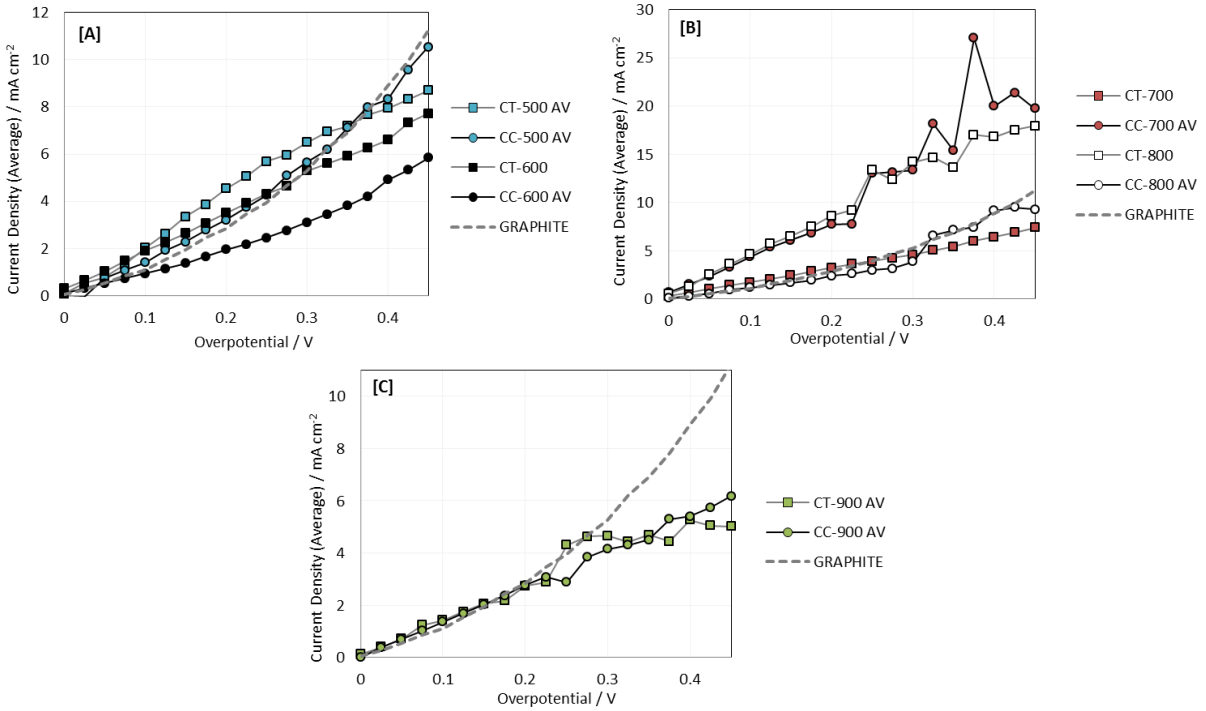

Figure 28: Comparison of CT and CC chars at different pyrolysis temperatures versus over-potential (OCP) [A] 500 and 600°C HHT, [B] 700 and 800°C HHT and [C] 900°C HHT

Comparison of results irrespective of OCP shows very similar behavior for the majority of coal chars to each other, as well as to a standard graphite electrode, also included in Figure 27 [A]-[C] for comparison. In the case of activated electrodes, CC-700 and CT-800 behaviour deviates from low overpotentials showing much faster kinetics for these activated electrodes which appear to follow a similar catalytic pathway to each other with a clear transition between low and high polarization, the change occurring at ~0.25 V. In the case of coal chars generated at 900°C, performance is almost identical between parent coals tested, both of which show an inhibited oxidative response at high polarization compared to graphite, again in the high potential region where instability is observed for activated electrodes (>0.25 V). Comparison of performance at the same polarization (OCP + 0.45 V) can be assessed including standard deviation calculated as described in Figure 23. This is shown in Figure 29.

When expressed as overpotential it can be seen clearly that the kinetics of coal char oxidation only vary significantly in the case of the activated cases of CC-700 and CT-800. Other coal chars result in very little variation where performance appears similar to, or, in most cases, inhibited from, graphite. The activated electrodes also show a high degree of standard deviation for activated coal chars at this polarization, most likely as a result of CO_2 bubble formation and dislodgement which has previously been observed on graphite at more elevated temperatures (750°C) [35]. Based on these observations it is suggested that the mechanism of oxidation on the activated electrodes follow an identical catalytic pathway, while inactive coal chars follow a similar mechanism to pure graphite.

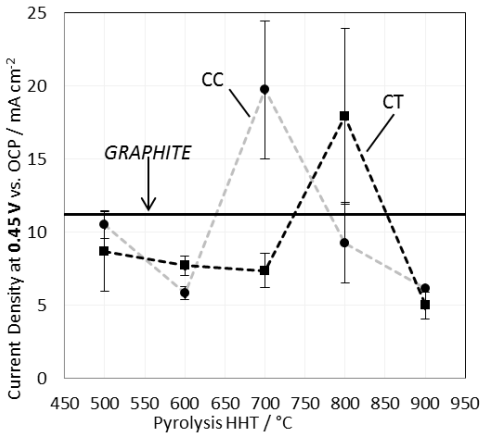

Figure 29: Average current density at 0.45 V vs OCP from LSV results of 25wt% coal chars at 600°C in ternary carbonate eutectic

Electrochemical Activation of Coal Chars: A clear relationship between the specific surface area, micropore volume and electrochemical activity of a slurry activated carbon system was observed by Cao et al. [36], the authors also suggesting changes in the relative 'acidity' or 'basicity' of the surface to effect electrochemical oxidative activity as a result of variation in surface functional groups. Increasing the surface functionalization of ashless carbon material, for example through chemical pre-treatment, has been suggested in the literature to lead to higher electrochemical activity for molten carbonate suspended carbon fuels [13, 36]. The importance of conductivity in a solid electrode has also been previously suggested by Hackett et al. when investigating solid carbon electrodes of various compositions [12], as might be expected when using the carbon fuel as a current collector also.

The performance of coal chars examined here can be explained to some extent using these observations for ashless carbon electro-oxidation including the importance of surface functional groups, BET surface area and, in the case of a solid anode, char resistivity. Performance can generally be explained in Figure 30 showing three regions of reaction which are influenced by properties shown here.

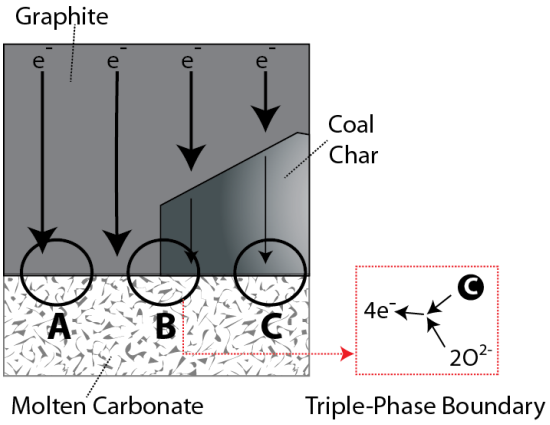

Figure 30: Defining regions of activity proposed for low conductivity, highly functionalized coal char with low ash

For a coal char of low conductivity but high functionalization and BET surface area, areas

outlined in Figure 30 would correspond to:

A. Low resistivity and low activity
B. Low resistivity and high activity
C. High resistivity and high activity

Performance is initially low for high resistance CT chars (CT-500 and CT-600). This is likely due to the high electrical resistivity of these chars limiting oxidation to Area (B) in Figure 30 where CT-500 outperforms CT-600 despite higher resistivity due to the higher functionalization and therefore activity of this char at the interface between graphite and coal char. When pyrolysed excessively; i.e., to a HHT of 900°C, activity of the carbon drops to that of graphite due to low levels of surface functionalization; i.e., Area (A) in Figure 30. The most active char however was CT-800, which might be a result of the further reduced resistivity for this char at a pyrolysis temperature of 800°C compared to 700°C (Figure 18). This seems unlikely however since similar activation is also observed for CC char at 700°C which has higher electrical resistivity than CT-800. The relative activation of CT-800 could be related to higher porosity, as suggested for ashless carbons [37], however the observed reduction in porosity through the plasticization stage of coking coal examined between HHT of 600 and 700°C apparently activated the coking coal tested here, meaning no clear relationship with porosity can be made.

The functionalization, surface area, porosity and electrical resistance do not appear to be the defining factor to cause a catalytic electrochemical pathway to be followed in the case of high ash coals investigated here. All of these conditions could be described to be necessary, but not sufficient for activation of coal chars electrochemically. Instead, it is suggested that ash type influences the electrochemical performance considerably for high ash coals. This is possibly a result of the interfacial mixing of carbon and ash. The dependence of this activation on pyrolysis temperature further suggests a change in the ash distribution and character with thermal treatment. In the case of CC chars, activation occurs at lower temperatures than CT chars and allows for a larger active window before destruction of activity at 900°C HHT for both coal types. The effect of coal ash pyrolysis has been investigated for gasification applications where it is established that coal ash acts catalytically and, further, that catalytic coal ash properties are affected by thermal treatment [26, 27]. For example iron oxides, which are known catalysts for coke gasification [38], are proposed to act as oxide mediators, enhancing gasification through the pathway [26]:

$$Fe_mO_n + CO_2 \rightarrow Fe_mO_{n+1} + CO \quad \textbf{(15)}$$

$$Fe_mO_{n+1} + C \rightarrow Fe_mO_n + CO \quad \textbf{(16)}$$

The oxidation state of the iron catalyst is dependent on thermal treatment conditions, including both gas atmosphere and temperature [26]. Eq (16) also suggests contact of the metallic catalyst with solid carbon is essential for activity, implying distribution and contact of the carbon and catalyst is a determining factor for activation.

3.2.4. Conclusions

Activity of coal chars cannot be simplified to optimization of porosity, surface functional groups or resistivity as, although trends in these properties do clearly occur, no definitive pattern for activation based on one or more of these factors can be observed for the two very different coal types investigated in this work. Instead it is suggested here that the ash composition and distribution in the coal particle plays a dominant role in catalytic activation, possibly through effect of ash on carbonate wettability and oxide mediation at the surface of the ash. Specific thermal treatment of the coal and coal ash appears to change these properties and lead to promotion of a catalytic reaction pathway at the solid carbon electrode.

3.3. Milestone 11: Electrode Catalyst Effects on Oxidation

3.3.1. Milestone Background and Aims

Catalysis in the carbon anodes can occur in two ways. The first involves the addition of foreign materials to the solid composite electrode. The second involves the addition of soluble species to the electrolyte. Both have the ability to catalyse or change the oxidation mechanism and identifying catalysts of this nature could significantly improve the performance of the DCFC. In this milestone our focus is on the effect that certain solid state catalysts have on the anodic rate performance of the carbon oxidation reaction.

3.3.2. Experimental Methods

Similarly to the previous section, experimental methods for this study, including anode pellet preparation and formation into an electrode as well as use in the DCFC have been outlined in Section 3.6.2. In addition, several other experimental techniques have been used here.

Proximate Analysis of Coals Investigated: Proximate analysis on the coal materials used the method ATSM D3175-11. Ash analysis was also performed on the coals using ASTM D4326-11.

Low Temperature Ashing: Low temperature ashing was performed in an oxygen plasma low-temperature asher (PE100 Plasma Etch) with a RF power supply providing 200-240 W at frequencies necessary to provide a sustained oxygen plasma (~13.65MHz). Selected, pre-dried (at 95°C), 20-30 g samples were evenly distributed on 150 mm Pyrex dishes and loaded into the ashing chamber, which was then evacuated to 0.15 Torr. Maintenance of the low-pressure oxygen (BOC industrial grade) atmosphere was through a bleed line (5-30 mL/min) and a scavenging vacuum pump. Samples were reweighed and gently overturned every 48 hour period. Ashing was assumed complete when the mass loss was no greater than 5 mg after a 48 hour cycle, complete ashing was observed after 3 weeks. After completion, samples were sealed in airtight containers until further analysis.

Structural Analysis: X-ray diffraction (XRD) patterns for selected samples were recorded using a Phillips PW1710 diffractometer. Cu K_α radiation (1.5418 Å) was used to analyse the sample at room temperature using settings of 40 mA and 40 kV, 2θ range of 10° – 90°, step size of 0.05° 2θ, scan step time of 2 seconds, divergence slit – receiving slit – scatter slit widths of 1° – 0.2° – 1°, respectively.

Morphological Analysis: Scanning electron microscopy (SEM) of manufactured electrode surfaces was carried out. To enable microscopic examination of the pelleted carbon samples, a polished specimen was prepared. This was achieved by initially mounting the carbon pellets under pressure in a two-part, cold setting, epoxy resin. The sample was then ground using various grades of silicon carbide paper on a rotating turn-table and finally polished using diamond and silica compounds. This resulted in a relatively flat, representative cross-section, making microscopic examination possible. For SEM examination the sample was mounted on an aluminium stub and carbon evaporation was carried out with a 20 nm conductive layer of carbon suitable for imaging and elemental X-ray analysis. SEM images were taken on a Zeiss MA15 instrument with a silicon drift X-ray detector (SDD) and a back-scattered electron (BSE) detector.

Contaminated Graphite Pellet Preparation: The particle size of the contaminants was kept below a standard size by dry-milling the mineral phases and passing them through a 40 μm test sieve prior to mixing with the graphite material. Kaolin was further heat treated at 500°C for 30 minutes prior to pelletising in order to minimise possible mechanical damage to pellets during electrochemical testing as a result of dehydroxylation of kaolin to metakaolin at elevated temperatures [3].

After sieving, contaminants were slowly introduced to the graphite powder while mixing in a mortar and pestle and combined for a further 5 minutes or until a homogenous powder was produced. Pellets were then prepared identically to pure graphite.

Contaminant materials including alumina (Al_2O_3), quartz (SiO_2) and anatase (TiO_2) were sourced from reputable chemical supplier (Sigma Aldrich), while kaolin, montmorillonite and pyrite were sourced from mineral deposits in the Hunter Valley region of Australia. To confirm their identity and the purity of the contaminant mineral phases sourced, all contaminants were analysed by XRD. All materials were found to match pure references of the material (found in Inorganic Crystal Structure Database) with minor deviations. Deviations observed include the presence of a very minor rutile phase within the anatase and minor traces of quartz in the pyrite material.

Electrochemistry

Electrode Preparation: Coal pellets for electrochemical assessment were formed using a mixture of graphite (SFG44 Timrex, Timcal Switzerland) and pyrolysed coal, using 25 wt% (dry basis) coal char for all pyrolysis temperature investigations. 0.8 g of the carbon mix in all cases was pressed into a pellet using an International Crystal Laboratories (Garfield, USA) 13 mm pellet die press under a pressure of 740 MPa. Once pressed, pellets were sintered at 500°C for 4 h under nitrogen flow. Pellets were then inserted into alumina electrode holders using the ceramic adhesive Resbond 989 (Ceramic Oxide Fabricators, VIC, Australia) and a paste of 1:1 Resbond 989 to graphite (weight percent) was compressed onto the back of the pellet over an electrical contact to ensure good connection.

Anodic Half-Cell Arrangement: The electrochemical half-cell used consisted of the working electrode as described above with counter and reference electrodes made from graphite rods. The rods were used several times and sanded back between experiments to refresh the surface, as well as renewing electrical connections which were inserted into a small hole drilled in the graphite rod. The electrodes were submersed in a pre-fused ternary carbonate eutectic once molten in an alumina bath with a weighted lid.

The eutectic was prepared from a mixture of lithium carbonate (Li_2CO_3, >99%), sodium carbonate (Na_2CO_3, >99%) and potassium carbonate (K_2CO_3, >99%, all Sigma-Aldrich) in the mole ratio 43.5:31.5:25 (eutectic composition [1]). The carbonates were firstly dried in air at 110°C for several days to remove moisture before being weighed separately and combined using a mortar and pestle. The eutectic was finally ball milled to ensure proper mixing (apparatus as described in 3.2.2). The eutectic was then fused at a temperature of 500°C in an alumina crucible before cooling.

Carbon dioxide (CO_2, Coregas, food-grade) was allowed to flow over the surface of the carbonate during electrochemical testing to maintain a carbon dioxide atmosphere (50 normal L/min flow rate, nitrogen basis) to ensure a stable reference electrode. Detailed cell and electrode drawings are provided in an earlier publication [4].

Electrochemical Test Procedure: In order to ensure consistent analysis, the same electrochemical method was used for assessment of all electrodes. Electrodes were at first partially inserted in the electrochemical half-cell to sit above the fused solid eutectic at room temperature. Carbon dioxide flow was started and the cell was heated at 6°C/min to the electrochemical assessment temperature of 600°C. The electrodes were immersed in the carbonate melt at 500°C prior to continuing to 600°C where the anode was held for 1 hour at open circuit potential (OCP) prior to testing to ensure good wetting of the carbon surface [5] and stable conditions within the cell (i.e., no temperature fluctuations from opening and closing the furnace door or movement of molten eutectic from insertion). Electrochemical testing was then carried out including sweeping of the electrode potential from the measured OCP to an overpotential of 0.5 V. Sweep rates of 1 and 5 mV/s were investigated.

For this work, the electrochemical apparatus used was a Pine Research Instrumentation (Durham, USA) WaveNow portable potentiostat, with AfterMath electrochemical software used for data collection. Current measured has been normalized for the geometric surface area of the pellet of 1.327 cm^2 (13 mm diameter) in all cases.

3.3.3. Results

Proximate and Ash Analysis Results

From the low ash content and high fixed carbon evident from the proximate analysis it is clear that the Coal-C sample has been processed to remove some of the ash producing phases. All of the other coal materials showed typical proximate analysis results for sub-bituminous coals.

As is commonplace, the elemental composition of the coal ashes were reported as oxides with composition indicated on a weight percentage basis, results shown in Table 6.

Table 5: Ash Constituent Analysis of Coals

	SiO_2	Al_2O_3	Fe_2O_3	TiO_2	Na_2O	CaO	SO_3	K_2O	MgO
COAL-A	56.5	27.6	6.4	1.4	1.3	1.5	2.1	1.2	0.9
COAL-B	58.2	27.4	4.6	1.3	3.8	0.9	1.2	1.5	0.8
COAL-C	73.5	14.8	1.7	4.8	0.6	0.6	0.2	1.1	0.4
COAL-D	41.6	23.5	20.3	1.1	0.8	5.4	3.5	1.7	1
COAL-E	72.4	14.6	5.8	0.1	3.6	0.9	1.2	0.6	0.7

Results here suggest all coal ashes are dominated by silica with significant inclusion of alumina and ferric oxides. Other constituents are minor and, combined; consist of less than ten per cent of the total ash. Coal-C again is shown to be different from other coals with notably smaller concentrations of silica, alumina and iron oxides – suggesting a preferential removal of these species in the pre-treatment process.

Identification of coal mineral phases of interest

Raw coals were analysed using XRD. Results are shown in Figure 31 along with XRD patterns for coals which have undergone the LTA procedure outlined in Section 3.3.2.

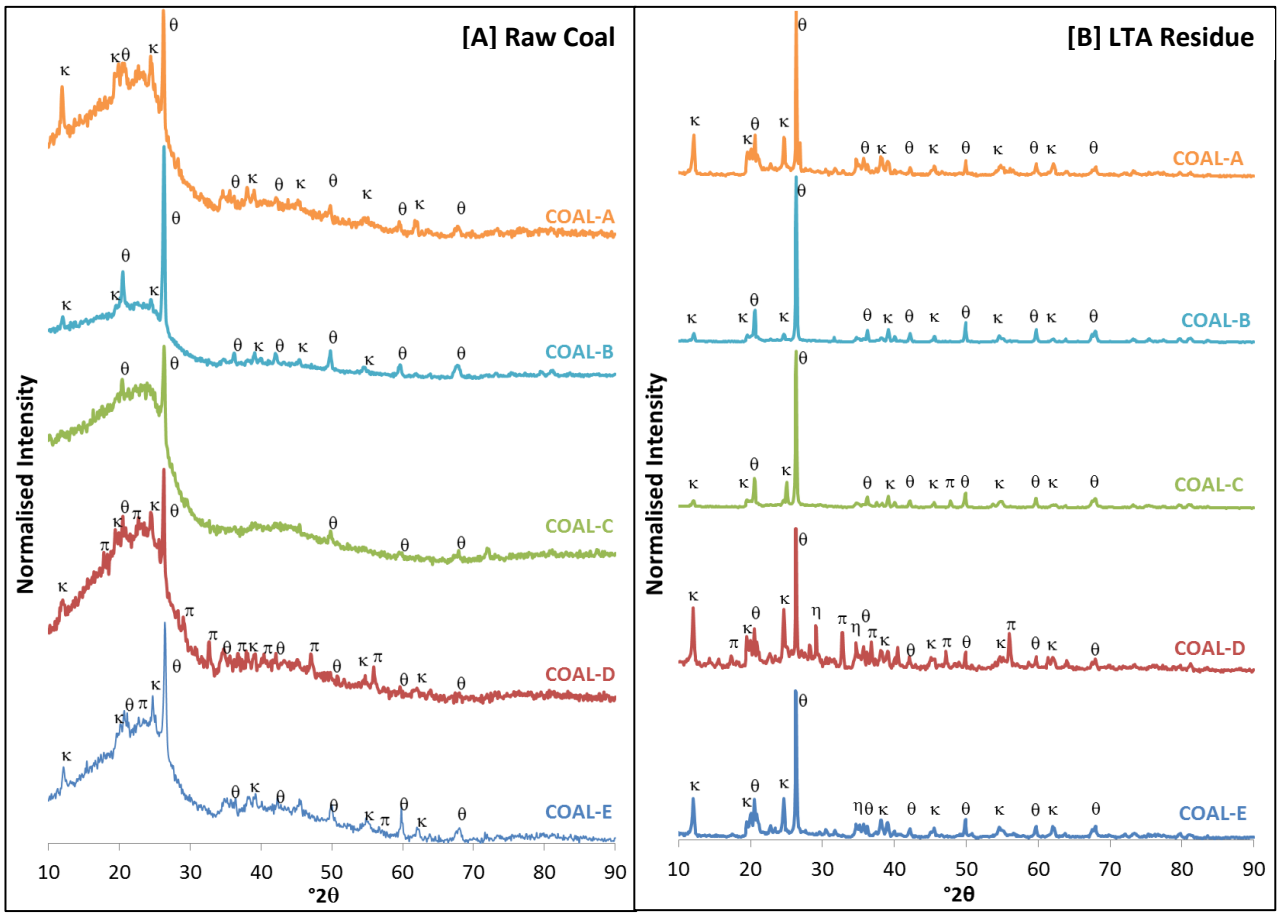

Figure 31: XRD patterns from [A] raw coal and [B] LTA residues (κ – kaolin, θ – quartz, π – pyrite)

All of the raw coal materials showed two broad peaks in the range 10-30°2θ and 30-60°2θ which are known to be characteristic of poorly crystalline carbon materials [6, 7]. Superimposed on the broad carbon peak there are several peaks from the crystalline mineral matter in the raw coal samples; namely kaolin (denoted with κ in Figure 31) and quartz (denoted with θ), with kaolin peaks at 12.1°2θ, 24.5°2θ and distinct multiple peaks at 20.5°2θ. The peaks due to quartz, 20.45°2θ and 26.4°2θ, are distinct for all the raw coal materials with the main quartz peak, 20.45°2θ, giving the largest peak in all the raw coal patterns. This peak from the quartz phase is exaggerated somewhat as the graphitic carbon in the coal material also has a main peak at 26.15°2θ. However, the secondary peaks at 49.3°2θ and 59.4°2θ confirm the presence of the quartz phase in the raw coals. In the case of Coal-D these secondary quartz peaks are minor peaks in the background, likely due to the fact that the majority of the quartz in the Coal-D raw coal is tied up in the clay materials in the sample. The XRD pattern of the raw Coal-D sample also showed small peaks at 32.55°, 36.5°, 40.35°, 46.95° and 55.8°2θ, which are the distinct major peaks from a pyrite (denoted with π) phase in the raw coal.

The large amorphous carbon peaks in the pattern can overshadow many peaks from other

mineral phases, meaning detailed information on the mineral phases present in the sample is difficult to establish. LTA was used to remove the carbon material in coal whilst preserving the mineral phases present in the samples through significantly reducing the severity of the ashing temperature and oxidative conditions. XRD patterns from LTA residues collected for each coal sample are shown in Figure 31.

The low temperature ash XRD patterns closely resemble that of their parent coal material with the shadowing broad carbon distortion removed. All of the patterns show strong kaolin peaks at 12.1°2θ and 24.7°2θ, and multiple peaks at 19.9°2θ and 38.1°2θ. A large quartz peak can be observed clearly at 26.4°2θ and minor peaks at 20.5°, 36.1°, 49.8° and 67.5°2θ are also evident. It is apparent from these features that the low temperature ashing has not disrupted the mineral phases present in the coal samples.

In comparing the Coal-C and Coal-E raw coal and LTA residue XRD results, it was apparent that the beneficiation process used on the Coal-C sample, whilst decreasing the overall mineral content of the coal sample, shows preference for the removal of certain phases. Evidence for this is the lack of any well-defined clay (kaolin) peaks in the Coal-C pattern, along with the significant reduction in peak height from the quartz mineral phase. From the proximate analysis the Coal-C and Coal-E coals both showed a high Si:Al ratio, indicating that there was likely to be a higher quartz phase present in these samples. Coal-E shows strong primary and secondary peaks from a quartz phase, whereas the secondary quartz peaks are almost lost in the background for the Coal-C raw coal spectra. From the XPert analysis software, only quartz and polymorphic graphite were identified in Coal-C.

It is evident from this analysis that the coal materials have a wider range of mineral chemistry than the basic oxides reported in the proximate analysis in . Through the use of both SiroQuant and XPert XRD analysis software a multitude of mineral phases were identified in these LTA samples. Table 6 highlights the range of mineral phases found in these LTA residues.

Quartz and anatase were the only significant oxide phases found in the LTA samples. This result is strongly supported by Ward [8] who also determined that the only significant oxides found in a compilation of LTA results were quartz (SiO_2) and anatase (TiO_2). This result illustrates that testing the effects of coal contaminants as they are likely to be introduced to the DCFC requires addition of the significant mineral phases and not their oxide counterparts.

Table 6: Identified mineral phases in the LTA samples of some of the coal materials

Coal-A

Quartz - SiO_2	Pyrite - FeS_2	Fluorapatite - $Ca_5(PO_4)_3F$
Kaolin - $Al_2Si_2O_5(OH)_4$	Calcium Sulfide - CaS	Muscovite- $KAl_2(Si_3Al)O_{10}(F,OH)_2$
Montmorillonite- $Na_{0.3}(Al,Mg)_2Si_4O_{10}(OH)_2 *H_2O$	Albite- $Na(AlSi_3O_8)$	Illite - $KAl_2(Si_3Al)O_{10}(OH)_2$
Jarosite - $KFe_3(SO_4)_2(OH)_6$	Siderite - $FeCO_3$	Dolomite - $CaMg(CO_3)_2$
Coal-D		
Kaolin - $Al_2Si_2O_5(OH)_4$	Quartz - SiO2	Pyrite - FeS_2
Muscovite- $KAl_2(Si_3Al)O_{10}(OH)_2$	Calcite - $CaCO_3$	Illite - $KAl_2(Si_3Al)O_{10}(OH)_2$
Coal-E		
Quartz - SiO_2	Bassanite - $CaSO_4\ 2H_2O$	Kaolin - $Al_2Si_2O_5(OH)_4$
Illite - $KAl_2(Si_3Al)O_{10}(OH)_2$	Calcium Sulfide - CaS	Muscovite- $KAl_2(Si_3Al)O_{10}(F,OH)_2$
Dolomite - $CaMg(CO_3)_2$	Hematite - Fe_2O_3	

Selective contamination of graphite electrode

From XRD and proximate analysis results on the original coal samples used in this study, and their low temperature residues, it was evident that quartz, clay (kaolin and montmorillonite in particular) and pyrite were amongst the more commonly found contaminant mineral phases. Mineral phases also present in high concentrations in the high temperature ash analysis (see Section 3.3.3) include anatase and alumina, which were also selected for contamination studies. Contaminant concentrations between 10-50 wt% with graphite were tested at 500°C and allowed to equilibrate for 30 minutes. Following equilibration repeated potential sweeps were made over the selected potential range; i.e., from the open circuit potential (OCP) of the cell to 0.5 V above the OCP versus the $C/CO_2/CO_3^{2-}$ reference at a scan rate of 5 mV/s with the third consecutive LSV used as a representative scan. Results for all contaminants tested with various contaminant loadings are shown in Figure 32 with a comparison of the achievable current density at two different applied potentials included in Figure 33.

Current density has been normalised in Figure 32 and Figure 33 to reflect the relative surface area of active graphite present at the electrode surface for each contaminant loading. As the amount of contaminant increases, the active area available for electrochemical oxidation decreases and therefore the reaction occurs on a reduced surface area (contaminants are assumed to be electrochemically inactive in the potential range investigated). The normalisation was carried out by calculating the volumetric weighting of each contaminant based on their density and the density of solid graphite. The geometric surface area used to normalise current per unit area was then changed to reflect the relative volumetric proportion of carbon present. This enables assessment of the current produced per unit area of graphite rather than the total surface area exposed to electrolyte.

SEM was carried out on the surface of each electrode material prior to electrochemical testing in order to confirm homogenization at the electrode surface and the normalization method used. Results, shown in Figure 34, show some differences in the distribution of contaminants within the graphite electrode.

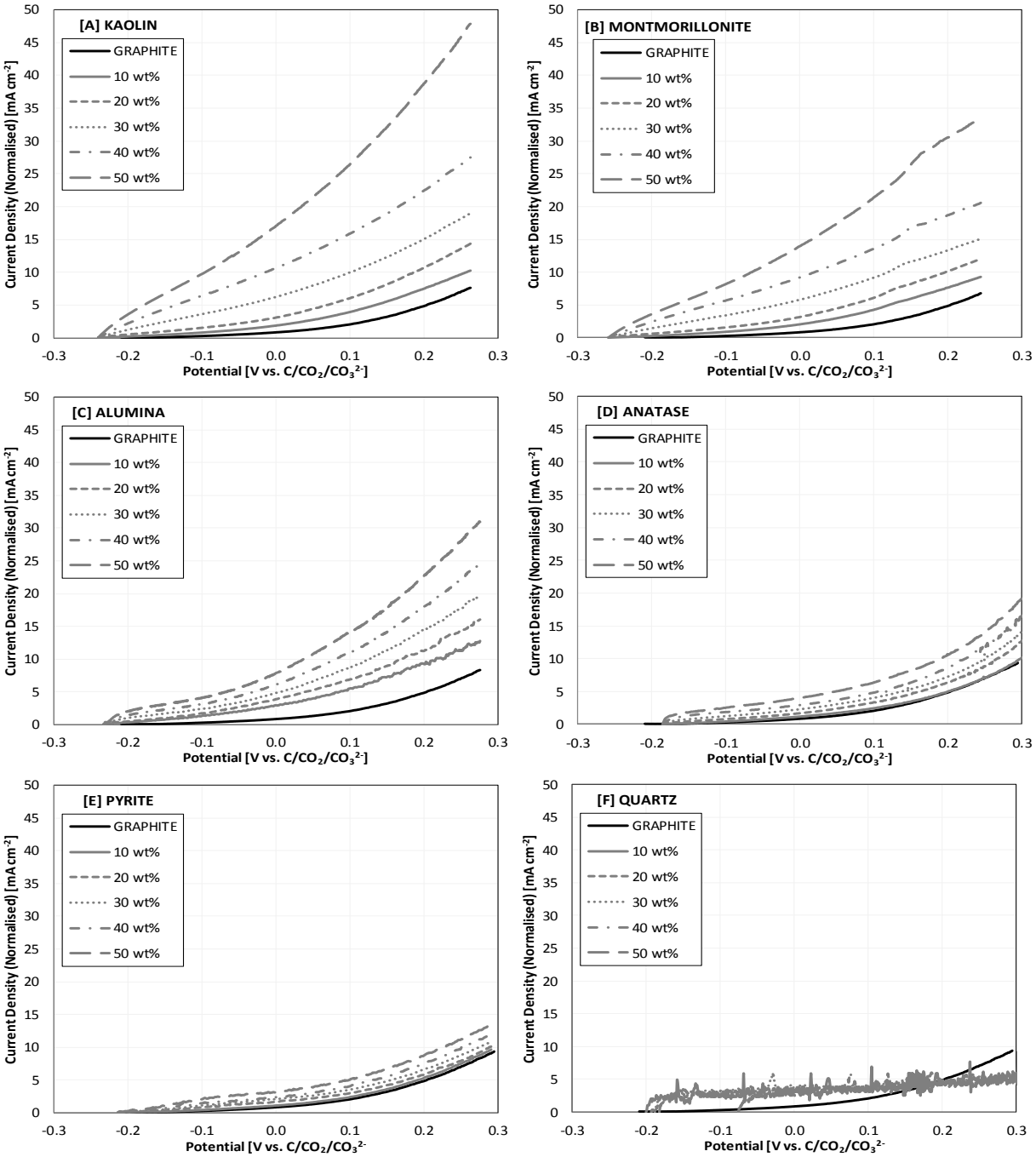

Figure 32: Electrochemical response for graphite contaminated with [A] kaolin, [B] montmorillonite, [C] alumina [D] anatase, [E] pyrite, and [F] quartz.

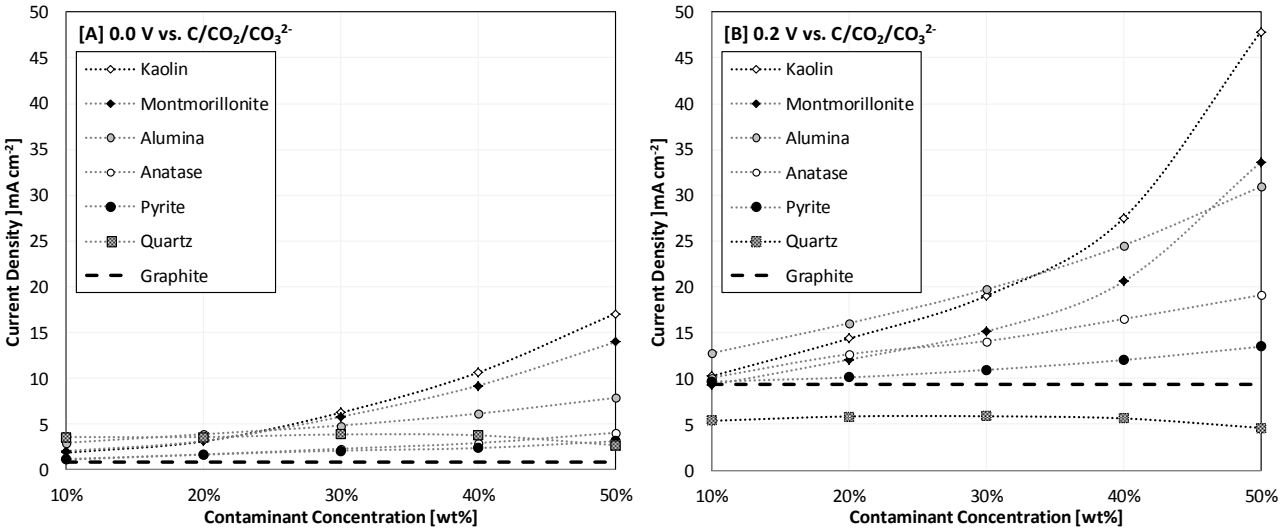

Figure 33: Comparative performance of graphite incorporated with different contaminants (indicated in figure) with current density measured at [A] 0.0 V vs. $C/CO_2/CO_3^{2-}$ and [B] 0.2 V vs. $C/CO_2/CO_3^{2-}$

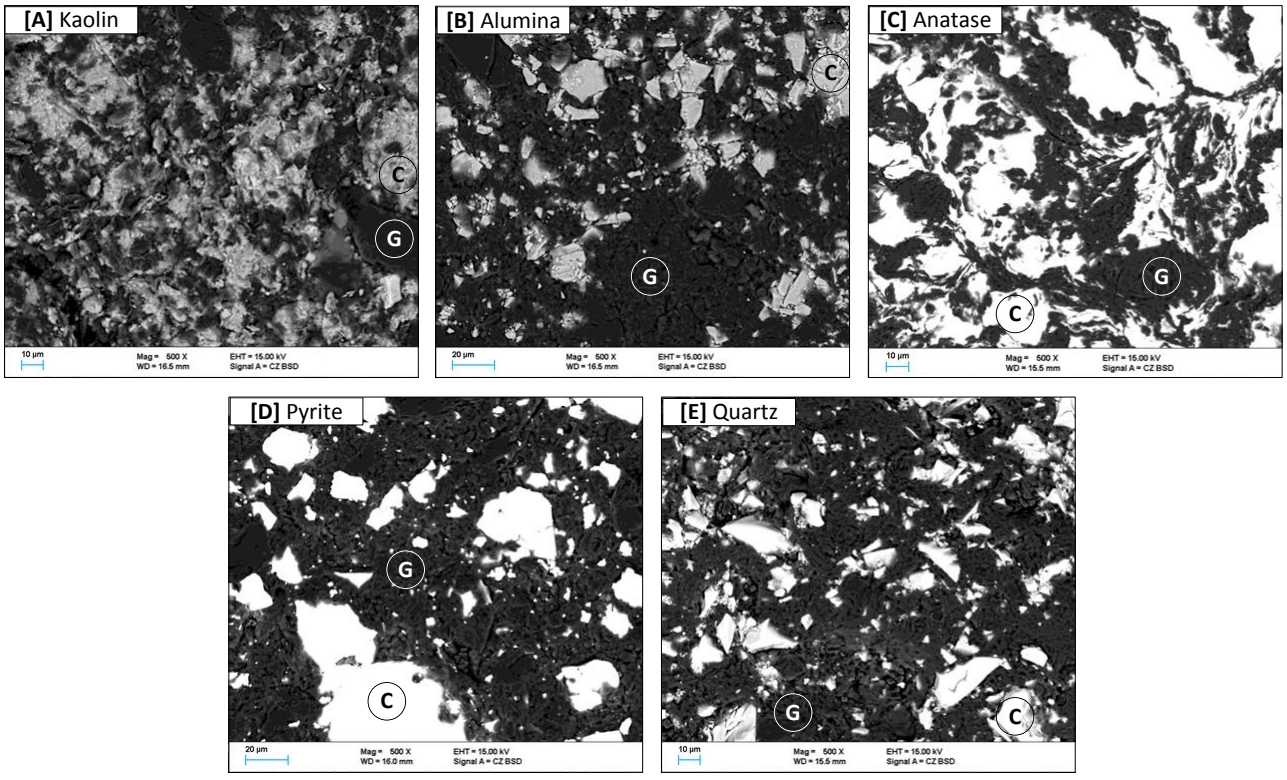

Figure 34: SEM images (500 x magnification) of working electrode surface prior to use with 50wt% contamination of [A] kaolin, [B] alumina, [C] anatase, [D] pyrite and [E] quartz. Areas identified as graphite are indicated with a 'G' while contaminant areas are indicated with a 'C'.

A 500x magnification was used in each case for comparison of the contaminant phases.

SEM images of the surface of the 50 wt% contaminated electrodes confirm that the contaminants are intimately mixed within the graphite material in all cases. However, clear differences in the surface structure are observed dependent on the type of contaminant used.

Kaolin (A) appears to be the most intimately mixed of the contaminants with high dispersion in the graphite. It can be seen that the kaolin contaminant has a particle size in the range of 3-8 μm. However, due to some agglomeration, some 'kaolin rich domains' can be as large as 25 μm. It is likely that the conversion of the kaolin to metakaolin caused a reduction in the particle size and the hardness of the kaolin material, resulting in a more finely and evenly dispersed contaminant from the milling step used to introduce the contaminant into the graphite. Very similar results to that of kaolin were found for montmorillonite.

Quartz and alumina (Figure 34E and B, respectively) appear to be similar in particle size and dispersion, although more graphite rich areas are observed in the case of the alumina. These particulates have a distribution of particle sizes from 4 – 5 μm up to ~45 μm, although average particle sizes appear to rest mostly in the 10-20 μm range.

The anatase contaminant formed larger agglomerated regions, as well as small finely divided particles (see Figure 34C). It is probable that the "marbling" type effect seen in the SEM images is a result of the preparation method used for the SEM. Preparations of the surface of the electrode for the SEM required wet polishing with a very fine abrasive, which would tend to remove the softer graphite material more easily from the surface and smear the anatase into the resulting cavities and clefts. What is evident from the SEM images of the anatase contaminated electrode is the clear difference between a contaminant phase that is significantly smaller than the graphite phase percolating through the graphite particles, rather than the graphite particles percolating through the contaminant phase

Pyrite shows the largest relative particle sizes and therefore the lowest contact between the graphite and contaminant. Pyrite was one of the hardest contaminants (6.5 - 7 mohs scale) and the grinding process used to reduce the particle size of the pyrite material resulted in a large range of particle sizes varying from 3 – 32 μm with a large incidence of particles in the upper range. As a consequence, the pyrite contaminant was expected to have a larger non-uniform particle size distribution compared to the other contaminants within the working electrodes.

The normalisation technique used is therefore thought to over-represent graphite in the case of anatase (current density is likely larger than appears) while under-representing graphite in the case of pyrite addition (current density is likely smaller than shown through normalisation), however in the majority of cases it is a good approximation for determining the active surface area. It can be seen from Figure 32 and Figure 33 that with this normalisation, addition of contaminants to electrodes have a significant effect on the reaction which generally increases with additions of the contaminant.

The electrode contaminated with Kaolin was found to exhibit the largest increase in current density. To further investigate this increase in performance an electrode composed of 25 wt% coal char (pyrolysed at 700°C), 5 wt% kaolin and 70 wt% graphite has been investigated was examined.

A comparison of *i*-*V* response curves for electrodes tested is shown in Figure 35 (left) along with Tafel analysis (right).

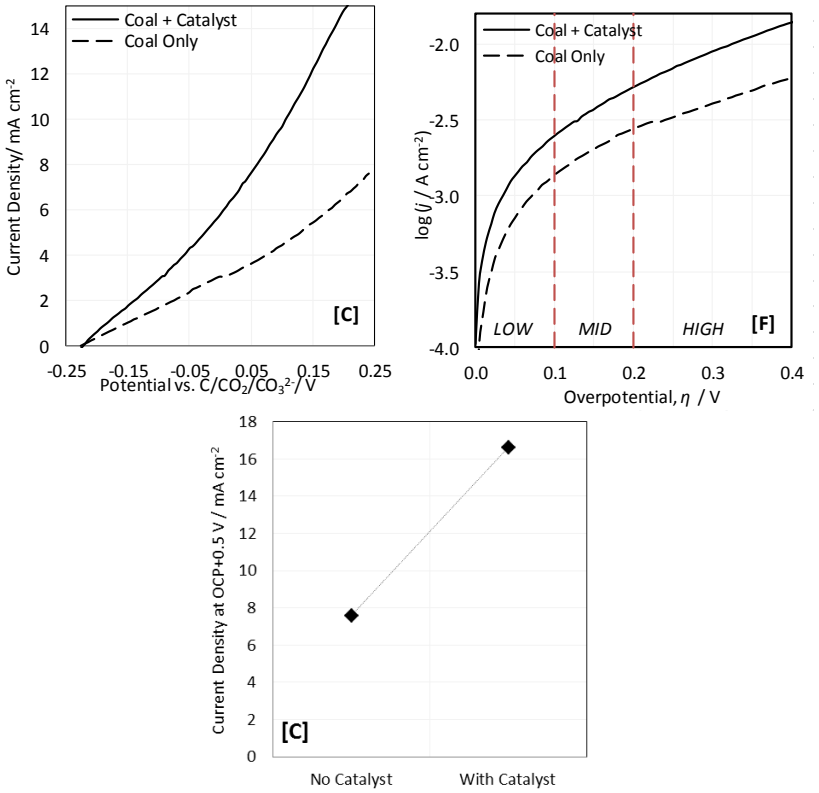

Figure 35: LSV (left) and Tafel Analysis (middle) for solid carbon electrode 25wt% coal char pyrolysed at 700°C with and without addition of 5wt% kaolin catalyst. Comparison of current density at OCP+0.5 V (right)

In this case, the OCP is seen to remain unchanged; however the current density achieved at polarisation of 0.5 V is more than doubled. Considering the doped electrode will have less overall carbon compared to the undoped electrode (95 and 100 wt% respectively), this demonstrates that the catalytic effect of the kaolin when incorporated in a solid carbon electrode is even more pronounced for a coal fuel than observed previously for graphite .

The kaolin doped electrode can be compared to an electrode using coal char pyrolysed at 800°C. This was seen in the previous section to be the most active coal char of the thermal coal pre-treatments investigated and can be seen to display a similar degree of activation to that of the inactive coal with kaolin. The latter however also displays behaviour not previously observed for the electrochemical oxidation in molten carbonate with highly unstable current density showing plateaus and jumps in current. It is likely that these jumps represent gas bubble formation on the carbon electrode since the arrangement of the electrode could result in entrapment of gas bubbles formed; i.e., carbon dioxide and carbon monoxide. This is a well-studied phenomena in terms of bubble formation at carbon anodes in aluminium reduction Hall-Heraoult cells and is possible in the case of carbonate solutions saturated with CO_2, i.e. flowing carbon dioxide atmosphere in this case. Holding the potential within the region of apparent bubble formation on an electrode using coal char formed at 800°C (Figure 36[A]) shows a current density with clear inhibition and activation regions.

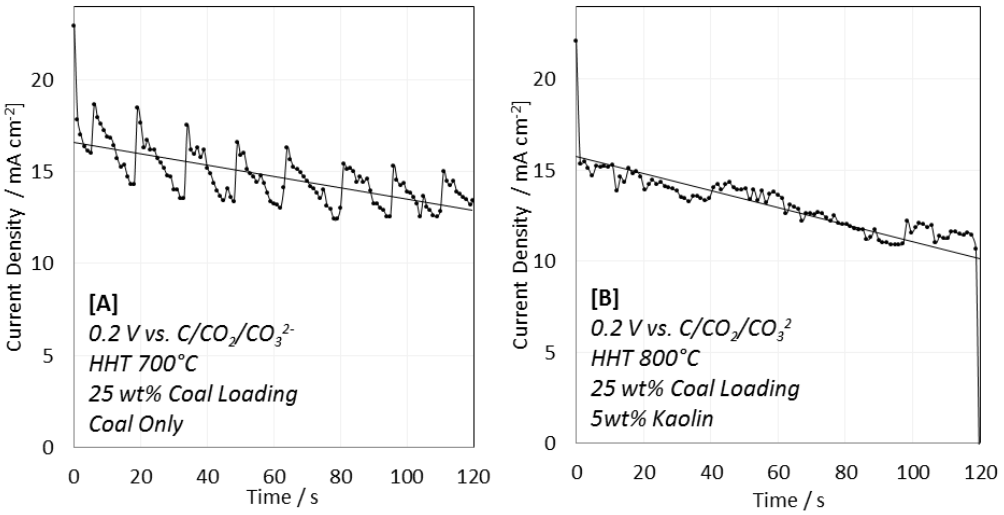

Figure 36: Potential hold results at 0.2 V vs. $C/CO_2/CO_3^{2-}$ for [A] coal char pyrolysed at 800°C (25wt% loading) and [B] coal char pyrolysed at 700°C with the addition of a 5 wt% kaolin

Bubble formation at this electrode could be the result of the relatively high current density observed for the coal char pyrolysed at 800°C, resulting in a higher volume of product gas expected to be formed and therefore enhanced inhibition from reduced surface area. However, this behaviour is not observed for a kaolin doped electrode where the current density achieved is similar to that of the electrode with coal char pyrolysed at 800°C. Both electrodes show a gradual decrease in the current density over a period of 2 minutes; however instability suggestive of bubble formation is only exhibited in the case of the coal char prepared at 800°C, despite the similar oxidation current. This suggests the formation and/or dislodgment of bubbles is different on each electrode, the inclusion of kaolin leading to a possibly less polar surface where the carbon dioxide gas formed might be expected to more easily dislodged, leading to a more stable current with constant gas dislodgement.

Contamination of Carbonate Electrolyte

Complementary to studying the electrochemical effects of contaminating the graphite working electrode, contamination of the electrolyte was also undertaken leaving the anode as solid graphite. The electrolyte was then purposefully contaminated with kaolin, montmorillonite, anatase, alumina, pyrite and quartz. Contamination studies were performed for the addition of both 1 and 5 wt% of contaminant to the electrolyte. The same electrochemical procedure as previously described for solid contaminant investigation was used to evaluate electrochemical performance of the graphite in the presence of the now liquid phase based coal based contaminants.

In contrast to addition of contaminants to the electrode, it was found that for almost all contaminants tested in the electrolyte no discernible change in the current response was seen for graphite electro-oxidation. Differences between LSV curves obtained were no more than normal variation in electrode fabrication procedures. The only contaminant which did show a small change in LSV behaviour was the quartz contaminant. Both the 1 and 5 wt% contaminant loadings had an effect on the *i*-V curve from the graphite working electrode at a scan rate of 5 mV/s, as shown in Figure 37.

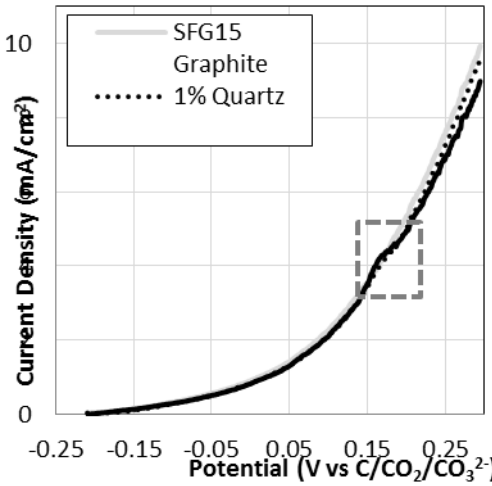

Figure 37: LSV performed on SFG15 graphite electrode pellet using a 5 mV/s scan rate. Electrolyte contaminant loading identified in Figure and region of interest highlighted.

A distinctive feature that can be seen in the i-V curves of the quartz contaminated electrolyte is the emergence of a peak in the current response in the 0.12 – 0.19 V region, indicating another oxidative process occurring at the electrode surface. Following this peak a discernible decrease in the normalised current response was observed, most noticeable in the 5% contaminated electrolyte. This decrease is not significant compared to changes observed on addition of contaminants instead to the solid electrode.

Discussion

Results show a clear interaction of incorporated contaminants with the graphitic carbon in the case of close physical contact; i.e., combined in a solid electrode. The order of activity for contaminants tested shows increased oxidative activity in the order of kaolin > montmorillonite > alumina > anatase > pyrite. Quartz was the only contaminant tested which showed a clear decrease in the oxidative activity of the graphite. The same effects are not observed in the case of other contaminant additions and increased effects are observed for increasing inclusion of contaminants.

Similar response to increasing contaminant concentration can be seen for each contaminant added at both low and high potentials with deviations observed at higher contaminant concentrations for kaolin and montmorillonite which increase beyond response from other contaminants.

The largest enhancement observed for anode contamination was for the pre-treated kaolin, which was also shown to have the most intimate contact with graphite on mixing (Figure 34A). Clear activation of the reaction occurs with increasing kaolin and montmorillonite concentrations, which is especially evident at concentrations >30 wt% in the low potential range (see Figure 33A) where an apparent activation of the oxidation reaction takes place.

The cause of the activation is difficult to determine, although some authors have previously postulated ways in which the anodic oxidation of carbon could be altered mechanistically. For example, the contaminant phase could act as a mediating site for the exchange of O^{2-} species, and possibly catalyse the reaction where the phases meet. Both Li *et al.* [6] and Wang *et al.* [9] note an enhancement on the performance of their test cell when specific metal oxides were introduced to the electrolyte. Li *et al.*, attributed performance enhancement observed for different

carbon sources tested to an increase in surface oxides within the carbon phase [6]. Both kaolin and montmorillonite contain surface oxides [2] and it is possible the oxides within these structures facilitate the adsorption of O^{2-} to the electrode surface and subsequent reaction with neighbouring carbon particles.

Alternatively, the catalytic effect of the contaminants could be a result of contact between the molten electrolyte and the carbon surface. Kaolin and montmorillonite give the biggest performance enhancement when incorporated in high concentrations and were also observed to have the greatest degree of mixing and contact between the graphite and contaminants (see Figure 33 A). Contaminant addition may enable more intimate contact between the molten electrolyte and the carbon by changing the wettability of the electrode surface in regions where the contaminant phase is present. Contact between carbon and carbonate electrolyte was identified as a possible limitation by Chen et. al [10] and was discussed as a possibly limiting issue in a recent review paper[11].

Overall, the effect of the inclusion of quartz to the electrode surface is the most dramatic result since it appeared to almost completely inhibit the oxidation of the graphite present at high potentials (Figure 33B). Given the soluble nature of quartz in the molten carbonate electrolyte [12] it is possible that the quartz contaminant is dissolving and forming a passivating layer at the electrode surface which reduces the CO_3^{2-} ion concentration in a localised area.

Devyatkin *et al*.[12] proposed a series of chemical equilibria that were possible within a molten tertiary eutectic carbonate - SiO_2 mixture, some of which are predicted to occur spontaneously and under non-electrolytic conditions. The reactions proposed by Devyatkin *et al*. between the SiO_2 and the molten carbonate (see Eqns (5) – (7) below), mean that the intermediate species M_2SiO_3 (where M = Li, Na, K) could be present in the electrolyte at the electrode interface causing a different series of electrochemical reactions through which the carbon is oxidised; i.e.,

$$Li_2CO_3 + SiO_2 \rightarrow Li_2SiO_3 + CO_2 \qquad \Delta G = -88.48 \text{ kJ/mol} \qquad \textbf{(17)}$$

$$Na_2CO_3 + SiO_2 \rightarrow Na_2SiO_3 + CO_2 \qquad \Delta G = -46.48 \text{ kJ/mol} \qquad \textbf{(18)}$$

$$K_2CO_3 + SiO_2 \rightarrow K_2SiO_3 + CO_2 \qquad \Delta G = -39.43 \text{ kJ/mol} \qquad \textbf{(19)}$$

An effect of the addition of quartz to the electrolyte was also observed Figure 37 in the form of a small oxidative peak in the 0.12-0.19 mV region. Other impurities were not seen to have any effect on the oxidation reaction of the graphite. Li *et al*. [6] report a notable difference in electrochemical performance with the inclusion of only 8 wt% SiO_2 on the basis of their carbon loading (which equates to 0.6 wt% with respect to the molten carbonate electrolyte), although subtle electrochemical impacts were not able to be observed due to the particulate carbon used for oxidation. This feature in quartz contaminated carbon sources is not discussed in literature relating to coal and utilisation in the DCFC such as Li et al. [6], Cherepy et al. [13] and Vutetakis et al. [14], and is likely overshadowed by mass transport limitations of the cells used in these studies. Devyatkin et al. [12] studied the electrochemical behaviour of SiO_2 in carbonate melts utilising, amongst other electrode types, a glassy carbon electrode. On glassy carbon, the emergence of a peak is seen in the same region of the anodic voltammogram (correcting for reference electrode used and cell temperatures). Furthermore, Devyatkin et al. report no corresponding cathodic process on the working electrode during the reverse potential sweep, indicating that the process is either non-reversible or kinetically very slow. It is suggested from the literature that the process, giving rise to the peak in the anodic sweep, is due to the electrochemical oxidation of silicon carbide, which is thought to form chemically at the electrode

surface during the heat-up procedure. Devyatkin *et al.* further confirm this with a series of experiments in which the carbon content was increased within the molten electrolyte, with reports of forming a black α-SiC coating on the working electrode. This effect could be due to the passivation of the reactive sites of the graphite surface due to SiO_2 formation

Effects of other contaminants were not observed, contrary to results of other authors adding metal oxides to the carbonate melt [6, 9]. Possibly the quiescent nature of the cell used had an effect in this investigation for both the kaolin and montmorillonite since both the clay materials precipitated from the electrolyte, forming a solid deposit on the cell bottom and preventing the materials from coming in contact with the electrode surface.

3.4. Milestone 12: Coal Oxidation Mechanism Characterisation

3.4.1. Milestone Background and Aims

Understanding the oxidation mechanism of the anodic reaction of the DCFC (carbon oxidation) is key fundamental knowledge and can be used to understand system effects and sensitivities. Understanding of the oxidation mechanism can also aid in catalyst development where identification of the rate determining step pinpoints where a catalyst may be applied and its nature. Here we conduct an electro-kinetic analysis of the high temperature carbon oxidation mechanism in an attempt to understand its sensitivities.

3.4.2. Results

A general oxidation mechanism involving single electron transfer steps and transformation of single species per step was envisaged as early as 1981 by Haupin and Frank [15], where the oxidation mechanism of carbon was established within cryolite for the production of aluminium. This mechanism was originally applied to the DCFC by Cherepy et. al. [13] and has been broadly accepted in the literature [11, 16, 17]. Cherepy *et al*. justify the adaptation of Haupin and Frank's mechanism on the basis of the strong dissociation of the ternary carbonate to the O^{2-} ion at the electrode surface [13]. The mechanism proposed is shown in Equations (20)-(26).

Step 1	$C_{SR} + O^{2-} \underset{k_{-1}}{\overset{k_1}{\rightleftarrows}} C_{SR}O^{2-}$	First Adsorption	**(20)**
Step 2	$C_{SR}O^{2-} \underset{k_{-2}}{\overset{k_2}{\rightleftarrows}} C_{SR}O^{-} + e^{-}$	Discharge	**(21)**
Step 3	$C_{SR}O^{-} \underset{k_{-3}}{\overset{k_3}{\rightleftarrows}} C_{SR}O + e^{-}$	Discharge	**(22)**
Step 4	$C_{SR}O + O^{2-} \underset{k_{-4}}{\overset{k_4}{\rightleftarrows}} C_{SR}O_2^{2-}$	Second Adsorption	**(23)**
Step 5	$C_{SR}O_2^{2-} \underset{k_{-5}}{\overset{k_5}{\rightleftarrows}} C_{SR}O_2^{-} + e^{-}$	Discharge	**(24)**
Step 6	$C_{SR}O_2^{-} \underset{k_{-6}}{\overset{k_6}{\rightleftarrows}} C_{SR}O_2 + e^{-}$	Discharge	**(25)**
Step 7	$C_{SR}O_2 \overset{k7}{\leftrightarrow} CO_{2(g)}$	Desorption	**(26)**

Following dissociation of the anion from its carrier (carbonate in the case of the MC-DCFC), the O^{2-} ion is proposed to adsorb at a surface reactive sites on the carbon (C_{SR}). The adsorbed $C_{SR}O^{2-}$ species can then undergo two, single electron transfers to form $C_{SR}O$. The relatively stable $C_{SR}O$ carbon site, it is suggested, then adsorbs a second O^{2-} adsorption to form $C_{SR}O_2^{2-}$. To finish the oxidation reaction the $C_{SR}O_2^{2-}$ species then undergoes two sequential single electron transfer reactions to form $C_{SR}O_2$, which is then discharged from the bulk carbon surface. This sequence has been visualised for the purpose of this work in a schematic, shown in Figure 38.

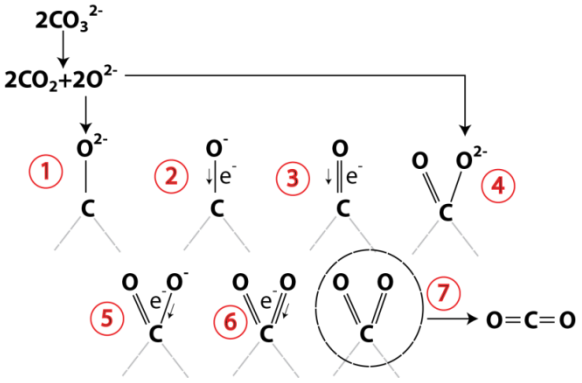

Figure 38: Possible reaction pathway for carbon oxidation from a single reactive surface site.

It is interesting to note that although Eqns (4)-(10) are commonly cited as the reaction pathway, indicating a single reactive surface site, initial representations of the mechanism in fact show adsorption of a single oxide anion to two active carbon sites. This is also shown schematically in Figure 39.

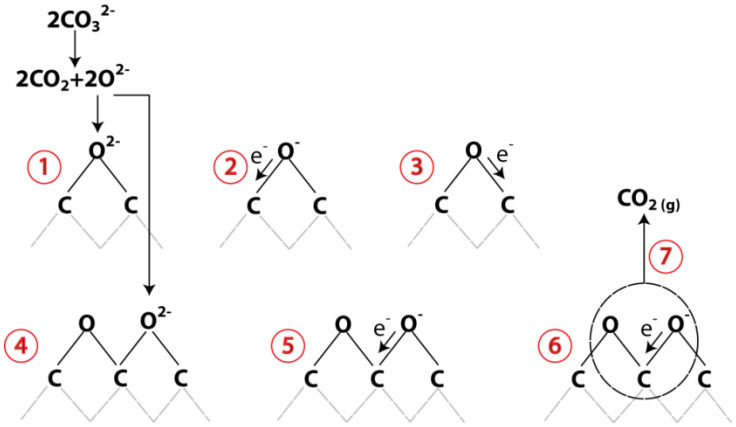

Figure 39: Possible reaction pathway for carbon oxidation from two reactive surface sites (Originally proposed by Cherepy et al. [13])

The adsorption of the oxide anion is shown in to occur over two carbon surface sites initially in a C_2O type adsorption, which was not reflected in the mechanistic proposal developed by Cherepy [13], although a dual reaction site scheme was outlined in the work of Wang et al. [9]. The initial adsorption is followed by a second adsorption, including the first carbon site and an adjacent site in a C_3O_2 arrangement. This arrangement results from proposals made by Cherepy et al. which are consistent with the more fully understood mechanism of the chemical oxidation of carbon in air [18]. It has been proposed that the relative stability of the C_2O group compared to C_3O_2 causes the main reaction product to be carbon dioxide rather than carbon monoxide, which reflects DCFC experimentation where carbon dioxide was found to be the favoured reaction species under most electrochemical conditions. Chemical formation of CO via the Bouduard reaction of carbon and carbon dioxide is thought to occur chemically and only when no potential is directly applied to the carbon species – for example in carbon slurry type arrangements [13, 15].

Regardless of single or double carbon site involvement, the second adsorption step (Eqn

8) has previously been proposed to be kinetically hindered, requiring a considerable over-potential, and has been presented as the rate determining step (RDS) in the carbon oxidation mechanism [9, 13, 15]. This proposal has not been supported by experimental evidence being based instead on the expected difficulty of physically attaching a second anion to the electrode surface. It is thought that after fast initial adsorption of oxide to preferred sites, liberation of CO_2 cannot proceed until less favourable sites located next to the initial adsorption are also occupied. This has been suggested to result in an increase in the driving potential required for oxidation and therefore a shift in the OCP away from that calculated thermodynamically [19].

In this Milestone, expected kinetic parameters for the proposed oxidation mechanism have firstly been derived using the Butler-Volmer approach for oxidation steps laid out in Eqns (20)-(26). Parameters of specific interest include the Tafel slope (*b*) and the anodic transfer coefficient (α_a) as these are easily measured using the experimental design developed in previous work [20]. These derived parameters are then compared to experimental data gathered on carbon based electrodes in order to give experimental evidence to kinetic limitations proposed.

Derivation of Rate Constant Expressions

The proposed mechanism through which the electrochemical oxidation of carbon is thought to occur is a series of chemical and electrochemical (charge transfer) steps ultimately resulting in the evolution of CO_2 (Eqns (20)-(26)). The Butler-Volmer model and equation for electrode kinetics allows the calculation of a predicted electrical current on an electrode as a function of the potential of that electrode. The high field approximation takes into account only the anodic region of the voltammogram (away from equilibrium) and can be used for assessment of the oxidation of carbon. The Butler Volmer high field approximation can be written as:

$$i = i_o \left\{ \exp\left(\frac{\alpha_a \eta F}{RT}\right) \right\} \text{ or} \qquad \textbf{(27)}$$

$$i = nFv = nFk_a[C_A]\left\{ \exp\left(\frac{(1-\alpha)\eta F}{RT}\right) \right\} \qquad \textbf{(28)}$$

where *i* is the electrode current density (A/m^2), i_O is the exchange current density (A/m^2), α is the charge transfer coefficient, η is the overpotential (*V*), *F* is the faradaic constant, *R* is the universal gas constant, *T* is the absolute temperature (K), k_a is the anodic reaction rate constant, C_A is the concentration of the reactant being oxidised, and v is the rate of reaction (mol/s). The value of (1-α) can also be referred to a α_a which is the overall anodic charge transfer coefficient.

Through the application of the high field approximated Butler-Volmer equation on the proposed mechanism, the transfer coefficient α_a can be calculated sequentially assuming each step of the electrochemical reaction mechanism is the rate determining step (RDS). Further assumptions that this approach makes are that all reactions/steps before the RDS are in quasi-equilibrium, there is only one reaction or step that controls the rate of the reaction, no step can have more than two chemical reactants, and that charge transfer steps are a one electron transfer step only.

(i) The rate of reaction (*v*) depends on three main driving forces including:
(ii) The rate constant (k_a), specific to the reaction taking place.
(iii) The amount of the reacting species available. This can be either the concentration of the ionic species in solution, available surface sites for adsorption or alternatively the coverage of the electrode surface with a species formed in previous steps.
(iv) If the reaction is electrochemical, it will also have a potential dependent driving force (involves the transfer coefficient).

The reaction scheme shown in Eqns (20)-(26) is heavily dependent on species adsorption and transformation at the carbon surface. Therefore, the surface coverage of the O^{2-} species on the reactive carbon sites needs to be defined. It can be assumed that not all of the reactive carbon sites are occupied at steady state and there is equilibrium between the occupied and non-occupied sites, and the fraction of occupied reactive sites can be expressed as a function of the surface coverage; i.e.,

$$\theta_T = \frac{\Gamma}{\Gamma_{max}} \quad \textbf{(29)}$$

where θ_T indicates the coverage of the electrode with adsorbed species, Γ the actual surface coverage of species on the active sites and Γ_{max} is the total number of reaction sites. It should be noted that Γ_{max} varies considerably depending on the carbon type used. In the case of graphite, this will be much smaller than a more porous and disordered material such as activated carbon or even coal [6, 21].

The surface coverage (θ_T) can be further defined as the sum of the occupied reactive sites throughout the entire reaction mechanism as Steps (1) - (7) occur through the same reactive site, i.e.,

$$\theta_T = \theta_{C_{SR}O^{2-}} + \theta_{C_{SR}O^-} + \theta_{C_{SR}O} + \theta_{C_{SR}O_2^{2-}} + \theta_{C_{SR}O_2^-} + \theta_{C_{SR}O_2} \quad \textbf{(30)}$$

At a point far from the equilibrium potential where the anodic oxidation is occurring at steady state, it is assumed for this analysis that the coverage of the electrode (θ_T) does not change and that, beyond this point, the total coverage will not change with increasing potential. It is further noted that θ_T will tend towards being equal to the coverage of species involved in the rate determining step as this species will remain at the electrode surface for a longer period of time than other more quickly consumed reactants.

The output of this analysis is a current prediction based on which step of the oxidation mechanism is the rate determining step (RDS). A summary of these outputs is shown in Table 7. Here the Tafel slope was calculated using constants R (universal gas constant) and F (Faradays constant) with a temperature of 500°C.

This data can be used to analyse experimental outputs for any molten carbonate systems to compare observed outputs with those predicted using the proposed mechanism of Cherepy et. al. [13] and the derivation carried out here. Generally, the Tafel slope and transfer coefficient are used to determine the relative rate of charge transfer for a specific reaction. Changes in the Tafel slope can indicate changes in the reaction mechanism since this will be related to a change in the charge transfer rate at the electrode surface and may be indicative of a changed RDS or mechanistic pathway. In this work, the Tafel slope and anodic transfer coefficient have been used for comparison to theoretically derived values in order to indicate possible rate determining pathways of the oxidation reaction.

Mechanistic Analysis using Fixed-Carbon Working Electrodes

LSV was carried out on both graphite and coal based working electrodes in order to observe changes to the Tafel behaviour of the respective carbon types. The LSV and respective Tafel plot for a pure graphite working electrode are shown in Figure 40.

Table 7: Equations derived for prediction of current, transfer coefficient and Tafel slope for each step as the RDS.

RDS	Predicted Current	α_a	$\partial V/\partial \log(i)$
(1)	$i_1 = 4Fk_1[O^{2-}](1-\theta_T)$	-	-

(2)	$i_2 = \frac{4Fk_2k_1}{k_{-1}}[O^{2-}](1-\theta_T)\,exp\left\{\frac{(1-\alpha)VF}{RT}\right\}$	0.5	0.307
(3)	$i_3 = \frac{4Fk_3k_2k_1}{k_{-2}k_{-1}}[O^{2-}](1-\theta_T)\,exp\left\{\frac{(2-\alpha)VF}{RT}\right\}$	1.5	0.102
(4)	$i_4 = \frac{4Fk_4k_3k_2k_1}{k_{-3}k_{-2}k_{-1}}[O^{2-}]^2(1-\theta_T)\,exp\left\{\frac{2VF}{RT}\right\}$	2.0	0.077
(5)	$i_5 = \frac{4Fk_5k_4k_3k_2k_1}{k_{-4}k_{-3}k_{-2}k_{-1}}[O^{2-}]^2(1-\theta_T)\,exp\left\{\frac{(3-\alpha)VF}{RT}\right\}$	2.5	0.061
(6)	$i_6 = \frac{4Fk_6k_5k_4k_3k_2k_1}{k_{-5}k_{-4}k_{-3}k_{-2}k_{-1}}[O^{2-}]^2(1-\theta_T)\,exp\left\{\frac{(4-\alpha)VF}{RT}\right\}$	3.5	0.044

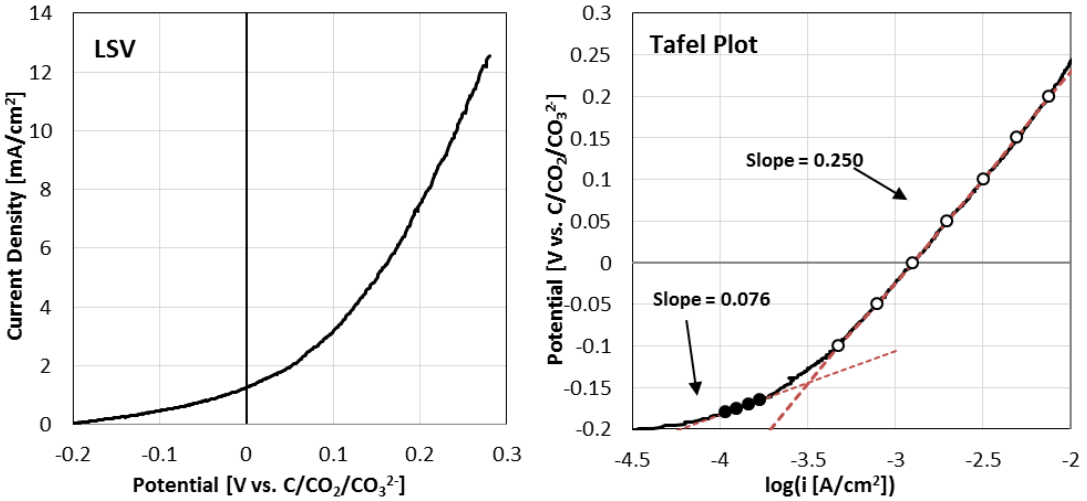

Figure 40: Graphite working electrode oxidation 1 mV/s, 500°C, Li/Na/K eutectic

The LSV behaviour for the electrochemical arrangement used to produce Figure 40 has previously been observed to be highly reproducible and stable [20]. Tafel analysis reveals two oxidation regions. The first is at low polarisation, close to the reversible potential of the system. The second continues over a wide potential region (between -0.1 V to 0.2 V vs $C/CO_2/CO_3^{2-}$) and is reflective of the main oxidation reaction occurring on the graphite electrode. Results shown here are consistent with the analysis of Cooper et al. who found two distinct oxidation regions occurring over experiments conducted by others under widely varied conditions [22]. However, Cooper et al. did not examine Tafel behaviour and instead suggested an inflection point from polarisation curves.

Results for the performance of a coal based working electrode are shown in Figure 41.

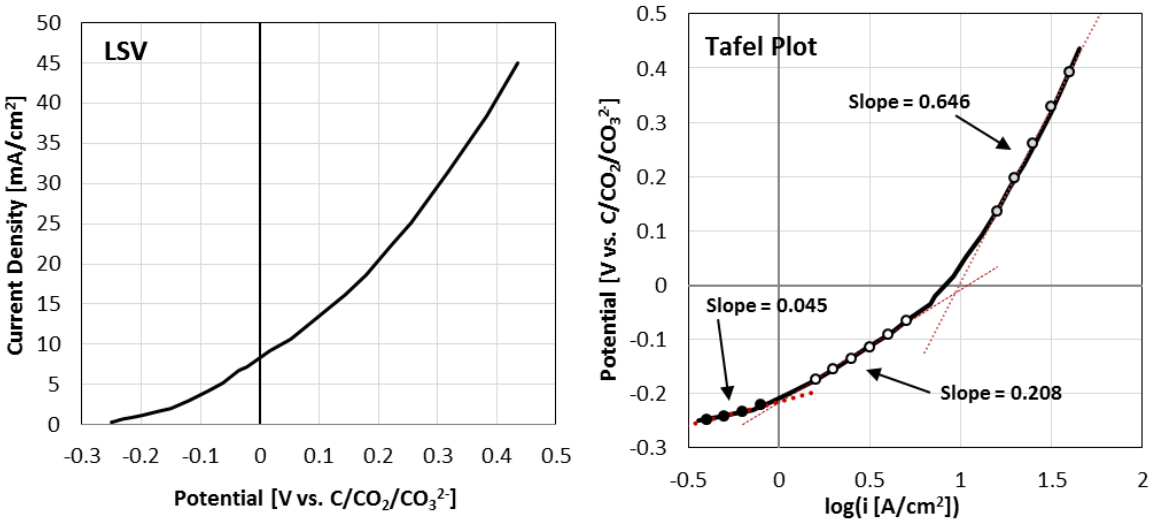

Figure 41: Coal based working electrode oxidation 1 mV/s, 500°C, Li/Na/K eutectic.

The coal based working electrode far outperforms that of the graphite with close to a two-fold increase in current density (9.97 and 19.95 mA/cm^2 at 0.2 V vs $C/CO_2/CO_3^{2-}$ on graphite and coal respectively). The improved performance of coal materials compared to graphite has not been observed to this extent previously, although improved behaviour on carbon with high surface functionalization has been previously investigated and found to have improved oxidative behaviour compared to graphitic counterparts [21].

Coal also shows different Tafel behaviour. In this case there are three clear Tafel regions including a low, mid and high potentials. The mid and high potential regions make up the majority of the oxidative activity occurring on the electrode while the low potential region may not have reached equilibrium where the Butler-Volmer model applies. A summary of observed Tafel slopes along with calculated anodic transfer coefficient and corresponding RDS is given in Table 8 for both graphite and coal working electrodes.

Table 8: Summary of Tafel behaviour, anodic transfer coefficient and rate determining step of the anodic oxidation on graphite and coal

	POTENTIAL REGION	δV/δlog(i)	α_a	*RDS*
GRAPHITE	LOW (<0.1 V)	0.076	2	Step 4
	HIGH (0.1<E<0.3)	0.250	0.6	Step 2-3
COAL	LOW (<-0.2 V)	0.045	3.5	Step 6
	MID (-0.2<E<0 V)	0.208	0.74	Step 2-3
	HIGH (0.4<E<0.1	0.646	n/a	n/a

It can be seen in Table 8 that the RDS for coal and graphite varies depending on the potential region. Under low polarisation, both materials tend towards limiting steps related to the second oxygen anion adsorption step, as previously suggested for the mechanism [9]. However the major RDS for graphite appears to fall within the region of the initial charge transfer. This is also the case for the mid-range potential region for coal. Oxidation on coal also has a further reaction region where the Tafel slope and anodic transfer coefficient do not fall within the range predicted by the derivation carried out here. This may be a result of variation in the coal surface

as it is consumed, however is more likely to stem from a change in the reaction mechanism.

All assumptions relating to the oxidation mechanism have previously assumed that the mechanism involves the oxide anion and that fast dissociation of the oxide in the carbonate melt occurs at the electrode double layer. However, it may be that the carbonate is in fact directly involved in the oxidation without dissociation to its oxide anion in the case of a carbonate melt. This could involve direct adsorption of the carbonate to the electrode surface and subsequent dissociation, or could be more complex involving replacement of surface functional groups. Since the change is specific to coal and not observed on graphite, it is likely to be related to the functionalised nature of the carbon undergoing oxidation.

3.5. Milestone 13: Electrolyte Composition Design

3.5.1. Milestone Background and Aims

The composition of the molten carbonate has the ability to impact on the performance of the DCFC for reasons outlined in Milestone 7 (thermal and electrochemical). The eutectic composition (mixture of lowest melting temperature) has been chosen for investigations, however variation of the eutectic may result in more favourable outcomes electrochemically at the cost of thermal inputs (change in dissociation and dissolution of oxide anions, change in wetting characteristics of molten carbonate etc). It is therefore of interest to test both thermal and electrochemical properties of various eutectic mixtures in order to ensure the composition used on a larger scale is the most ideal both thermally and electrochemically.

3.5.2. Experimental Methods

TGA and DTA

As described in Section 3.1.2, TGA is a useful technique for measuring the mass change of a sample over time under a controlled temperature and under a gaseous atmosphere. This is measured as the change in weight of a small sample compared to a stable, unchanging reference. Differential Thermal Analysis (DTA) however is used to measure the heat flow of the sample compared to the reference. This gives an energy output or input of the sample representative of an exo or endo thermic reaction respectively. In this way, the phase change of an unchanging mass can be examined through the heat input or output required by the reaction which causes the sample to be different than the unchanging reference material (α-alumina has been used in all cases here). Using a controlled temperature program identical to that outlined in Section 3.1.2 for examination of the effect of impurity addition to thermal properties, the thermal behaviour of 6 carbonate compositions around the eutectic composition have been examined. Calculations for the heating temperature are taken at the temperature where the DTA response returns to zero on a normalised scale, i.e. 100% conversion of solid to liquid. This is an acceptable method for determining the melt temperature in this case as the heating rate used was slow enough to consider the melt to be at equilibrium.

Carbonate Mixture Preparation

Carbonate mixtures were prepared from lithium, sodium and potassium carbonates supplied from Sigma Aldrich. Carbonates were dried in an oven at 110°C prior to weighing to ensure no moisture was contained in the sample, which can lead to error in composition of mixtures. Carbonates were mixed together manually by tumbling them together for a period of 20 minutes initially. Following tumbling, mixtures were combined by hand using a mortar and pestle to ensure good mixing. In one case, the carbonate mixture was also ball milled to ensure thorough mixing and en even consistency.

DTA analysis was conducted on a small carbonate sample size (<1 g) which was added to an aluminium crucible as a powder (unfused). Electrochemistry was conducted in a mixture of 400 g which was fused at 600°C and cooled to room temperature prior to use to ensure consistency. All mixtures chosen fell under a melting temperature of 500°C.

Electrochemistry

The electrochemical arrangement for testing of the effect of carbonate mixtures on graphite oxidation is the DCFC half-cell anode, outlined in 3.6.2. Graphite working electrodes were used to ensure consistency with SFG44 graphite from Timcal, Switzerland used. Electrochemical

procedures included equilibration of the graphite electrode in the carbonate for a period of 1 hour at open circuit potential to ensure good wetting of the carbonate. The LSV was conducted following this and several scans were repeated with the OCP measured in between to ensure consistency. The final experiment consisted of holding the potential at 0.2 V for 90 seconds to determine the steady state current.

3.5.3. Results

Carbonate Mixture Compositions

From a ternary phase diagram of lithium, sodium and potassium carbonate, the eutectic mixture (mixture of lowest melting point) was used as the centre of a study of 6 other ternary compositions. These were chosen at a 10% radius to the initial composition point on the ternary diagram indicating the eutectic point. The base and resulting carbonate compositions are indicated on the ternary diagram in Figure 42.

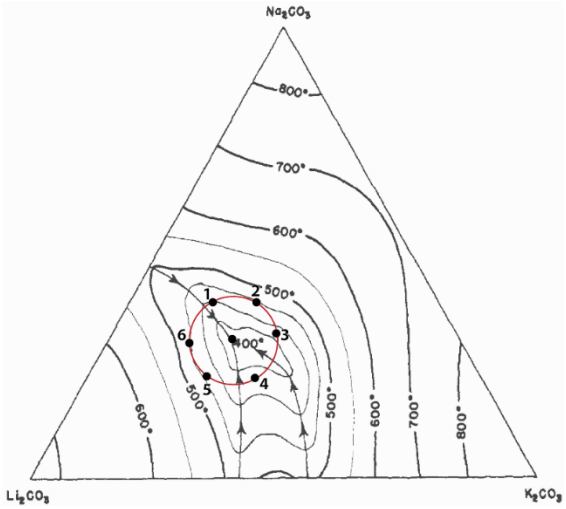

Figure 42: Ternary diagram [1] used as the basis for the different carbonate compositions analysed.

The mole percentages for each carbonate mixture were calculated for each of these 6 points from interpolation of the ternary diagram. Final mixtures prepared are shown in Table 9.

Table 9: Resulting eutectic compositions with conversion to mass to be analysed with 1 to 6 at a difference of 10% along with the eutectic composition

Mixture	Percentage composition		
	Li_2CO_3 [mol%]	Na_2CO_3 [mol%]	K_2CO_3 [mol%]
EUTECTIC	43.5	31.5	25.0
CM#1	44.0	39.0	17.0
CM#2	36.0	39.2	24.8
CM#3	35.9	32.0	32.1
CM#4	44.4	22.0	33.6
CM#5	53.3	22.6	24.1
CM#6	53.4	30.2	16.4

Thermal Behaviour of Carbonate Mixtures

Each sample was placed in the TG/DTA and the DTA response was analysed to determine the melting point and activation energy of the carbonate mixtures. Figure 43 shows the 7 carbonate mixtures graphed as the normalised, baseline corrected DTA response in microvolts per gram as a function of the sample temperature.

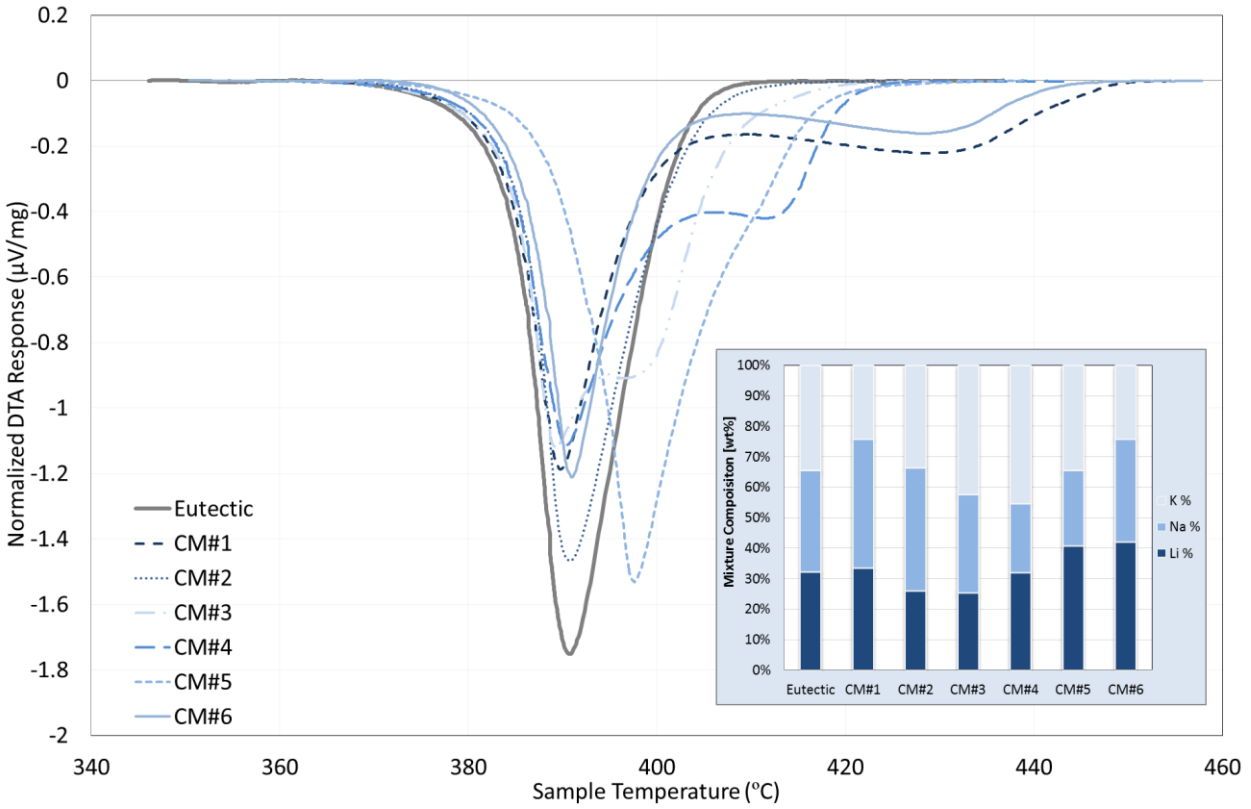

Figure 43: Normalized DTA response for each carbonate mixture investigated (temperature increasing). Inset – relative weight percent of each cation carbonate in mixture

Thermal behaviour varied from the expected single melting peak observed for the eutectic composition with the appearance of secondary peaks, in some cases showing a substantial tail. It was originally thought that this may be a result of incomplete mixing of the carbonates and therefore formation of separate phases within in the melt. Carbonate Mixture #4 in particular showed several peaks initially for a tumbled mixture and as a result of this several mixing methods were trialled to determine the effect of incomplete mixing on the thermal behaviour. Results for carbonate mixture #4 which has been (1) tumbled only, (2) tumbled and mixed with mortar and pestle and (3) ball milled are shown in Figure 44.

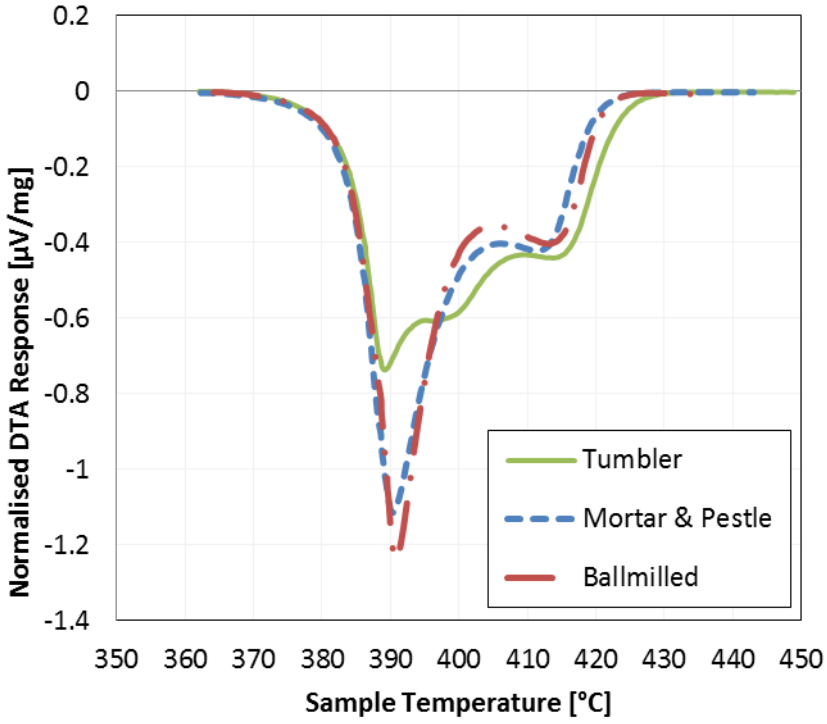

Figure 44: DTA response for Carbonate Mixture #4 prepared using different mixing methods

The shape of the DTA response is shown in Figure 44 to be dependent to some extent on the method of mixing with an extra DTA peak observed in the case of the least homogenised sample. However, the difference between using a mortar and pestle and ball milling is minimal. Results in are therefore that of a sample which has been homogenised using a mortar and pestle.

The melting point for each eutectic was taken to be when the solid to liquid phase conversion had reached 100%, hence the melting point of the eutectic mixture would be the final DTA response that reached zero indicating no more phase change and a fully liquid melt. This was done in order to incorporate the prominent secondary peaks, which as a function of the DTA response indicated a remaining solid phase. The resulting melting point measured is compared with the literature value approximated from the ternary diagram (Figure 42) in Figure 45.

Results measured are generally in agreement with literature values for the experimental melting points observed. It should be noted that literature values are only approximated from the ternary diagram and some measurement error may be possible from the estimation technique used to determine the literature values. Further, literature data was interpolated and not all points were measured, meaning some variation can occur from this also. The method for determining the melting temperature in the literature was also not as accurate as that used in this case since the literature method involved visual observations of seeding behaviour.

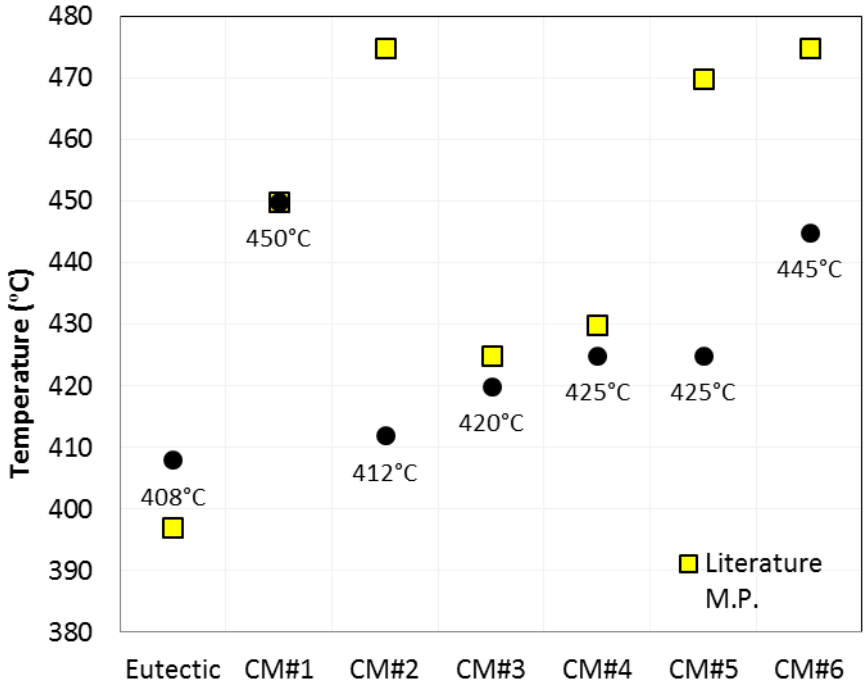

Figure 45: Comparison of literature and experimental melting points for each eutectic mixture.

The appearance of double peaks is thought to be related to reasons also outlined in Section 3.1.3 which describes the impacts of different ions contained in the melt on the thermal behaviour of the mixture. Since the molar ratio is changed to be uneven for the carbonate mixtures investigated, the prevalence of different cations (Li/K/Na) is thought to impact on the melt behaviour.

The activation energy for the carbonate mixtures was also calculated with use of a model previously outlined. The solid to liquid phase conversion is modelled as percentage vs the sample temperature based on initial estimated activation energy. The experimental conversion percentage is then compared against the model and an error is calculated. Figures 46 and 47 show the relative accuracy of the experimental results in relation to the model for two carbonate mixtures.

The influence of the broad secondary peak is clearly seen when fitting the conversion model in the case of carbonate mix #6 (Figure 47). The experimental conversion does not show typical first order behaviour and therefore means the conversion is skewed away from the model. The fit in the case of carbonate mixture 1 and 6 therefore gives high error in the fit (25%) and this is carried through to the activation energy error.

Calculated activation energies for each carbonate mixture are shown in Figure 48, note that error for Carbonate Mixture 1 and 6 is expected to have high error while other mixtures are modelled well.

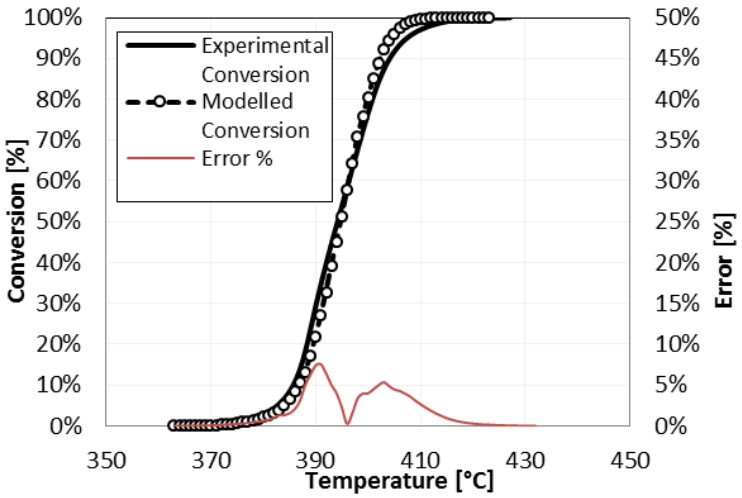

Figure 46: Comparison of modelled and experimental conversion % for carbonate mixture #3, with a max error of 8%.

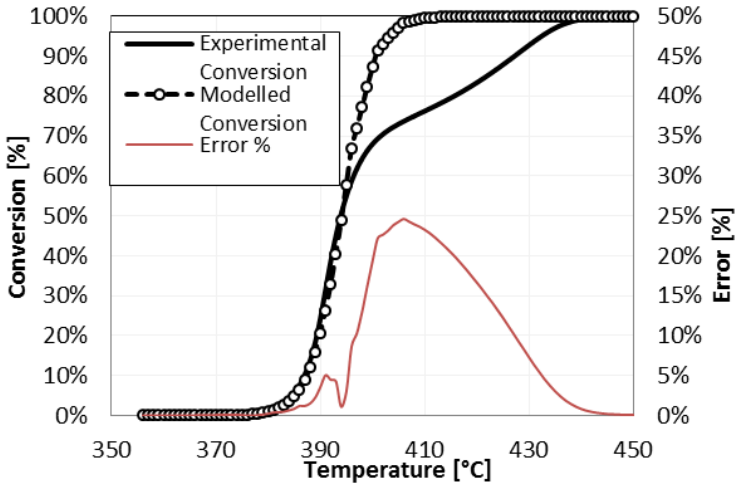

Figure 47: Comparison of modelled and experimental conversion % for carbonate mixture # 6, with a max error of 25%.

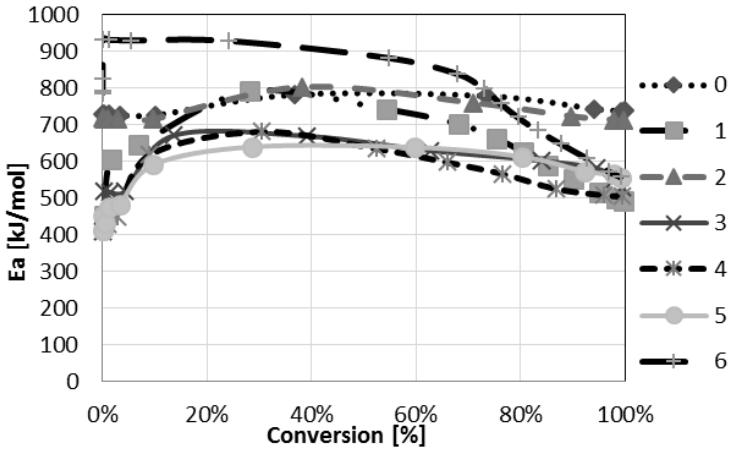

Figure 48: Activation energy as a function of solid to liquid phase conversion for each carbonate mixture.

Conversion energy can be seen to vary somewhat for each carbonate mixture. This is expected since changing the melting temperature will change the required energy for melting. Interestingly, although the melt temperature increases for mixtures beyond the eutectic, less energy overall is required for the different carbonate mixtures leading to a lower activation energy in some cases. This means at the same temperature (above the melting point) it will take the eutectic mixture longer to reach equilibrium than other carbonate mixtures which will impact on the energy required for initially heating the DCFC to reaction temperature. In the case of a continuous plant this would represent a large impact on overall operation, however if continuous cooling and heating of carbonate is required could result in considerable energy differences of the mixtures.

Electrochemical Investigation

The impact of variation to the carbonate molten electrolyte on graphite electro-oxidation was investigated. The eutectic composition has been used previously in both the literature and in work carried out by our group since it has the lowest melting temperature of any carbonate combination. However, the effect of this carbonate carrier on the oxidation reaction has not been investigated previously. Therefore several carbonate mixtures were prepared and tested in the half-cell DCFC to determine the impact of changing the composition. Results for carbonate mixtures #1 to #4 are shown in Figure 49 compared to behaviour in the eutectic composition.

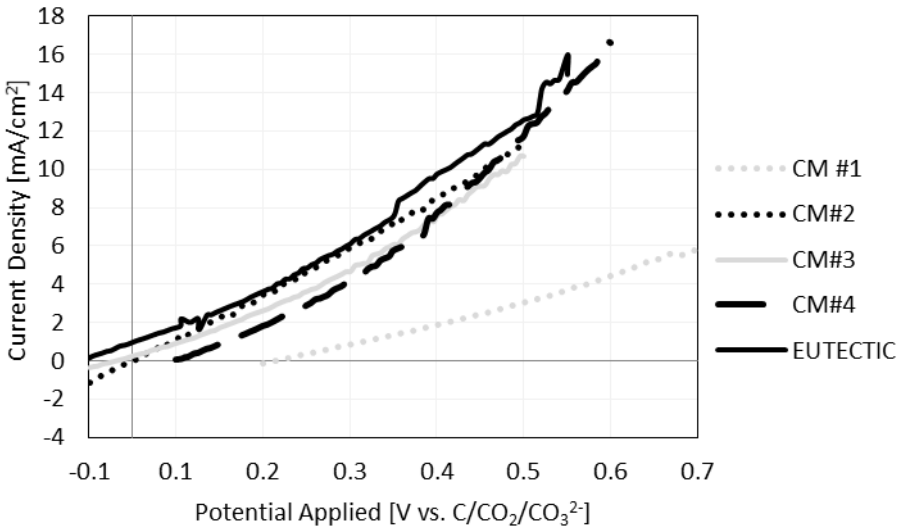

Figure 49: Electrochemical behaviour of graphitic carbon oxidised in different carbonate mixtures. LSV at 5 mV/s (600°C)

Interestingly, results do vary however the eutectic composition shows the most favourable behaviour with a low OCP and comparable current density. The largest difference in behaviour is observed from carbonate mixture #1 which has the highest melting temperature of mixtures examined in Figure 49 (see Figure 45). This is somewhat unexpected as at temperatures examined (600°C) the carbonate will be completely liquid and viscosity effects will be minor. This suggests an electrochemical factor as the reason for variation. This could potentially be the method of oxide migration/diffusion to the anode surface, dissociation of oxide at the electrode surface, solubility of carbon dioxide in the carbonate solution for example.

It is difficult to know at this stage the origin of the observation limitation in Figure 49 is, however it is clear that optimisation of the DCFC should include consideration of the electrochemical impact of the molten carbonate medium. In the case of a ternary carbonate, the best electrochemical response will be observed for the eutectic composition. However, that is only for the mixtures investigated and in fact a more suitable medium may exist. Until fast throughput screening of compositions is possible, it will be difficult to determine this without further detailed study.

3.5.4. Conclusions

Activity of carbon oxidation depends on many factors. It has been demonstrated here that one of these is the molten carbonate composition. Varying the ratio of cations in the mixture heavily influences not only thermal behaviour of the anode compartment (including melting temperature and activation energy of melting) but also the electrochemical activity of a graphite electrode towards oxidation. The inhibition observed here for the oxidation reaction in specific combinations of molten carbonate is unprecedented and has not previously been investigated or even commented on in literature regarding the DCFC. It has been shown that this is possibly a major oversight since some research groups use only binary carbonate mixtures which have far higher melting temperatures than the carbonate mixtures observed here. This thermal variation is likely to result in electrochemical change and results from these binary systems might be limited by the carbonate media as much as by any other system variable which is the subject of the study.

Of the mixtures studied to date it has been seen here that the most advantageous carbonate mixture for electrochemical activity is indeed the eutectic carbonate mixture, which has been used in other milestone investigations by our group and will continue to be the focus of our research.

Summary of Fundamental Outcomes

Fundamental outcomes from this project can be summarized as follows:

(i) Electrolyte Composition: The experiments conducted here focus on the role that contaminants play on the behaviour of a ternary molten carbonate electrolyte. Common coal impurities were included into the electrolyte and the effects of these impurities on the speciation and melt-freeze characteristics of the electrolyte were examined. All of the impurities had an effect on the melt temperature of the electrolyte, causing changes in the melt temperature in either direction; i.e., either raising or lowering the melting temperature. This also indicates that impurities were dissolved into the electrolyte, although the rate at which this occurred was not the same for each impurity examined. Dissolution of these coal impurities into the electrolyte had the potential to influence the electrochemical behaviour of the coal oxidation; however, this effect was found to be minimal. Electrolyte composition is an important design characteristic for a commercial DCFC because the dissolution of impurities into the electrolyte will eventually reach saturation, and so the electrolyte will need regenerating to remove the impurities, otherwise impurity precipitation will occur within the DCFC, and it is believed that this will be detrimental for DCFC behaviour. However, it also represents an opportunity to reclaim value added materials from the electrolyte component.

(ii) Carbon Properties: As the fuel for the DCFC, the properties of the carbon source can have a big impact on DCFC performance. Here we have examined a range of different carbon samples, in particular different coal types and their pre-pyrolysis on anode performance in the DCFC. The baseline material used for comparison in all of this work was graphite because of its thermodynamic stability. All coal samples examined performed better in the DCFC anode because of their lower stability and hence higher activity. A particularly significant comparison made in this milestone was between a thermal and coking coal, which had different structures and impurity contents. It was found that a thermal pre-treatment activated the coals, although this was different for both coal samples. Thermal pre-treatment had the effect of removing volatiles, functionality and graphitizing the coal samples. At lower pre-treatment temperatures volatiles were removed but the coal was not sufficiently conductive to achieve good electrode performance. At higher pre-treatment temperatures significant loss of functionality occurred together with graphitization of the coal. While this improved coal conductivity, it also lowered activity because some functionality is required for high activity. The initial difference between thermal and coking coals was primarily their ash content, and it would seem apparent that this influenced their electrochemical activity and optimal pre-treatment contact.

(iii) Catalysis: In any fuel cell system catalysis is critical since it improves the energy and power densities of the fuel cell. The DCFC is no exception, and in this work we have examined extensively the role that various impurities in the coal ash have on improving coal oxidation kinetics and hence anode performance. It was found that most common impurities in coal improve anode performance, and in the worst case, there was no effect on performance. The catalyst that improved oxidation kinetics the most was the clay, kaolin, which had a profound effect on performance. For example, a 5 wt% loading of kaolin in coal doubled anode performance, which is very significant. It was also found that the distribution of kaolin in the anode influences performance, suggesting that the interface between the kaolin and coal was critical. This suggests that the kaolin catalyzes the transfer of oxide from the electrolyte to the coal which is a new finding.

(iv) Coal Oxidation Mechanism: Significant mechanistic studies were also carried out the examine in more detail the experimental sensitivities of the coal oxidation mechanism. To enable this a thorough electrochemical kinetic analysis of the oxidation mechanism was carried out, assuming that each step in the mechanism was the rate determining step for electrochemical oxidation. The predicted kinetic parameters resulting from the analysis and its application to electrochemical data enabled identification of the rate determining step as a function of active material type and condition, as well as at the applied overpotential. In most instances the first adsorption step and the first charge transfer step were identified as being rate determining. The addition of catalysts to the electrode enabled better adsorption, which is consistent with the previous hypothesis resulting from direct catalysis studies.

(v) Electrolyte Design: For the bulk of experiments conducted here a ternary molten alkali metal carbonate eutectic was used. This was chosen because it represents the minimum melting temperature eutectic, and hence requires the least energy input to retain a molten state. Nevertheless, a range of other molten carbonate combinations were examined, including binary combinations. The main conclusion here is that binary carbonate combinations lead to better electrode performance, in particular those that contain a significant proportion of lithium carbonate, so much so that a binary sodium and potassium carbonate eutectic performed very poorly. The role of lithium is still under investigation; however, it is hypothesized that lithium inclusion into the carbon structure, as in a Li-ion battery negative electrode, facilitates superior anode performance.

Applied Outcomes

3.6. Milestone 14 and Milestone 15: Construction and Performance Optimisation of a Bench-Scale DCFC

3.6.1. Milestone Background and Aims

Up until this stage of the project the majority of experimental work has been focused on exploring the fundamental behavior of carbon oxidation in a molten carbonate medium. In particular, this is in reference to outcomes from Milestones 7, 8 11, 12 and 13 focused on understanding the effects of the molten carbonate electrolyte, carbon pre-treatment and type, and catalysts on the oxidation kinetics in the DCFC anode.

The next logical step in the process of full cell DCFC development and optimization is to implement these fundamental findings into a functioning small scale DCFC. This stage of development is essential to ensure the transition of the material, system and process advantages observed in fundamental studies into a fully functioning system. Therefore, the main aim of these milestones is to carry out the development of a bench-scale DCFC and implement our fundamental findings into a functioning system, as well as use the bench-scale system to complement the activities associated with the development of the pilot scale system. Further, in development of these milestones, practical cell set-up and assembly knowledge will be gained including materials handling and electrode construction issues. Workable reference and counter electrodes able to give reproducible results are key to the half-cell design while cathode design will impact heavily on the full bench-scale operation.

3.6.2. Experimental Methods

Anode Pellet Preparation

Pellets are manufactured in a 13 mm diameter pellet press and the desired graphite/coal/contaminant mixture filled in the press (pre-dried, and weighed before combination to create a pressing powder) before compressing at 740 MPa for 5 minutes. To ensure stability under test conditions, all pellets, including pellets containing pre-pyrolysed coal and graphite only pellets, are then sintered for 4 hours under a nitrogen atmosphere at 500°C.

Anode Construction

Contact to the anode pellet is made through a chromel wire cemented in place with a conductive ceramic adhesive (Resbond 989, mixed with 25 wt% graphite). The conductive adhesive, pellet and wire contact were allowed to dry at room temperature for 4 hours after which they are heated in a nitrogen atmosphere to 90°C, 120°C and 300°C for 2 hours, 1 hour and 1 hour, respectively, to dry, cure and post cure the adhesive. The carbon pellet and contact were then mounted into a ceramic tube, cemented and cured in place using ceramic adhesive (Resbond 989) using the same procedure as the conductive glue curing. A general arrangement diagram of the anode is shown in Figure 50.

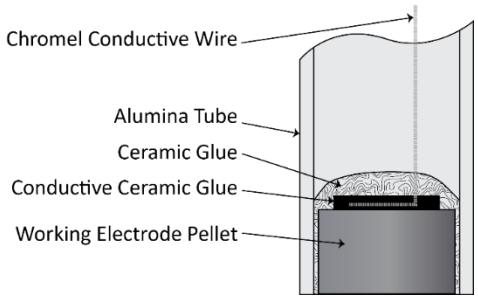

Figure 50: General arrangement of anode

The surface of the working electrode was polished flat on 1000 grit carbide abrasive paper and well rinsed with Milli-Q water to remove any surface contaminant. This procedure produced a working electrode with a cross sectional geometric area of 1.766 cm^2 (allowing for surface roughness), which has been used to normalise currents recorded in electrochemical testing (along with normalisation used for active carbon surface area as discussed in Section 3.3).

Cathode Construction

The cathode consists of a ready-made solid oxide membrane with catalyst spot produced by Fuel Cell Materials. The solid electrolyte is composed of the trademarked 'Hionic' substrate (zirconia based, 150µm) which has both high strength and good oxide conductivity with a LSM/LSM-GDC catalyst spot of 50µm thickness (strontium-doped lanthanum manganite (LSM) and gadolinium-doped ceria (GDC)) for oxygen reduction applied. This is fixed to the end of an alumina tube using two kinds of ceramic paste in order to ensure a good seal against carbonate incursion as the oxygen reduction reaction must occur at the surface of the solid electrolyte and cannot proceed on this substrate if submersed in the carbonate. Contact is made to the catalyst spot with a piece of platinum wire while a stainless steel tube is inserted into the tube to allow turbulent air flow. The general arrangement of the cathode design is shown in Figure 51.

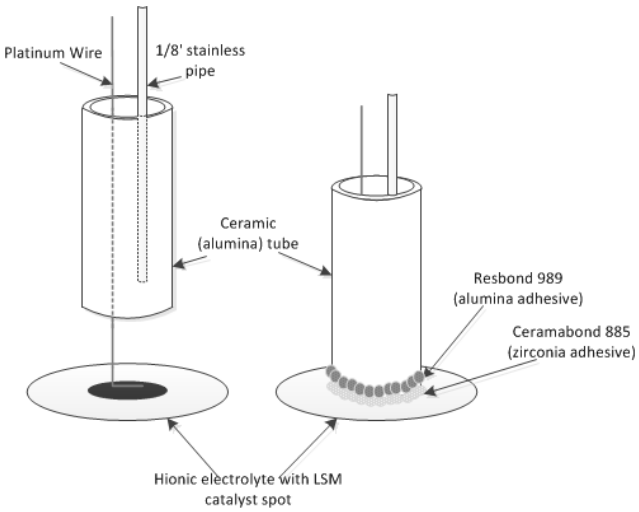

Figure 51: Cathode design for DCFC half-cell

Electrochemical Cell Set-Up (HALF CELL)

Electrochemical experimentation conducted in this work was performed using a portable WaveNow potentiostat from Pine Instruments and using AfterMath software for data collection (data analysis was done in MS Excel).

The half-cell includes the use of three electrodes: the working electrode, which can be either the anode or the cathode, the counter electrode (measures current flow between working electrode and it) and the reference electrode. The cell itself was constructed of high-density alumina (ceramic), prepared and machined by Ceramic Oxide Fabricators (Australia). The cell consisted of a circular ceramic dish with a specially manufactured ceramic tile lid to allow the working (WE), reference (RE) and counter (CE) electrodes to be held securely in place. A constant carbon dioxide (BOC grade 4.5) atmosphere was maintained within the cell via an external gas feed line flowing at a rate of 50 mL_N/min in order to maintain constant reference electrode conditions. The temperature within the furnace was controlled through a thermocouple which terminates within the furnace. A schematic of the half-cell (anode) test arrangement is shown in Figure 52.

Both the counter and reference electrode consist of a graphite rod (GrafTech, Cleveland OH) with electrical contact through an internally cemented chromel wire (conductive ceramic adhesive and curing regime as above). The geometric surface area of the counter electrode was approximately 3.7 times that of the working electrode (based on an electrolyte depth of 15 mm), ensuring that any surface area limitations were not a result of the counter electrode.

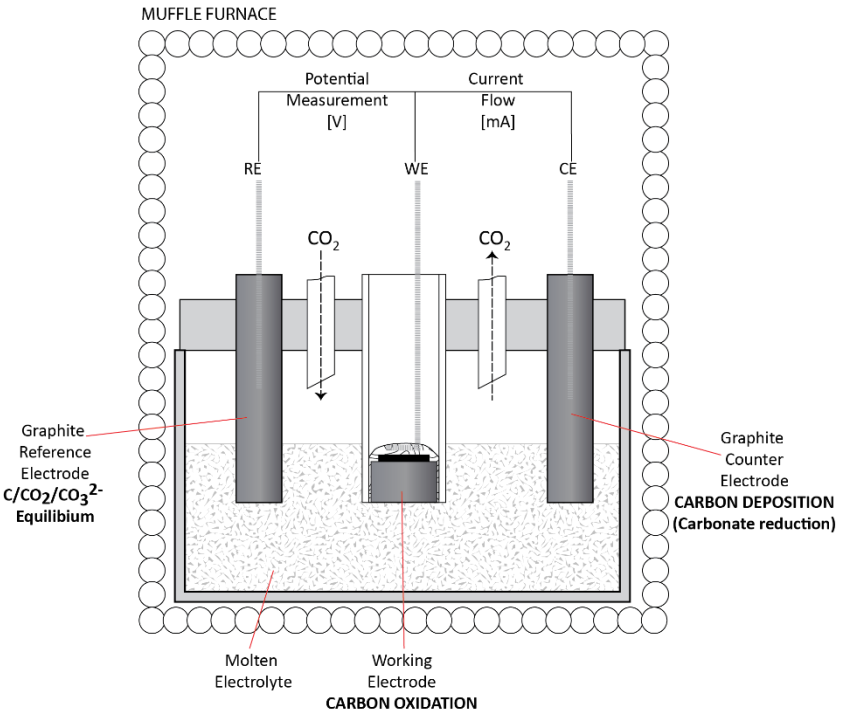

Figure 52: Half-cell DCFC arrangement including working, counter and reference electrode

Electrochemical Cell Set-Up (FULL CELL)

The full DCFC arrangement consists of the anode and cathode directly connected and operating in an inert atmosphere. The general arrangement as well as the reaction scheme of the full cell is shown in Figure 53.

Tertiary Carbonate Electrolyte

Sodium carbonate (Na_2CO_3), lithium carbonate (Li_2CO_3) and potassium carbonate (K_2CO_3) (Sigma >99% pure) are dried at 110°C under vacuum for 24 hours prior to combining. The three carbonate powders are, in most cases, combined in a mole ratio of 43.5% Li, 31.5% Na, 25% K (eutectic composition) and gently homogenised with a mortar and pestle for 5 minutes. The tertiary carbonate precursor is then fused at 600°C prior to use.

3.6.3. Results

The performance and optimisation of the bench scale arrangements design for this work have been presented in detail for previous milestones. Replication of the previous fundamental findings has been carried out using the full cell configuration shown in Figure 53. This has shown that the performance found in the fundamental half-cell studies can be reproduced in the full cell configuration. Alternately, it means the performance of the air cathode does not impact on anode performance in this configuration, and that the intrinsic performance of the cathode is sufficient to ensure that the cathode is the limiting electrode in this case.

As the design and construction of the pilot-scale cell was being carried out, concepts were tested in the bench-scale DCFC for applicability prior to integration in the pilot. Successful optimisation of the set-up has meant the arrangement is flexible and able to be applied to several different aspects of the full DCFC including separate testing of anode, cathode and combined cell operation.

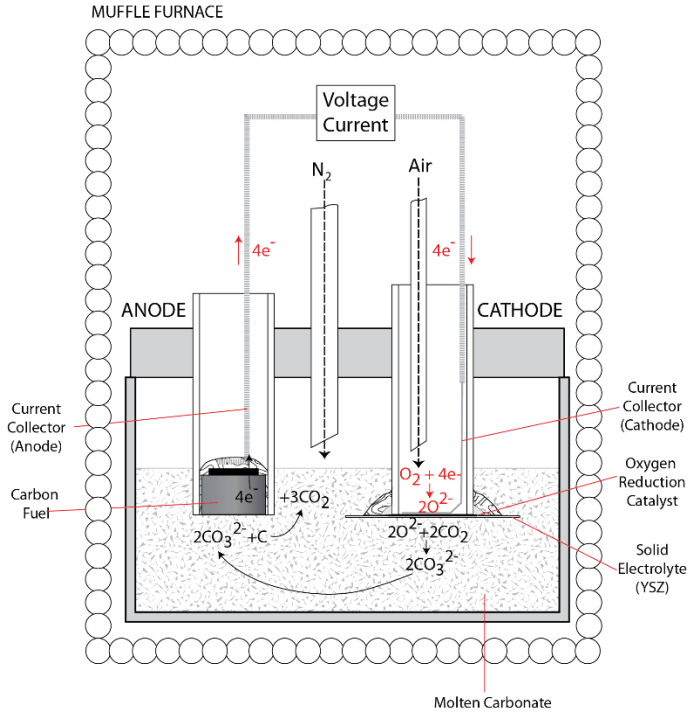

Figure 53: Full Cell DCFC Arrangement

3.6.4. Summary and Conclusions From Bench-Scale DCFC Testing

The construction of the bench-scale DCFC demonstrated that a small scale DCFC could be prepared and utilized to consolidated existing findings from fundamental studies. This bench-scale DCFC consisted of a carbon anode (for carbon oxidation) of similar construction to the half-cell used extensively for fundamental studies. The main difference was the use of an air

cathode (for oxygen reduction) instead of a graphite rod onto which carbon electrodeposition occurred. The size and hence capacity of the air cathode was sufficiently large so as to ensure that its performance was not limiting in the bench-top DCFC. Aside from this difference, the bench-top DCFC was assembled and used in a similar way to the half-cell used for fundamental studies.

Due to its similarity, the bulk of experiments conducted with the bench-top DCFC were carried out to confirm the findings in the fundamental studies portion of this project. Along these lines, experiments using the bench-scale DCFC were conducted to examine the following, together with the highlighted findings:

(i) Impurity effects in the electrolyte originating from coal contaminants. Here it was found that the majority of common coal contaminants are soluble in the molten carbonate electrolyte, with their effect on carbon oxidation kinetics being minimal. However, their effect on the molten carbonate eutectic melting temperature was substantial, with shifts in the melting temperature to both higher and lower potentials.

(ii) The effect of coal type and its pretreatment on oxidation kinetics. Comparisons were made here with respect to graphite as the baseline carbon source. Here, optimal pretreatment temperatures were identified for a number of coal samples, with the preferred conditions being a trade-off between volatile removal and retention of surface functionality at lower temperatures, and lower activity graphitization and increased conductivity at higher temperatures.

(iii) Carbon anode catalysis with a variety of common coal contaminants. Extensive studies were conducted here with a range of common coal impurities, some of which were found to be excellent catalysts for carbon oxidation. The most effective catalyst was kaolin, which even at the 5 wt% level in coal doubled the resultant current output.

(iv) Molten carbonate eutectic electrolyte composition effects. Here the presence of lithium carbonate in the electrolyte was identified as being critical, likely through a mechanism consist with that found in Li-ion battery anodes; i.e., intercalation of Li into the structure to facilitate further oxidation.

3.7. Milestone 16: Construction of a Pilot Scale DCFC

3.7.1. Milestone Background and Aims

The ultimate objective of this project was the design, construction and optimization of a pilot-scale DCFC able to incorporate the fundamental findings of the project into a larger scale functioning system. To some degree this was accomplished with the bench-scale DCFC, which had considerable success in replicating the fundamental findings. However, what the bench-scale cell lacked was some of the electrochemical engineering aspects of effective fuel cell design, which is critical for development of a working commercial system. As such, in addition to implementation of the fundamental findings, the pilot scale system was intended to explore certain other aspects of DCFC operation.

Scaling up the bench-scale DCFC to a pilot scale is a key part of the DCFC commercialisation pathway and enables learning from the bench scale equipment to be applied on a larger scale. It was an embedded design principle of this project that the pilot scale rig was flexible in its construction and operation so as to be easily modified and optimised as new information comes to light.

3.7.2. Pilot Cell Design

This milestone unfortunately had a major early set-back after disappointing communication from a key supplier, Ceramic Oxide Fabricators. A second version of the pilot cell has been developed as a result using a stainless steel body instead of alumina, as planned. A stainless steel cell was not initially considered due to materials specific limitations including:

(i) Corrosion of stainless steel in the molten carbonate environment;
(ii) Differences in thermal expansion between stainless steel (cell body) and zirconia (solid oxide membrane), meaning sealing of cell would be difficult and, once fixed to stainless steel cell, the membranes would be extremely prone to breakage during heat-up/cool down – which could result in molten carbonate leakage and cell failure; and
(iii) Electrically conductive and needs specific isolation from cell components

Problems in the use of stainless steel have been addressed through several design modifications of the alumina cell. Firstly, the stainless steel will be internally coated with Resbond or a similar ceramic based adhesive in order to increase resistance to corrosion by molten carbonate. Practicality of this measure has been investigated using stainless steel rods coated in Resbond and taken to 600°C to determine adherence at temperature. Results for initial coating and heating are shown in Figure 54. Overall, some of the advantages of using stainless steel as the main body of the cell include:

(i) Cost effective
(ii) Ability to manufacture in-house without reliance on external suppliers
(iii) More flexible and tunable due to ease of machining (compared to alumina which required specialist grinding tools)
(iv) Able to weld joints together to ensure liquid/gas tight sealing
(v) No need for spacer plate as stainless steel can be procured in lengths long enough for the full cell

Figure 54: LEFT – Stainless rod before and after painting with Resbond, RIGHT – After heating to 600°C

Corrosion of various steels has been investigated for use of molten carbonates for application to the Molten Carbonate Fuel Cell (MCFC) and it has been found that specific alloys have better corrosion resistance towards molten carbonates than stainless steel [4]. However, for this initial cell design it was thought that the cost and speed of manufacture should be prioritised since corrosion appears to be sufficiently addressed by coating of the steel with alumina/zirconia adhesive faster and more cost-effectively than through ordering of specific steel alloys for this version of the cell. After initial testing and development of this cell a higher resistance alloy will be procured depending on cost impediments and corrosion behaviour of alumina coated Stainless Steel. More work with respect to materials corrosion issues in molten carbonates will be investigated in Milestone 18.

The second modification is more extensive and required the external casing of the cell to be modified as well as the method of securing membranes to be changed. The use of an alumina walled cell allowed the electrolyte discs to be fixed in place through use of a ceramic binder – which was tested and found to be sufficient in Q3 2014. The coefficient of expansion however for stainless steel and zirconia/alumina is very different and it is thought that permanent fixing of solid membranes in the cathode windows of the cell would not seal due to cracks and destabilization of the alumina binder. Both membrane and stainless steel must be allowed to expand without fixing of electrolyte components in place. The design was therefore modified to allow for physical compression and fixation of solid electrolyte membranes in place through the use of a gasket arrangement. Alumina felt gaskets are commonly used in solid oxide fuel cells in order to allow a gas tight seal between the cathode and anode using a solid electrolyte, as used here. Alumina felt is also easily cut to specific sizes and is cheap to obtain on a roll basis (US $64 for a piece ~60 x 60 cm). It is also electrically insulating and careful design allows the cathode to be electrically isolated from the main cell body through the use of these gasket materials. This electrical isolation through use of the alumina gasket also solves the final issue of using a stainless steel cell. Samples of different grades of alumina gaskets have been sent from a manufacturer in the US and are ready for testing. The gasket system to be used is shown in Figure 55with the full cell outline shown in Figure 56.

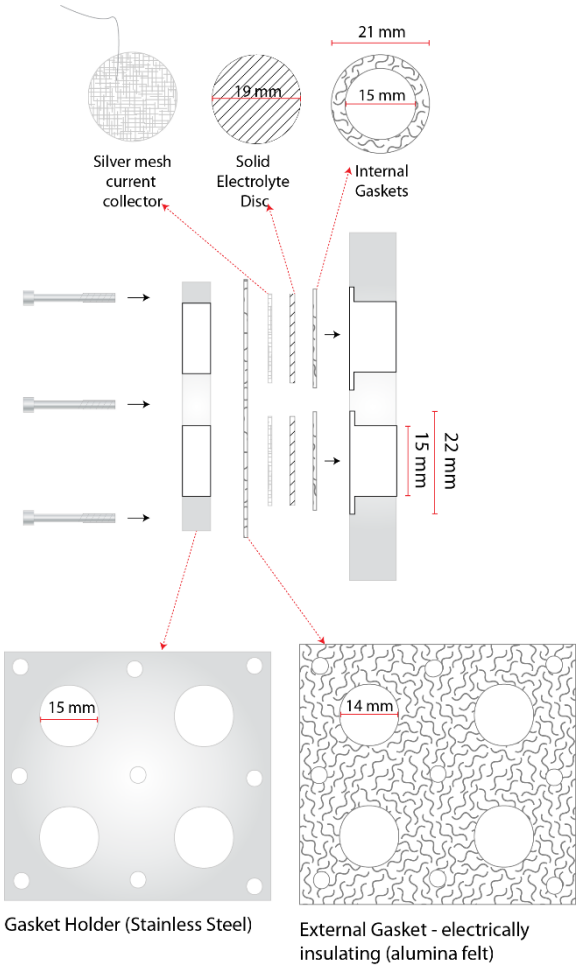

Figure 55: Gasket system for DCFC pilot cell – Version 2: Stainless Steel

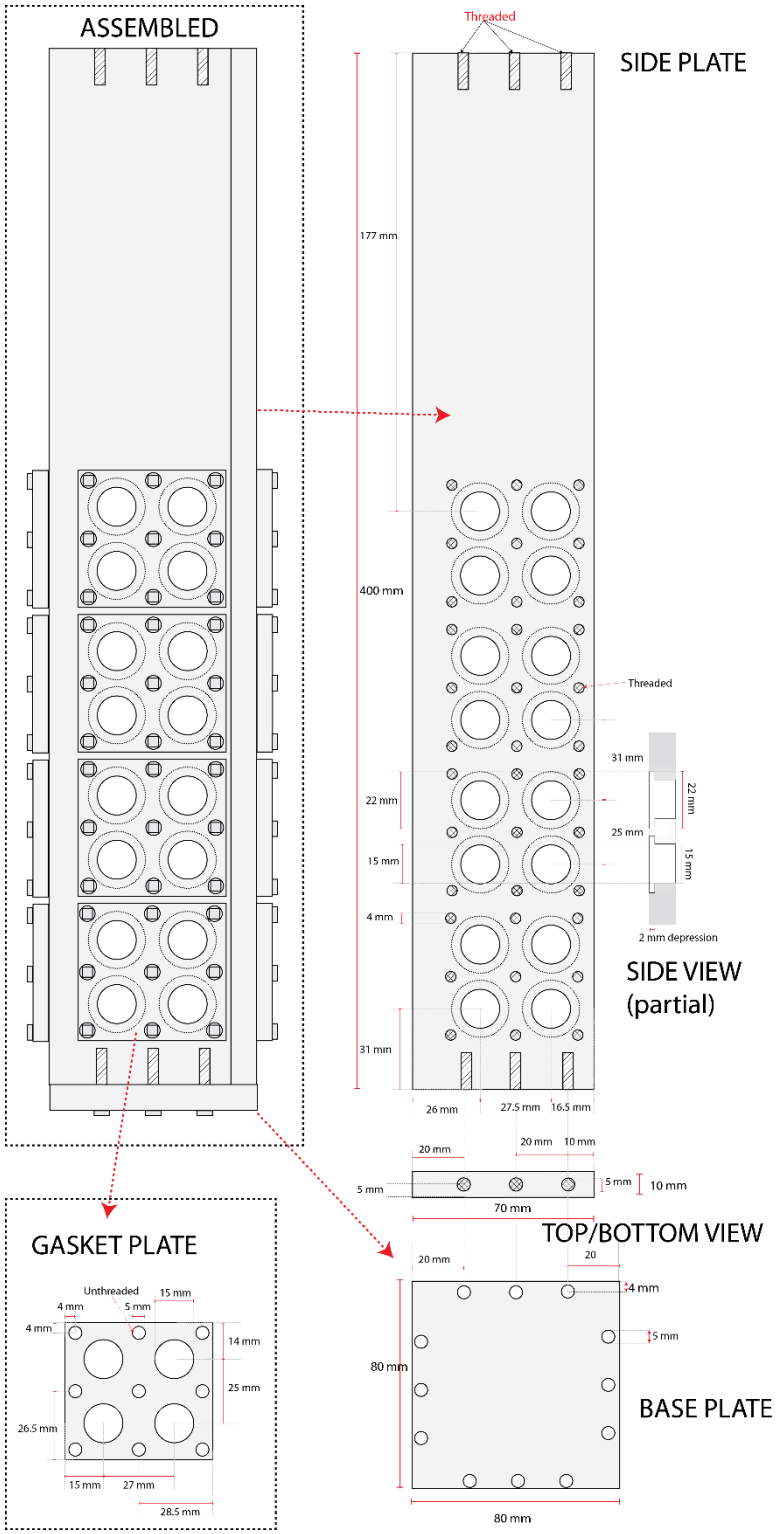

Figure 56: DCFC Pilot cell body – Version 2: Stainless Steel

Another advantage of the stainless version of the DCFC pilot is the ability to insert and remove solid electrolyte materials. This would not have been possible with the alumina version of the cell and means different electrolyte discs can be trialed and updated without building a new cell. Damaged discs can also quickly be replaced.

Ideally the same system in alumina could be used, although it is now thought that this will be prohibitively expensive in any sort of laboratory arrangement due to the difficulty of moulding and shaping alumina to customised arrangements. Potentially moulds could be developed commercially specific for the direct carbon fuel cell and this updated design would solve issues of both Version 1 and Version 2 of the design. For the budget and time allowed for this project however, Version 2 was sufficient and it is thought that any possible problems have been addressed.

3.7.3. Commissioning

Extensive work was carried out in 2014 into the design of a workable pilot scale DCFC design. This design was based on the use of alumina materials due to their high stability in molten carbonates and similarity in expansion coefficient to solid electrolyte discs which were required in this design to be permanently fixed to the cell walls using alumina high temperature adhesive. In designing the cell, a local ceramic manufacturer was consulted and had some input in the finalisation of the design in terms of realistic plate sizes and machining capabilities. This manufacturer gave an initial quote estimate of $3-4K and, based on this design, a test plate was ordered in order to ensure the cell design was workable before outlay of funding for the full cell. After successful testing of this plate (including an initial delay in this milestone) a final quote was sought for approval and ordering of the full cell. The quote took 4 weeks to arrive despite multiple emails and phone calls to the manufacturer and when it arrived it was more than double the original quote estimate of <$4K provided by the supplier, the final price given was $10K for a single set of plates. This is despite making it clear to the manufacturer early on in the design process that a maximum amount of $5K could be spent on the cell design and very little change in design between the initial and final quote. This unreasonable quote meant the cell design had to be rethought and seemed to be a substantial set-back in the progress of the project. However, a workable design was completed in late 2014 for a stainless steel based cell and a final quote of <$1000 for a single set of plates with the majority of work carried out in-house at the University of Newcastle workshop. It is now thought that this new design is superior to the original design as it allows for easy replacement of the solid electrolyte membranes and is a cheaper, more flexible design since it can be made in-house at the University of Newcastle.

The assembled cell is shown in Figure 57 and the unassembled plates shown in Figure 58.

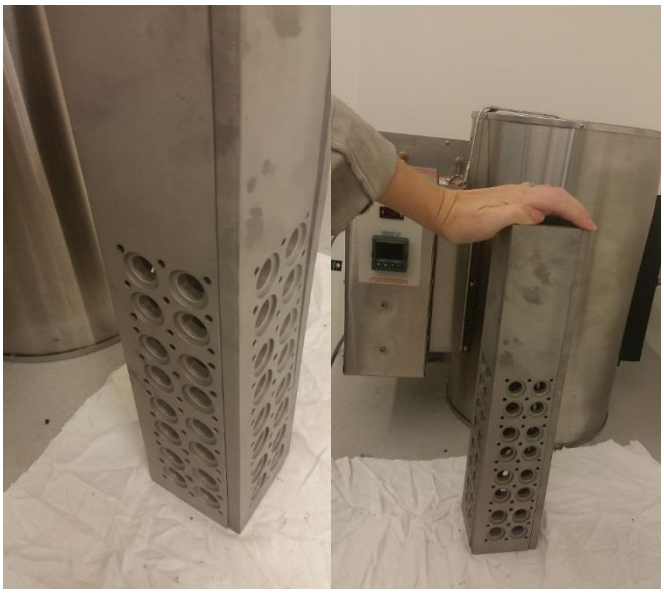

Figure 57: Assembled cell (vertical tube furnace also shown on RHS for scale)

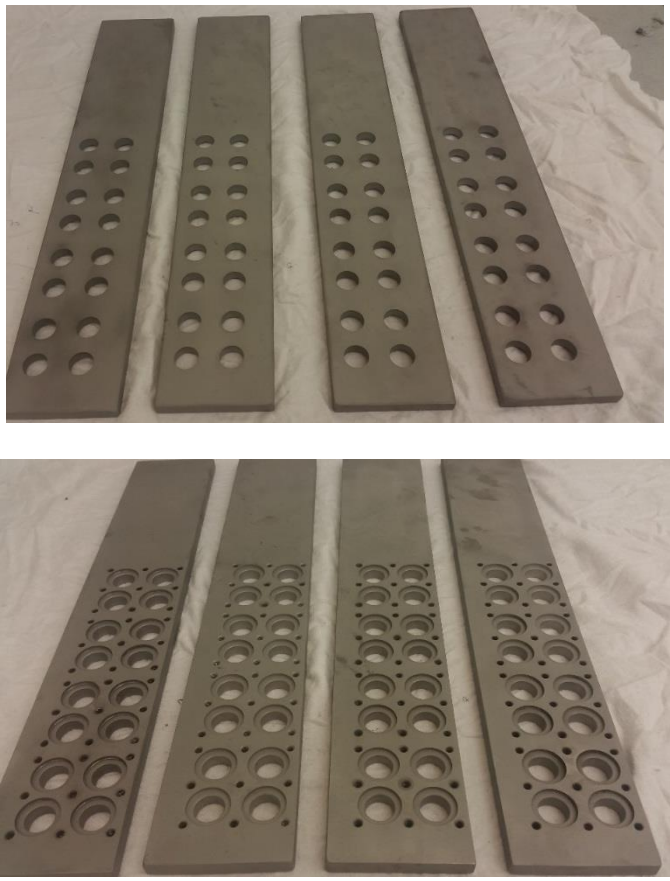

Figure 58: TOP - Inner side (carbonate contact) and BOTTOM - Outer side (cathode placement)

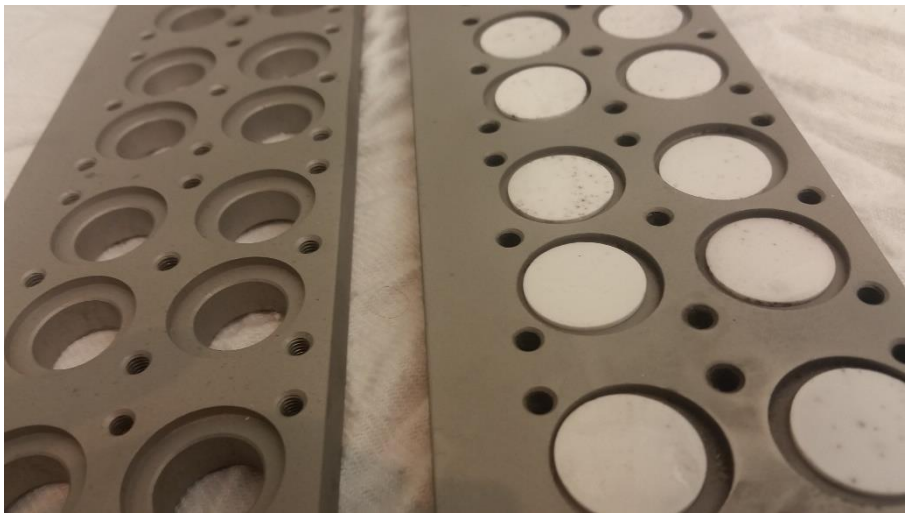

Figure 59: Outer side without (LHS) and with (RHS) YSZ membranes in place

3.8. Milestone 18: Performance Optimisation of Pilot Scale DCFC

3.8.1. Milestone Background and Aims

The practical and reliable operation of the pilot scale DCFC utilizing knowledge gained from previous milestones, including the bench scale arrangement, is the culmination of all work carried out to date. This milestone is essential for the continued development and commercialization of the DCFC.

This milestone describes in detail the activities that have been conducted regarding the optimization of the pilot-scale DCFC. The description that follows contains elements of fundamental research, optimization and performance data for the pilot-scale DCFC. Some of the topics discussed may be considered fundamental in nature; however, they have been included here because they relate directly to the operation of the pilot-scale DCFC. In terms of optimization of the pilot-scale DCFC, selected outcomes have been taken from the fundamental studies conducted in this project and implemented into the pilot-scale DCFC to demonstrate their validity on the large scale.

3.8.2. Cell Component Fabrication

Cathode/Membrane (LSM/YSZ)

Customised fabrication of solid electrolyte discs is desired as this will allow variation in interface design as well as electrolyte thickness and, as mentioned above, the interface between oxide anion conduction and the carbonate electrolyte. Extensive work has been carried out to prepare and test solid electrolyte/cathode discs. YSZ powder was used to dry press solid electrolyte discs. These discs proved difficult to prepare and were determined to be highly sensitive to moisture present in the dies used for pressing and the YSZ powder, meaning the disc was difficult to remove following pressing and frequently became stuck to the die and was unable to be removed whole. Drying of YSZ in a high temperature oven prior to pressing aided in this procedure as did use of warm dies which had also been dried in a hot oven. Even once removed however the YSZ discs prepared were highly fragile and prone to breakage. Initially, due to underestimation of the densification of discs upon sintering, discs were twice as thick as intended with a thickness of over 2 mm. The amount of YSZ powder however was then adjusted and discs almost exactly 1 mm thick were produced, outlined in Table 10 and shown in Figure 60 before and after sintering.

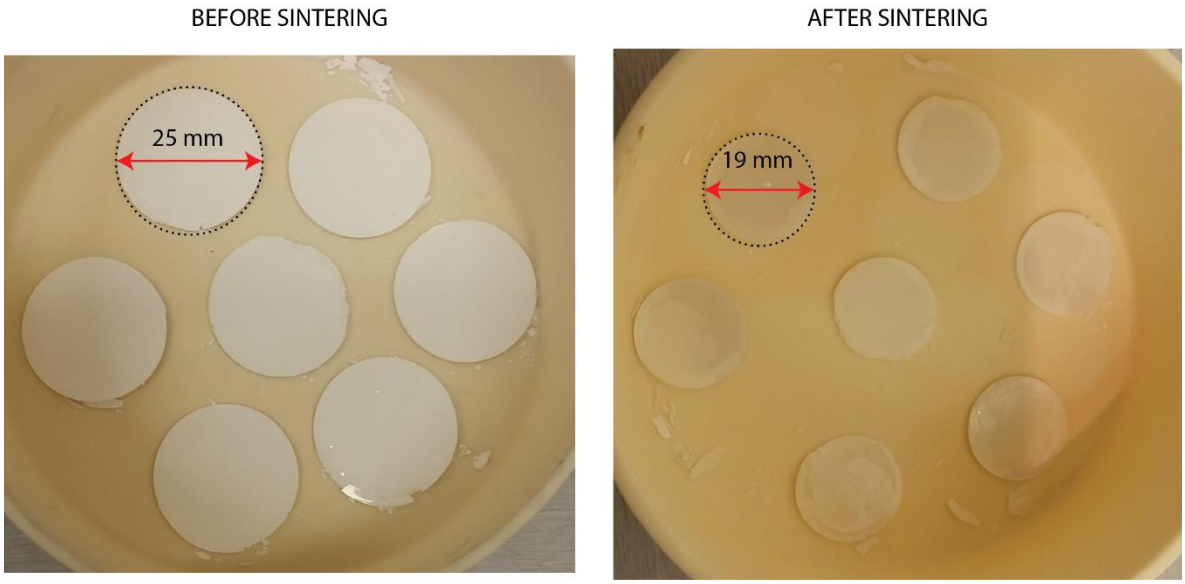

Figure 60: YSZ solid electrolyte pellets prepared prior to sintering at 1500°C (LEFT) and after (RIGHT)

Table 10: Measured density for unsintered (green) and sintered YSZ pellets prepared (average values used for 7 prepared pellets)

		Green	Sintered
Diameter	mm	25.00	19.59
Thickness	mm	1.42	1.02
Volume	mm^3	694.65	307.89
	cm^3	0.69	0.31
Mass	g	1.66	1.66
Density	g/cm^3	2.38	5.38
Theoretical Density (YSZ)	g/cm^3	5.96	5.96
Theoretical Percentage		40.00%	90.25%

Sintering was performed in a high temperature muffle furnace through heating of the discs in an alumina crucible to a temperature of 1500°C where the temperature was held for 2 hours and cooled to room temperature. Once sintered YSZ discs were prepared, LSM and YSZ/LSM inks were prepared and spray coated onto the YSZ disc. A test disc was also prepared which was spray coated with pure YSZ powder, as shown in Figure 61.

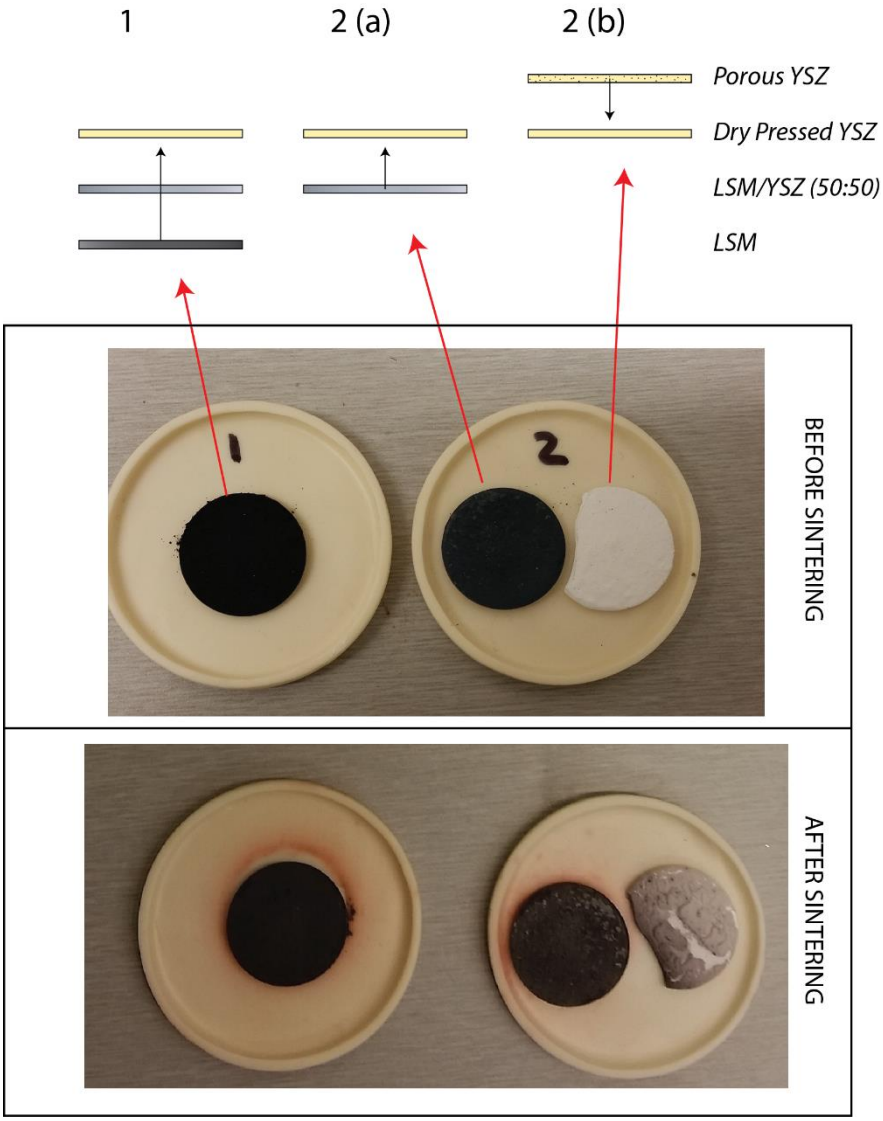

Figure 61: Solid electrolyte and cathode discs prepared for testing using (1) YSZ|LSM/YSZ|LSM (2a) YSZ|LSM/YSZ (2b) YSZ|YSZ

Spray coating was found to be an effective method for application of cathode inks, however it was determined that an organic filler and use of a binder would give better results for the application of YSZ as the porous layer applied was found to be inconsistent, clearly seen in Figure 61. The presence of LSM in close proximity to the YSZ disc also appears to have caused some contamination of the YSZ disc and should therefore be separated in future experiments.
After this initial testing, methods for producing solid electrolytes and cathodes were investigated in more detail and finalised. Finding the necessary information for the fabrication of the DCFC cathode/membrane proved to be a challenge. There are many papers available showing studies of the DCFC, however very few supplied adequate information that was needed to repeat the process.

Synthesising LSM (cathode catalyst): There are many different processes used to synthesis LSM powder for the cathode of the direct carbon fuel cell. In some papers LSM powder was purchased pre-made [23] and others synthesized it themselves. Lanthanum (III), strontium (II)

and manganese (II) nitrates were the most commonly used base chemicals for the synthesis of the LSM powder [24-29] with acetates being the next frequently used [30, 31]. Other base chemicals that have been used previously were a combination of lanthanum (III) nitrate, strontium (II) chloride and manganese (II) nitrate [32] or lanthanum (II) nitrate, strontium (II) nitrate and manganese (II) acetate [33] although these were not frequent. The base chemicals were dried in an oven to evaporate any hydrate they may have and weighed to the appropriate ratios, which also varied within the literature [23, 26, 29, 33-35]. The ratio we chose was 0.4 mole of lanthanum acetate, 0.6 mole of strontium acetate and 1 mole of manganese acetate since it was stated that this is the best ratio for facilitating four-electron reduction [30]

The next step is to dissolve the acetates, the most common solvent is pure or deionised water [24, 27-30, 33, 36] which is what we chose to use. The solution was then heated on a hotplate and stirred until all the water had evaporated. Once all the water had evaporated the mixture was placed in an oven at 200°C for 48 hours and ground to a free flowing powder using a mortar and pestle. To complete the fabrication process, the LSM was compressed into pellets and sintered at 950°C for 72 hours before again being ground to generate a loose powder.

Methods for coating the cathode: The most common method used for coating the cathode with the LSM mixture was screen printing [23, 27, 37-41] with other methods including dip-coating [42], smearing [24], painting [35, 43] and spraying [29, 44-47]. The spraying method is the most practical method for the equipment we have, although not much information was provided on making the ink. The basic method of making the ink is to mix the LSM with a binder which is then dissolved with an organic solvent before spraying and allowing the solvent to evaporate. Many different binders and solvents have been employed in the literature. These include:

(i) nafion 117 solution [30]
(ii) polyethylene glycol [23]
(iii) ethanol and diethylene glycol [48]
(iv) a mixture of glycine, polyvinyl pyrrolidone and ethanol [36]
(v) a mixture of ethanol and diethylene glycol monobutyl ether [32]
(vi) a mixture of terpineol and ethyl-cellulose [35]
(vii) ethylene glycol dimethyl ether [44]
(viii) a mixture of ethylcellulose and polyvinyl butyral [45]

The final ink mixture chosen was poly (vinylidene fluoride) as a binder, and ethanol as a solvent. This mixture was chosen as previous work for supercapacitor testing in the laboratory used PVF successfully as a binder while ethanol is the least harmful organic solvent of those available. Since the mixture will be sprayed, creating aerosols, safety was considered carefully.

After the LSM ink has been sprayed onto the cathode it then needs to be sintered, the temperature and time of this is also widely disputed with the most common being 1100°C for 2 hours [37, 40, 41, 49] with 1200°C for 2 hours [25, 35, 37] being the next frequently used. Other temperatures and times include 1250°C [38, 50], 1050°C for 2 hours [39], 1150°C for 2 hours [23], 850°C for 2 hours [34], 1000°C for 2 hours [26, 28], 1500°C for 5 hours [46] and 1200°C for 6 hours [42]. Since little overall effect on performance is expected compared to limitations of the anode, the most commonly used procedure of sintering at 1100°C for 2 hours was chosen.

Cathode Half Cell Performance: Leak issues of the half-cell cathode were addressed through extensive testing and the performance of a cathode window was successfully evaluated. This was carried out initially in half cell configuration so as to avoid having to operate a full cell

in the bench-scale system, as well as enable optimization of the cathode performance. Performance was not high initially, however temperatures were not elevated too greatly to allow an overall cell performance metric to be evaluated based on previous cell performance measured at 600°C. A sample of the results are shown in Figure 62.

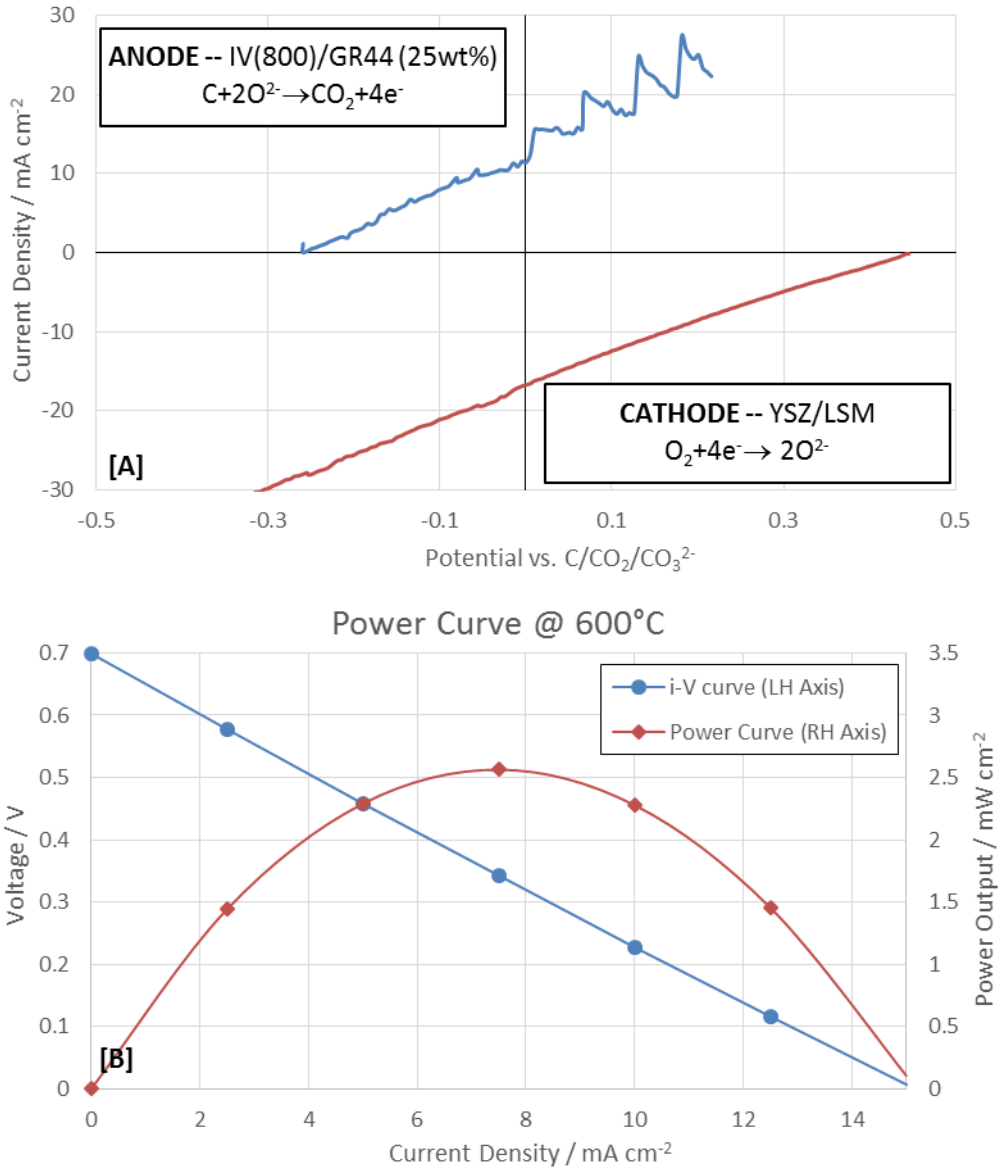

Figure 62: Bench scale cell overall performance using two half-cell set-ups [A] Half cell performance of IV(800) coal anode and LSM/YSZ cathode [B] Combined performance data for overall cell power output (Max 2.5 mW cm^2)

Results show similar performance of each carbon oxidation and oxygen reduction reactions. The oxygen reduction reaction is expected to be better kinetically than the carbon oxidation, however at 600°C YSZ is not ideally ionically conductive and is likely limited. Higher temperature would give exponentially better oxidation behavior, leaving the anodic reaction to be limiting. Carbon oxidation will also be improved in this case and the need for an anodic catalysts is shown to be of high importance from this analysis. Further testing of cathodes used

in the pilot cell at higher temperatures are required.

3.8.3. Anode Development

It was shown in a recently submitted publication the activity of a solid anode is heavily dependent on not only the activity of the most active component at the electrode surface, but also its conductivity. A literature search reveals limited work on the use of a solid anode, however one study showed the preferential consumption of a highly active anode binder used to hold the coal fuel together, resulting in mechanical failure of the electrode. Ideally therefore, the binder needs to be both more conductive as well as less active than the main coal fuel. We have developed the hypothesis that therefore the best coal binder will be a highly pyrolysed and demineralised form of coal fuel, which would have less surface functionalization than the main reacting fuel as well as better conductivity as a result of the pyrolysis process.

Acid washing techniques have also been used in the literature to remove the mineral content of coals prior to introduction into the DCFC, producing 'demineralised' coal. The acid washing process however also removes active volatiles from the coal and represents a loss in efficiency of the process. It is expected to be more efficient to firstly pyrolyse the coal followed by acid washing in order to drive off volatiles for useful production of heat in the pyrolysis process. Mineral impurities in the coal have also been shown by our research group to act effectively as catalysts for the electrochemical oxidation process and it therefore does not make sense to remove them completely from the DCFC. The most active form of coal is also thought to involve some partial oxidation, leading to increased functionalised surface groups on the coal material. Therefore, pyrolysis followed by brief exposure to small amounts of air at elevated temperature is likely to result in the most active coal type.

Therefore, it is thought that in fact the solid anode could be composed of a mixture of the same coal pre-treated in two different ways, plus solid catalyst kaolin, in order to achieve an anode of high mechanical stability and sustained activity. The pre-treatment processed involved in this are shown in Figure 63.

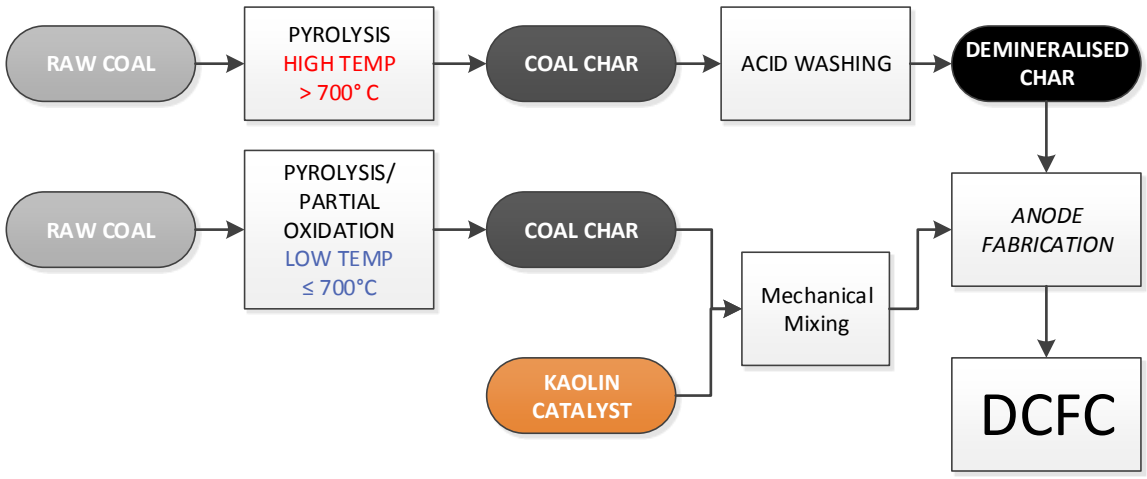

Figure 63: Anode formulation – proposed pre-treatment of coal for DCFC anode fabrication

The use of a comparatively low activity binder (high conductivity) and a highly active coal (moderate conductivity) is expected to produce a highly active, stable and conductive anode.

Coal fuels have been prepared for testing on the small scale (bench-scale cell) prior to

incorporation as a larger test solid anode. Fabrication methods of the solid anode have also been brainstormed and the current design involves the use of a roller press and a current collecting mesh as shown in Figure 64.

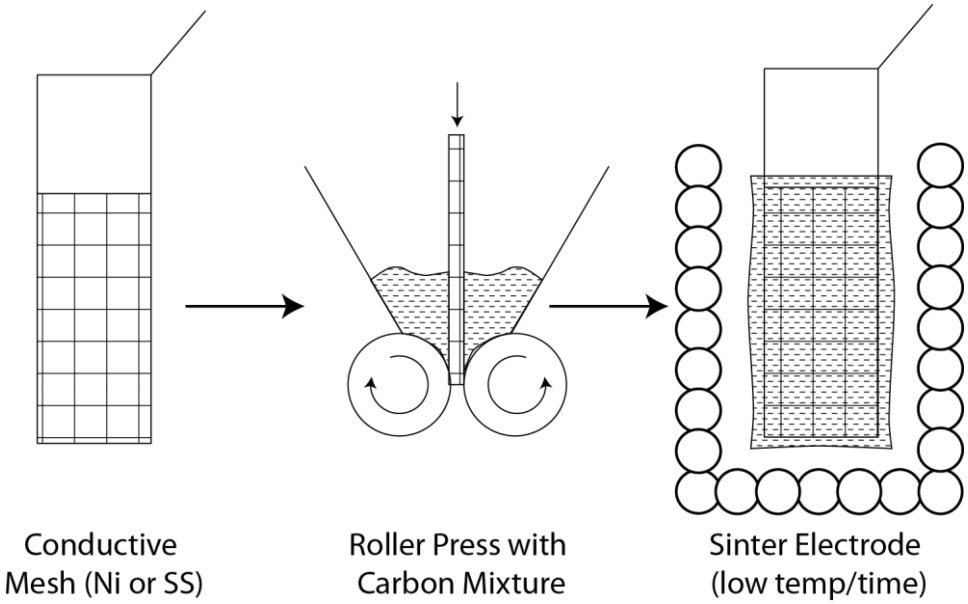

Figure 64: Proposed anode configuration for pilot cell

In a practical operating plant, the roller press is envisaged to be a heated roller which operates on coal directly after pyrolysis and in a semi-continuous nature. The mesh will be re-used after the anode has been run and carbon remaining burnt to remove contamination. The mesh type will need to be investigated, most likely a nickel or stainless steel mesh will be used, and stability in the carbonate melt will need to be confirmed. A small version of the mesh design will firstly be tested in the half-cell arrangement to investigate the mechanical strength of different coal/binder/graphite mixtures. First, the formula will be finalised to ensure conductivity, mechanical stability and high electrochemical activity on the bench scale.

Anode Catalyst Development Work

Further catalyst development work has also occurred with a clear demonstration of the effect of kaolinite as a catalyst material made using graphite based electrodes within the pilot scale DCFC. This series of experiments has been described and reported here because of its relevance to the practical operation of the DCFC.

In order to confirm the importance of mineral distributions within the solid carbon anode, the activity of graphite has been assessed using kaolinite distributed in the electrode in two different arrangements. In the first, kaolinite was sieved to a particle size below 32μm and intimately mixed with graphite powder using a mortar and pestle. The resulting mixture was pressed into an electrode pellet and tested for electrochemical activity. In the second arrangement, pure kaolin was compressed into a pellet and cut into a solid square. This square of kaolinite was then placed below pure graphite powder and compressed, resulting in an electrode where the solid kaolinite square was surrounded by graphite powder (referred to as ‘bulk’ kaolinite electrode).

Both electrodes were subsequently tested for electrochemical activity at 600°C in a ternary carbonate eutectic using standard electrochemical test procedures. Results for pure graphite,

distributed kaolin and bulk kaolin are shown in Figure 65 where they have been normalised for total geometric surface area, which was the same for each electrode.

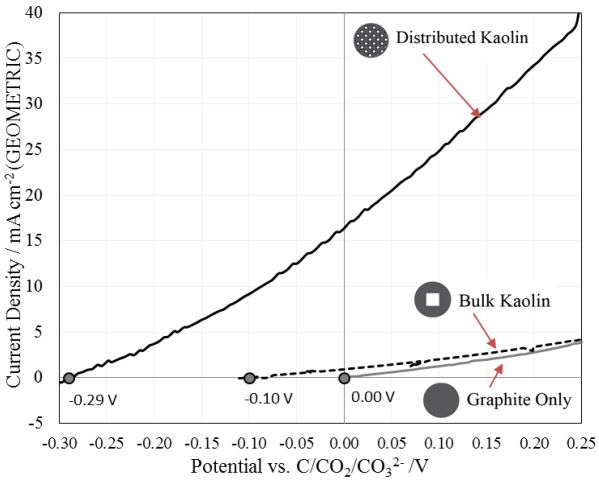

Figure 65: Electrochemical response for graphite with and without addition of kaolinite of different particle size (5 mV/s, ternary carbonate eutectic, 600°C).

It can be seen that the distributed kaolinite electrode shows an extremely high level of activation and shifted onset potential compared to both the pure graphite and the bulk kaolinite electrode. Indeed, compared to active coals investigated previously, the average current density measured over a 5 minute interval while holding at 0.5 V vs $C/CO_2/CO_3^{2-}$ is more than four times as high for the distributed kaolinite electrode (72.6 mA cm^{-2}) as that seen for a 25wt% CC-700 electrode (16.8 mA cm^{-2}). Mesoporous surface area and a high O/C ratio [51], as well as bulk lattice disorder and conductivity [13] have previously been said to be key to activity of carbon in the DCFC, however clearly the involvement of mineral matter has a more dramatic effect on the electrochemical activity since even 'inactive' graphite, which has none of the desirable physical characteristics for carbon electroactivity, can display performance observed in Figure 65. The bulk graphite electrode shows comparatively limited activity when normalised for geometric area, the main difference compared to pure graphite being the onset potential (0.1 V compared to 0.0 V for graphite). The surface area of carbon available for oxidation is slightly less (kaolinite chunk of 0.19 cm^2 used in a 1.33 cm^2 electrode), which might be expected to decrease the current density, however a similar result is achieved and current density observed at 0.5 V is almost identical (14.0 mA cm^{-2} for graphite, 13.8 mA cm^{-2} for bulk kaolinite electrode). It is likely therefore that activity at the interface of graphite and kaolin leads to some limited improvement in performance for the bulk electrode which counteracts expected decrease in activity from reduction of the available carbon area.

It has previously been proposed that kaolinite may act as a catalyst through different mechanisms including enhanced wetting of the carbonate at the electrode surface, or through mediation of oxide transfer to reactive sites [4]. There is a third possibility which has not previously been discussed and is specific to solid anodes incorporating kaolinite. This mechanism involves the selective dissolution of kaolinite in the molten carbonate electrolyte, leading to enhanced carbon surface area. Kaolinite solubility in a ternary carbonate eutectic was discussed as a possibility recently by Glenn et al. to explain shifts in melt behaviour of alkali-metal carbonates when the mineral was intimately mixed with the salt [52]. All three catalytic mechanisms are shown graphically in Figure 66.

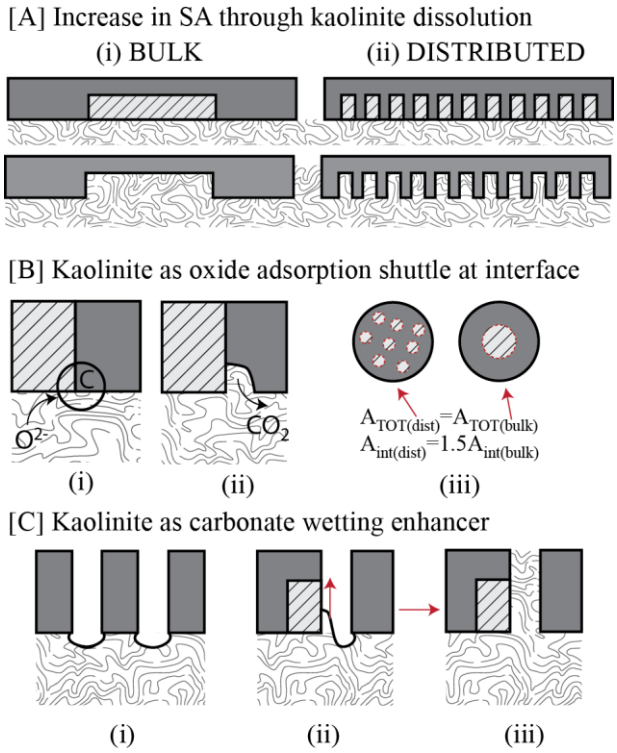

Figure 66: Role of kaolinite as a catalyst [A] through surface area increase [B] through oxide shuttle mechanism [C] through pore saturation (improved wetting)

If the kaolinite present were to dissolve, the enhanced performance of the distributed electrode can be understood through the resulting dramatic increase in surface area compared to the bulk or pure graphite electrode. However, this does not explain the change in open circuit potential observed for the electrode which becomes more negative as more kaolinite is added (Figure 65).

Chen et al. showed that the OCP can be observed to vary depending on the immersion length and immersion time of a solid carbon electrode [5]. This was said to be a result of a change in the wetting of the carbon surface with molten carbonate on a micropore level. The OCP measured was seen by Chen et al. to become more negative (versus a different reference system) when wetting was increased either as a function of immersion time or immersion level in the molten carbonate melt [5]. The negative shift in OCP observed for the distributed kaolinite electrode (-0.29 V compared to 0.00 V for pure graphite) could well be explained through this observation. However, this would appear to essentially be an enhancement of surface area of the electrode since more active carbon sites would be available as shown graphically in [C] where (i) shows the limited contact of carbonate with carbon micropores in the absence of kaolinite. When kaolinite is present it could possibly allow flooding through change in contact angles in and around pores, as shown in [C] (ii)-(iii). Since the OCP is an intrinsic property of the electrode, it would not be expected to change simply as a functional of surface area. It is therefore also possible therefore that the OCP is related to a change in the activity of the electrode due to a shift in the mechanism.

[B] outlines a different catalytic enhancement mechanism involving the use of kaolinite as oxide adsorption sites. This would mean the interfacial area between the kaolinite and carbon would be extremely active and would explain why smaller, distributed particles give better results compared to a single large chunk of kaolinite. In the example given in [B] (iii), kaolinite

has the same geometric area (A_{TOT}) for each electrode shown, however in the distributed case the interfacial area (A_{int}) is 1.5 times that of the bulk case. Since very small particles were used compared to a single large chunk in Figure 65 this difference would be expected to be much larger. This catalytic mechanism would be expected to have a different dominating reaction mechanism or rate determining step for the electrochemical oxidation, especially in the case of the distributed electrode. To assess whether this is the case, Tafel analysis has been carried out on LSV results, similarly to that presented in previous work [53], shown in Figure 67.

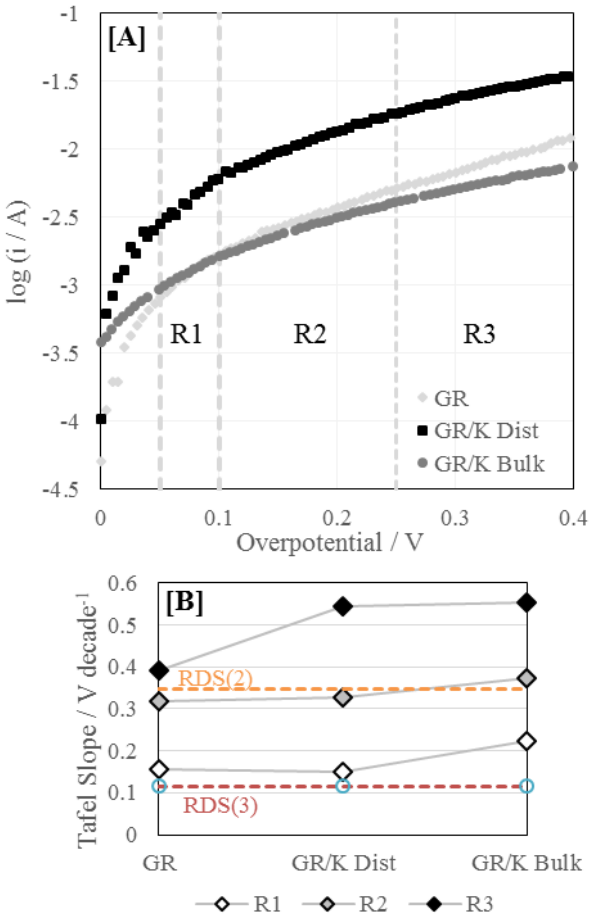

Figure 67: [A] Tafel plot of electrochemical performance of graphite only (GR), graphite containing distributed kaolin (GR/K Dist) and graphite containing bulk kaolinite (GR/K Bulk) submersed in ternary molten carbonate eutectic at 600 C (LSV of data used shown in Figure 65) [B] Calculated Tafel slope in overpotential region 1, 2 and 3 (denoted R1, R2 and R3) as marked in [A] for each electrode trialled

Three oxidation regions are defined here with the Tafel slope calculated with a fit of R>0.99 in the specified potential range. Tafel slopes calculated are compared in Figure 67[B] where theoretical Tafel slopes are also shown for the mechanism outlined in Figure 68, kinetic analysis for these results presented in a previous publication [54].

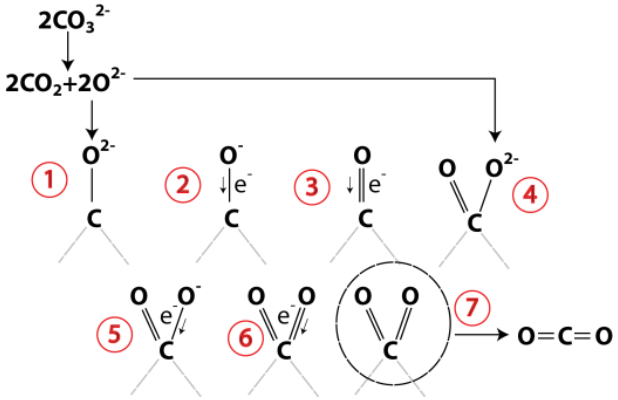

Figure 68: Proposed reaction mechanism for carbon electrochemical oxidation with rate determining steps numbered

All three electrodes show a Tafel slope which agrees closely with RDS (2) and (3) in region 1 and 2 respectively, which is in agreement with previous results presented for different carbonate compositions using pure graphite anodes at elevated temperatures [53]. In region 3 however, the kaolinite electrodes show significant deviation away from that of graphite at this temperature and Tafel slopes no longer agree with the kinetics expected for the mechanism shown in Figure 68. This deviation likely stems from a change in reaction mechanism which occurs at high polarisation. Since it is only observed in the case of the kaolinite doped electrodes investigated here, it is likely that kaolinite does indeed change the reaction mechanism of carbon electro-oxidation to enable a more activated oxidation pathway, likely involving an interaction of the kaolinite mineral with the carbon surface.

From analysis presented here, inclusion of kaolinite mineral is suggested to activate a solid carbon anode through both a change in the wetting of carbonate to the electrode surface (seen through change in OCP) as well as a shift in the electrochemical oxidation mechanism at high polarisation. Small mineral particle size and intimate contact with reactive carbon is crucial to observing both of these effects.

3.8.3.1. Impact of Coal Ash Distribution

The effect of pyrolysis temperature on the electrochemical performance of coal has been discussed in this report in detail and recently we have published a journal article in this area. It was concluded that the electrochemical oxidation of coal and carbon materials was dependent on both the form of carbon present (functionalization, crystal structure, porosity etc) as well as the mineral or ash content of the coal. In fact, it was shown very clearly that activation during pyrolysis occurs at different pyrolysis temperatures depending on the coal type investigated. Use of the optimum pyrolysis temperature did not result in major changes between coal properties normally measured (volatiles, porosity/surface area, functional groups) and it was instead postulated that ash undergoes a transition at a specific temperature and the change in the association of the carbon with the ash component can cause a catalytic activation of the carbon material. However, it is difficult to determine changes in the ash distribution with pyrolysis temperature since most methods involve high temperature ashing of the coal to drive off all carbon materials prior to assessment. Even low temperature ashing results in modification of the ash and the carbon component is no longer present to observe association with ash particulates.

We were notified of a new method of interest which was developed by CSIRO QCAT and contacted them to find out more. After some discussion, a scoping study was suggested and

accepted where 4 coal chars which had been electrochemically assessed were analysed using combined CGA/MLA analysis which allows identification of ash size distribution, mineral type (without ashing), and char class. Chars chosen for testing are shown in Table 11.

Table 11: Coal chars suggested for analysis in scoping study

Sample	Parent Coal Type	Pyrolysis HHT	Ash content	Electrochemical Activity
1	Thermal	700°C	~30%	Low
2	Thermal	800°C	~30%	High
3	Coking	700°C	~10%	High
4	Coking	900°C	~10%	Low

An example of the data provided by CSIRO from the study is included here in Figure 69 to Figure 71.

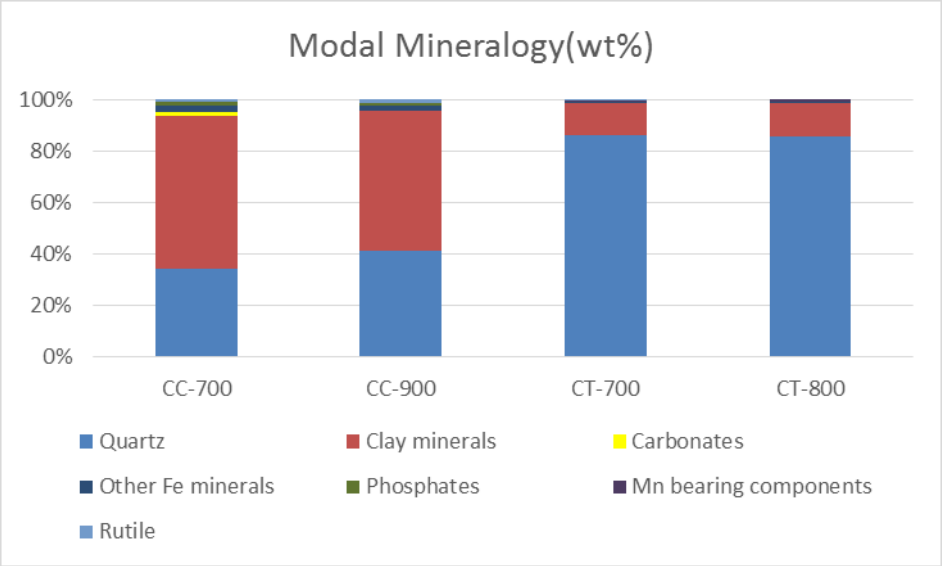

Figure 69: Mineral Composition

The data contains valuable information and the method has not previously been applied to coal chars, meaning it is a first of a kind study. It is difficult to determine trends from only four samples, however changes and similarities observed between coal types and coal chars will give another piece of the puzzle in terms of understanding activity of coal chars in the DCFC.

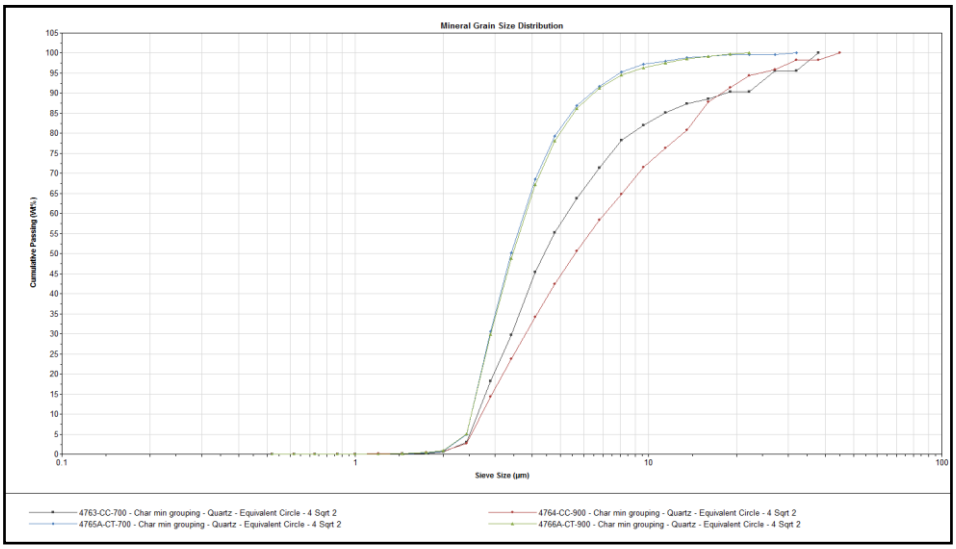

Figure 70: Mineral Size Distribution - Quartz

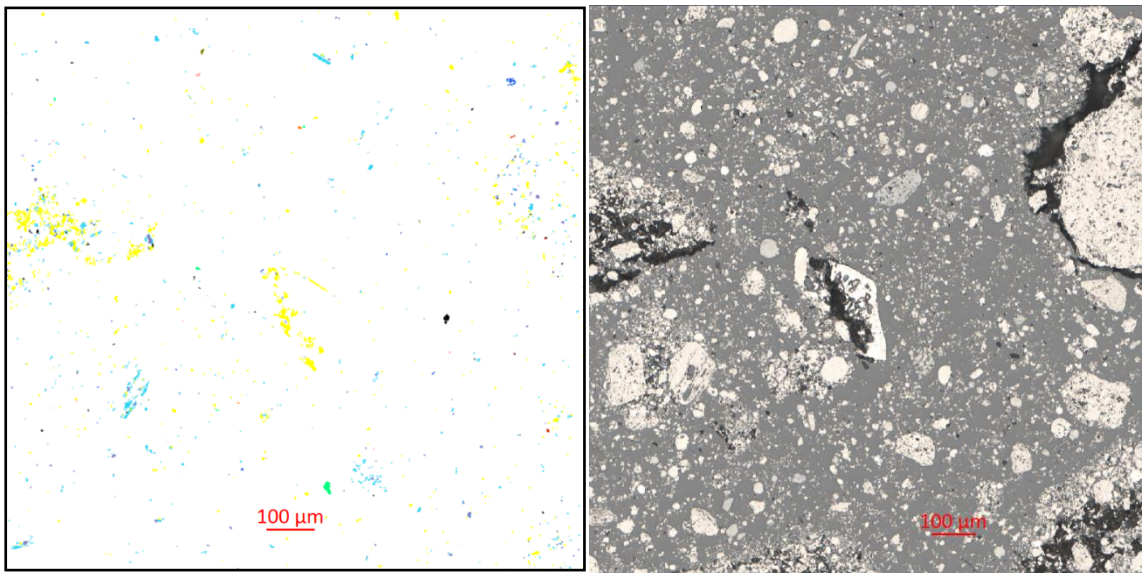

Figure 71: Matched Optical/MLA analysis (portion)

3.8.3.2. Performance Analysis – Literature Review

In DCFC studies, a variety of membrane and cathode catalysts have been employed over a wide range of temperatures, arrangements and carbon fuels. A summary by fuel type was shown by Rady et al. in 2012 [55], however research interest in this area has intensified since with publication of over 20 new articles related to DCFC performance in 2013 and 2014. In this review, the maximum performance of each study is shown as a function of temperature in with publication dates up to and including 2014 only.

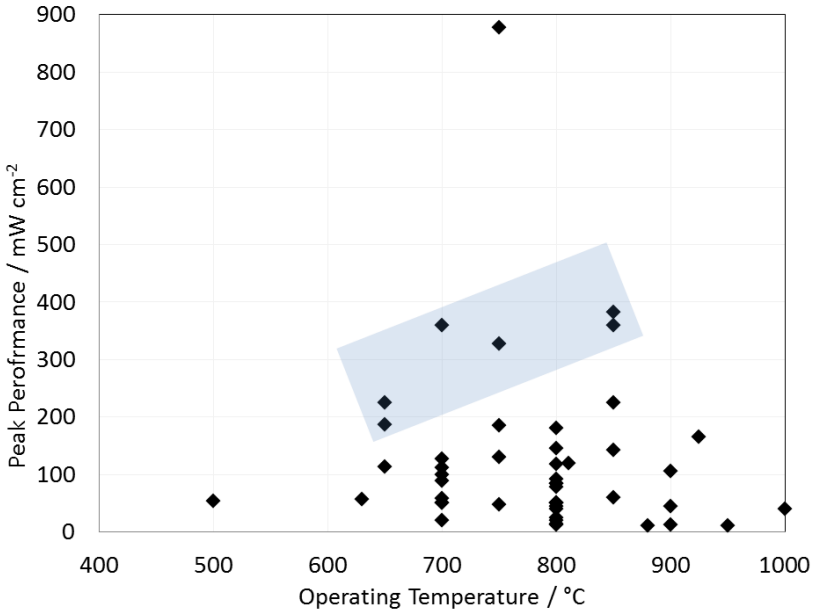

Figure 72: Cell performance as a function of temperature. Ref in order of lowest to highest performance for each temperature range: 500°C [56] 630°C [57] 650°C [10, 58, 59] 700°C [60-68] 750°C [37, 69-71] 800°C [13, 38, 40, 49, 72-83] 810°C [84] 850°C [85, 86]

Concentration of effort at operational temperatures of 700 and 800°C can be observed in this figure. The publication year and fuel cell arrangement type of cells outlined in have also been assessed and are shown in Figure 73.

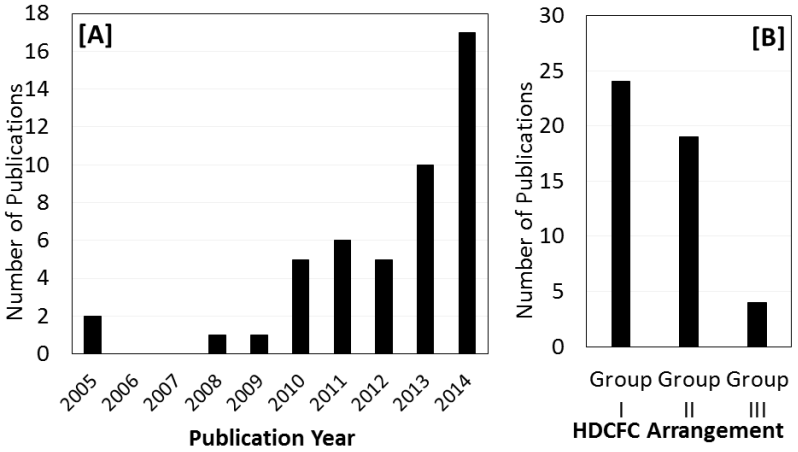

Figure 73: [A] Publication year and [B] Cell arrangement of cells assessed in Figure 72

Clearly, research interest in this area is high with more studies published in 2013 and 2014 to date than in all previous years (Figure 73[A]), a trend which is expected to continue increasing. Most investigations have made use of a carbonate secondary electrolyte with the second most common being direct contact and very few making use of a molten anode, a few select research groups engaged in this specialized area.

Trends in best cell performances observed does not appear to obey any clear relationship with temperature, shown in Figure 72 . Indeed it is difficult from analysis of published results to

determine the key to high performance. Best performance was reported by Jiang et al. [69] where the reported power density is double that of the second best performing cell. The authors attributed this high performance to the use of a thin solid membrane of YSZ, being anode supported in preference to membrane supported. However, for an almost identical arrangement with a very thin solid oxide membrane and the same carbon fuel, pyrolysed MDF, performance for Chien et al. [81] was a tenth of the output of Jiang et al. In fact results are of Jiang et al. are anomalous when compared with other similar arrangements and we are sceptical of their reality, indeed they may have been skewed through normalisation or other mistake on the behalf of the authors. Until this result is replicated, it will be regarded with scepticism.

Cells with more realistically high performance (above that of 300 mW cm^{-2}) have significantly different arrangements including different solid oxide membranes (SDC, YSZ and LSGM), cathode catalysts (BSCF, LSM, GDC and LSC/CGO), fuels (activated carbon, pyrolysed MDF, carbon black) and arrangements (molten anode, secondary carbonate electrolyte and direct contact). All primary electrolytes used were below 200 μm for these highly active cells, however the thickness of the membrane does not necessarily determine performance, considering the work of Dudek et al. who managed to achieve a power density of over 100 mW/cm^2 with a YSZ membrane 2 mm thick [65, 68], compared to Kulkarni who also used a direct contact arrangement with a YSZ membrane less than 30 μm thick [61, 77] yet achieving less than half the power output of Dudek et al.

A summary of key arrangement variables used in the best performing cells highlighted in are shown in Table 12.

SOURCE	*Lead Author*	Chen	Hao	Jayakumar	Xu	Lee	Zhang
	Year	2010	2014	2011	2013	2014	2014
	Ref.	[10]	[59]	[68]	[71]	[87]	[88]
CATHODE	*Cathode*	Lithiated NiO	LSCF	LSF-ScSZ	BSCF	LSM/YSZ	GDC/Ag
	Current Collector	n/s	Silver Paste	Silver Paste	Silver Paste	Platinum Mesh/Wire	Silver Mesh
MEMBRANE	*Type*	$(Li_2CO_3–K_2CO_3)–Al_2O_3$ (7:3)	SDC	ScSZ	SDC	YSZ	LSGM ($La_{0.9}Sr_{0.1}Ga_{0.8}Mg_{0.2}O_{3\,d}$)
	Thickness / mm	1	0.02	0.15	0.2	0.25	0.15
ANODE	*Current Collector*	n/s	Silver Paste	Rhenium Wire	Rhenium Wire	Platinum Mesh/Wire	Silver Paste
	Anode	n/s	NiO/SDC	Molten Sb-Sb_2O_3	n/a	Ni/YSZ (porous)	GDC/Ag
	Fuel Delivery	Carbon:Carbonate Pressed Pellet (8:3)	Particulate Carbon	Molten Anode	Molten Anode	Carbon:Carbonate Slurry (2:3)	Particulate Carbon
	Secondary Electrolyte	Li_2CO_3-K_2CO_3 (62:38)	None (direct contact)	Molten Sb-Sb_2O_3	Molten Sb-Sb_2O_3	Li_2CO_3/K_2CO_3 (62:38)	None (direct contact)
	Carbon type	Needle Coke	Waste Paper Carbon	Sugar Char	Activated Carbon	Super-P Carbon	Fe-loaded Activated Carbon
CELL OPERATION	*Operational Temperature (°C)*	650	650	700	750	850	850
	Maximum Power Density (mW/cm^2)	187	225	360	327	359	383

Table 12: Performance and Variables of Best Performing DCFC Arrangements to date

Although publications do not generally note the normalization method used to obtain current as current density, use of a molten anode while normalizing via cathode surface area is likely to overestimate kinetic activity of a DCFC in this arrangement since it is essentially operating with an extended anode area due to liquid anode arrangement. Presumably the effective

anode area cannot be realistically measured and therefore the results are normalized against the cathode. Since the anode is the limiting reaction, this allows enhanced performance not through enhanced oxidation kinetics but through enhanced oxidation area. There is also an argument of the reduced ohmic resistance observed in these cells, which show good contact between the solid electrolyte and anode/carbon, and therefore low resistance over the cell, can be attributed mainly to resistance over the membrane and cathode. The efficiency of these cells is also highly limited. Generally for identical components, cells which utilize molten carbonate outperform those using direct contact between the carbon and solid electrolyte [50], although performance has been seen to improve for direct contact cells at temperatures higher than 800°C [50], most likely as a result of partical gasification of the fuel to form carbon monoxide, which again limits the efficiency of the cell performance.

It is thought that in fact the most important aspect of achieving a high performing cell is the contact between the fuel, current collector and oxide anion, i.e. triple phase boundary. This is best achieved using molten carbonates as an oxide ion conducting medium and when the carbon fuel acts as a current collector with sufficient conductivity. This is the working design of this grant and once optimised, with careful selection of cathode, membrane and cell components, a high performing DCFC can be achieved. Analysis of previous work suggests our design, once realised, may be expected to outperform all reported values.

3.8.4. Coal Ash Distribution Investigation

This work is currently under review in the Journal of Power Sources.

For the first time, a combination of coal grain analysis (CGA) and mineral liberation analysis (MLA) has been applied to coal chars prepared at different pyrolysis temperatures. Information collected from these powerful techniques is used here to assess electrochemical activity of coal chars in a solid anode of the direct carbon fuel cell.

It is shown here that coal char ash type and distribution vary considerably between parent coal types. It is proposed that this variation in coal ash leads to different activating conditions for coal chars trialled in terms of electrochemical performance. The coking coal chars analysed had larger particles than the raw coal and are more intimately mixed with mineral ash component of the char. These chars also have a high kaolinite content, determined through MLA analysis, which has previously shown catalytic effects on carbon electro-oxidation. Coking coal chars trialled therefore were shown to have activity closely linked to the chemical composition of the mineral content. Thermal coals investigated have a high quartz content as well as small ash particle sizes, which have minimal interaction with the organic component of the coal char. Quartz has been shown previously to be inhibiting to electrochemical oxidation of carbon fuels and, although a clear inhibition is not observed for the thermal coal investigated here, activation of the char does not occur at the same pyrolysis temperature as the coking coal. It is suggested here that the lack of clay catalysts in this material reduces its electrochemical activity when treated at the same pyrolysis conditions and that, instead, physical properties such as crystallinity and resistivity of the thermal coal char determine its final activation. The mineral content of raw coal applied to the direct carbon fuel cell is clearly of key importance in terms of activation of coal chars and has been observed here to dictate the required thermal pre-treatment to allow activation.

Results and Discussion

Coal Physical and Electrochemical Properties

Results found previously for coal chars investigated here are presented in Table 13.

Table 13: Coal Char Properties [87]

COAL CHAR	CC-700	CC-900	CT-700	CT-800
C / wt% (db)	79.80	83.17	64.67	65.50
H / wt% (db)	2.40	1.43	1.03	0.54
N / wt% (db)	1.76	1.22	1.39	1.29
S / wt% (db)	0.22	0.09	0.21	0.24
O / wt% (db)	4.78	2.55	4.16	3.41
Ash / wt% (db)	11.05	11.56	28.55	29.03
Pyrolysis Yield (db) / wt%	80.77	77.92	76.45	76.50
Resistivity / $m\Omega.cm^{-1}$	2271	2	267	31
BET SA / $m^2.g^{-1}$	69	37	96	98
Average Current Density at 0.5 V vs $C/CO_2/CO_3^{2-}$ / mA cm^{-2}	16.78	5.08	6.32	14.75

These chars were selected for further analysis due to differences in performance. The chars also have different pyrolysis HHT. For ashless carbon sources, it has been shown clearly that electrochemical activity in slurry-type arrangements can be linked to carbon functionalisation and BET surface area [13, 21, 51, 88]. It can be seen in Table 13 that there is no clear dependence on these simplified properties in the case of coal chars investigated here. In particular, the thermal coal used shows a substantial difference in electrochemical performance between 700-800°C HHT despite little to no change in chemical composition or BET surface area. Since the only major change appeared to be in the electrical resistance of these chars, it could be suggested that electrical conductivity is key to performance in a solid electrode, such as those used in this work. However, CT-700 has a 10-fold lower resistance than CC-700 and yet this coal char demonstrated very high activity. It was therefore thought that electrochemical observations may be explained through differences in the ash component of the coal chars investigated, in particular, the particle size of the char. Ash and specific identification of ash components were concluded to be key to determining electrochemical activity. A mixture of CGA/MLA analysis techniques were used in order to investigate this further.

Char Particle Size and Classification

Particle Size

Raw coals were prepared via ball-milling and sieving to less than 45 μm as outlined in [87] and Section 3.2.2. However, once the initial raw coal was sieved, it was then pyrolysed and used with no further treatment other than gentle separation of particles with a mortar and pestle. Char particle size was therefore measured to give a realistic reflection of the final char size used in electrochemical investigations. Results for each coal type and HHT are shown in Figure 74.

It can be seen in Figure 74that particle size of chars do not match raw coals which were sieved to below 45 μm size. This is especially true in the case of the coking coals investigated where particle sizes of larger than 150 μm are common, indeed outnumbering smaller particles in the case of CC-900. Thermal coals show smaller particles with the majority in the expected size region, however they do include some few larger particles. Differences between the two

different types of coals used can be clearly seen in optical images taken of the coal chars embedded in resin as per Section 3.3.2, shown in Figure 75.

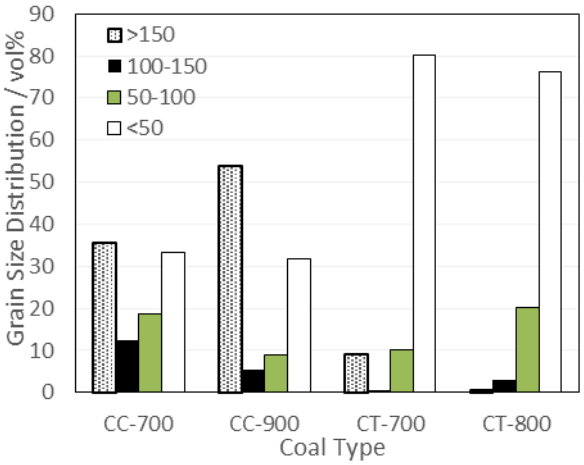

Figure 74: Coal char particle size distribution

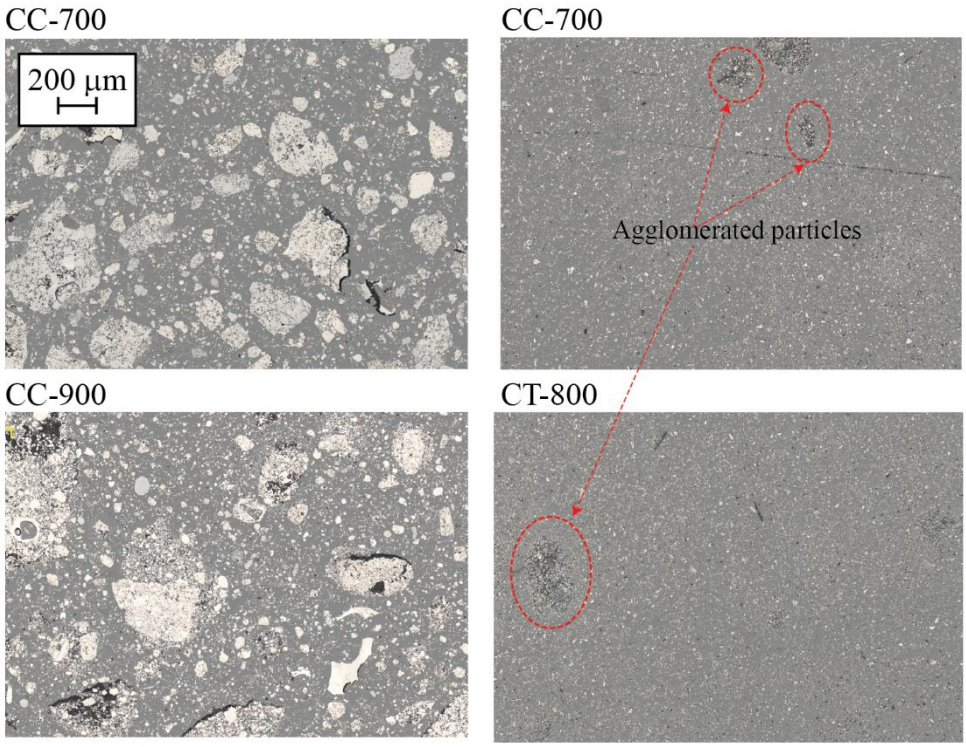

Figure 75: Optical image of coal chars embedded in resin

It is possible that larger particles are simply agglomerates of smaller particles, however it can be seen in Figure 75for CC chars that the large particles observed are not agglomerates but rather are indeed large single particles. This does not occur in the case of CT chars and, considering smaller portion of over-sized particles, agglomeration could be a factor for CT rather than CC chars. Some examples of possibly agglomerated particles are circled in Figure 75. These are visually very different to the large particle seen to dominate in CC chars.

Coking coals are known to have a plasticisation stage, more so than thermal coals. It is

likely that, since no further processing occurs during pyrolysis that the particle size of the coking chars changes during this plasticisation stage [89]. This fusing appears to be less likely to occur in the case of thermal chars investigated here.

Char Mineral Composition and Distribution

Char Composition

Using MLA software, minerals were identified in each coal char from a representative segment of the char encased in resin. A normalization procedure was used in order to identify mineral components in the chars as these were expected to be different to raw coal minerals present in the database.

MLA analysis yielded a range of different particles, the relative weight percent of which was calculated by the software. This method allows detailed identification of minerals present in the char without thermally or chemically altering the char. Therefore, results reflect real concentration observed in an electrode composed of this char. This method also allows differentiation of complex minerals such as kaolin compared to quartz. These minerals cannot be differentiated through normal ash analysis where elemental composition are determined through ashing and overall elemental balance assuming oxides of each element. A combination of quartz, clays, carbonates and other minor mineral components were found in each char type, as show in Table 14

Table 14: Minerals present in coal chars analysed according to MLA

Mineral (wt%)	Composition	CC-700	CC-900	CT-700	CT-800
Quartz	(SiO_2)	34.15	41.42	86.25	85.43
Kaolinite	$Al_2Si_2O_5(OH)_4$	21.90	15.53	0.86	0.55
Illite	$K_{0.6}(H_3O)_{0.4}Al_{1.3}Mg_{0.3}Fe^{2+}_{0.1}Si_{3.5}O_{10}(OH)_2 \cdot (H_2O)$	31.33	34.30	10.95	11.87
Clay	$(Mg_3,Fe_2)Al(AlSi_3)O_{10}(OH)_8$	6.16	4.17	0.79	0.87
Calcite	$Ca(CO_3)$	0.25	0.01	0.00	0.00
Siderite	$Fe^{2+}(CO_3)$	1.19	0.39	0.02	0.02
Pyrite	Fe_2S_2	2.03	0.27	0.00	0.01
Fe	Fe	0.63	1.46	0.14	0.25
Apatite	$Ca_5(PO_4)(F,Cl,OH)$	1.58	1.19	0.00	0.00
Manganite	$Mn^{3+}O(OH)$	0.02	0.00	0.37	0.80
MnSulfate	$MnSO_4$	0.03	0.00	0.37	0.10
MnS	MnS	0.00	0.00	0.03	0.00
Rutile	TiO_2	0.73	1.25	0.22	0.10
Total		**100.00**	**100.00**	**100.00**	**100.00**

It can be seen in Table 14 that the majority of the ash for each char type is quartz and clay (including, kaolinite, illite and clay in this category) which make up a combined total of more than 90 wt% of the total ash. Carbonates, iron minerals, phosphates, manganese bearing compounds and rutile make up a combined total of less than 10%, in some cases less than 5 wt%. Thermal and coking coal chars investigated show very different compositions, although only small differences can be seen between char HHT. The thermal coal used here clearly has a high quartz content, more than 85% of the ash component is identified as silica. Between 700 and 800°C this does not appear to change drastically, with the biggest changes being a slight decrease in silica and increase in illite when increasing temperature from 700°C to 800°C.

Coking coals however do show a large change in ash composition with pyrolysis

temperature which is beyond the expected error for these measurements. When the HHT is increased to 900°C, the amount of kaolinite present in the ash drops by more than 5 wt%, while the amount of quartz increases by the same amount. The decomposition of kaolinite has been reported to involve several temperature dependant steps, forming metakaolinite (AS_2, or $Al_2O_3.2SiO_2$) and even quartz at elevated temperatures [90], i.e.;

$$Al_2O_3.2SiO_2.2H_2O \xrightarrow{450-700°C} Al_2O_3.2SiO_2 + 2H_2O \quad \textbf{(31)}$$

$$2(Al_2O_3.2SiO_2) \xrightarrow{925-1050°C} 2Al_2O_3.3SiO_2 + SiO_2 \quad \textbf{(32)}$$

The decomposition temperature of kaolinite has been seen to be dependent on the type of coal due to differences in initial kaolinite composition [90]. Results shown for CC-char heated at 900°C see a decrease in the kaolinite measured and increase in quartz, which suggests the decomposition reaction shown in Eqn (31)-(32) is likely occurring at the slightly lower temperature of 900°C.

The total amount of mineral present in each char as a whole should also be considered since the ash component of the coking and thermal coals investigated here are different. The overall weight percent of combined clays and quartz are compared in Figure 76.

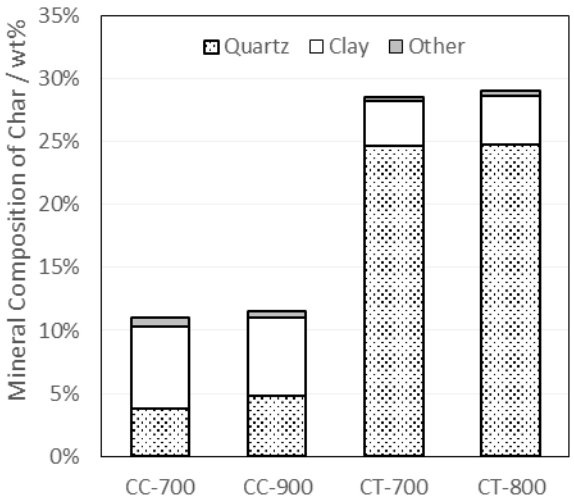

Figure 76: Main mineral composition of ash present in CT and CC chars

Carbonates and other minerals make up a very small portion of both coal char types and are therefore not considered in further detail. Overall, each char has a similar amount of clay (~ 5 wt%) although CC chars are dominated by kaolinite while CT chars include mostly illite. The larger overall ash content, combined with the high percentage of quartz in CT char ash, reveals far more total quartz in CT chars than CC chars.

Impact of Minerals

To determine the effect of kaolinite on coal chars, CT-700 coal was mixed with 5wt% kaolinite and tested in a graphite based electrode for activity. Results for both the initial, inactive CT-700 char and kaolin modified CT char electrode are shown in Figure 77. It was seen in a previous publication [4] that kaolinite increases the comparative electrochemical performance of graphite substantially when normalised for the amount of kaolin present. In Figure 77, no normalisation has occurred other than for the geometric surface area of the electrode, and yet the observed current density is seen to more than double by a potential of 0.2 V (6.46mA.cm^{-2} for

CT-700, 14.61 mA cm^{-2} for CT-700 with kaolinite). Clearly, CT-700 can be activated through the addition of small amounts of kaolinite, and this is observed to a greater degree than activation on graphite.

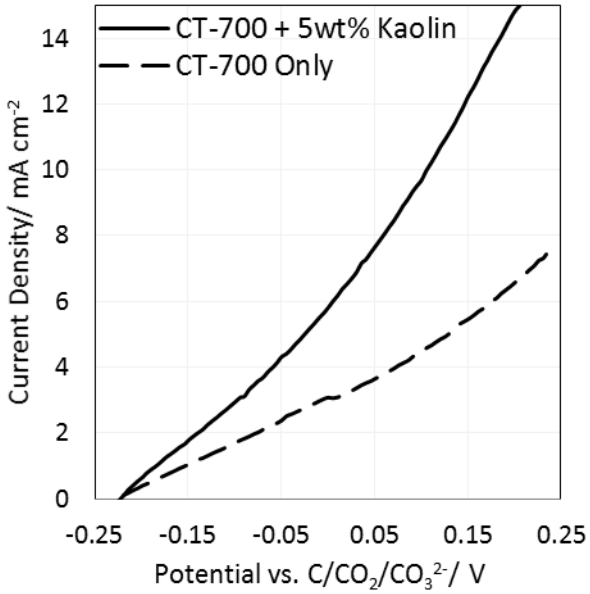

Figure 77: Kaolinite catalyst effect on CT-700 char

The effect of quartz is more difficult to understand. Inhibition by quartz addition has been observed previously [4, 6], however CT-800, which still includes a large amount of quartz, shows high activity. This could be a result of distribution within the electrode, quartz particle size and association with coal char or, most likely, total amount of quartz present in the solid electrode. In this case a maximum of 25 wt% of the char is quartz and only 25 wt% of the electrode is char, meaning approximately ~6 wt% quartz total in the electrode. In the previously reported results, the inhibiting influence of quartz was investigated from 10wt% SiO_2 up to 50wt% of the total solid electrode and this is therefore outside the previously reported on range. At a lower loading and elevated temperature (600°C compared to 500°C), quartz does not inhibit performance. It may not enhance it as observed for other minerals, but certainly carbon oxidation is not blocked in this case.

Ash particle size

Where inhibition was observed by quartz contamination of a solid graphite electrode, particle sizes in the 10-20 µm size range were used [4]. In the case of the CT chars, particle size of the quartz is much smaller, the majority in the 2-5 µm range, and all less than 10 µm, as shown in Figure 78[B].

CC chars also contain a comparatively small amount of quartz and some of this is present in larger particle sizes than the CT chars, extending out to 38 µm in size. This can also be seen for clay distribution where the distribution of clay in the CC chars includes larger particles than seen in CT chars (Figure 78).

The interfacial area expected for the quartz and clay minerals has also been calculated using the density of the mineral and chars. Mineral density was calculated based on the combination of clays present in proportions seen in Table 14, while char density was measured

by compressing char under the same conditions as electrode pellet formation (740 MPa) and measuring resultant volume. Density of chars ranged from 1.43-1.78 g/cm^3. Particles are assumed to be spheres with diameters of the specified particle size. Results for the surface area of ash contacting the char per square centimeter are shown in Figure 79.

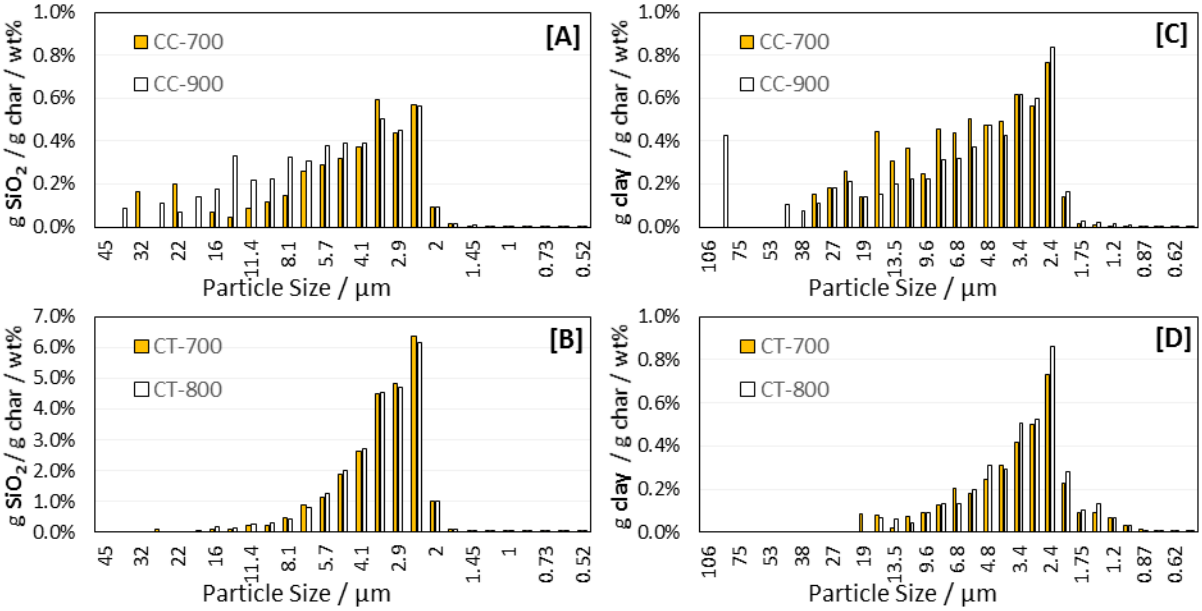

Figure 78: Particle size distribution of SiO_2 and clay minerals in thermal and coking coals from MLA analysis

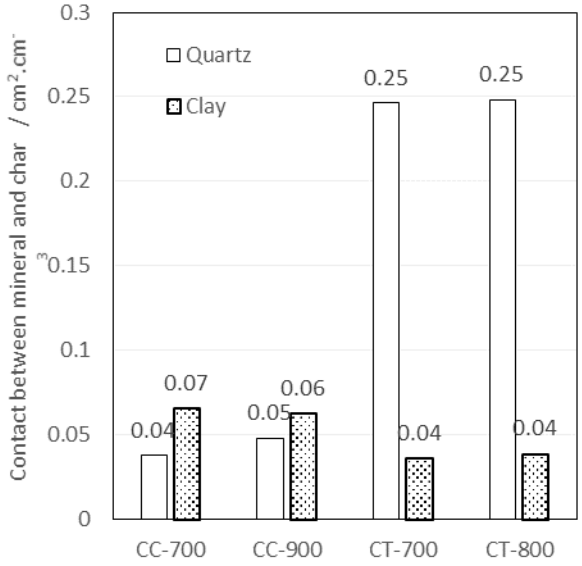

Figure 79: Comparative contact area of SiO_2 and clays for thermal and coking coals

The interfacial area of quartz and clay is reflective of the weight percentage. There is large contact area observed with quartz for the CT chars, reflective of the smaller particle size of the quartz in this case. For CC-chars there is higher contact area with clays. No major differences can be observed between pyrolysis temperatures for coal chars of the same parent coal origin

other than a slight increase in quartz contact area between CC-700 and CC-900.

Ash Distribution

Combining optical images and mineral liberation analysis enables mineral distribution within the char to be observed and to qualitatively understand contact between char and ash. Several example particulates for CC-700 and CT-700 are shown in Figure 80 and

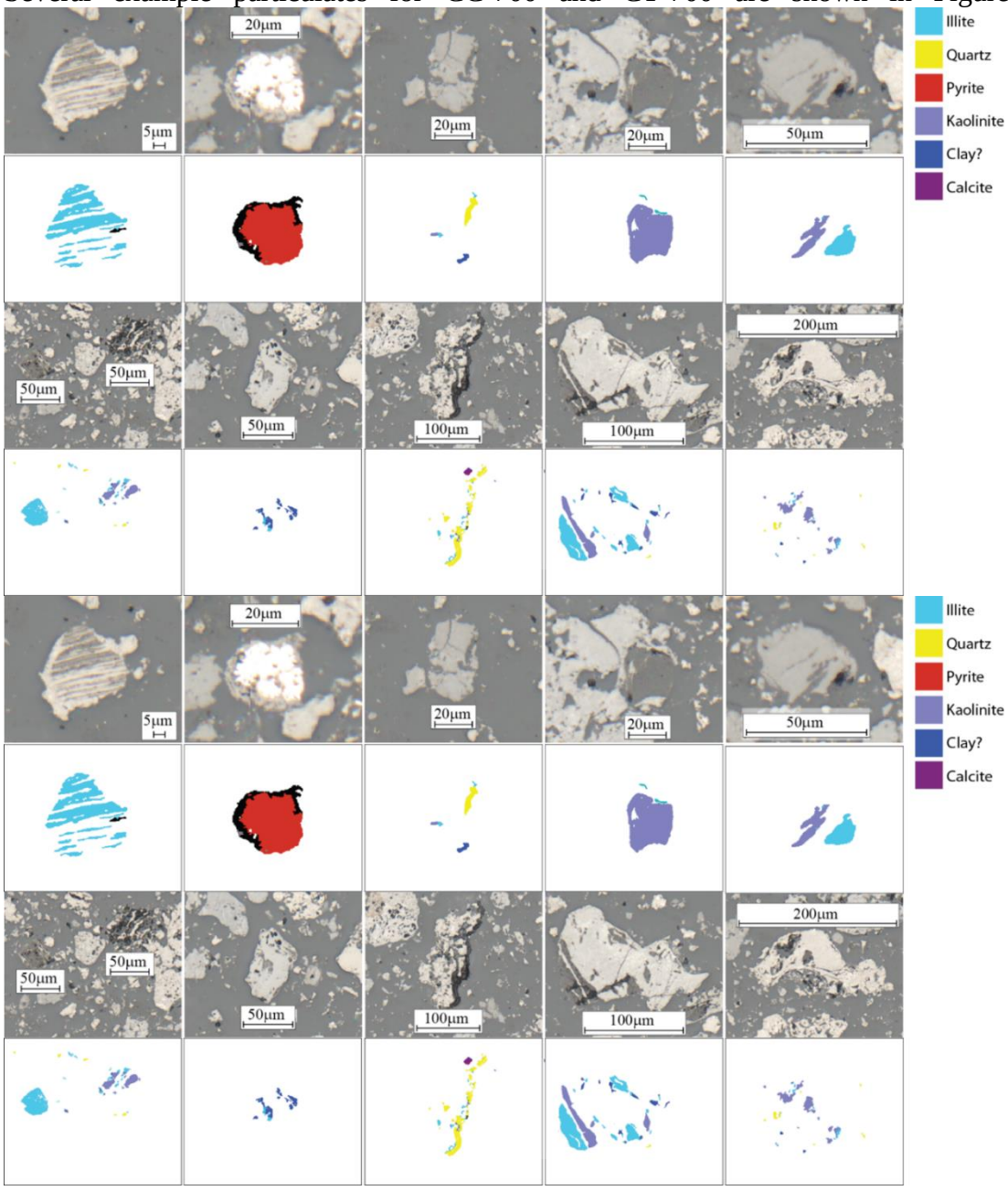

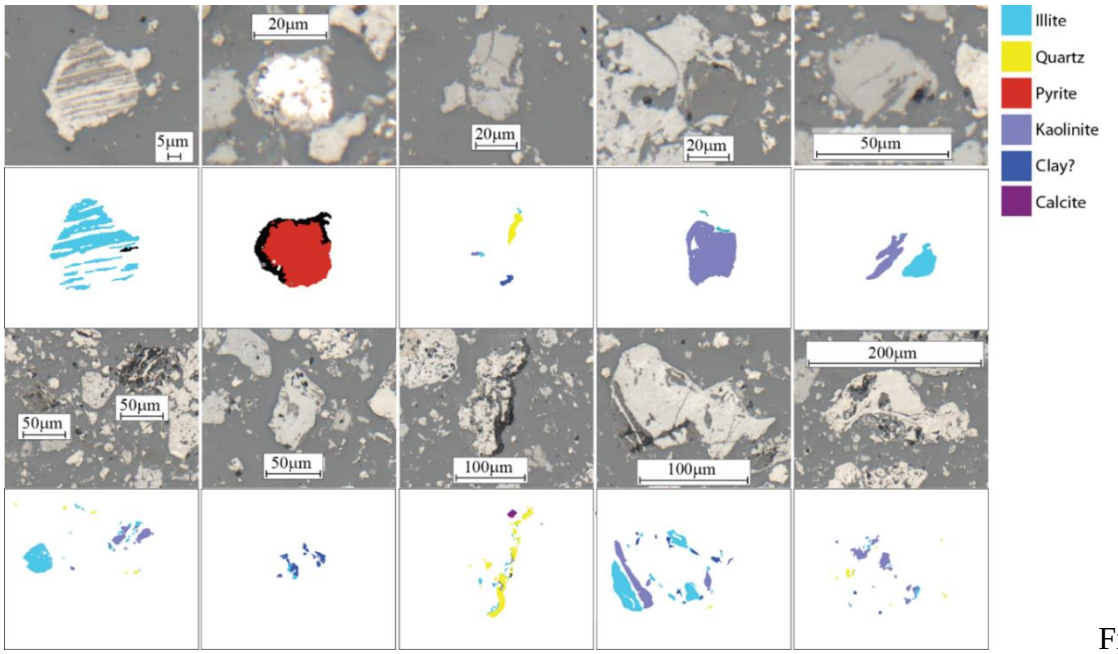

Figure 81.

No major differences observed between char HHT for each char type.

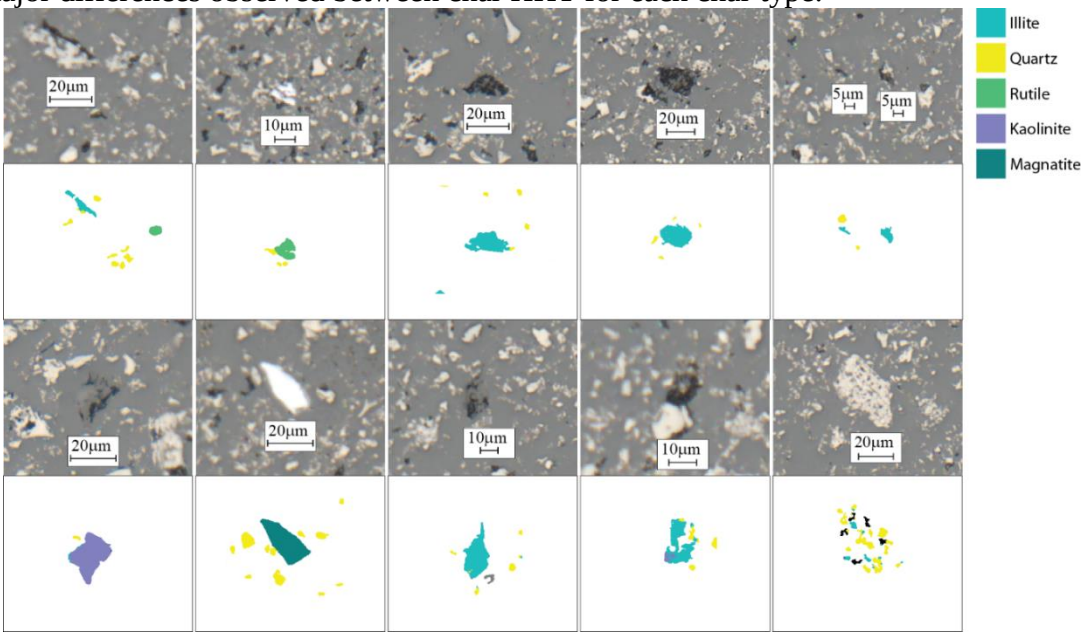

Figure 80: Physical ash distribution of minerals within char particles shown with optical

and MLA analysis technique – CT-700

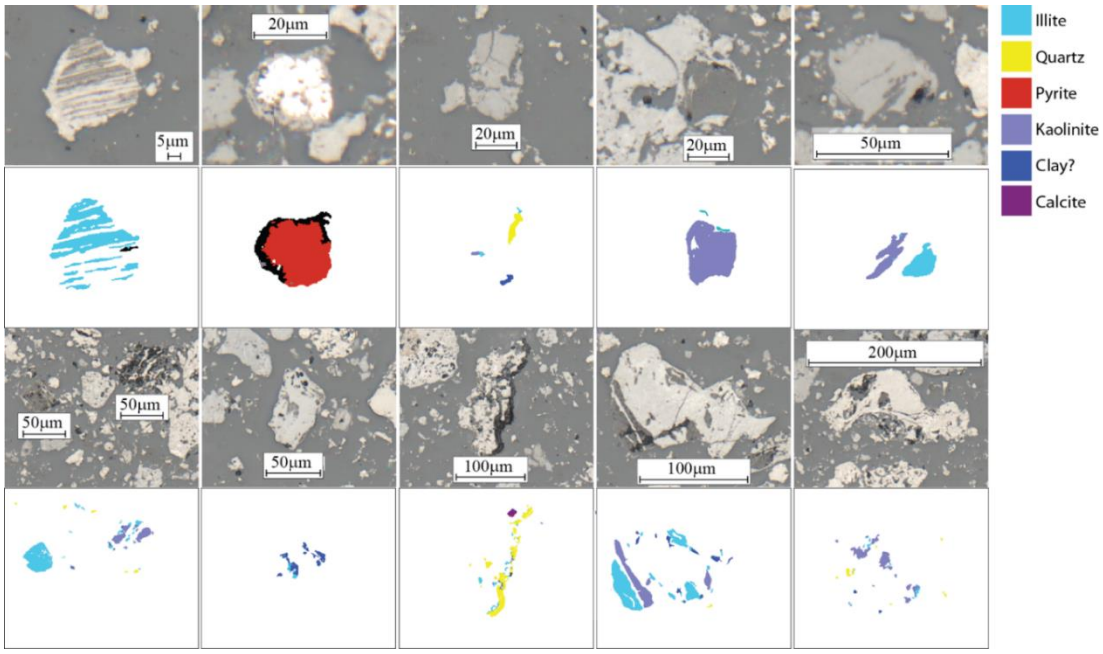

Figure 81: Physical ash distribution of minerals within char particles shown with optical and MLA analysis technique – CC-700

Qualitative analysis of a representative sample of particulates shows some trends and interesting observations for different coal chars investigated here. Ash particles in the case of CT coals are far less closely intermixed with the carbon component than with CC chars, as well as being smaller, as expected from particle size and ash size distributions (Figure 80 and Figure 81, respectively). Quartz is also prevalent in CT chars, although MLA data is difficult to match directly with optical images as quartz is not clearly delineated in optical sampling, being grey similar to the background colour. Intimate contact with char however does not appear to

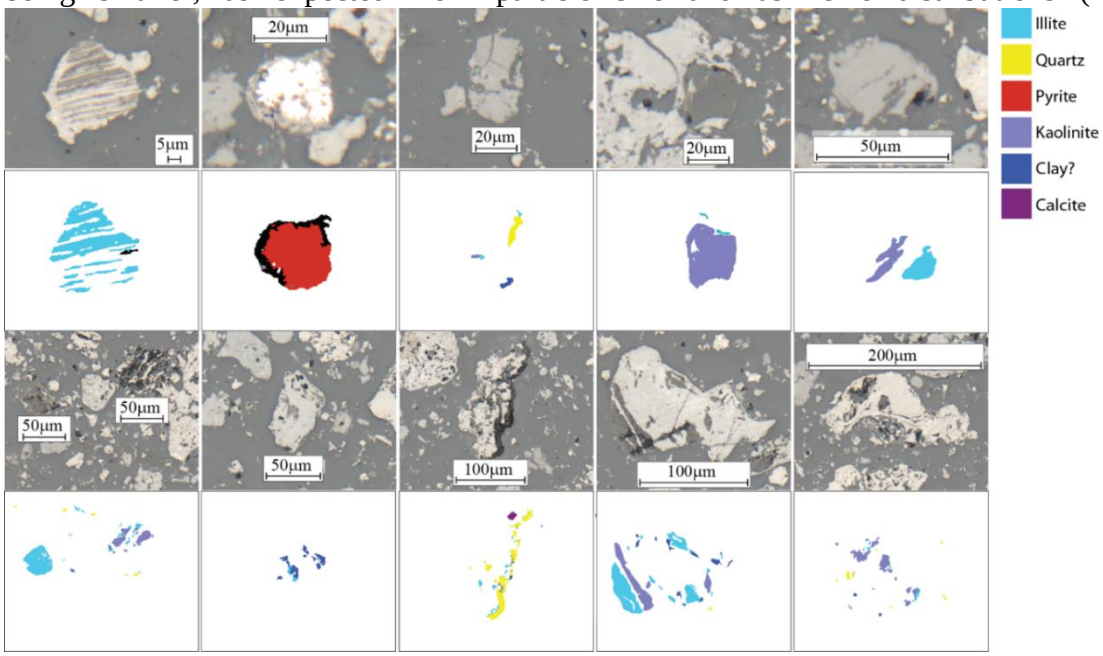

occur with quartz to the same extent as clay components, and smaller char particles in the case of CT-chars also means very little intimate contact can be observed.

CC-chars however show very close intermixing and association of char with minerals, especially in the case of clays. Here, particles as well as mineral components are larger, although minerals are for the vast majority still smaller than the raw coal sieve size of 45 μm.

Discussion

Analysis of ash distribution and type in coal chars is a useful tool for assessing characteristics of the carbon fuel. The technique enables assessment of the ash type and mineral content without high temperature treatment of the fuel prior to assessment. It also allows accurate identification of minerals and their particle sizes compared to the particle size of the coal char. Qualitative assessment of the distribution of mineral components with carbonaceous particles can also be carried out. Matched with electrochemical analysis of these chars, this is a powerful technique which can help to understand differences in electrochemical oxidation performance.

Optical analysis of chars has shown that initial particle sizing of the raw coal is not a sufficient description in the case of coking coals as these coal chars tend to be composed of particles which have fused, forming larger char particles. This immediately introduces a point of difference between the chars and suggests they are not directly comparable despite similar pyrolysis temperatures.

Clear differences between coal types in terms of ash distribution including mineral composition, size and contact with char can be observed. CC chars investigated show substantially lower quartz content than the thermal coal chars with the majority of the ash composition being kaolinite. Both overall char and individual mineral particle sizes were seen to be larger for the CC than CT chars and the minerals were more intimately mixed with the char particles for CC chars. CT chars showed a prevalence of physically separated mineral matter in individual particles while CC chars were more likely to have mineral matter combined into a larger particle.

Between pyrolysis temperatures for the same chars, very little variation can be observed. No clear difference quantitatively or qualitatively can be seen for mineral matter present in CT-700 and CT-800. Since there is a difference in electrochemical activation, the reason does not appear to be related to the mineral content, as previously proposed. Between CC-700 and CC-900, however, changes in the mineral content can be observed. Differences include an increase in the quartz content and decrease in kaolinite content when the pyrolysis temperature is increased from 700°C to 900°C. Small changes in kaolinite content are shown here to make a big difference in overall activation of coal. Addition of only 5wt% kaolin to the otherwise inactive CT-700 demonstrated activation in terms of electrochemical performance with current density doubled at the same polarisation.

Activation observed in CT coals with change in HHT is likely related to the tipping point observed for the material resistance since the resistivity of CT-800 is substantially lower than CT-700. Change in resistivity is results from change in carbon structure at 800°C. Structural change impacts degree of carbon crystallinity and crystallite size, which has been shown to impact on electrochemical performance of carbon in particulate form [16].

It is suggested here that CC coals appear to be activated when they still have lower conductivity due to enhancement effect of clays present and close contact of mineral content throughout larger char particles observed in the case of CC chars. Deactivation of CC chars is likely a result of decreased functionalisation (O/C, H/C ratios) but could also be due to changes in clay composition which occur showing a decrease in the kaolin composition which is shown

here to have dramatic enhancement effects on electrochemical activity for only 5 wt% inclusion.

Conclusion

Although ash distribution and consideration of particle size gives very useful information in terms of showing differences between chars of differing origin, differences between pyrolysis HHT are not observed here and an alternative hypothesis is required to explain change in behaviour of solid char based anodes with pyrolysis temperature. Electrochemical activation of coal chars at a solid anode in molten carbonate appear to be dependant on two different properties. The first is the 'physical' properties of the char including its porosity, resistivity, surface area and crystalline structure. The second is the prevalence, size and type of mineral matter in the coal char and its contact with char particles. Ideal properties in terms of physical characteristics hinge on low resistivity, while the activating properties of kaolinite mineral are clearly observable and can lead to activation without optimisation of physical characteristics if it is distributed intimately with carbonaceous matter.

3.8.5. Coal Pre-treatment Investigation

The effects of thermal and chemical pre-treatment of a bituminous coal from a NSW coal deposit have been investigated in terms of electrochemical performance in a solid anode half-cell set-up for use in a hybrid solid oxide DCFC.

It was found that demineralisation alters the composition of the coal char, with the resultant electrochemical activity related to whether acid or base demineralisation was used. Demineralisation with a strong base (NaOH) led to an electrochemical activity increase of almost 70% from the untreated coal char, with the lowest resistivity obtained for this pre-treatment option. Use of HNO_3 had little effect on this coal type, except for a slight conductivity increase. Demineralisation with HCl resulted in significantly lower surface activity of the coal char with no change in conductivity. The influence of different mineral matter present in the untreated coal is reported as the cause of differences in electrochemical performance of the coal chars after demineralisation.

Obtaining a suitable method of carbon-oxygen functionalisation of the coal chars for increase in surface activity was another objective of this investigation. Pre-treatment of coal by partial oxidation with air at high temperatures (800°C) led combustion of volatile surface groups rather than the anticipated formation of carbon-oxygen surface groups. This was despite low oxygen partial pressures used, leading to a systematic decrease in surface activity of the coal chars with increasing exposure time to the air.

Results and Discussion

<u>Obtained mass yields after coal pre-treatment</u>

Thermal treatment by pyrolysis at two different temperatures, 800 and 900°C, has been tested for a thermal, bituminous coal from the NSW Australia coal deposit. Previous study by Allen et al. [87] investigated the effect of increasing pyrolysis temperatures on the same thermal coal. The relative activity at the surface of this coal was found to be highest at a pyrolysis temperature of 800 °C. A partial oxidation trial at a temperature of 800 °C has been performed for investigation of the possible increase in surface functionalisation. Additionally, demineralisation steps by acid and base has been performed on the untreated coal for the removal of mineral impurities. The resulting coal was then pyrolysed at 900 °C for comparison with untreated coal pyrolysed at the same temperature. The percentage yields after defined treatment (Table 15) show mass losses of between 20-30 % after pyrolysis. This supports previous analysis

done on the characteristics of the selected coal in that Ivanhoe North (IV) contains a considerable amount of volatile compounds driven off by the high heating temperatures [87].

Table 15: Yields obtained of IV coal after treatment, where indicated treatment steps are given in order (abbreviations are used throughout the report)

Treatment	Abbreviation	Yield-%
Pyrolysis at 800 °C	IV(800)	76.4
Pyrolysis at 900 °C	IV(900)	77.0
Partial oxidation at 800 °C 240 min N_2, 10 min O_2	IV(800)-10minO2	77.1
Partial oxidation at 800 °C 240 min N_2, 30 min O_2	IV(800)-30minO2	75.0
Acid demineralisation with 4 M HNO_3	IV(HNO3)	98.4
1: 4 M HNO_3 2: Pyrolysis at 900 °C	HNO3-IV(900)	73.9
Acid demineralisation with 4 M HCl	IV(HCl)	98.8
1: 4 M HCl 2: Pyrolysis at 900 °C	HCl-IV(900)	71.8
Base demineralisation with 4 M NaOH	IV(NaOH)	101.1
1: 4 M NaOH 2: Pyrolysis at 900 °C	NaOH-IV(900)	74.9

Expected difference in obtained yield is seen between the coal pyrolysed at 800 and 900 °C as the higher temperatures would lead to a slight increase in the removal of volatile compounds. Little difference is seen for the mass loss of the partial oxidation procedure, however a difference of 1.4 % is observed for the sample which was exposed to 30 minutes of introduced air at high temperature; a possible indication of the removal of more volatile compounds, or that some coal char has been burned off by combustion instead of fixing oxygen to the coal surface as desired. Very small mass losses are seen from the acid demineralisation treatments. The bituminous coal used consists of about 20 % mineral matter, which should lead to a lower percentage yield if demineralisation removed this component, thus harsher conditions might be necessary for future analysis in order to successfully remove mineral matter from the char. The base demineralisation shows a slight increase in mass after treatment. It is possible that functionalisation of the coal surface has led to a higher mass than initial mass; however it is more likely a result of the procedure used for obtaining the mass yield, which involved filtration and drying steps.

Resistivity measurements of coal samples

The resistivity has been measured as an indication of the conductive nature of the resulting coal chars after thermal treatment. The columns in blue colour show resistivity of samples pyrolysed at 900 °C (Figure 82). Pre-treatment with a strong base (NaOH) and two strong acids

(HCl and HNO_3) were compared with initially untreated coal. Columns in red show calculated resistivity values (Equation 4) of the coals undergoing partial oxidation treatment compared with untreated coal pyrolysed at 800 °C.

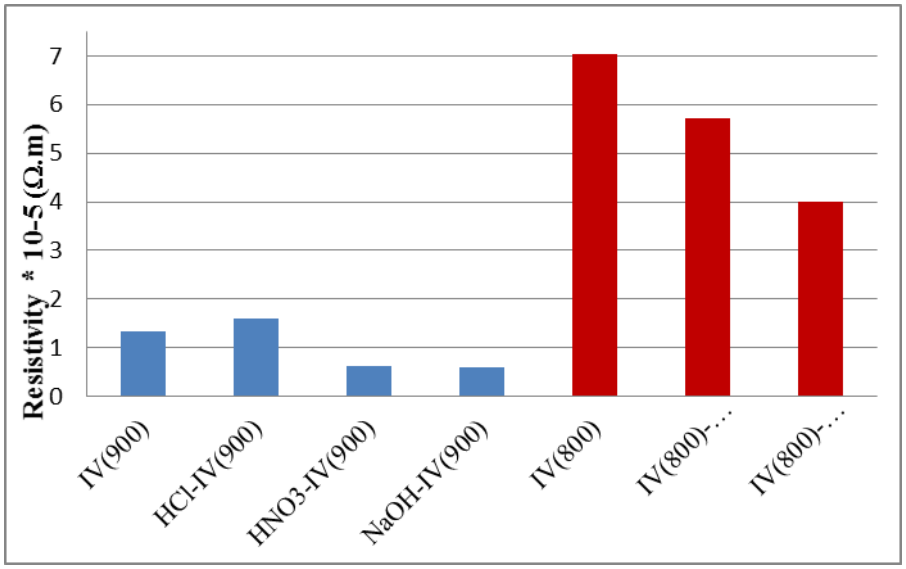

Figure 82: Calculated resistivity of the different coal samples

A clear decrease in resistivity is observed for increasing applied time of partial oxidation at the high heating temperature (800 °C). This is an indication that more volatile matter is removed by the introduction of air, supporting the possibility of a combustion process happening at the coal char instead of desired partial oxidation. The resulting relative increase of carbon would likely be the cause of conduction increase in the coal char.

It is difficult to say from Figure 82 whether or not the resistivity of the demineralisation pre-treatments resulted in significant difference from the untreated coal pyrolysed at 900°C. It seems like the most notable difference resulted from the demineralisation with HNO_3 and NaOH, where demineralisation with HCl show a resistivity pretty much on par with the untreated coal char. As previously explored by Li et al. [88], will the HNO_3 possibly functionalise the coal surface in addition to removing some of the minerals that inhibit electrochemical activity (like Al_2O_3 and SiO_2). This might be the reason for the resistivity decrease in the coal char treated with HNO_3. As little research has been done on the demineralisation of coal with NaOH in literature, further interpretation of electrochemical analysis is necessary to achieve a possible understanding of what reactions might have happened in this sample.

Thermogravimetric analysis of demineralised coal

Three different demineralisation procedures were tested for the removal of mineral impurities in the thermal coal investigated (Table 16). The resulting ash content after heating of demineralised IV coal was determined at temperatures between 20-1000°C, and subtraction of water content was performed by disregarding mass losses up to about 150°C.

Table 16: TGA analysis of ash content in demineralised IV coal at mass loss measured between 20-1000 °C

	Ash content (wt% dry basis)

IV(raw)*	22.4
IV(NaOH)	15.2
IV(HNO3)	16.5
IV(HCl)	17.2

** Allen et al. [87]*

The ash content of raw IV coal is about 22 %. Small changes in ash content was seen from the demineralisation treatments. The largest difference of 7.2 % from the raw coal was obtained from the treatment with NaOH. The type of mineral matter in the thermal coal investigated cannot be clearly determined as the ash contents from the three demineralisation treatments are very similar. However, the small difference seen for the lowest ash percentage obtained from the NaOH treatment compared to treatment with HCl and HNO_3, might possibly be an indication of the presence of mineral matter that is more reactive to the strong base rather than acid. Further electrochemical analysis are performed to appropriately assess resulting difference in activity by current density of the demineralisation treatments.

Electrochemical analysis of pre-treated coal in the anodic working electrode

Linear Sweep Voltammetry

Linear sweep voltammograms were collected for a 25 wt% loading of each coal sample in a coal char/graphite mixture. All the coal samples show negative open circuit potentials (OCP, where current density is zero). The OCP gives an indication of the voltage difference between the reference electrode (RE) (graphite) and the working carbon electrode (WE) at the conditions investigated. The WE is higher in activity as it contains coal as opposed to the pure graphite hich the RE consists of.

Cyclic fluctuations with differing amplitudes were observed for each of the voltammograms above zero potential. This has previously been proposed by our research group to be a result of bubble formation at the anode from CO_2 production. When a bubble is forming, the current decreases until the bubble is released due to coverage of the active surface area with the product gas. The current then jumps up to the actual current density of the surface, where size and frequency of the jumps are likely related to the surface properties of the coal. However, recent study by Allen et al [91] links the difference in bubble formation to the combination of cations in the carbonate melt and to the possible intercalation of lithium into the surface pores [91]. Despite this, will differences in bubble formation at the anode surface be explained by differences in the coal samples that were tested, as the same carbonate eutectic mixture was used in every electrochemical testing procedure. If more oxygen is fixed to the coal, which would possibly increase the surface activity, then more CO_2 will be formed and bubble formation will increase as a result [87].

Figure 83 shows the predicted higher activity of IV(800) as opposed to IV(900), which is comparable to work previously done for the same thermal coal [87].

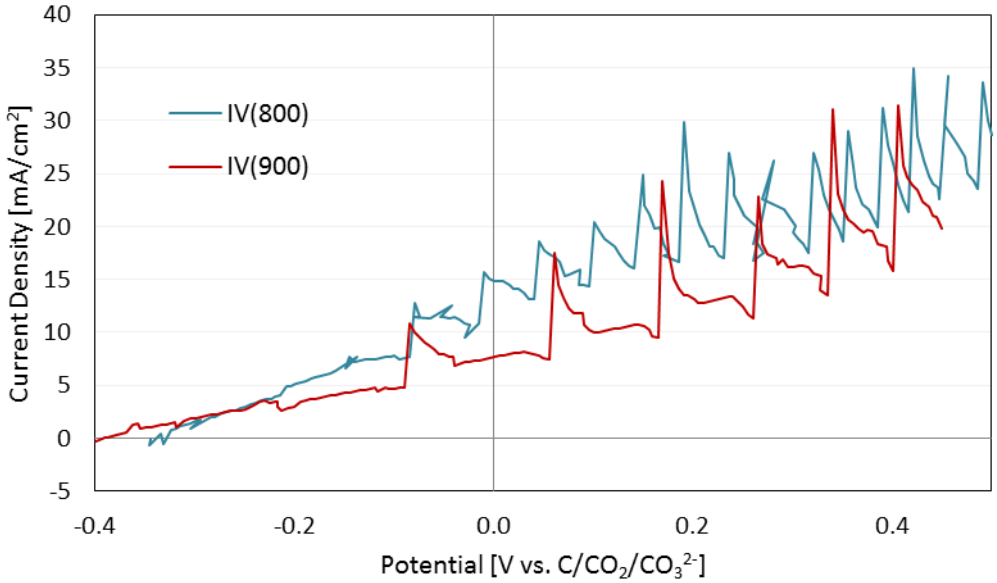

Figure 83: Increase in current density vs applied potential of IV coal pyrolysed at 800 and 900 °C (1 mV/s from OCP to 0.5 V)

The lower activity of coal pyrolysed at 900°C is possibly related to a higher loss of oxygen and nitrogen groups, leading to graphitisation of the coal. Bubble formation is also more frequent in the IV(800) compared to IV(900), which might be another indication of higher surface activity. At higher potentials however, we observe current densities that appear to overlap with each other. A possibly inhibiting reaction pathway for IV(900) at lower voltages compared to IV(800) is therefore suggested.

The voltammogram from the partial oxidation trial is given in Figure 84. Results indicate that as more air is introduced more surface active material is driven off, most likely through combustion, leading to a decrease in the current density vs. applied potential.

The voltammogram obtained from the coal char pyrolysed at 800 °C lies above the coals with introduced air, and the coal that had air introduced for 30 minutes lies slightly below the coal with 10 minutes introduced air. The partial oxidation thus seems to lead to a systematic decrease in surface activity with the increase in time period of air introduction. At increasing potentials however (0.4-0.5 V), observations show that the coal sample with 30 minutes introduced air is slightly higher in activity at the maximum peaks than the sample with 10 minutes of air. However, this may also be a result of variation between the electrode testings and repetition of data is necessary to see if these are reproducible results. Further characterisation of the coal contents and possibly testing at higher applied potentials would also be necessary to fully understand the impact of this treatment.

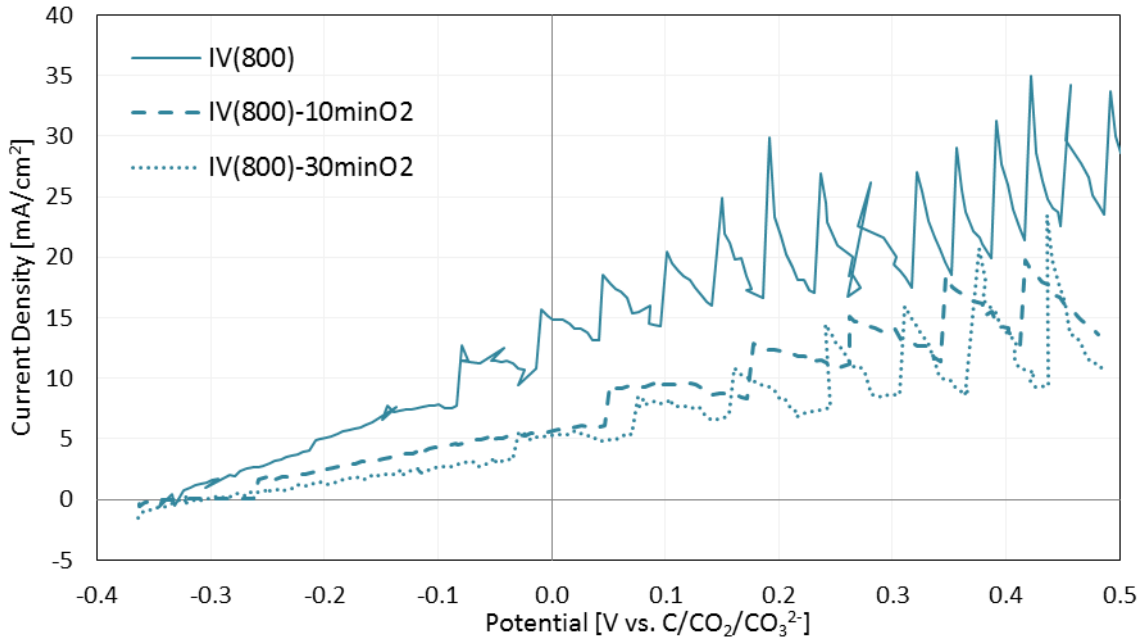

Figure 84: Increase in current density vs applied potential of pyrolysed IV coal with 10 and 30 min introduced air for partial oxidation (1 mV/s from OCP to 0.5 V)

Figure 85 reflects the activity differences between all coal samples pyrolysed at 900 °C, where demineralisation treatments are compared with untreated coal pyrolysed at the same temperature. The increase in activity of the coal demineralised by sodium hydroxide is likely' explained by the removal of Si and Al, which are previously stated as inhibitors for the electrochemical activity of the coal char [6, 92, 93]. It is also possible that activity increase came from an additional functionalisation by OH groups as oxygen participate in the surface activation of coal chars [6, 88]. The highest current density obtained is at about 65 mA/cm^2 for the coal treated with NaOH, with an applied voltage of about 0.43 V. The frequency of bubble formation supports the observed activity increase with the highest bubble formation frequency observed for NaOH-IV(900) and lowest for HCl-IV(900).

Low values are seen for the HCl-IV(900) and almost no bubble formation. It is likely from these results that the hydrochloric acid might have removed essential mineral matter for activation of the oxidation process. It might be that the catalytically performing minerals in coal are more important for the reaction process than pyrolysis higher heating temperature [87]. As the HCl is not strong enough for sufficient removal of SiO_2 [93], it is also possible that the relative percentage increase of this mineral after HCl treatment strictly inhibits the oxidation of the carbon further. However, the small obtained difference in yield of this treatment means that appropriate analysis of sample must be obtained for further conclusion to be made.

The HNO3-IV(900) show similar activity to IV(900), however an increase in, and less reproducible, bubble formation can be seen from the curves. HNO_3 would lead to the functionalization of the coal as previously stated [6], but it is possible that the treatment was not strong enough to remove sufficient ash material that inhibit the oxidation of the carbon.

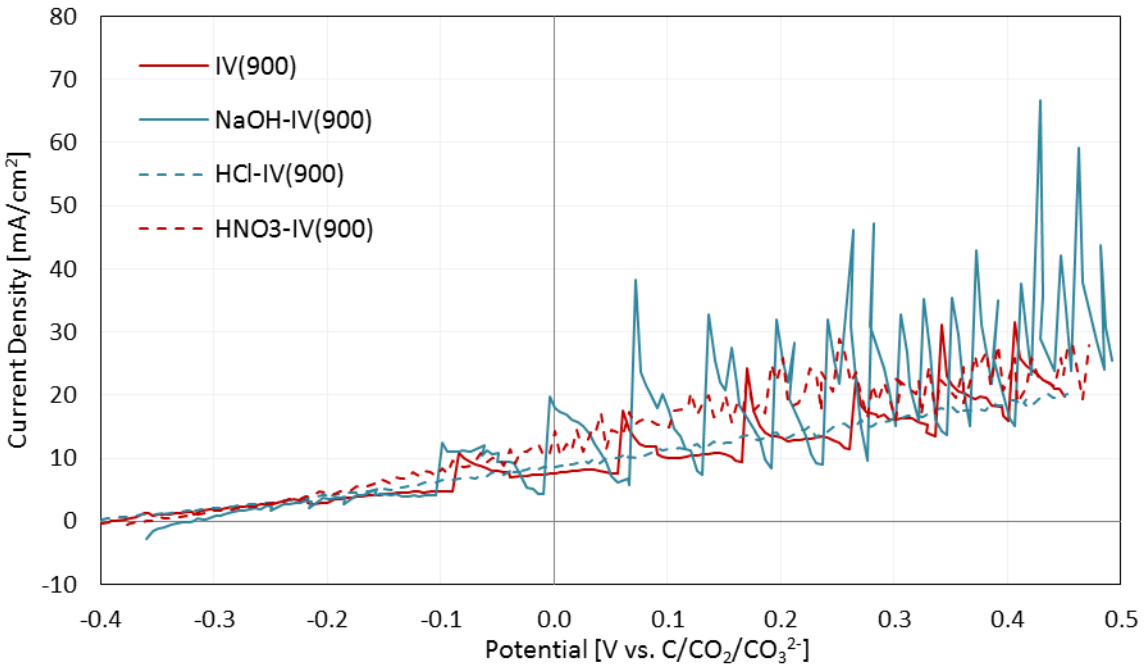

Figure 85: Increase in current density vs applied potential of different demineralisation treatments of IV coal followed by pyrolysis at 900 °C (1 mV/s from OCP to 0.5 V)

Chronoamperometry

After performing chronoamperometry on the coal/graphite based pellets, current density was averaged from an applied voltage of 0.5 V. The current density was used as a measure of the surface activity of the coal. In **Table 17**, we see that the IV(900) has a lower activity than IV(800), which was expected and explained previously as being related to the possible graphitisation of the selected coal after 800 °C and removal of active functional groups at this comparatively higher pyrolysis temperature [87]. The graphitisation of coal may make it useful as a possible binder in a solid carbon anode, however demineralisation steps are necessary for decreasing porosity and lack of structure in the carbon source.

A somewhat unexpected occurrence was seen for the partial oxidation procedure. As more air was introduced to the coal after pyrolysis at 800 °C, a decrease in the current density was observed. It is clear that, as opposed to fixing oxygen to the surface of the coal, the air likely reacted with the carbon-oxygen functional groups on the surface of the coal char to form carbon dioxide via combustion at the high temperature used. This would be seen as a decrease in the surface activity of the coal possibly because the presence of oxygen promotes wettability of the carbon surface with the molten carbonate electrolyte [94]. When compared with the decreased resistivity of the coal samples with increasing introduction of air, it might be that the removal of C-O functional groups, and other volatile compounds with air, allowed for a further "packing" of the coal chars, which essentially led to the conductivity increase in the samples.

The use of HCl in demineralisation decreased coal activity below the initial activity of IV(900). As clay materials are said to possibly increase the activity of coal, and quartz and aluminium materials will work as inhibitors, the results from the acid wash of HCl and HNO_3 are not particularly unexpected [6, 87, 93]. The HCl would have been expected to remove some of the catalytically performing materials, leading to a decrease in activity from initial coal char. Demineralisation by this method shows it is more useful in the production of a better binder

material.

Table 17: Difference in average current density of the working anode with different coal samples at an applied potential of 0.5 V

Coal sample	Average current density (mA/cm^2)
IV(900)	27
NaOH-IV(900)	40
HNO3-IV(900)	24
HCl-IV(900)	18
IV(800)	30
IV(800)-10minO2	15
IV(800)-30minO2	17

It was previously reported by Li et al. [6] that coal chars increased considerably in electrochemical activity after demineralisation with HNO_3. The average current density in this analysis however shows reasonably similar activity between the IV(900) and the HNO_3 demineralised coal. A further assessment of mineral material would be necessary for observation of changes in coal structure by this treatment.

The most substantial change in electrochemical activity was seen from the pre-treatment of coal char with a strong base (NaOH).The average current density shows an increase of about 68 % from raw coal pyrolysed at the same temperature. This might be an indication of a considerable removal of activity inhibiting material like quartz [4, 93], and possibly further functionalization of the surface.

When comparing the current density values with the resistivity of the different coal samples, no clear relationship is seen for the demineralised samples pyrolysed at 900 °C. However, the decrease in resistivity of the partially oxidised samples is also seen as a decrease in activity by current density. If compared, despite possible correlation issues, it can be seen that leaving of volatile matter of the coal might be the cause of conductivity increase in the coal samples. This might be an observation of importance for the future investigation of a suitable coal binder for a solid working anode, as conductive and stabilised carbon material will be needed for this [87].

Conclusion

Several pre-treatments of Ivanhoe North, a thermal, bituminous coal from the NSW Australia coal deposit have been analysed for the purpose of optimising the solid working anode in a direct carbon fuel cell. A partial oxidation trial procedure was performed with little success in fixing oxygen to the coal char surface as the electrochemical analysis of current density showed decreasing surface activity outputs from the use of this method. This conclusion is additionally supported from the increasing conductivities seen from increasing time of air introduction as a sign of the removal of volatile groups from combustion processes.

Three demineralisation steps have been analysed for the selected coal using strong base

and strong acid (NaOH, HCl and HNO_3). Results show the highest possible increase in surface activity of the coal demineralised with NaOH upon pyrolysis at 900 °C. The highest current density was observed at around 65 mA/cm^2 with the applied voltage being 0.43 V. The average current density of this coal obtained at an applied voltage of 0.5 V showed an increase in surface activity of almost 70 %. Activity inhibitors given in literature as being the presence of Al_2O_3 and SiO_2 might have been selectively removed by the pre-treatment with NaOH and a possible carbon-oxygen functionalisation might have occurred. A resulting conductivity increase was also observed for this coal, which was recorded as a resistivity value of 0.62 *10^{-5} Ω.m. The features obtained for pre-treatment of NaOH might make the coal char useful as the active component of a solid anode in the direct carbon fuel cell. It is likely an even more highly activated coal could be obtained by pre-treating coal pyrolysed at 800 °C with NaOH..

Little noted difference was seen from the pre-treatment with HNO_3 for the surface activity, which had a relatively insignificant increase in the conductivity, of the resulting coal. The results from pre-treatment with HCl however showed the lowest surface activity by an averaged current density of 18 mA/cm^2 at 0.5 V. A limited change was observed in resistivity, but the surface activity decrease might indicate loss of ash-impurities that are catalytically active in the coal char. Stronger conditions are necessary to investigate the change in conductivity for the possible use of HCl as a pre-treatment in producing a stable coal binder for the solid carbon anode.

3.8.6. Materials Corrosion Investigation

This work is currently being prepared as a manuscript for submission to the journal "Journal of the Electrochemical Society"

Molten carbonate salts are of interest for several applications including the molten carbonate fuel cell (MCFC), the direct carbon fuel cell (DCFC), as a solar energy thermal storage medium as well as more recently in the electrochemical deposition of carbon for electrochemical storage applications. The high temperatures and aggressive nature of the salt means it is expected to be highly corrosive to plant equipment and components used in these varied applications. Extensive work has been carried out into the corrosion of stainless steels, alloys and pure metals under conditions relevant to the MCFC, the most developed of applications utilising molten carbonates. However, surprisingly little information is available about corrosion of these materials under varied conditions more relevant to solar thermal or DCFC applications. This is even more surprising considering the observed sensitivity of the extent of materials corrosion in different gas environments.

Extensive work has been carried out under both reducing ($H_2/CO_2/H_2O$) and oxidising (CO_2/O_2) atmospheres, which correspond to the anode and cathode gas environment of the MCFC respectively. It has been shown that corrosion is exacerbated under reducing conditions (fuel gas conditions in MCFC) and that the presence of oxygen gas allows generation of a more stable passive film, protecting surfaces from extensive damage. Carbon dioxide atmospheres have been shown by Frangini and Loretti [95] to encourage corrosion, although a systematic investigation of materials under these conditions has not been carried out

For DCFC arrangements which utilise both solid oxide membranes and molten carbonates as an oxide transfer medium, the most relevant conditions include higher temperatures than that used for the MCFC (generally around 650°C) as well as gas atmospheres with high carbon dioxide partial pressure and, ideally, no oxygen present. This is also expected to be more applicable to solar thermal applications since carbonate stability and degradation would be keys issues, and carbonate decomposition has been observed to be exacerbated under nitrogen, argon and air atmospheres compared to its apparent chemical stability under carbon dioxide [96].

The effect of carbonate salt composition on the observed corrosion behaviour has had very little attention since the MCFC generally does not vary from using LiK carbonate eutectics, unlike the DCFC which has used both ternary and binary combinations in various investigations. It has been shown for both DCFC and carbon deposition investigations that variation in the carbonate salt composition effects the electrochemical performance of these systems. The use of different combinations of these salts therefore may well be relevant to the final materials choice for these technologies.

In this work, an assessment of the corrosion behaviour of sodium, lithium and potassium carbonate salts in both ternary and binary compositions has been investigated for standard pure metals including titanium and copper, as well as several stainless steel alloys, to determine bench mark corrosion behaviour under conditions relevant to the DCFC. Nickel is commonly used as the anode material in DCFC applications and has been shown to have low corrosion in oxidising and reducing atmospheres for MCFC applications. Presumably the metal would also be protected during operation through polarisation, however in DCFC conditions may still undergo corrosion during heat up and cool down cycles of the cell operation. This is also true for silver which is also used as a current contact in molten carbonates under many different operating conditions. Comparison of these standard materials to observed behaviour under different gas atmospheres is also possible due to the number of studies which have assessed these materials.

This corrosion investigation has been carried out electrochemically at 700°C (unless specified) with the corrosion current used to compare performance and calculate expected corrosion rates over extended exposure times of surfaces. The same technique has been applied at room temperature in standard corrosive environments for comparison including 1 M H_2SO_4 and 1 M NaCl. Surfaces are also been imaged here using SEM after exposure to molten salts in order to observe bulk structural changes.

Stainless steels investigated are shown in Table 18, purchase from Vulcan Steel, Newcastle.

Table 18: Stainless steel compositions used for corrosion investigations

	C	Si	Mn	P	S	Cr	Ni	Mo	N	Cu	Fe (balance)
SS-304	0.30	0.3	1.8	0.04	0.030	18.5	8.5	0.0	0.00	0.00	70.53
SS-316	0.03	0.3	1.8	0.04	0.030	17.0	10	2.1	0.00	0.00	68.70
SAF-2205	0.03	1.0	2.0	0.03	0.015	22.5	5.5	3.2	0.18	0.00	65.55
SAF-2705	0.03	0.8	1.2	0.035	0.015	25.0	7.0	4.0	0.30	0.05	61.57

Rods of each material were procured and cut to size. They were then paint with Resbond to limit the exposed surface area to the end of the electrode only, diameter of 1.528 cm. The same reference system used in other high temperature electrochemical work by our group was used ($C/CO_2/CO_3^{2-}$). Procedure for testing including firstly fusing of eutectic under carbon dioxide atmosphere at 500 C. The eutectic was allowed to cool before setting up the cell for testing. The assembly was then heated to 700 C under CO2 and electrodes pushed down into the carbonate once molten (above 400°C). Open circuit potential of the electrode was measured for 10 minutes followed by a slow potentiodynamic sweep from the OCP to a point 0.5 V negative of OCP, then positive +1.0 V from the OCP. A scan rate of 1 mV/s was used to ensure quasi-equilibrium conditions around the Tafel region of the measurement. Results for the OCP measured and CV scan are shown for all conditions analysed in Figure 86.

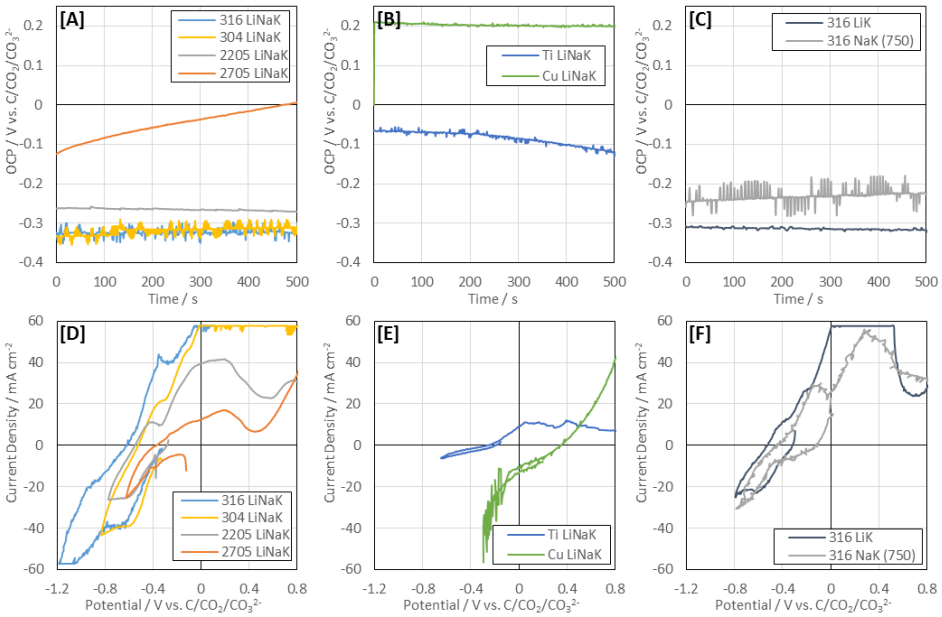

Figure 86: Electrochemical data for investigated materials at 700°C [A]-[C] Initial open circuit potential, [D]-[F] Cyclic voltammetry at 1 mV/s. Max current reached in some cases for potentiostat being used.

Some variation can be observed between steels investigated for both OCP measured as well as CV shape. However, the majority of steels showed a fairly stable OCP around -0.3 V vs. $C/CO_2/CO_3^{2-}$. Exceptions include SS2705 which appears to have a much more positive potential which was less stable, increasing towards zero with time. The measurement requires reproduction for confirmation. CV data looks very different however for pure metals tested and peak positions and heights appear to vary somehwat between types of steel tested. In order to evaluate these differences quantitatively, we can focus on the tafel behaviour around the corrosion potential, Ecorr, which is the potential at which the current density becomes zero during polarisation. This shows performance at the point where a reduction reaction becomes an oxidation reaction. If the tafel plot is then taken, valuable information can be obtained after fitting the Butler-Vomer model to experimental data to determine corrosion parameters including the corrosion current, i_{corr} and the corrosion potential , E_{corr}, i.e.;

$$i = i_{corr}\left\{exp.\left(\alpha_a \frac{nF}{RT}(E - E_{corr})\right) - exp\left(\alpha_c \frac{nF}{RT}(E - E_{corr})\right)\right\} \quad \textbf{(33)}$$

An example of data analysis for SS2705 is shown in Figure 87.

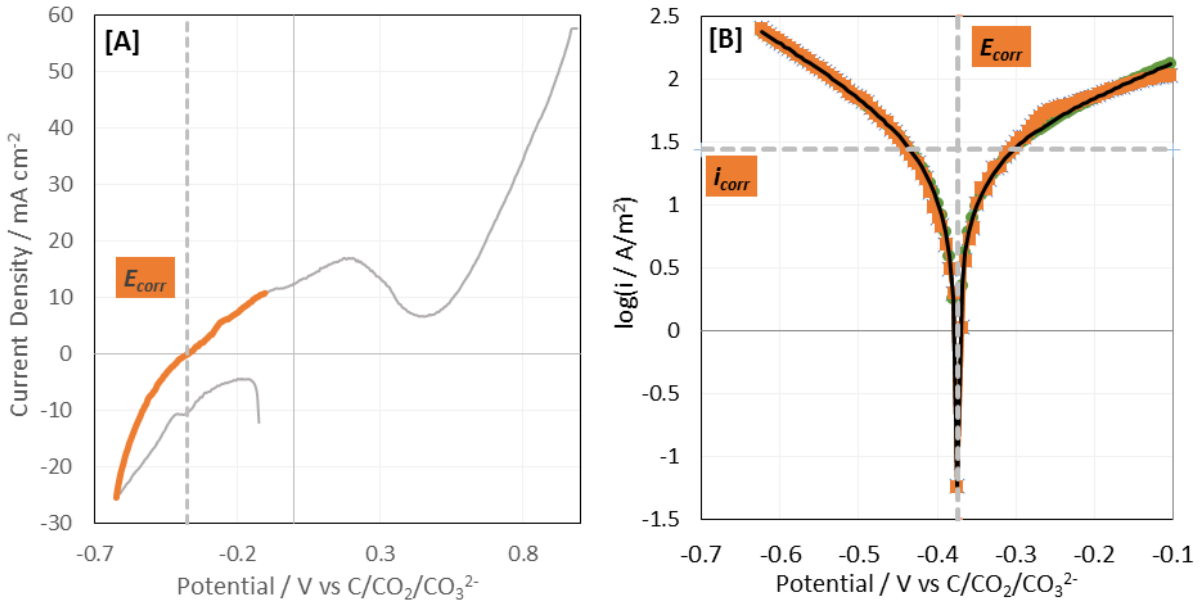

Figure 87: Tafel analysis to determine corrosion parameters [A] Initial CV with area of interest selected (orange), corrosion potential also marked on graph and [B] Tafel plot of selected data demonstrating corrosion current and corrosion potential determined from data (orange squares) using model (black line).

Tafel analysis plots for all data collected, using selected region of interest only are shown in Figure 88.

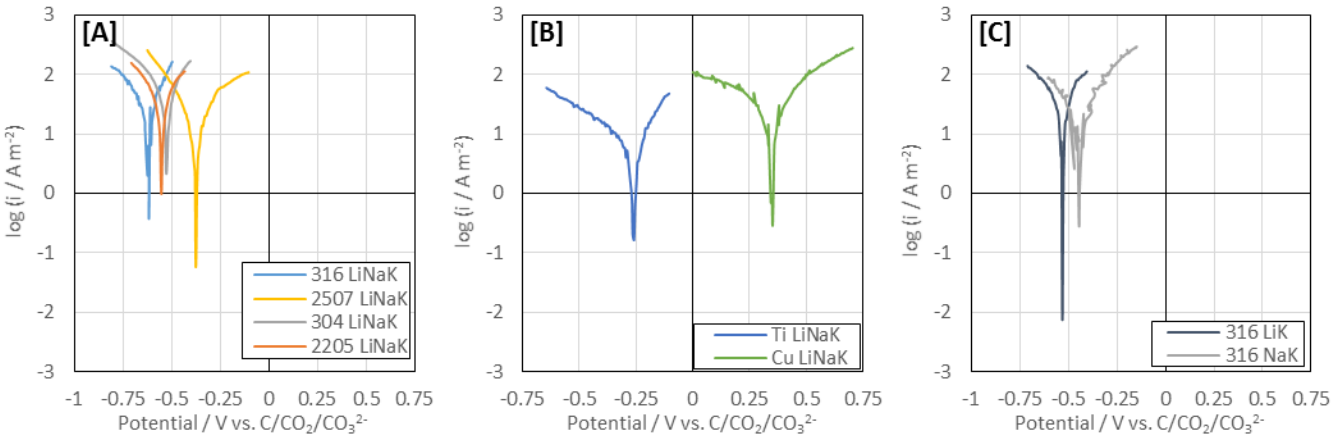

Figure 88: Tafel plots for all materials investigated, taken from original CV data collected as shown in Figure 86 [D]-[F]

Model parameters fitted to this data are shown in Figure 89 and Table 19.

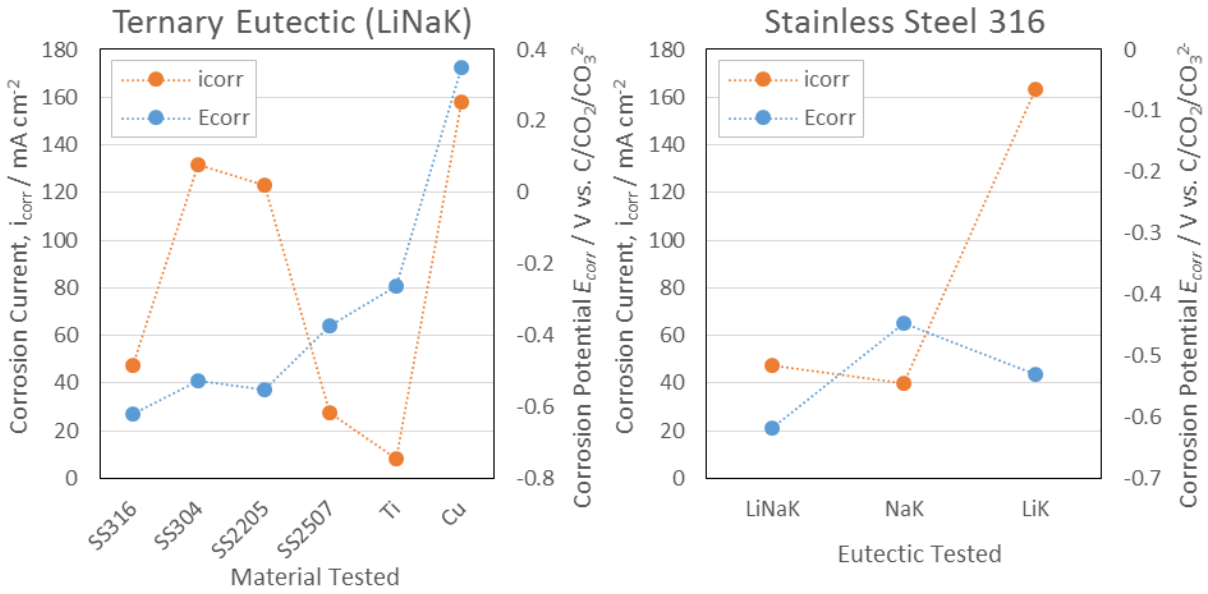

Figure 89: Corrosion current (Icorr) and potential (Ecorr) for materials tested in the termary eutectic (LHS) and for SS316 tested in various carbonate eutectics (RHS).

Table 19: Transfer coefficients calculated along with corrosion parameters for fitting of model outlined in Eqn (3)

	α_a	α_c
SS316 (LiNaK)	0.93	0.50
SS304 (LiNaK)	0.48	0.31
SS2705 (LiNaK)	0.49	0.73
SS2205 (LiNaK)	0.35	0.34
SS316 (LiK)	0.30	0.14
SS316(NaK)	0.60	0.50

The corrosion current is strongly linked to the stability of the material being tested as it represents the consumption of the metal, i.e.;

$$Me \rightarrow Me^{2+} + 2e^{-} \quad \textbf{(34)}$$

The higher the current, the faster the material will corrode. The most stable materials tested in the ternary carbonate eutectic (containing Li_2CO_3, Na_2CO_3 and K_2CO_3) include the pure metal titanium as well as SS316 and SS2705. The least stable materials include copper as well as SS304 and SS2205. It can also be seen in Figure 89 that the carbonate eutectic composition impacts on the corrosion rate with the corrosion proceeding at increased rates on SS316 in LiK compared to LiKNa and NaK. These results show it is possible to alter corrosion rates of materials through change in composition of both the material and the carbonate eutectic and is a good baseline investigation to start more detailed studies including determination of the mechanism of corrosion and the nature of the oxide layer formed during oxidation/corrosion.

3.8.7. Pilot Cell Commissioning and Initial Testing

Experimental Design and Scale-Up

The trials conducted with the pilot-scale DCFC were aimed at implementing selected outcomes from the fundamental testing stage into the operating DCFC. Primarily, this included

the effects of coal (carbon) type and the inclusion of kaolin as a catalyst into the anode, since these were the parameters that had the most profound effect on anode performance during the fundamental testing. Throughout all of the pilot-scale DCFC trials the electrolyte used was the lowest melting point ternary eutectic of Li_2CO_3-Na_2CO_3-K_2CO_3, with a cell operating temperature of 600°C, and a gas phase composition of pure CO_2. Other operational aspects of the pilot-scale DCFC were also considered. This included anode fabrication, cathode fabrication, leak prevention, corrosion prevention and short circuit prevention. Experiments conducted to evaluate these system aspects were as follows:

Carbon (Coal) Type

The initial carbon sample investigated was graphite. This material was chosen because of its well defined chemistry, structure and morphology, thus standardizing these features within the anode of the DCFC.

The thermal coal sample used for evaluation was Ivanhoe that had been pre-pyrolysed at temperatures ranging from 600°-900°C, as per the fundamental section of this report.

A metallurgical (coking) coal sample was also used for comparison, again pre-pyrolysed at temperatures ranging from 600°-900°C.

Catalyst (Kaolin) Inclusion

The catalyst that provided the most significant improvements in performance during the fundamental studies was the clay, kaolin. As such, it was included (at the 5 wt% level) into the anode with a coal sample to demonstrate its improved performance compared to the baseline coal.

Anode Fabrication

The initial design intent with the anode was to develop a system whereby the carbon could be introduced into the DCFC as a compressed electrode around an electronic conductor in a continuous manner. As such we developed a procedure where a nickel mesh was fed through a ring-roller together with the anode material. This electrode could then be fed continuously into the DCFC.

As a hybrid alternative (battery/fuel cell hybrid), solid compact anodes were also prepared and incorporated into the DCFC. This eventuated to be the approach of choice for testing of the pilot-scale system.

Cathode Fabrication

The cathode within the pilot-scale DCFC was designed so as to not be the limiting performance aspect of the cell, and since oxygen reduction is used as the cathode reaction in essentially all fuel cells, standard components were used throughout.

Leak Prevention

Here the focus was on the gasket assembly around the cathodes, with a number of materials used to prevent leakage of the molten carbonate eutectic from around the solid oxide ion conductor.

Corrosion Prevention

The molten carbonate ternary eutectic used in the DCFC is very corrosion to materials at elevated temperatures. As such, various alumina coating strategies were examined during the

operation of the pilot-scale DCFC to determine their effect on material stability. This involved the use of two different thermally stable alumina paints to coat the exposed steel surfaces in the DCFC.

Scale Up Factors

The pilot-scale DCFC system was intended to examine the effects of various material and system features on a larger scale within an operating DCFC. Within the fundamental testing and bench-scale pilot system, the limiting anode area was 1.33 cm^2. In the pilot-scale DCFC the limiting anode area was 50 cm^2, and almost 40 times increase in active area.

Throughout all of the investigations we have carried out, the design intent was to have the anode performance be the limiting factor for DCFC performance. The reason for doing this was to ensure that the focus of the DCFC was on the anode. Of course in a practical commercial system the anode and cathode performance will need to be matched, so that neither is individually limiting, and then the performance is reflective of the system. Here, in the case of the fundamental studies, the counter electrode area was ~10 times larger than that of the working electrode (anode). In the bench-scale testing the cathode area was ~3 times larger than the anode area. While in the pilot-scale DCFC the cathode area was ~1.7 times larger than the anode area. Note that as the scale and complexity of the DCFC system was increased the balance between the anode and cathode areas approached a balance.

The volume of electrolyte used was considered in a similar way. For the fundamental studies the volume of molten carbonate electrolyte used was ~350 cm^3, which was massive compared to the anode area (1.33 cm^2), thus ensuring the electrolyte availability is not limiting DCFC performance. A similar ratio of electrolyte volume to electrode area was apparent in the bench scale DCFC. For the pilot-scale DCFC the electrolyte volume was ~900 cm^3, compared to the anode area of ~50 cm^2. Thus the electrolyte volume to electrode area ratio was much smaller (~18 cm) for the pilot-scale system compared to the fundamental and bench-scale systems (~250 cm). Electrolyte volume is an important consideration for a commercial DCFC system because it has to remain in the liquid state for cell operation which requires the input of energy. Thus the smallest electrolyte volume possible is required for highest cell efficiency.

Anode Development Work

Anode development work, apart from compositional formulation work regarding the anode (as discussed above), has been carried out. This work has been toward physical preparation of a large graphite anode supported in a nickel current collection mesh. Indeed this is not a simple matter of roller pressing the graphite with the mesh, which was initially planned, as this results in three separate layers. The mesh does not adhere to the graphite pressed with it with the pressed graphite layer flaking apart almost instantly after rolling under various configurations. Very low level of stability is observed when using only the roller press for anode manufacture (roller press arrangement shown in Figure 90.

Figure 90: Roller press used for initial anode fabrication investigation

It is possible that less fine mesh would allow for the graphite to be pressed and held in place. It is also likely that a thicker, less flexible mesh would prevent separation through holding the graphite in a stable matrix. However materials currently available and ordered for the procedure will not allow this and therefore a different method is required. Initial testing has been carried out for block pressing the anode around the nickel mesh. Initial tests were not successful as shown in Figure 91.

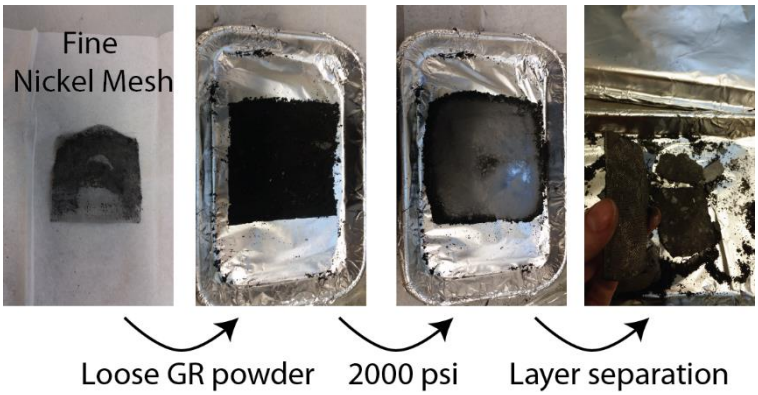

Figure 91: Initial bulk anode pressing test

Layer separation still occurred in this case. However, the structure was far more stable and extensive testing showed that allowing the graphite to completely surround the nickel mesh would result in a stable, solid anode. Therefore, a design for a specific press to manufacture larger solid block anodes has been prepared and is currently in discussion for fabrication with University of Newcastle workshop staff. The press has been kept as simple as possible to avoid costly manufacture and involves four separate pieces which have been designed to allow both pressing and removal of the solid block electrode with stainless steel connectors attached. This

is key as the connectors will both allow direct electrical contact to nickel mesh and the rest of the graphite anode as well as acting to insert and remove the anode during electrochemical testing. The arrangement devised can be seen in Figure 92 with final anode dimensions of approximately 7 cm x 15.5 cm x 1 cm.

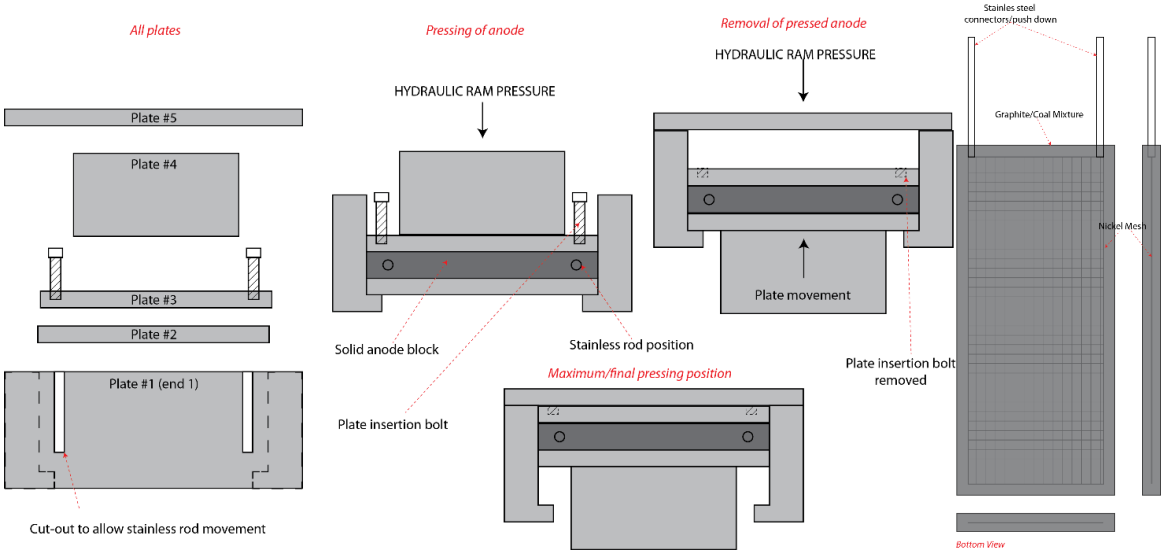

Figure 92: Outline of proposed pressing block function (from bottom view of anode) (LHS) and expected dimensions of fabricated block anode (RHS)

This will allow the pressing of solid anode blocks in a fashion similar to the way anodes are fabricated for the bench scale cell, i.e. through compression with hydraulic press. The larger press will not be able to accommodate as high pressures as used in the small die press used to make anode pellets, however it has been seen through trials without specialised press that a pressure of 2000 psi is achievable and will be sufficient to make a mechanically stable block anode. The use of nickel mesh within the graphite/coal mixture will allow for better electrical conduction throughout the anode and connection of this mesh with stainless steel rods used means external electrical connection to the cell can be made.

After completing this design, a suitable, although somewhat smaller than designed, assembly was found in the Applied Electrochemistry laboratory and has been used to create a solid anode, shown in Figure 93. The anode dimensions were 5 cm x 5 cm x 2 cm. An anode block made in this way will be effective, however it was found that pressing at 5000 psi is unlikely to be a high enough pressure as the final electrode was fragile and brittle, tending to break off in places. This is likely to be exacerbated in the case of a coal based anode which does not have the soft malleable properties of graphite. Further anode development in terms of fabricating a more stable solid block is required.

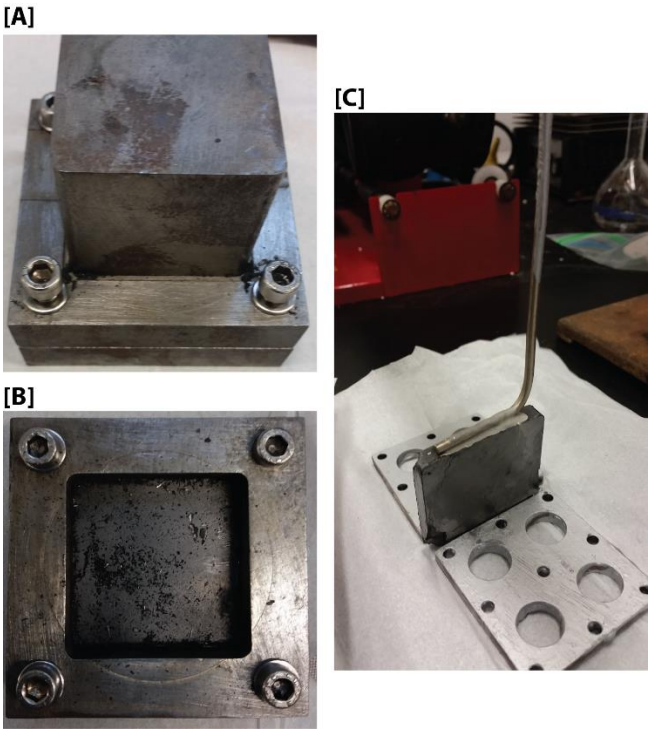

Figure 93: Solid anode block fabrication [A] Full press assembly with ram in place [B] press assembly without ram containing partially pressed block [C] final block anode with pilot cell connection made

Corrosion Protection of Surfaces

As found in corrosion investigation, stainless steel alloys are not corrosion resistant and corrosion behaviour shows substantial mass loss after moderate exposure times to carbonate salt at elevated temperatures. In order to avoid corrosion of the as-built cell, initial corrosion protection with Cermabond was carried out to the inner steel surface. Cermabond is alumina based sealant commonly used in manufacturing for protection of engines from corrosive conditions (generally acidic environments). Since Resbond, another alumina based paste, has shown good resistance to attack from molten carbonate corrosion, it was thought that Cermabond would provide similar protection with an easier coating enabled. However, after initially coating and curing the inner steel plates with Cermabond, it became apparent that the expansion coefficient of the alumina and the steel were very different and a stable layer was not able to be maintained and the protective coating flaked away from the stainless steel. A different sealant was then trialled called Corrpaint (Aremco Products Inc), also used for corrosion protection in engines. This coating had much better adhesion to the steel plates and will provide at least initial protection from corrosion even if re-application of coating is required after running the cell a few times. Successful protection has been observed through running gasket leak tests.

Leak testing and gasket trial

Two types of gasket materials were ordered after trial including RS-3000 (1/8'') and RS-99R (1/32''), ZIRCAR Refractory Composites, Inc. It was seen that although some small amount of leakage was observed during the initial trial, this appeared to be minor and likely to be avoided by use or torque wrench when tightening gaskets, as well as through variation in combination of gasket materials used. Results of a trial carried out using only alumina felt (RS-3000) as the

gasket material is shown in Figure 94.

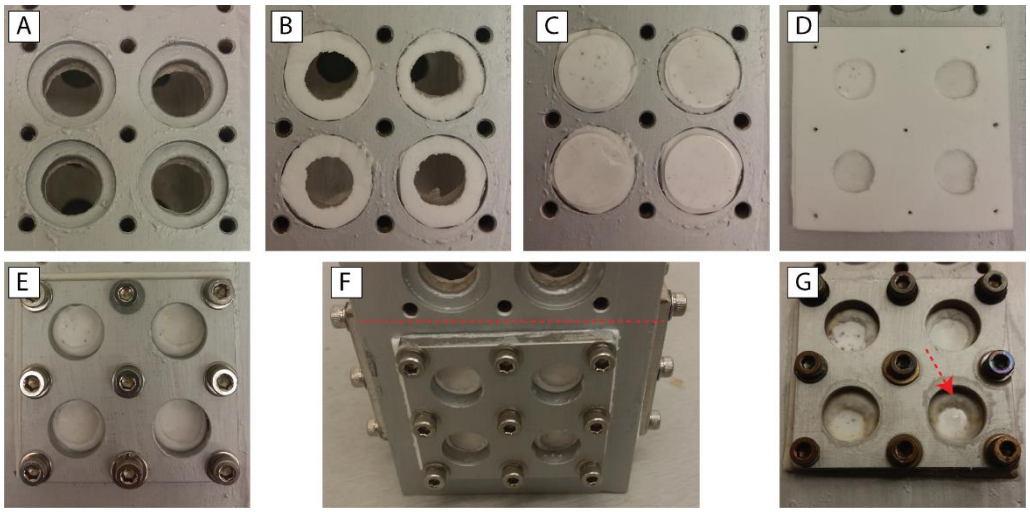

Figure 94: [A] Bare pilot cell [B] Inner gasket [C] YSZ membrane (~1mm thick) [D] Outer gasket [E] gasket plate [F] final assembly before testing [G] final assembly after testing showing carbonate leakage

It was found after testing that carbonate leaked through the gasket slowly, appearing to absorb into the alumina felt gasket material. Therefore, a trial was repeated with the inner gasket made from RS-99R and the outer gasket made from alumina felt. It was thought that since the alumina felt is made for SOFC operation, it would be better suited to the outer gasket rather than the inner gasket. This trial was more successful with only a very small amount of leakage through the gasket. More major leakage was observed in cases where YSZ plates appeared to have cracked during testing, likely a result of over-tightening gaskets or most likely flaws in YSZ membranes developed during the manufacturing process, causing weakness in the structure (commonly observed). However even a small amount of carbonate leakage can be enough to cause a short circuit and severely limit cathode performance. Therefore another trial using RS-99R as both the inner and outer gasket was used as well as fresh YSZ membranes and a torque wrench tightening system to ensure even distribution of pressure over gasket plates. This trial was more successful and will be the preferred arrangement. Some few YSZ membranes still cracked however and the fabrication procedure for these requires review to ensure optimal preparation.

3.8.8. First Pilot Cell Run

Initial Assembly and Preparation

Assembly involved first preparation of all components for the cell including solid oxide/cathode assemblies, gaskets materials cutting and fitting, solid anode preparation and preparation of cathode current collection aspects. Prepared components are shown in Figure 95 and Figure 96.

Figure 95: All pilot cell components (including auxiliary measurement devices) - unassembled

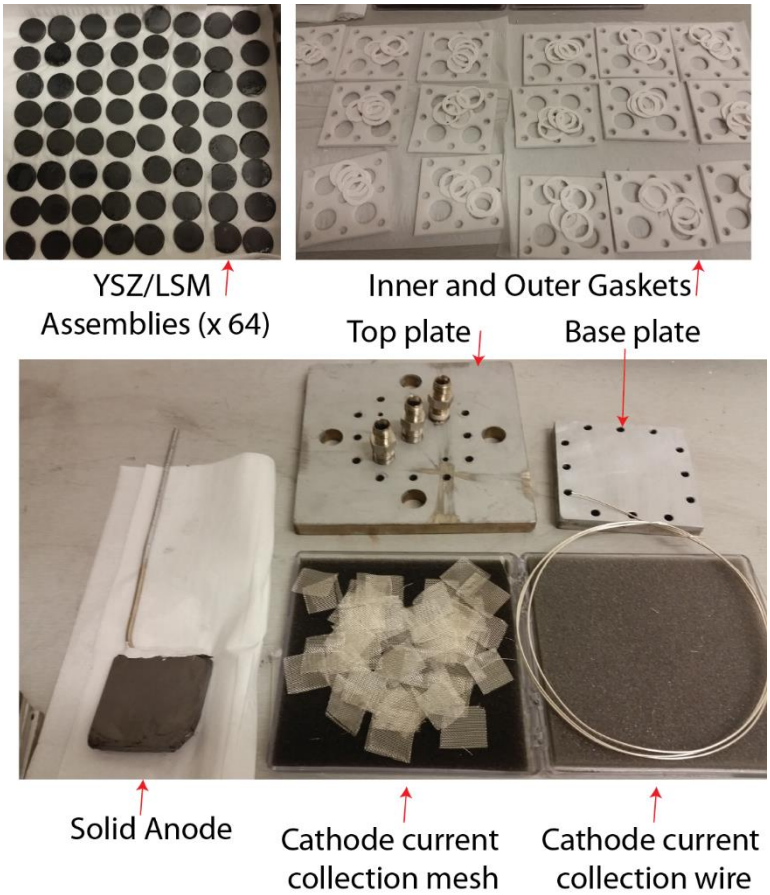

Figure 96: Major pilot cell components prepared for cell testing

Components were then assembled in the pilot cell to enable a test run with baseline performance. Assembly of the cell is shown in Figure 97 with final operation ready cell shown in Figure 98.

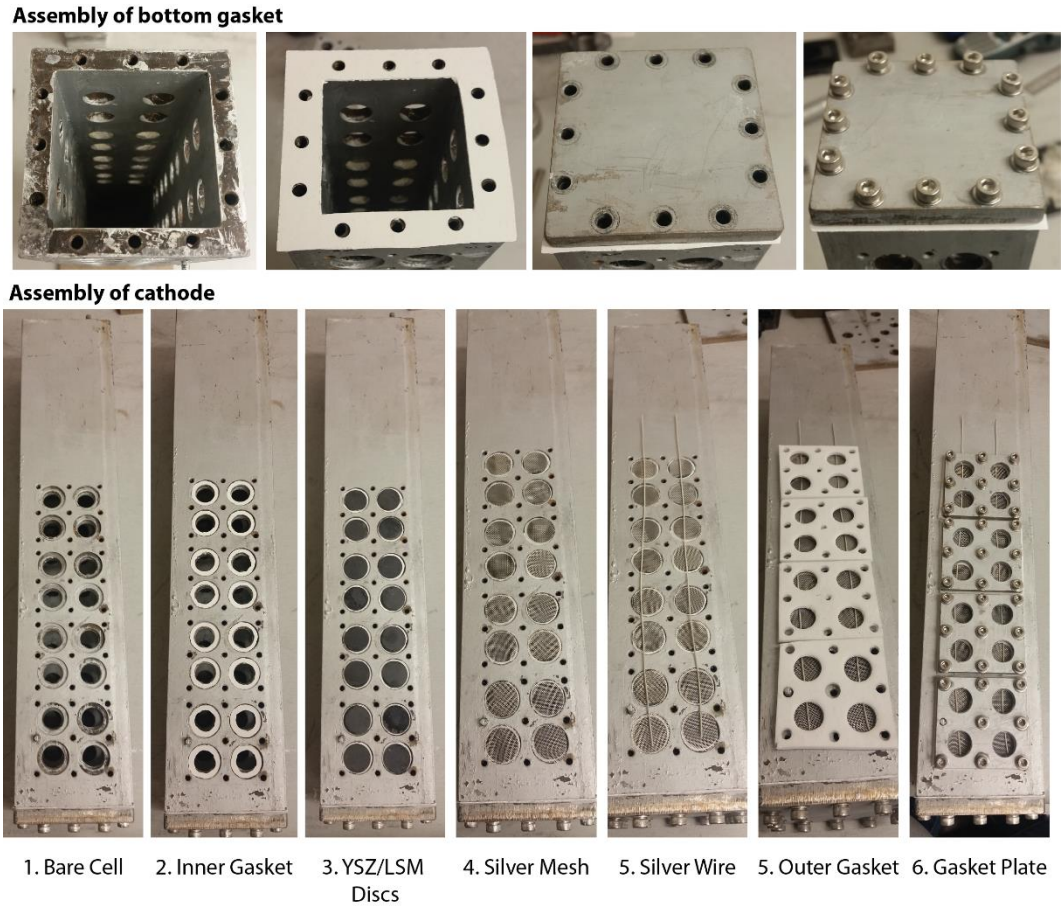

Figure 97: Assembly of pilot cell outer body

Once the cathode discs and gaskets were in place, the top plate could be added along with auxiliary components and the entire cell inserted into the vertical tube furnace. The cell was filled with pre-fused carbonate eutectic, broken into chunks, prior to sealing. Anode was also inserted from below before sealing upper plate in place. The final assembled cell and cell inserted into furnace is shown in Figure 98.

Electrochemical Protocol

The electrochemical protocol used for the pilot-scale DCFC was designed to examine the performance of the DCFC in terms of output power, rather than to run the system for an extended time. The hybrid system employed was best suited to evaluate performance rather than extended lifetime, due to the limited amount of fuel included in the cell.

The electrochemical protocol involved varying the potential (V) of the DCFC in a staircase manner from the open circuit potential down in ~0.1 V increments until a cell voltage of ~0.1 V was reached. During each step the current flow (i) was recorded over the course of ~30 minutes to establish a stable current. This stable current was then used to plot the i-V relationship for the

DCFC, as well as then calculate the power output from the DCFC as a function of applied potential; i.e., P = iV. Ideally what is required from the system is a high current flow as a result of only small changes in potential from open circuit.

Pilot Cell Run and Outcomes for Future Work

The cell run started out promising, however a successful run was not achieved in this initial test. Major issues included carbonate leakage and apparent shorting of the cell (measured open circuit potential was 0-0.2 V, suggesting cell had shorted). It is also thought that not enough carbonate was added to the cell to allow the anode to be submersed in the electrolyte, partially due to leakage observed. There are several issues arising from this run.

ANODE: As mentioned above, the anode after pressing was found to be brittle and fragile, likely due to the step-wise pressing procedure required due to press dimensions, as well as not enough pressure being applied. Further work on both anode stability as well as on final connection and use within the pilot cell is required, including a method to hold the anode at set distance from the molten carbonate. Ceramic beads should also be used over the silver wire connection to prevent short circuiting of the anode with the cell. Pilot cell testing should also be conducted over a period of two days. The first day should include initial fusing of eutectic within the cell as well as leak testing of the cathode system. The eutectic level within the cell will then be known and the distance the anode must be lowered can then be determined. Using the block anode without knowing the final eutectic height made it difficult to determine how far the anode must be lowered so that it was suitably immersed in the melt.

Figure 98: Final assembled cell on bench (LHS) and within vertical tube furnace ready for testing

CATHODE and SEALING: Firstly, a highly performing cathode needs to be confirmed within the half-cell arrangement at a temperature of 700°C. This then needs to be fabricated in bulk. Secondly, it is that cathode assemblies are tightened sufficiently to avoid carbonate leakage. In

the initial test, all gasket plates were tightened using a torque wrench to a pressure of 100cN cm^2, however clear evidence of leakage was seen for all plates meaning a higher pressure is likely required. Alternatively, a different gasket material may need to be considered or a more permanent sealing solution once active cathodes have been identified, such as cementing cathodes in place with Resbond. Some cathode plates appear to have performed worse than others with clear leakage in several cases. They may have cracked during heat-up, meaning a lower heating rate should be used in the next test, but could also be a result of the imperfect nature of the pressed YSZ disc. Substantial work was done in this quarter to fabricate a YSZ disc with no weakness or flaws, using different sintering temperatures and pressures when fabricating, however in all cases a slight weakness in the disc occurred and was not able to be avoided. Possibly this can be remedied with the use of a different membrane material (i.e. SDC) or through further modification in the pressing method (change in amount of YSZ used/pressed etc). A different gasket material may also perform better, although a carbonate resistant and high temperature gasket is difficult to find. Nevertheless this may be required to completely solve leakage issues.

CELL ARRANGEMENT: In order to lift the cell into the real heating zone of the furnace, it was required to be propped up and protruded somewhat from the furnace (see Figure 98). This likely results in large thermal losses through airflow over the cell and may account for the low internal temperature observed via the thermocouple reading. The furnace could also be lowered closer to the bottom desk to prevent large circulation of air and to provide some insulation to the bottom of the furnace. The furnace itself was reading a temperature of 810°C during the test run while the inner thermocouple showed a maximum temperature of only 535°C. This would be an issue in future runs as the cell must reach at least 700°C to achieve high performance. It is possible however that the eutectic is at higher temperature than the gas atmosphere in the cell, which has flow of either nitrogen or carbon dioxide over the top also. The temperature of the carbonate itself will need to be confirmed in later tests with the longer thermocouple purchased for this used instead of the short one.

SHORT CIRCUTING: The cell arrangement involved contact between the silver wire used as cathode contact and the cell wall (see Figure 97). The cell was coated in Corr-paint prior to running, which has been observed to be insulating, however if the coating is not perfect, or if it is damaged during heat-up then immediate contact between the silver wire and the cell wall will be made. This could be avoided through insulating silver wire used where it contacts the cell, perhaps through intermittent coating of silver wire with Resbond between plates or through use of ceramic beads between plates. Care should also be taken to ensure a full coat of Corr-Paint on gaskets plates as these may also contact the silver wire. The single coat applied in this test run was likely insufficient. The anode also likely contacted the top plate. Again this can be avoided through use or ceramic beads coating the silver contact wire or through strategic use of Resbond. Both methods may require use to avoid any electrical contact between anode and cathode and the cell walls.

Further Improvements and Modifications

CATHODE FABRICATION

YSZ membranes were initially fabricated using the method used for the previous test run (1.6750 g, pressed at 2000 PSI for 10 mins). However, this method was not as successful in subsequent tests, with a much lower success rate for producing solid, uniform discs. This was

likely due to the increased sticking of the dry YSZ to the die used to press it. To overcome this, more rigorous drying conditions were used. The YSZ powder was dried at 160°C prior to pressing discs and was placed back into a 160°C oven between making each disc. Additionally, the die was cleaned with acetone and dried in an oven after making ~ 2-3 discs. Whilst this did result in more successful discs being produced, those produced had more defects than in the initial test run.

The pressure under which the discs were pressed was also varied and it was found that a pressure of 2100-2200 PSI produced discs with fewer defects.

The procedure for making the YSZ disc may still need to be improved as the current method has proven inefficient given the number of discs that must be produced for a full run (64).

PILOT CELL DESIGN

During initial test runs, the cell had to supported above the top of the vertical tube furnace so that the functional part of the cell was in the heating zone of the furnace (Figure 99). This meant that the cell protruded significantly above the furnace and likely resulted in thermal losses due to airflow around the top of the cell.

The cell was redesigned so that the top portion of the cell was removed (~10 cm) so that the cell could be placed in the heating zone with the top plate sitting flat on the top of the furnace (Figure 99).

Figure 99: (LEFT) Initial pilot cell design (during test run) (RIGHT) updated pilot cell design (during leak test)

PILOT CELL ASSEMBLY AND LEAK TESTING

Initial trial runs of the cell showed evidence of some leakage of the electrolyte. Although this did not impact on our ability to carry out electrochemical experiments it was decided to

explore this further to optimize the process. This leakage is likely caused by a deficiency in the sealing of each gasket plate. A number of solutions to this were considered including (a) greater tightening of the gasket plates (> 100 cN cm^2) (b) different gasket arrangement (c) different gasket material.

Leaks tests were conducted to identify the cause of the leakage. For a leak test, only the bottom 16 cathodes (four gasket plates) were used (Figure 100) and the LSM catalysts was not included. No electrochemical testing was carried out during the leak tests.

The first leak test used the same gasket material and arrangement as the first test run but with different levels of tightening. Each gasket plate was tightened to a different level of either: 100, 110,120,129 cN cm^2.

During this run, some leakage of the cell occurred. It appeared that many of the YSZ discs had cracked, causing the electrolyte leakage. Therefore it could not be determined if the greater tightening of the gasket plates lead to better sealing.

Figure 100. Cell setup used for leak testing.

The second test run used a different gasket arrangement consisting of circular inner and outer gasket (Figure 101). Using this arrangement, the gaskets could not be tightened more than 80 cN cm^2 before cracking of the YSZ disc occurred.

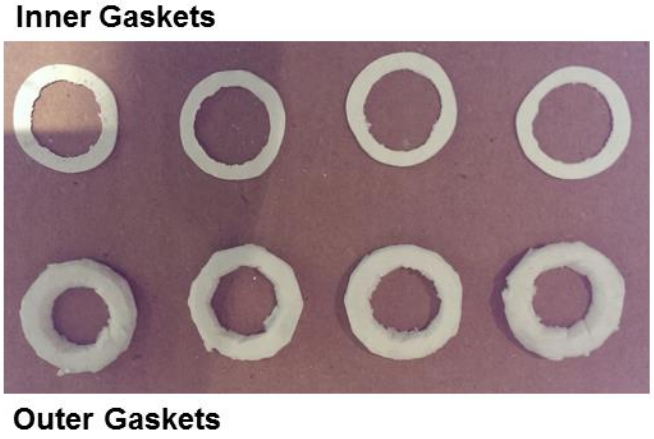

Figure 101. Alternative gasket arrangement

A leak test run using this gasket arrangement indicated that significant leakage of the eutectic occurred at the cell operating temperature.

HEATING CAPACITY TESTING

The first trial of the pilot cell indicated that significant heat losses occurred due to airflow around the cell. The furnace read a temperature of 810°C during the test run whilst the thermocouple inside the pilot cell showed a maximum temperature of 535°C.

A test run with the new cell design improved the heating significantly. During this run, the furnace reading was 800°C and the thermocouple reading inside the cell was 717°C, which is above the temperature required to achieve high performance (700°C).

PILOT CELL PERFORMANCE

The cell was run on a number of occasions to examine the implementation of the fundamental advances made earlier in the project. This mainly revolved around the use of catalysts incorporated into the carbon fuel, as well as the effects of using pre-treated coal as a fuel since these reflect the fundamental outcomes impacting the most of anode behaviour.

A typical example of the output from the pilot-scale DCFC is shown below in Figure 102. A typical example has been included, rather than the entire suite of experimental data collected, because for all intents and purposes, the appearance of the data is the same, with the only changes apparent in the magnitude of current flowing.

The current versus voltage data shown in Figure 102 shows the expected behaviour of a fuel cell system; i.e., a sigmoidal curve as expected from Nernstian electrode behaviour. The open circuit potential of the pilot-scale DCFC for the examples shown in Figure 102 is ~0.72 V. This open circuit potential will be greatly influenced by the type of carbon source used in the DCFC, with the more active materials (such as coal) having a higher OCP. This will be advantageous for the operation of the DCFC since it will mean a greater power output can be extracted from the DCFC for the same current flow.

The following table details the data collected from each of the successful pilot-scale DCFC experiments. Note that for each of these experiments the ternary molten carbonate electrolyte was used, temperature was fixed at 700°C, the atmosphere was 100% CO_2, and the air cathode composition was fixed.

Table 20. Output data from each of the pilot-scale DCFC experiments conducted.

#	Description	Open Circuit Voltage (V)	Maximum Power (mW/cm^2)
1	Graphite anode	0.72	2.5
2	Graphite anode + 5% kaolin	0.72	5.0
3	Ivanhoe (600°C pyrolysis)	0.95	18
4	Ivanhoe (700°C pyrolysis)	0.91	20
5	Ivanhoe (800°C pyrolysis)	0.88	23
6	Ivanhoe (900°C pyrolysis)	0.86	17
7	Ivanhoe (800°C pyrolysis) + 15% kaolin	0.89	47
8	Coking coal (700°C)	0.90	22

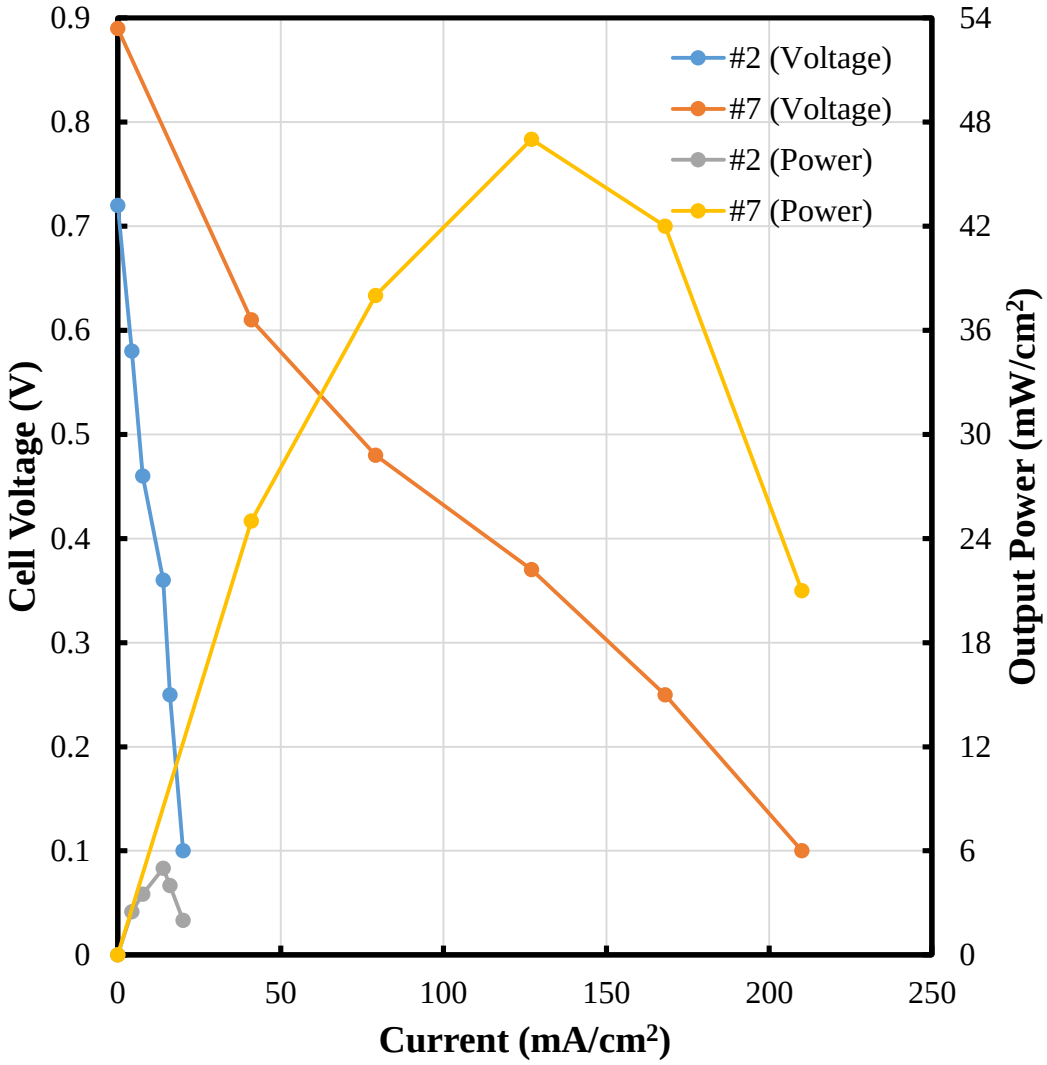

Figure 102. Examples of pilot scale DCFC performance.

The data in Table 20 show performance improvements in line with the fundamental

outcomes from the project. They emphasize the role that the catalyst plays in improving performance, as well as the effect that varying the coal type has on performance. In terms of comparison with literature data (Figure 72) the best results we have obtained are comparable for the temperature used. Of course there are many more optimization experiments that could have been conducted with alternate coals, catalyst loadings, cell configurations and electrolytes.

DCFC Efficiency

Now that some electrochemical data has been collected from the pilot scale DCFC we are in a position to estimate the efficiency of energy conversion. For electrochemical energy conversion systems the efficiency (η) is the ratio between the Gibbs free energy (ΔG; the maximum energy that can be converted to electrical work) and the enthalpy (ΔH; the total chemical energy stored in the fuel) for the overall cell reaction; i.e.,

$$\eta = \frac{\Delta G}{\Delta H} \quad \textbf{(35)}$$

In the case of the DCFC where the entropic difference (ΔS) between the reactants and products for the overall reaction; i.e.,

$$C(s) + O_2(g) \rightarrow CO_2(g) \quad \textbf{(36)}$$

is very small, due to the presence of similar numbers of gas molecules on either side of the reaction, it is anticipated through the definition of Gibbs free energy; i.e.,

$$\Delta G = \Delta H - T\Delta S \quad \textbf{(36)}$$

that in this case the Gibbs free energy should be essentially the same as the enthalpy. The implication is then that the theoretical efficiency of the process is close to unity.

In this case we have estimated the efficiency of the pilot scale DCFC by comparing the chemical energy of the coal (heating value or enthalpy) to the power output from the DCFC, from which can be determined the electrochemical energy output (Gibbs free energy). A sample calculation is shown below in a step-wise sequence.

Step 1.

For the anodic oxidation of carbon ($C + 2O^{2-} \rightarrow CO_2 + 4e^-$) we first calculate the amount of charge (q; C) passed over a set time period (t; say 1 s) using the current flow (I; A) at a certain cell voltage (V). Therefore, using say the peak power point from Figure 102 for #7 (V = 0.37 V; I = 0.127 A/cm^2; P = 0.047 W/cm^2):

$$q = I \times t = 0.127\,(\text{A/cm}^2) \times 1\,(\text{s}) = 0.127\,(\text{C/cm}^2)$$

Step 2.

From this the moles of electrons passed, and hence the moles of carbon atoms consumed, are determined; i.e.,

$$\text{Moles of electrons} = \frac{q}{F} = \frac{0.127\,(\text{C/cm}^2)}{96486.7\,(\text{C/mol})} = 1.32 \times 10^{-6}\ (\text{mol/cm}^2)$$

$$\text{Moles of carbon atoms consumed} = \frac{\text{Moles of electrons}}{4} = 3.29 \times 10^{-7}\ (\text{mol/cm}^2)$$

This second step was based on the stoichiometry of the anodic reaction.

Step 3.
The mass of carbon consumed can then be determined; i.e.,

$$\begin{aligned}\text{Mass of carbon consumed} &= \text{Moles of carbon consumed} \times \text{MW(C)} \\ &= 3.29\times10^{-7}\ (\text{mol/cm}^2)\times12.01\times10^{-3}\ (\text{kg/mol}) \\ &= 3.95\times10^{-9}\ (\text{kg/cm}^2)\end{aligned}$$

where MW(C) is the atomic weight of carbon.

Step 4.
Given now the heating value for the carbon source, the total chemical energy (ΔH; J/cm^2) available from this amount of material can be determined; i.e.,

$$\begin{aligned}\Delta\text{H}\ (\text{J/cm}^2) &= \text{Mass of carbon consumed} \times \text{Heating value} \\ &= 3.95\times10^{-9}\ (\text{kg/cm}^2)\times19\times10^{6}\ (\text{J/kg}) \\ &= 0.075\ (\text{J/cm}^2)\end{aligned}$$

Step 5.
Now, from the power (P; W/cm^2) at this point the amount of electrochemical energy (ΔG; J/cm^2) passed can be determined; i.e.,

$$\Delta\text{G}\ (\text{J/cm}^2) = \text{P}\times\text{t} = 0.047\ (\text{W/cm}^2)\times1\ (\text{s}) = 0.047\ (\text{J/cm}^2)$$

This calculation is based on the fact that 1 W is equivalent to 1 J/s.

Step 6.
The efficiency (η) can then be determined; i.e.,

$$\eta = \frac{\Delta\text{G}}{\Delta\text{H}}\times100\% = \frac{0.047\ (\text{J/cm}^2)}{0.075\ (\text{J/cm}^2)}\times100\% = 63\%$$

Table 21 details the data used to compute the energy efficiency at the peak power output for the pilot scale DCFC runs carried out (cf. Table 20). Firstly, what can be seen here is that the efficiencies resulting from operation of the pilot scale DCFC are quite good, certainly within the expected bounds of operation of the DCFC. Interestingly, the efficiency is in general dependent on the type of carbon source used, with those materials possessing the highest heating value demonstrating the lowest efficiency. What this implies is that those materials with the highest energy content find the liberation of energy the most difficult. In other words, the kinetics of charge transfer is the slowest for these materials. This is consistent with our fundamental studies on different carbon sources, where it was found that the fastest kinetics resulted from materials that were the most disordered, and with the greatest surface oxygen content. These also corresponded to the materials with the lowest open circuit potentials in the fundamental cells

relative to a graphite reference electrode, or the highest open cell voltage in the pilot scale DCFC. Ultimately the efficiency of the DCFC is determined by the power output of the system, which is ultimately a function of the kinetics of carbon oxidation and the operating voltage of the DCFC. The optimum is an ideally polarized electrode with little change in potential with increasing current. This represents the design challenge for next generation fuels.

Table 21. Calculated electrochemical efficiency for the pilot scale DCFC experiments.

#	Carbon	Heating Value (MJ/kg)	Maximum Power (mW/cm^2)	Efficiency
1	Graphite	33	2.5	35
2			5.0	34
3	Ivanhoe	19	18	61
4			20	59
5			23	59
6			17	61
7			47	63
8	Coking Coal	27	22	54

The same calculation described above can also be applied to all reported points obtained for an i-V curve for the DCFC. What this will do is show how the efficiency of operation varies with load on the DCFC. As such, efficiency calculations were carried out on the data shown in Figure 102, with the results shown in Table 22.

Table 22. Sample efficiency calculations for the DCFC pilot operation data reported in Figure 102.

(a) Experiment #2: Graphite anode

Voltage (V)	**Current (mA/cm^2)**	**Power (mW/cm^2)**	**Efficiency (%)**
0.72	0	0	
0.58	4.31	2.5	57
0.46	7.61	3.5	45
0.36	13.89	5.0	34
0.25	16.00	4.0	25
0.10	20.00	2.0	10

(a) Experiment #7: Ivanhoe coal anode

Voltage (V)	**Current (mA/cm^2)**	**Power (mW/cm^2)**	**Efficiency (%)**
0.89	0	0	
0.61	41.0	25	103
0.48	79.2	38	81
0.37	127.0	47	63

0.25	168.0	42	42
0.10	210.0	21	17

The data in this table shows quite clearly that increasing the load on the DCFC decreases the efficiency of DCFC operation. This was entirely to be expected, although what was previously unknown was the extent to which the efficiency decreases. As noted in Table 21, the efficiency is initially dependent on the carbon source, with the more stable carbon source, graphite in this case, having the lower initial efficiency. What is perhaps surprising is how fast the efficiency decreases, in particular for the Ivanhoe coal anode. What this suggests is that the overpotential for carbon oxidation increases quicker for this material, or in other words the rate of oxidation kinetics does not increase as fast for this material. The cause of this may be related to the difference between the surface and bulk chemistry of the coal; i.e., the surface chemistry, in particular oxygen content, is such that coal oxidation kinetics are fast, whereas in the bulk of the coal structure, which has been exposed less to the environment, may have less oxygen and hence slower kinetics.

Post Cell Operation Analysis

After cell operation the current was turned off, the carbon anode was raised out of the electrolyte (but still kept in the CO_2 atmosphere), and the electrolyte was drained from the cell. This essentially represents best practice in shutting the system down, while minimizing the impact on electrodes. The appearance of the carbon anode after experimentation indicated that it had been consumed extensively during the cell operation. Consumption of the anode was uniform across the surface indicating a god current distribution in the cell.

Pilot Scale DCFC Summary and Conclusions

A pilot scale DCFC system was designed and constructed to implement some of the fundamental findings made during the initial stages of this project. The pilot scale DCFC was based on a hybrid fuel cell/battery design, with a fixed volume solid carbon anode and a continuous flow air cathode. This design proved more than effective for demonstrating the improved DCFC performance that results from using the fundamental outcomes determined in this project.

During the commissioning stage of the pilot scale DCFC many different aspects of its operation were explored so as to ensure its effective operation. This included leak testing, coal preparation (washing, etc.), solid oxygen ion conductor preparation, gasket materials, anode preparation and formulation, etc. In each of these cases experiments were conducted to improve the effectiveness of DCFC operation.

The experiments carried out with the pilot scale DCFC were designed to implement the fundamental findings made previously. This included the use a catalyst in the anode to assist with carbon oxidation kinetics, the initial heat treatment conditions on the coal (bituminous thermal coal), as well as the use of a coking coal. The pilot scale DCFC was used under standard conditions, with these changes only being made in the carbon anode. Standard conditions refer to the use of a ternary alkali metal carbonate eutectic, at a temperature of 600°C.

The efficiency of DCFC operation was also determined by considering the chemical energy content of the coal and comparing it to the electrical energy output. In most instances the pilot scale DCFC showed very good performance, with peak power efficiencies of >54% for real carbon feedstocks; i.e., coals. The efficiency was also found to decrease considerably with an increase in load on the DCFC. This latter feature points towards the requisite material properties

for carbon fuels. That is, the feedstock coal must have a high energy content, and this energy must be able to be released quickly through high current demands, all the while maintaining a high cell operating voltage; i.e., low overpotential. Further catalysis studies are required to demonstrate this capability.

4. TECHNICAL OUTCOMES

4.1. Overall Outcomes and Learnings

Fundamental investigations of the electrochemical oxidation of carbon in a molten carbonate eutectic were carried out during this project in order to design and implement a pilot scale DCFC.

Areas of investigation included optimizing the electrochemical performance of the molten carbonate eutectic with a particular focus on the effects of coal impurities in the eutectic (Milestone 7). The kinetic behaviour of melting and freezing of the eutectic with different impurities was determined. Results obtained from this research was used to design an ideal electrolyte for use in the DCFC (Milestone 13).

Additionally, investigation into the fundamental oxidation mechanism and the influence of coal properties and catalysts on the electrochemical performance were investigated. Specifically, the impacts of different coal types and pre-treatment procedures was examined leading to an understanding of what an active, solid anode may consist of which may include coal of various rank and combination of pre-treatment options including coals which have been variously treated by ash removal, pyrolysis or partial oxidation. The oxidation of carbon in the DCFC has also been studied extensively with a proposed oxidation mechanism having been developed.

Results arising from these fundamental studies of the electrochemical behaviour of the DCFC have been utilized for the design and development of a pilot scale DCFC. This pilot cell has been designed and constructed. After some initial failures, the cell was trialed in baseline mode leading to a successful outcome (~2.5 mW/cm^2). Subsequent experiments were conducted with the objective of optimizing performance, ultimately leading to a highest performance of 47 mW/cm^2 for an anode containing kaolin catalyst and an optimally pyrolyzed coal.

4.2. Discussion of Project Challenges

The most significant challenge arising in this project was the design and commissioning of the pilot DCFC. Significant delays were encountered when commissioning the cell due to changes in the quoted price from suppliers. This required that the cell be redesigned with different materials (stainless steel instead of alumina) which slowed down the progress of this particular milestone. Nevertheless, we were able to achieve a series of experiments using an enhanced anode.

4.3. Publications Arising from Project

All publications to date:

[1] Tulloch J, Allen J, Wibberley L, Donne S. *Influence of selected coal contaminants on graphitic carbon electro-oxidation for application to the direct carbon fuel cell*. Journal of Power Sources. **2014**;260:140-9.

[2] Allen, JA, Tulloch J, Wibberley L, Donne SW. *Kinetic Analysis of the Anodic Carbon Oxidation Mechanism in a Molten Carbonate Medium*. Electrochimica Acta. **2014**;129:389-95.

[3] Allen JA, White J, Glenn M, Donne SW. *Molten carbonate composition effects on carbon electro-oxidation at a solid anode interface*. Journal of the Electrochemical Society. **2015**;162(1):F1-F8.

[4] Allen, J.A., M. Glenn, and S.W. Donne, *The effect of coal type and pyrolysis temperature on the electrochemical activity of coal at a solid carbon anode in molten carbonate media*. Journal of Power Sources, **2015**. 279: p. 384-393.

[5] M. Glenn, J. Allen, S. Donne *Thermal Investigation of a Doped Alkali Metal Carbonate Ternary Eutectic for Direct Carbon Fuel Cell Applications* Energy & Fuels, **2015**: 29 (8), 5423-5433

5. CONCLUSIONS

5.1. Overall Progress in Meeting Project Objectives

5.1.1. Objective #1

Understanding the mechanism through which coal is oxidized to form CO_2, and identifying and optimizing the important process variables for optimum performance, as defined by the kinetics of carbon oxidation to CO_2. Following on from above, the important process variables include the type and impurity level of the coal and whether coal washing is necessary, the nature and composition of the electrolyte (molten carbonate), the anodic catalyst, the operational temperature, and the gas-phase composition (CO_2/O_2 ratio).

This objective was met relatively early in the project, with the fundamental understandings gained from this objective utilized to address Objective #2.

The oxidation reaction has been both investigated and manipulated with a working hypothesis as to the origin of activity of specific carbon materials developed. Coal impurities have been shown to have the ability to both improve and inhibit electrochemical performance depending on their type and concentration and fundamental reasons for this have been proposed. Further, the carbonate composition has been shown to be thermally sensitive to coal impurity addition and changes to composition, which has both operational and electrochemical implications for the direct carbon fuel cell.

Additionally, the effect of pyrolysis, coal type and successful introduction of a catalyst and activation of an inactive coal has been examined. Traditional characterisation methods were determined to be insufficient to explain electrochemical behaviour of coals pyrolysed, instead it is suggested that the ash distribution and thermal transitions could hold the key to explaining electrochemical performance. Further, partial oxidation and optimised pyrolysis conditions will enhance carbon oxidation kinetics.

5.1.2. Objective #2

Development of an operational (bench and pilot scale) DCFC, in particular, taking into account the mode of coal introduction to the catalyst surface.

The pilot cell has been designed and constructed. Trial runs were carried out successfully, together with some optimization experiments. A trial run of the cell in baseline mode was conducted, leading to a maximum power output of ~2.5 $mW.cm^2$. In addition to performance testing, some optimization experiments were conducted. The introduction of catalyst to the coal surface has already been tested whereby simple mechanical mixing of components prior to formation into a solid anode. The pilot cell has been shown to be operational, however further improvements to the setup can be used to further improve outcomes.

6. References

1. G. J. Janz and M. R. Lorenz, (1961), *Journal of Chemical & Engineering Data*, 6 (3), 321-323
2. M. Castellano, A. Turturro, P. Riani, T. Montanari, E. Finocchio, G. Ramis and G. Busca, (2010), *Applied Clay Science*, 48 (3), 446-454
3. F. Moodi, A. Ramezanianpour and A. S. Safavizadeh, (2011), *Scientia Iranica*, 18 (4), 906-912
4. J. Tulloch, J. Allen, L. Wibberley and S. Donne, (2014), *Journal of Power Sources*, 260 140-149
5. C. C. Chen, T. Maruyama, P. H. Hsieh and J. R. Selman, (2012), *Journal of the Electrochemical Society*, 159 (10), D597-D604
6. X. Li, Z. H. Zhu, R. De Marco, J. Bradley and A. Dicks, (2010), *Journal of Power Sources*, 195 (13), 4051-4058
7. L. Lu, V. Sahajwalla, C. Kong and D. Harris, (2001), *Carbon*, 39 (12), 1821-1833
8. C. R. Ward, (2002), *International Journal of Coal Geology*, 50 (1), 135-168
9. C. Q. Wang, J. Liu, J. Zeng, J. L. Yin, G. L. Wang and D. X. Cao, (2013), *Journal of Power Sources*, 233 244-251
10. M. Chen, C. Wang, X. Niu, S. Zhao, J. Tang and B. Zhu, (2010), *International journal of hydrogen energy*, 35 (7), 2732-2736
11. T. M. Gür, (2013), *Chemical Reviews*, 113 (8), 6179-6206
12. S. V. Devyatkin, A. D. Pisanenko and S. V. I., (2002), *Russian Journal of Applied Chemistry*, 75 (4), 562-564
13. N. J. Cherepy, R. Krueger, K. J. Fiet, A. F. Jankowski and J. F. Cooper, (2005), *Journal of the Electrochemical Society*, 152 (1), A80-A87
14. D. G. Vutetakis, D. R. Skidmore and H. J. Byker, (1987), *Journal of the Electrochemical Society*, 134 (12), 3027-3035
15. W. E. Haupin and W. B. Frank, *Electrometallurgy of Aluminium*, in Comprehensive Treatise of Electrochemistry,(1981), Plenum Press, New York, 301-325
16. S. Giddey, S. P. S. Badwal, A. Kulkarni and C. Munnings, (2012), *Progress in Energy and Combustion Science*, 38 (3), 360-399
17. D. Cao, Y. Sun and G. Wang, (2007), *Journal of Power Sources*, 167 (2), 250-257
18. G. Blyholder and H. Eyring, (1957), *Journal of Physical Chemistry*, 61 (5), 682-688
19. H. Li, Q. Liu and Y. Li, (2010), *Electrochimica Acta*, 55 (6), 1958-1965
20. J. Tulloch, J. A. Allen, L. Wibberley and S. W. Donne, (In Press), *Journal of Power Sources*,
21. X. Li, Z. Zhu, J. Chen, R. De Marco, A. Dicks, J. Bradley and G. Lu, (2009), *Journal of Power Sources*, 186 (1), 1-9
22. J. F. Cooper and J. R. Selman, (2012), *International Journal of Hydrogen Energy*, 37 (24), 19319-19328
23. Y. Leng, S. Chan, K. Khor and S. Jiang, (2004), *Journal of applied electrochemistry*, 34 (4), 409-415
24. G. Wang, Y. Bao, Y. Tian, J. Xia and D. Cao, (2010), *Journal of Power Sources*, 195 (19), 6463-6467
25. M. Gaudon, C. Laberty-Robert, F. Ansart, L. Dessemond and P. Stevens, (2004), *Journal of power sources*, 133 (2), 214-222
26. J. X. Wang, Y. K. Tao, J. Shao and W. G. Wang, (2009), *Journal of Power Sources*, 186

(2), 344-348
27. J. Kong, Y. Zhang, C. Deng and J. Xu, (2009), *Journal of Power Sources*, 186 (2), 485-489
28. J. Piao, K. Sun, N. Zhang and S. Xu, (2008), *Journal of Power Sources*, 175 (1), 288-295
29. D. Marrero-López, L. dos Santos-Gómez, J. Canales-Vázquez, F. Martín and J. R. Ramos-Barrado, (2014), *Electrochimica Acta*, 134 159-166
30. J. Tulloch and S. W. Donne, (2009), *Journal of Power Sources*, 188 (2), 359-366
31. J. X. Wang, J. L. Sun, C. R. He, Q. Wang and W. G. Wang, (2014), *Journal of Power Sources*, 253 424-430
32. A. Princivalle, D. Perednis, R. Neagu and E. Djurado, (2004), *Chemistry of materials*, 16 (19), 3733-3739
33. M. Zhi, G. Zhou, Z. Hong, J. Wang, R. Gemmen, K. Gerdes, A. Manivannan, D. Ma and N. Wu, (2011), *Energy & Environmental Science*, 4 (1), 139-144
34. X. Xu, C. Cao, C. Xia and D. Peng, (2009), *Ceramics International*, 35 (6), 2213-2218
35. R. Liu, C. Zhao, J. Li, S. Wang, Z. Wen and T. Wen, (2010), *Journal of Power Sources*, 195 (2), 541-545
36. H. Ju, S. Uhm, J. W. Kim, R.-H. Song, H. Choi, S.-H. Lee and J. Lee, (2012), *Journal of Power Sources*, 198 36-41
37. T. Siengchum, F. Guzman and S. S. Chuang, (2012), *Journal of Power Sources*, 213 375-381
38. Y. Nabae, K. D. Pointon and J. T. Irvine, (2009), *Journal of The Electrochemical Society*, 156 (6), B716-B720
39. L. Deleebeeck and K. K. Hansen, (2014), *Journal of The Electrochemical Society*, 161 (1), F33-F46
40. C. Jiang, J. Ma, A. Arenillas and J. T. Irvine, (2013), *ECS Transactions*, 57 (1), 3013-3021
41. C. Jiang and J. T. Irvine, (2011), *Journal of Power Sources*, 196 (17), 7318-7322
42. C. C. Wei and K. Li, (2008), *Industrial & Engineering Chemistry Research*, 47 (5), 1506-1512
43. K. Kendall and M. Palin, (1998), *Journal of power sources*, 71 (1), 268-270
44. H. A. Hamedani, K.-H. Dahmen, D. Li, H. Peydaye-Saheli, H. Garmestani and M. Khaleel, (2008), *Materials Science and Engineering: B*, 153 (1), 1-9
45. J. Ding and J. Liu, (2008), *Solid State Ionics*, 179 (21), 1246-1249
46. H. Shi, W. Zhou, R. Ran and Z. Shao, (2010), *Journal of Power Sources*, 195 (2), 393-401
47. J. Ding, J. Liu, W. Yuan and Y. Zhang, (2008), *Journal of the European Ceramic Society*, 28 (16), 3113-3117
48. D. Beckel, U. P. Muecke, T. Gyger, G. Florey, A. Infortuna and L. J. Gauckler, (2007), *Solid State Ionics*, 178 (5), 407-415
49. A. C. Chien, A. Arenillas, C. Jiang and J. T. Irvine, (2014), *Journal of The Electrochemical Society*, 161 (5), F588-F593
50. Y. Nabae, K. D. Pointon and J. T. Irvine, (2008), *Energy & Environmental Science*, 1 (1), 148-155
51. D. X. Cao, G. L. Wang, C. Q. Wang, J. Wang and T. H. Lu, (2010), *International Journal of Hydrogen Energy*, 35 (4), 1778-1782
52. M. Glenn, J. A. Allen and S. W. Donne, (IN PRESS 2015), *Energy & Fuels*,
53. J. A. Allen, J. White, M. Glenn and S. W. Donne, (2015), *Journal of the Electrochemical Society*, 162 (1), F1-F8
54. J. A. Allen, J. Tulloch, L. Wibberley and S. W. Donne, (2014), *Electrochimica Acta*, 129

(0), 389-395
55. A. C. Rady, S. Giddey, S. P. Badwal, B. P. Ladewig and S. Bhattacharya, (2012), *Energy & Fuels*, 26 (3), 1471-1488
56. L. Guo, J. M. Calo, E. DiCocco and E. J. Bain, (2013), *Energy & Fuels*, 27 (3), 1712-1719
57. S. Zecevic, E. M. Patton and P. Parhami, (2005), *Chemical Engineering Communications*, 192 (12), 1655-1670
58. X. Xu, W. Zhou, F. Liang and Z. Zhu, (2013), *international journal of hydrogen energy*, 38 (13), 5367-5374
59. W. Hao, X. He and Y. Mi, (2014), *Applied Energy*, 135 174-181
60. L. Deleebeeck and K. K. Hansen, (2014), *Journal of Solid State Electrochemistry*, 18 (4), 861-882
61. A. Kulkarni, S. Giddey and S. Badwal, (2011), *Solid State Ionics*, 194 (1), 46-52
62. L. Kouchachvili and M. Ikura, (2011), *international journal of hydrogen energy*, 36 (16), 10263-10268
63. A. Elleuch, J. Yu, A. Boussetta, K. Halouani and Y. Li, (2013), *International Journal of Hydrogen Energy*, 38 (20), 8514-8523
64. A. C. Rady, S. Giddey, A. Kulkarni, S. P. Badwal, S. Bhattacharya and B. P. Ladewig, (2014), *Applied Energy*, 120 56-64
65. L. Jia, Y. Tian, Q. Liu, C. Xia, J. Yu, Z. Wang, Y. Zhao and Y. Li, (2010), *Journal of Power Sources*, 195 (17), 5581-5586
66. J. Yu, B. Yu and Y. Li, (2013), *International Journal of Hydrogen Energy*, 38 (36), 16615-16622
67. A. Elleuch, A. Boussetta, J. Yu, K. Halouani and Y. Li, (2013), *international journal of hydrogen energy*, 38 (36), 16590-16604
68. A. Jayakumar, R. Küngas, S. Roy, A. Javadekar, D. J. Buttrey, J. M. Vohs and R. J. Gorte, (2011), *Energy & Environmental Science*, 4 (10), 4133-4137
69. C. Jiang, J. Ma, A. D. Bonaccorso and J. T. Irvine, (2012), *Energy & Environmental Science*, 5 (5), 6973-6980
70. J. Yu, Y. Zhao and Y. Li, (2014), *Journal of Power Sources*, 270 312-317
71. X. Xu, W. Zhou and Z. Zhu, (2013), *Industrial & Engineering Chemistry Research*, 52 (50), 17927-17933
72. N. Kaklidis, V. Kyriakou, I. Garagounis, A. Arenillas, J. Menéndez, G. Marnellos and M. Konsolakis, (2014), *RSC Advances*, 4 (36), 18792-18800
73. C. Li, Y. Shi and N. Cai, (2011), *Journal of Power Sources*, 196 (10), 4588-4593
74. A. Kulkarni, S. Giddey, S. Badwal and G. Paul, (2014), *Electrochimica Acta*, 121 34-43
75. A. Kulkarni, S. Giddey and S. Badwal, (2015), *Journal of Solid State Electrochemistry*, 19 (2), 325-335
76. Y. Tang and J. Liu, (2010), *international journal of hydrogen energy*, 35 (20), 11188-11193
77. A. Kulkarni, F. Ciacchi, S. Giddey, C. Munnings, S. Badwal, J. Kimpton and D. Fini, (2012), *International Journal of Hydrogen Energy*, 37 (24), 19092-19102
78. C. Munnings, A. Kulkarni, S. Giddey and S. Badwal, (2014), *International Journal of Hydrogen Energy*, 39 (23), 12377-12385
79. H. Wang, T. Cao, Y. Shi, N. Cai and W. Yuan, (2014), *Energy*, 75 555-559
80. B. Cantero-Tubilla, C. Xu, J. W. Zondlo, K. Sabolsky and E. M. Sabolsky, (2013), *Journal of Power Sources*, 238 227-235
81. A. C. Chien, G. Corre, R. Antunes and J. T. Irvine, (2013), *International Journal of*

Hydrogen Energy, 38 (20), 8497-8502
82. M. Dudek, R. Tomov, C. Wang, B. Glowacki, P. Tomczyk, R. Socha and M. Mosiałek, (2013), *Electrochimica Acta*, 105 412-418
83. J. Ruflin, A. D. Perwich, C. Brett, J. K. Berner and S. M. Lux, (2012), *Journal of Power Sources*, 213 275-286
84. M. Dudek, P. Tomczyk, R. Socha and M. Hamaguchi, (2014), *International journal of hydrogen energy*, 39 (23), 12386-12394
85. A. C. Rady, S. Giddey, A. Kulkarni, S. P. Badwal and S. Bhattacharya, (2014), *Electrochimica Acta*, 143 278-290
86. Y. Xie, Y. Tang and J. Liu, (2013), *Journal of Solid State Electrochemistry*, 17 (1), 121-127
87. J. A. Allen, M. Glenn and S. W. Donne, (2015), *Journal of Power Sources*, 279 (0), 384-393
88. X. Li, Z. H. Zhu, R. De Marco, J. Bradley and A. Dicks, (2010), *Journal of Physical Chemistry A*, 114 (11), 3855-3862
89. X. Shu and X. Xu, (2001), *Energy & Fuels*, 15 (6), 1347-1353
90. H. Cheng, Q. Liu, J. Yang and R. L. Frost, (2010), *Thermochimica Acta*, 507–508 (0), 84-90
91. J. A. Allen, J. White, M. Glenn and S. W. Donne, (2015), *Journal of the Electrochemical Society*, 162 (1), F76-F83
92. J. Wang, Z. G. Zhang, Y. Kobayashi and A. Tomita, (1996), *Energy & Fuels*, 10 (2), 386-391
93. N. Wijaya and L. A. Zhang, (2011), *Energy & Fuels*, 25 1-16
94. E. K. Lee, H. H. Chun and Y. T. Kim, (2014), *International Journal of Hydrogen Energy*, 39 (29), 16541-16547
95. S. Frangini and S. Loreti, (2007), *Corrosion Science*, 49 (10), 3969-3987
96. R. I. Olivares, C. L. Chen and S. Wright, (2012), *Journal of Solar Energy Engineering-Transactions of the Asme*, 134 (4),

Direct Carbon Fuel Cell – Preliminary Life Cycle Analysis

Abstract

A life cycle analysis (LCA) has been conducted on the operation of the direct carbon fuel cell (DCFC) in comparison with a coal fired power station (CFPS) with the same inputs. The base case for comparison was a CFPS with 10 Mt pa input of coal leading to the generation of 94.5×10^{15} J of energy with an emissions efficiency of 0.9369 tCO_2-e/MWh. Adding post-combustion capture of the carbon dioxide with an energy penalty of 13%, the resultant emissions efficiency is 1.0587 tCO_2-e/MWh. In comparison, DCFC operation with the need for an increased transportation network, an electrochemical efficiency of 80%, pre-pyrolysis of the coal, requisite heating and sequestration (2% energy penalty) leads to an emissions efficiency of 0.4825 tCO_2-e/MWh. In conclusion, the DCFC is a much more efficient technology, with emissions efficiency of only 45.6% of that of a comparable CFPS. Additionally, there are additional energy savings that can be made with the DCFC to further improve this emissions efficiency.

Introduction

For any energy generation system in today's day and age it is necessary to conduct a life cycle analysis of the complete process to effectively account for all inputs and outputs. Of course the focus is largely on the quantity of emissions per unit of energy produced; however, a detailed life cycle analysis can also be used as a tool to measure system efficiency and highlight aspect of the overall process that require attention. In this project sponsored by Coal Innovation NSW, the focus has been on the development of the direct carbon fuel cell. As such, this report presents a life cycle analysis of this system.

Energy Generation

The traditional approach to energy generation si through the use of a coal-fired power station, a schematic of which is shown below in Figure 1. In the CFPS the chemical energy stored in coal undergoes a number of energy transformations processes, leading ultimately to electrical energy leaving the plant. Each of these energy transformations has an associated inefficiency, and so a CFPS typically produces electrical energy with 35-40% efficiency. While this represents a very inefficient way to produce energy, the abundance of coal in Australia and around the world has meant that this has been the preferred approach to energy generation since the Industrial Revolution in the early 1800's.

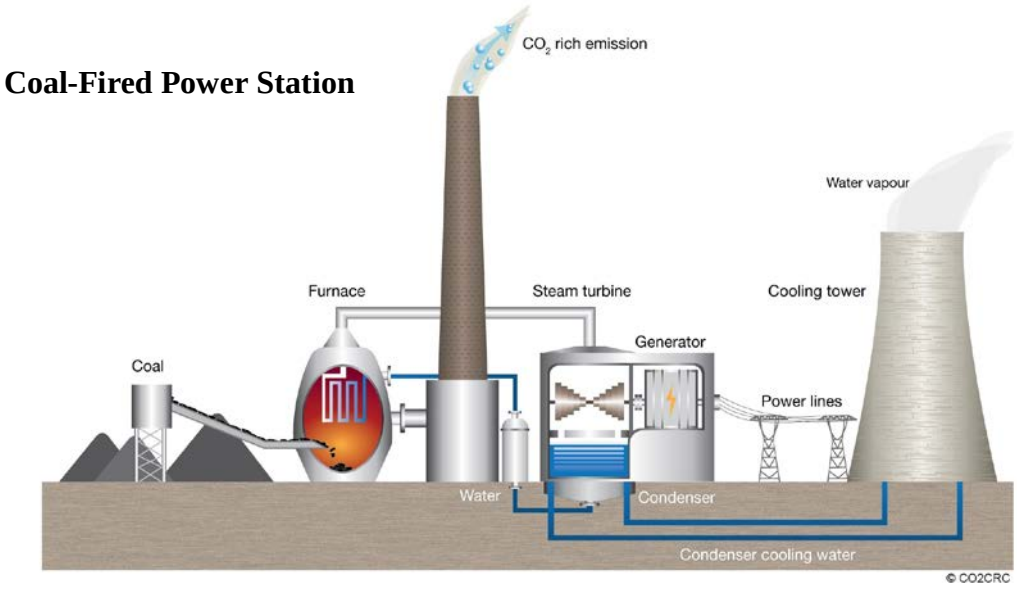

Figure 1. Schematic of a coal fired power station.

As a source of energy, coal is a limited resource. The majority of global coal reserves were deposited during the Carboniferous geological period (359-299 million years ago; 60 million years duration). Global consumption of coal by humans began in earnest during the Industrial Revolution, and at this stage, estimates are that all this coal will be consumed within ~500 years. This rate of consumption, with a rate of coal generation compared to rate of coal usage of $\sim 1.2\times10^{5}$ times, guarantees that coal is a limited resource.

At present rates of coal consumption it is estimated that there is somewhere between 100-150 years of coal remaining. During this time it is expected that other forms of energy production will be developed and implemented on the global scale. In the interim, the efficiency of coal utilization needs to be improved, as does a reduction in emissions from the use of coal. A possible approach is to improve the efficiency of CFPSs; however, these will always be limited by thermodynamic efficiencies, which are intrinsically low. Another alternative, which is the focus of this research, is the direct carbon fuel cell.

The direct carbon fuel cell (DCFC) is a fuel cell technology employing the direct electrochemical oxidation of carbon (specifically coal here) to produce electrical energy. In the DCFC there is only one energy transformation process employed; namely the electrochemical conversion of the chemical energy in coal to electrical energy, and as such the DCFC is often referred to as being an efficient means of direct energy production. The overall reaction involved in the DCFC is the same as in a CFPS; i.e.,

$$C + O_2 \rightarrow CO_2 \quad \ldots(1)$$

except in the case of the DCFC this is broken down into two electrochemical half reactions; i.e.,

$$C + 2O^{2-} \rightarrow CO_2 + 4e^- \text{ (anodic process)} \quad \ldots(2)$$
$$O_2 + 4e^- \rightarrow 2O^{2-} \text{ (cathodic process)} \quad \ldots(3)$$

where the oxide anion (O^{2-}) is the ionic charge carrier. Each of these half reactions is carried out in separate compartments of the fuel cell, as shown in the schematic in Figure 2. Separating the compartments is an ionically conducting medium, or electrolyte. In Figure 2 this is a combination of a solid oxide ion conductor; e.g., yttria stabilized zirconia (YSZ), and a molten mixture of Li_2CO_3, Na_2CO_3 and K_2CO_3. The solid YSZ physically separates the two compartments, while still allowing for ionic transport, while the molten carbonate media essentially acts as a carrier for oxide anions to facilitate their ready access to the carbon surface.

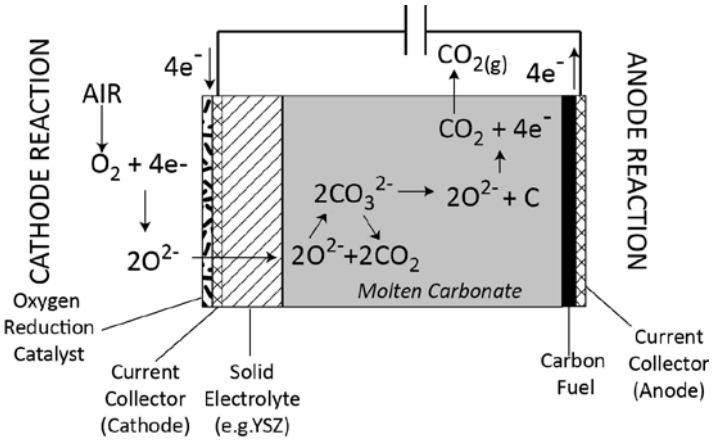

Figure 2. Schematic of the direct carbon fuel cell.

The efficiency of a fuel cell system such as the DCFC is assessed electrochemically, and revolves around how much of the chemical energy in the fuel is converted into electrical energy.

Therefore, for the overall reaction in Eqn (1) we can define a reaction enthalpy ($\Delta_r H$) corresponding to the amount of chemical energy present in the fuel (carbon). Likewise, for the electrochemical oxidation of carbon (Eqns (2) and (3)) we can define a reaction Gibbs energy ($\Delta_r G$) which in ideal terms corresponds to the maximum amount of electrical work the reaction can do, or in practical terms the amount of electrical work actually done by the system. The efficiency (η) is then defined as

$$\eta = \frac{\Delta_r G}{\Delta_r H} = \frac{\Delta_r H - T\Delta_r S}{\Delta_r H} = 1 - \frac{T\Delta_r S}{\Delta_r H} \quad \ldots(4)$$

where $\Delta_r S$ is the entropy change on reaction. For the oxidation of carbon (Eqn (1)) the reaction entropy is always close to zero, and as such the theoretical efficiency of the DCFC will be close to unity. For example, the standard entropy of formation for graphite (carbon source), oxygen and carbon dioxide (at 298.15 K and 1 atm pressure) are 6, 205 and 214 J/K/mol, respectively. Therefore, $\Delta_r S$ for Eqn (1) is 3 J/K/mol. Under the same conditions, the enthalpies of formation are 0, 0 and -394 kJ/mol for graphite, oxygen and carbon dioxide, respectively, leading to an overall reaction enthalpy of -394 kJ/mol. Substitution in Eqn (4), for a temperature of 298.15 K, leads to a theoretical efficiency of 1.002, or just over 100% efficient. Of course this can vary depending on the heat content of coal compared to graphite, as well as in terms of the entropy of formation of coal relative to graphite. Nevertheless, the calculation shows that high efficiencies are expected, much greater than a CFPS. In practice the amount of electrical work extracted from the DCFC is limited by overpotentials associated with the individual redox half reactions. Literature has reported efficiencies in the range of 80%, and we have also reported similar efficiencies.

Comparative Life Cycle Analysis

For the purposes of the life cycle analysis we will be carrying out a comparative analysis between the DCFC and a CFPS. This is considered to be the most straightforward approach, essentially allowing for a direct comparison between the technologies. Furthermore, it also makes sense to use such an approach since many features of both technologies are common, as highlighted in the block diagram in Figure 3.

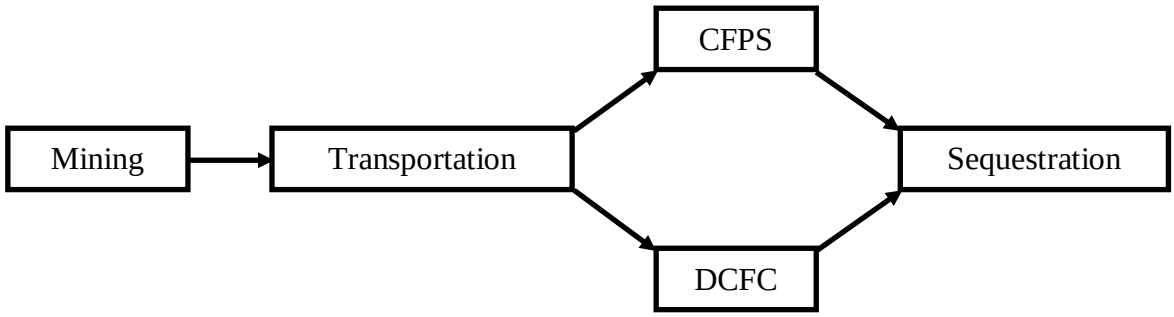

Figure 3. Block diagram of the alternative energy generation systems.

As can be seen in Figure 3 common aspects of energy generation include mining, transportation and ultimately sequestration.

Coal Mining

Of course, coal mining is essential for operation of both a CFPS and the DCFC. For a CFPS thermal coal is used, while for the DCFC there is no particular differentiation in place presently to assign a specific coal type for DCFC usage. In fact, most of the experimental work conducted thus far with the DCFC has been with the use of a thermal coal, with only selected experiments conducted with a metallurgical coal. As such, at this time we will assume that the process for

mining coal will be the same irrespective of the end use application of the coal; i.e., a CFPS or DCFC.

Transportation

Transportation of the coal from the mine to its end application is also a critical aspect of the LCA. Thermal coal usage for a CFPS will involve transportation of the coal primarily from the mine to either a port for exportation or directly to the CFPS. Certainly export coal (via ship) will require additional energy inputs to travel the longer distances. Transportation costs and energy consumption to use coal in the DCFC has the potential to be very similar to the CFPS particularly if the DCFC system used is a large centralized energy generation facility, like a CFPS. However, if the DCFC system used is much smaller, perhaps on the community scale, then there will be a need for additional transportation infrastructure to distribute the coal more broadly to the smaller scale systems.

Sequestration

For a CFPS post-combustion capture of emissions is a viable alternative for emissions reduction. The flue gas coming from a CFPS is composed primarily of carbon dioxide resulting from coal combustion. However, there are other gaseous (SO_x and NO_x gases) and particulate species present that must be removed first before sequestration can occur. This incurs a significant energy penalty in the separation process before sequestration can occur. For the DCFC the situation is quite different. In the absence of a combustion process where air is required, there will be no NO_x gases generated, and minimal SO_x gases. Furthermore, there will be no particulates produced, instead these will be contained within the molten carbonate electrolyte used in the DCFC.

LCA Points for Consideration

Throughout this LCA we will endeavour to make as fair a comparison as possible between the emissions and energy outputs coming from both CFPS and DCFC systems. It is important to specify what will and will not be focussed on in the analysis. Here we will try and focus on as many aspects of the systems as possible, but one aspect that will not be examined is the energy consumption and emissions coming from the construction of both the CFPS and DCFC systems. At least for the DCFC system this is a very large unknown, particularly on the large scale, and so we have chosen to ignore it at this stage. Similarly, the energy consumption and emissions resulting from the construction of mining equipment and transportation infrastructure used in the operation of the CFPS or DCFC systems will not be considered.

Base Case – Coal Fired Power Station (CFPS)

The base case for LCA comparison is the CFPS, the energy inputs and emissions from which can be summarized in Table 1. This data was sourced from a Worley Parsons publication, and relates to the energy inputs and outputs, materials usage and emissions arising from the extraction and processing of 10 Mt of black coal per year.

Table 1. Base case energy and material inputs and emissions arising from the mining, transportation and use of 10 Mt per annum black coal.

Base Case	**Energy and Material Input**		**GHG Outputs**	
10 Mt pa Production	**Sources**	**Quantities**	**Source**	**tCO_2-E pa**

Coal Mining	Diesel use	42,600 kL (1.7 PJ)	Diesel	115,000
	Use of grid power	174,800 MWh (0.63 PJ)	Grid power Explosives	180,000 2,500
	Explosives	14,700 t	Fugitives Slow combustion	375,200 18,500
	Other materials	n/a	Slow oxidation	1,800
Transportation	Diesel use	7600 kL (0.3 PJ)	Diesel	20,500
Energy Generation	Coal use	270 PJ	Combustion	23,880,000
Total Energy Consumption		**272.63 PJ**	**Total Emissions**	**24,593,500**

Based on the data in Table 1 we are now in the position of being able to calculate the total emissions resulting from the production of electrical energy. So for a total of 270×10^{15} J of input energy from coal, and assuming a CFPS efficiency of 35%, the total electrical energy output is therefore 94.5×10^{15} J, or 26.25×10^{6} MWh. With total emissions arising from this energy production amounting to 24,593,500 tCO_2-e per year, the emissions efficiency equates to 0.9369 tCO_2-e/MWh.

DCFC Specific Features

To assess the emissions efficiency of the DCFC we have to examine the features of the system that are specific to the DCFC. To do that we will begin with a naïve interpretation of the DCFC system, and work from there incorporating more of the complexities of the DCFC system, essentially outcomes from the fundamental studies we have conducted.

Naïve Interpretation

As a first assessment of the emissions efficiency of the DCFC we can take the total energy input from the coal (270×10^{15} J), with the theoretical efficiency of DCFC operation (100%), with the same emissions, and determine an emissions efficiency of 0.3279 tCO_2-e/MWh. This is best considered as the optimum emissions efficiency, representing ~35% of the emissions from a CFPS.

Increased Transportation Network

A point made previously was that the transportation network for the DCFC may need to be larger depending on the size of the DCFC system. Certainly if a single DCFC system was sufficiently large enough to cope with the 10 Mt per annum of coal used in the base case in Table 1, then the transportation network would be the same in both cases. However, if the operational DCFC systems were smaller and more distributed in nature, then a greater transportation network would be needed. Concomitant with that are greater emissions from transportation. For the purposes of this LCA we will presume that the diesel consumption will double to accommodate this need for an increased distribution network; i.e., 15,200 kL, amounting to emissions of 41,000 tCO_2-e per annum. This brings the total emissions to 24,614,000 tCO_2-e per annum, and again assuming a 100% efficiency for DCFC operation, the emissions efficiency increases slightly to 0.3282 tCO_2-e/MWh.

DCFC Efficiency

Previously it was naively assumed that the DCFC operates at its optimum efficiency. In practice this is not the case, with reported experimental efficiencies being closer to 80%. Under

these circumstances the total input energy from the coal (270×10^{15} J) transforms into 216×10^{15} J of electrical energy, or 60×10^{6} MWh. Assuming again the emissions from the expanded transportation network, the emissions efficiency becomes 0.4102 tCO_2-e/MWh, which is still only 43.8% of the emissions from a comparable CFPS.

Coal Pre-Pyrolysis

As an outcome of the fundamental studies we have conducted it was determined to be necessary to pre-pyrolyze the coal prior to use to remove volatiles that would otherwise adversely affect the operation of the DCFC. To examine the energy requirements necessary to do this we have assumed that the coal will be heated from ambient temperature (25°C) to 700°C, a temperature difference of 675 K. We have also assumed a heat capacity for coal of 1.38 kJ/K/kg. So, for the total amount of coal used on an annual basis (10×10^{6} t), the energy input required is 9.315×10^{12} kJ, with a thermal efficiency of 100%. More realistically with a heating efficiency of say 80%, the required energy input is 11.64×10^{12} kJ. This energy input equates to 3.234×10^{6} MWh, which when comes from a CFPS with an efficiency of 35%, equates to an additional 3.030×10^{6} tCO_2-e per annum, bringing the total emissions to 27,644,000 tCO_2-e per annum. Combining the reduced efficiency of the DCFC (80%) and expanded transportation network leads to an emissions efficiency of 0.4607 tCO_2-e/MWh, which is 49.2% of the emissions from a comparable CFPS.

The volatile species arising from the pre-pyrolysis of the coal can also be used as a source of energy rather than just being considered as emissions. The volatiles given off are essentially mid-range chain length hydrocarbons, which can be combusted directly to produce heat and steam for a mini-turbine. In the absence of knowing the thermal content of these volatiles, which will be specific to the type of coal used in the DCFC, it is not possible to calculate with any certainty the energy available here. As an estimate, if we assume that 2% of the coal is lost as volatiles, then the quantity lost is ~0.2 Mt per annum. Again now assuming an average alkane chain length of C10, the energy available from these volatiles is $\sim9\times10^{15}$ J, which is available for recovery.

Heating of the DCFC

The DCFC is a high temperature fuel cell and so energy has to be input to maintain operating temperature. For the sake of this LCA analysis we will assume that the operating temperature of the DCFC is 700°C, in line with the pre-pyrolysis temperature of the coal. This is not a random temperature. Fundamental experimentation we have conducted has shown that 700°C is sufficiently high a temperature to ensure fast anodic and cathodic kinetics, but not too high a temperature to facilitate Boudouard gasification of the coal; i.e., chemical corrosion of coal.

Under these conditions, the main component that requires heat to remain at this temperature is the molten carbonate electrolyte. We have assumed here that the coal entering the DCFC still remains at the pre-pyrolysis temperature, and thus does not require additional heating. At this time it is unknown with any certainty how much of the electrolyte will be required to operate the DCFC under such large scale conditions. It is a component of the DCFC that is not consumed, and so what we have assumed for the LCA is that the amount of molten carbonate electrolyte required is 20% of the total amount of coal used; i.e., 10 Mt of coal are used annually, suggesting the use of 2 Mt of the molten carbonate electrolyte. The heat capacity of the molten carbonate electrolyte is quoted in the literature (Trans. Faraday Soc., 1963, 59, 841-845) as being 168.9 J/K/mol or 1.687 kJ/K/kg. Therefore, for 2×10^{9} kg of electrolyte the heat input required is 2.277×10^{12} kJ. At 80% thermal efficiency this is an energy input of 2.847×10^{12} kJ. This energy input equates to 0.791×10^{6} MWh. When this energy comes from a 35% efficient CFPS, it adds a further 0.741×10^{6} tCO_2-e per annum, leading to total emissions of 28,384,900 tCO_2-e per annum. This leads to an emissions efficiency of 0.4731 tCO_2-e/MWh, which is 50.5% of the emissions from a comparable CFPS.

DCFC Inefficiency

As discussed previously the DCFC is a high efficiency process. With a working efficiency of 80% the power output from coal is far superior to that coming from a CFPS. While this working

efficiency is high, the inefficiency can also contribute to the operation of the DCFC. For an input energy of 270×10^{15} J, and with an 80% electrochemical efficiency, this leads to an output of 216×10^{15} J, or 60×10^{6} MWh. The inefficiencies in the process (54×10^{15} J) are associated with electrochemical overpotentials for the anodic and cathodic processes and resistances in the DCFC. This energy is not lost from the DCFC, but are instead evident as heat contributions to the DCFC, in effect contributing to the ongoing heating of the DCFC. If this is indeed the case, then the thermal energy arising from the inefficiencies in the DCFC are considerably larger than that required to heat the molten carbonate electrolyte in the cell; i.e., 2.847×10^{15} J, or only 5.3% of the energy lost due to inefficiencies in coal utilization. Therefore, even assuming poor thermal insulation within the DCFC, the emissions arising from heating the DCFC can be negated, and potentially even those arising from pre-pyrolysis of the coal.

Waste Gas Stream

The carbon dioxide emissions arising from the DCFC also carry a considerable amount of energy tied up with the heat capacity of the gas. This can also be used as a means of energy recovery before release. If we consider the base case in terms of carbon dioxide emissions (24,593,500 tCO_2-e per year), then with a heat capacity of 37 J/K/mol, the amount of energy available for capture associated with the carbon dioxide stream is (assuming a temperature drop from 700°C to 25°C) 13.96×10^{15} J. This energy can be used for heating the DCFC, or even direct energy generation. Whatever the application, the use of the heat associated with this waste carbon dioxide stream will diminish the external energy requirements even further.

Sequestration

Sequestration of the carbon dioxide waste stream is expected to be more energy efficient for the DCFC compared to a CFPS. The main reason for this is that no post combustion separation of the carbon dioxide is required for the DCFC. If we assume the energy penalty for sequestration is 13% for a CFPS, based on the energy output, this adds an additional energy requirement of 12.29×10^{15} J and emissions of 3,197,155 tCO_2-e per annum. This ultimately leads to total emissions of 27,790,655 tCO_2-e per annum, and an emissions efficiency of 1.0587 tCO_2-e/MWh.

For the DCFC where no post-combustion separation is necessary, much less energy is required to capture the essentially pure carbon dioxide stream coming from DCFC usage. To assess the energy requirement, we have assumed an energy penalty of 2% based on the total output energy. This requires an input energy of 4.32×10^{15} J, which corresponds to emissions of 567,698 tCO_2-e per annum. This brings the total emissions from the DCFC to 28,952,598 t-CO_2-e per annum, and registers an emissions efficiency of 0.4825 tCO_2-e/MWh, which is 45.6% of the CFPS with a similar sequestration requirement.

Summary

As a result of this life cycle analysis we have shown that the DCFC is a lower emissions energy generation technology. Table 2 is a summary of the energy generated, emissions and emissions efficiency for the DCFC compared to the CFPS.

Table 2. Summary of the DCFC emissions performance.

	Energy (J pa)		Emissions	
Situation	**Input**	**Output**	**tCO_2-e pa**	**tCO_2-e/MWh**
CFPS				
Base case	270×10^{15}	94.5×10^{15}	24,593,500	0.9369
+ Sequestration	282.3×10^{15}	94.5×10^{15}	27,790,655	1.0587
DCFC				
Naive analysis	270×10^{15}	270×10^{15}	24,593,500	0.3279
+ Increased transportation network	270.6×10^{15}	270×10^{15}	24,614,000	0.3282

+ Lower efficiency	270.6×10^{15}	216×10^{15}	24,614,000	0.4102
+ Coal pre-pyrolysis	282.2×10^{15}	216×10^{15}	27,644,000	0.4607
+ DCFC heating	285.0×10^{15}	216×10^{15}	28,384,900	0.4731
+ Sequestration	289.3×10^{15}	216×10^{15}	28,952,598	0.4825
DCFC inefficiency	↓	216×10^{15}	↓	↓
Waste gas stream	↓	216×10^{15}	↓	↓